Dissertation zur Erlangung des Doktorgrades

der Fakultät für Chemie und Pharmazie

der Ludwig-Maximilians-Universität München

Synthesis, Identification, and Characterization of Novel, Condensed Oxonitridophosphates and Phosphorus Oxonitrides
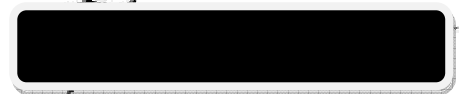
Stefan Josef Sedlmaier

aus

Freising

2011

Meinen Eltern

Ich bin vom Glauben zum Wissen konvertiert.

Hamed Abdel-Samad

Table of Contents

10.   Unprecedented Zeolite-Like Framework Topology Constructed from Cages with 3-rings in a Barium Oxonitridophosphate   119

11. SrP_3N_5O: A Highly Condensed Layer Phosphate Structure Solved from a Nanocrystal by Automated Electron Diffraction Tomography   148

1.   Introduction

The overall towering topic of mankind for the future is the sustainable management of natural, non-renewable resources. In this context, the finite fossil energy sources like crude oil, gas and coal or the scarce drinking water reserves and the narrowed access to them in many parts of the world reside permanently in the awareness of the public, by regarding the gasoline prizes or by tracking the news about the recent drought in East Africa.

In the meantime it is also known that there are shortages for some metals, as popular high-technological products like mobile phone, laptop or flat screen are affected. The very rare metals such as tantalum, niobium, and indium, where the mineable resources are ambiguous, are increasingly used in the growing electronics industry.[1] Even the narrow in the availability of the more frequent lithium is discussed more often, because this prevents mostly advance in electromobility.[2]

Another critical global resource, which receives much less attention, however, is phosphorus, although the element with the atomic number 15 is a nutrient essential for whole life (plants and animals). Processed to 90 % as fertilizers, phosphorus is, besides nitrogen and potassium, a limiting factor for successful agriculture and so for the world's food production.[3] As recently acquired by *Cordell*,[4] a similar situation for phosphorus as for oil is currently prevailing. The main raw material for phosphate fertilizers, phosphate rock (calcium phosphates, mainly apatite and phosphorite), is like oil, a non-renewable resource that will be depleted within the next 50 to 100 years. From the imminent *peak phosphorus* (Figure 1) onward,[5] the global reserves of phosphate rock, which are mainly concentrated in only few countries (China, Morocco and Western Sahara), are more difficult to extract and become more and more expensive (Figure 2).[6] The growing food demand, triggered by an increasing population, a global trend towards more meat and dairy-based diets and an expansion of the biofuel industry melts down the phosphorus reserves even more rapidly. And the situation turns out to be more severe as there are, in contrast to oil, no alternatives for phosphorus in agriculture and so for future food security of civilization. In the face of the immense importance and scarcity of phosphorus, besides the development of effective recovery technologies, research on phosphorus topics is mandatory to get chances to develop worthwhile functional materials from this invaluable commodity.
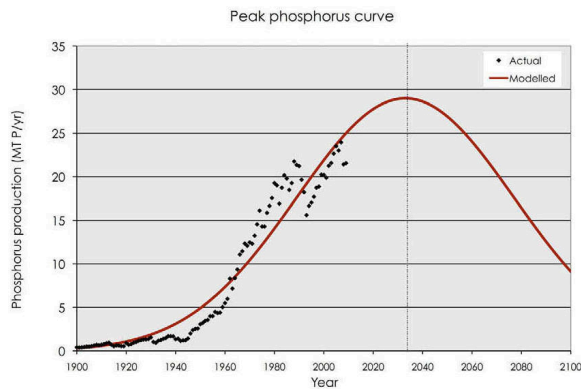
Figure 1. *Hubbert curve* based on industry data, indicating a peak year of global phosphate rock production before 2035; production will decline afterwards.[4,5]
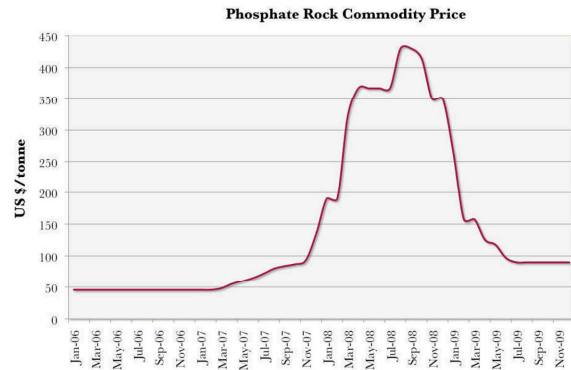
Figure 2. Phosphate rock commodity price (Morocco) increased 800 % between 01/2007 and 09/2008.[4,6]

Aside from the usage as fertilizers, phosphorus finds further industrial applications in different fields. In the second largest market, phosphorus is manufactured to $Na_5P_3O_{10}$ and used as water softener in detergents. Additionally, phosphorus is further consumed—also in industrial scale—for the fabrication of matches and in form of manganese-, iron- and zinc-phosphates as corrosions protection coatings.[7] Furthermore transferred to organo-phosphorus compounds, diverse usages e.g. as plasticizers ($POCl_3$), flame-retardants or herb- and pesticides ($POCl_3$, P_4S_{10}) are existent.[8] In a wide range of more special niche applications, phosphorus is additionally included e.g. in beverages (as H_3PO_4 e.g. in Coca Cola®), in toothpaste or in military artefacts (white P),[9] only to name few.

Solid-state chemistry and materials science made sure that phosphorus also penetrated high-tech applications. Besides elementary phosphorus as alloy component in electronics (e.g. GaP semi-conductor, as *n*-dopant or P together with Ni for better solderability on circuit boards[10]), phosphorus appears first and foremost in functionalities in form of phosphates such as $(VO)_2P_2O_7$, acting as catalyst in organic syntheses.[11] A highly relevant field are particularly special glasses. Alumo-phosphate glasses with a glass transition temperature below 400 °C and an expansion coefficient larger than $150 \cdot 10^{-7}$ °C^{-1} are for example suitable as special hermetic seals,[12] biocompatible phosphate glass ceramics are used in medicine[13] and amorphous lithium phosphates exhibit useful solid-state electrolytes.[14] A more famous

Figure 3. Nd^{3+} doped phosphate glass for laser applications (FOCtek Photonics Inc., Fujian, China).

material for the latter functionality is the superfast Na^+ ion conductor $Na_{3-x}Zr_2(PO_4)_{1+x}(SiO_4)_{2-x}$ known as NASICON.[15] Phosphates are also very important for laser materials. With Er^{3+} or Nd^{3+} doped glass compositions (Figure 3) highly energetic (up to 10^6 J) and powerful (up to 10^{15} W) lasers can be built.[16] Further compounds in the field of optic materials are KH_2PO_4[17] and $KTiOPO_4$,[18,19] exhibiting efficient second harmonic generators (SHGs). In this series of optics, $Na_3Ce_{0.65}Tb_{0.35}(PO_4)_2$,[17] orthophosphates of the rare-earth metals or as well with α-$Sr(PO_3)_2$:Eu^{2+},Mn^{2+}[20] luminescent materials join as well in phosphate-based applications.

As obvious above, nearly all applications for phosphorus are based oxidic. However, with intensive research in the last few decades, non-oxidic materials have often proved to be chemically, thermally and mechanically more resistant. Besides carbides, nitrides are particularly prominent. Through more frequently appearing of higher anion coordination numbers and thus higher condensed structures in combination with an increased covalent bonding character involved, nitridic compounds are among high-performance materials in several fields. The most famous examples are Si_3N_4 that is used as an especially light hardening treatment for i.e. gas tubes and BN, which is either applied as high-temperature lubricant (*h*-BN) or as abrasive (*c*-BN). From the latter derived Si/B/N materials by *Jansen*[21-23] impress as ultra high-temperature materials. Another highly important nitride is GaN, a III/V semiconductor with a wide direct bandgap. The technological access to a *p*-doped variant enabled the fabrication of highly efficient blue (405 nm) laser light-emitting diodes (LEDs). This invention created the conditions for another, in the meantime prominent application-oriented research topic within nitrides. The (oxo)nitrido(alumo)silicates afforded very stable compounds which, doped with rare earth ions (Eu^{2+}, Ce^{3+}), work as efficient luminescent materials for pc-LEDs based on GaN blue primary LEDs to emit white light (Figure 4). Driven by this application highlight and some other promising properties (e.g. lithium ion conduction), through the development of different synthesis strategies (high-temperature reactions, reactions in liquid alkali metals,

Figure 4. Principle of a two pc-LED with nitridosilicate phosphors and a blue GaN primary LED.[24]

precursor routes or carbothermal reduction- and nitriding processes) within nitridosilicates and its related classes including SiAlONs a structural diversity was found in the last few decades, which outperforms the already high structural variability of the oxosilicates.[24]

In contrast to the latter multifaceted Si/N compound class, the phosphorus nitride chemistry, however, has not led to such a blossoming, although the chances are theoretically not worse. As there also nitride anions are incorporated in tetrahedral networks, the respective benefits like the higher valence (connecting three or four tetrahedra centers) and the more flexible bond lengths and angles could come to effect and result also in a variety of stable structures beyond that of oxosilicates. Up to now the group of ternary phosphorus nitrides and phosphorus oxonitrides is rather compact, whereas the individual examples, however, are very different. After the series $M^I_3M^{III}P_3O_9N$ (M^I = Na, K; M^{III} = Al, Ga, In, Ti, V, Cr, Mn, Fe),[25] $M^I_2M^{II}_2P_3O_9N$ (M^I = Na; M^{II} = Mg, Mn, Fe, Co),[26] and $Cs_3M^{II}_2P_6O_{17}N$ (M^{II} = Mg, Fe, Co)[27] which rather rank among the oxophosphates, there are three nitridophosphates with finite anions, namely Li_7PN_4[28] exhibiting an orthophosphate with isolated PN_4^{7-} anions, $Li_{12}P_3N_9$[29] as one cyclotriphosphate and $Li_{10}P_4N_{10}$[30] containing P_4O_{10}-analogous, adamantane-like anions. Ascending in degree of condensation, besides only two compounds with chain-structures ($M^{II}_2PN_3$ with M^{II} = Mg, Ca),[31] the rest of the compounds within this compact compound class divide over several TX_2 and higher condensed structure types. These comprise three-dimensional framework structures like cristobalite related M^IPN_2 (M^I = Li, Na),[32,33] megakalsilite ($M^{II}P_2N_4$ with M^{II} = Ca, Sr, Cd),[34,35] phenakite (BeP_2N_4),[36] the HP-CaB_2O_4 IV type (BaP_2N_4)[37,38] and the series of $M^IP_4N_7$ with M^I = Na, K and Rb[39] and $M^IP_6N_{11}$ with M^I = K, Rb and Cs.[40] In addition to those dense P/N networks, besides sinoite-like $SiPN_3$,[41] few compounds with three further structure types must be added. These are impressive open-frameworks, namely the nitrido-[42] and oxonitridosodalites,[43] the first nitridic zeolite $Li_{12-x}H_{x-y+z}[P_{12}O_yN_{24-y}]X_z$ (X = Cl, Br) (three letter code *NPO*, Figure 5)[44] and the first nitridic clathrate $P_4N_4(NH)_4 \cdot NH_3$ (Figure 6).[45] Besides the ternary, metal-containing phases, the sparseness of compounds further continues with the binary and the pseudo-binary phases. Compared to the variety of alone SiO_2 polymorphs (14 representatives),[46] there are only nine† different phases, although twice as much elements and increased structural possibilities are involved. Instead, in compounds like P_3N_5,[47,48] P_4N_6O[49] and HP_4N_7[50] exceptional und rare structural motifs like edge-sharing tetrahedra and square pyramids (γ-P_3N_5)[48] are appearing. The remaining few compounds in this regard, PON (cristobalite, moganite and quartz)[51-55] and HPN_2 (cristobalite and another monoclinic one),[56,35] adopt mainly structures known from SiO_2.

---

† without $P_4N_4(NH)_4 \cdot NH_3$, which actually belongs to the category of the pseudo-binary phases
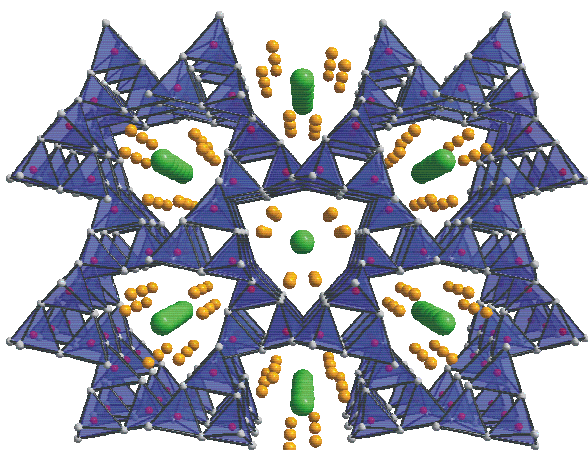
Figure 5. Crystal structure of $Li_{12-x}H_{x-y+z}[P_{12}O_yN_{24-y}]X_z$ (X = Cl, Br) with view along [100]; yellow spheres represent Li^+, green spheres Cl^-, pink spheres P and white spheres O/N. [44]
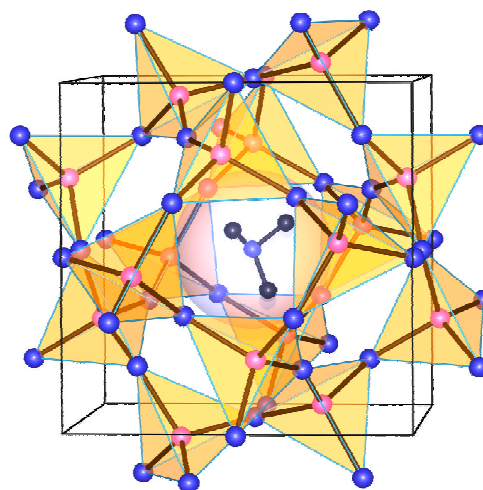
Figure 6. Crystal structure of $P_4N_4(NH)_4 \cdot NH_3$ with view approx. along [001]; blue spheres represent N; pink spheres P, dark gray spheres H; the 4^28^4 cages encapsulate NH_3 molecules. [45]

But why is there such a scarcity in the compound class of (oxo)nitridophosphates and phosphorus (oxo)nitrides and why was it not possible so far to exploit their potential? The reason for this question is rooted in both, preparative and analytical difficulties. In most of the cases, the reaction products show poor crystallinity without including single crystals big enough for conventional X-ray based structure determination. So, fast identification of new phases is impeded. Samples are notoriously micro- or even nanocrystalline, which require usually at first phase-purity before from powder X-ray diffraction data or a combination of analytical methods (including electron microscopic methods or solid-state NMR spectroscopy) new compounds can be identified and structurally characterized. Phase-pure P/O/N samples, however, are also often not available but further accompanied by high amorphous proportions. This problematic behavior may originate from a less bonding strength P–N (molar bonding energy (MBE): 290 kJ mol^{-1}).[57] Compound classes like oxophosphates (MBE P–O: 407 kJ mol^{-1}), nitridosilicates (MBE Si–N: 335 kJ mol^{-1}) and especially oxosilicates (MBE P–O: 444 kJ mol^{-1}) include much higher bonding strengths and crystallize by far better.

By regarding the facts above, it should indeed be worth the effort, despite these problems, to accept the challenge of discovering novel oxonitridophosphates and phosphorus oxonitrides and try to develop this field to a level, where other tetrahedra network building compound classes already are. The diverse structural chemistry in the few already existing P/O/N compounds alone, indicating a still hidden abundance, is promising enough. As shown impressively for borates in the last years, a helpful tool for the development of PON chemistry could be high-pressure conditions.[58] Besides the pure

academic interest, however, as compounds like $Li_{12-x}H_{x-y+z}[P_{12}O_yN_{24-y}]X_z$ (X = Cl, Br) with Li+ ion conductivity[44b] and $P_4N_4(NH)_4 \cdot NH_3$ potential for catalysis, gas storage and separative membranes[59] show that also applications are imaginable, make the P/O/N chemistry especially exciting.

The objective of this thesis was the synthesis, the identification, and the structural characterization of novel oxonitridophosphates and phosphorus oxonitrides. Therefore, building the unifying thread throughout, different synthesis strategies were pursued. They cover potential precursor compounds in the first part, followed by the development of new P/O/N starting materials and the utilization of high-pressure conditions with applying the latter to classical solid-state chemistry employing multi-component reactant systems. The analytical methods used for the identification and characterization exhibit just the same importance as synthesis strategies. X-ray diffraction (mainly executed on powders) served as main analytical method while in some cases it was combined with supplementing ^{31}P and ^{1}H solid-state NMR. Electron microscopy methods including both imaging and diffraction techniques, played also a crucial role in this thesis. The introduction of the new method 'automated electron diffraction tomography' ADT and its (nearly to routine) utilization within this thesis includes an outstanding benefit for the future in material science research in general and P/O/N chemistry in particular.

REFERENCES

[1]   U. Bilow, A. Reller, *Nachr. Chem.* **2009**, *57*, 647.

[2]   http://www.spiegel.de/wissenschaft/technik/0,1518,649579,00.html, **accessed 12/10/2011**.

[3]   http://phosphorusfutures.net/, **accessed 15/09/2011**.

[4]   D. Cordell, Doctoral Thesis, Univ. Sydney (Australia) and Univ. Linköping (Sweden), **2010**.

[5]   D. Cordell, J.-O. Drangert, S. White, *Global Environmental Change* **2009**, *19*, 292.

[6]   a) World Bank, *Commodity Price Data (Pink Sheet), Prospects for the Global Economy*, World Bank **2009**, http://go.worldbank.org/5AT3JHWYU0, **accessed 15/09/2011**; b) Minemakers Limited, *Rock Phosphate Price Rockets to US$200/Tonne*, ASX and Press Release, Perth **2008**.

[7]   W. Foerst, *Ullmanns Encyklopädie der technischen Chemie*, Verlag Urban & Schwarzenberg, München, Vol. 10, **1958**, pp. 669.

[8]   N. N. Greenwood, A. Earnshaw, *Chemistry of the Elements*, 2nd edn., Butterworth-Heinemann, Oxford, **1997**.

[9]   K. Dockery, *Special Warfare Special Weapons*, Emperor's Press, Chicago, **1997**.

[10]   C. Schmetterer, H. Ipser, *Nachr. Chem.* **2011**, *59*, 831.

[11]   P. T. Nguyen, A. W. Sleight, N. Roberts, W. W. Warren, *J. Solid State Chem.* **1996**, *122*, 259.

[12]   R. K. Brow, L. Kovacic, R. E. Loehman, *Ceram. Trans.* **1996**, *70*, 177.

[13]   J. Vogel, P. Wange, P. Hartmann, *Glastech. Ber.* **1997**, *70*, 23.

[14]   J. Fu, *J. Mater. Sci.* **1998**, *33*, 1549.

[15]   A. R. West, *Grundlagen der Festkörperchemie*, Verlag Chemie, Weinheim, **1992**.

[16]   M. J. Weber, *J. Non-Cryst. Solids* **1990**, *123*, 208.

[17]   C. N. R. Rao, J. Gopalakrishnan, *New directions in solid state chemistry*, Cambridge University Press, Cambridge, **1986**.

[18]   R. Masse, J. C. Grenier, *Bull. Soc. Fr. Mineral. Cristallogr.* **1971**, *94*, 437.

[19]   M. M. Eddy, T. E. Gier, N. L. Keder, G. D. Stucky, D. E. Cox, J. D. Bierlein, G. Jones, *Inorg. Chem.* **1988**, *27*, 1856.

[20]   H. A. Höppe, M. Daub, M. C. Bröhmer, *Chem. Mater.* **2007,** *19,* 6358.

[21]   H. P. Baldus, M. Jansen, *Angew. Chem.* **1997**, *109*, 338; *Angew. Chem., Int. Ed. Engl.* **1997**, *36*, 328.

[22]   R. M. Hagenmayer, U. Müller, C. J. Benmore, J. Neuefeind, M. Jansen, *J. Mater. Chem.* **1999**, *9*, 2865.

[23]   P. Kroll, R. Hoffmann, *Angew. Chem.* **1998**, *110*, 2616; *Angew. Chem., Int. Ed. Engl.* **1998**, *37*, 2527.

[24]   M. Zeuner, S. Pagano, W. Schnick, *Angew. Chem.* **2011**, *123*, 7898; *Angew. Chem., Int. Ed.* **2011**, *50*, 7754.

[25]   W. Feldmann, *Z. Chem.* **1987**, *27*, 100.

[26]   R. Conanec, W. Feldmann, R. Marchand, Y. Laurent, *J. Solid State Chem.* **1996**, *121*, 418.

[27]   W. Feldmann, P. L'Haridon, R. Marchand, *J. Solid State Chem.* **2000**, *153*, 185.

[28]   W. Schnick, J. Lücke, *J. Solid State Chem.* **1990**, *87*, 101.

[29]   W. Schnick, habilitation treatise, Univ. Bonn (Germany), **1992**.

[30] W. Schnick, U. Berger, *Angew. Chem.* **1991**, *103*, 857; *Angew. Chem., Int. Ed. Engl.* **1991**, *30*, 830.

[31] a) W. Schnick, V. Schultz-Coulon, *Angew. Chem.* **1993**, *105*, 308; *Angew. Chem., Int. Ed. Engl.* **1993**, *32*, 280; b) V. Schultz-Coulon, W. Schnick, *Z. Anorg. Allg. Chem.* **1997**, *623*, 69.

[32] W. Schnick, J. Lücke, *Z. Anorg. Allg. Chem.* **1990**, *588*, 19.

[33] K. Landskron, S. Schmid, W. Schnick, *Z. Anorg. Allg. Chem.* **2001**, *627*, 2469.

[34] F. W. Karau, L. Seyfarth, O. Oeckler, J. Senker, K. Landskron, W. Schnick, *Chem. Eur. J.* **2007**, *13*, 6841.

[35] F. Karau, Doctoral Thesis, Univ. München (LMU), **2007**.

[36] F. J. Pucher, S. R. Römer, F. W. Karau, W. Schnick, *Chem. Eur. J.* **2010**, *16*, 7208.

[37] F. Karau, W. Schnick, *J. Solid State Chem.* **2005**, *178*, 135.

[38] F. Karau, W. Schnick, *Z. Anorg. Allg. Chem.* **2006**, *632*, 231.

[39] K. Landskron, E. Irran, W. Schnick, *Chem. Eur. J.* **1999**, *5*, 2548.

[40] K. Landskron, W. Schnick, *J. Solid State Chem.* **2001**, *156*, 390.

[41] H. P. Baldus, W. Schnick, J. Lücke, U. Wannagat, G. Bogedain, *Chem. Mater.* **1993**, *5*, 845.

[42] a) W. Schnick, J. Lücke, *Angew. Chem.* **1992**, *104*, 208; *Angew. Chem., Int. Ed. Engl.* **1992**, *31*, 213; b) W. Schnick, J. Lücke, *Z. Anorg. Allg. Chem.* **1994**, *620*, 2014; c) W. Schnick, N. Stock, J. Lücke, M. Volkmann, M. Jansen, *Z. Anorg. Allg. Chem.* **1995**, *621*, 987; d) F. Wester, W. Schnick, *Z. Anorg. Allg. Chem.* **1996**, *622*, 1281.

[43] N. Stock, E. Irran, W. Schnick, *Chem. Eur. J.* **1998**, *4*, 1822.

[44] a) S. Correll, N. Stock, O. Oeckler, W. Schnick, *Angew. Chem.* **2003**, *115*, 3674; *Angew. Chem., Int. Ed.* **2003**, *42*, 3549; b) S. Correll, N. Stock, O. Oeckler, J. Senker, T. Nilges, W. Schnick, *Z. Anorg. Allg. Chem.* **2004**, *630*, 2205.

[45] F. Karau, W. Schnick, *Angew. Chem.* **2006**, *118*, 4617; *Angew. Chem., Int. Ed.* **2006**, *45*, 4505.

[46] http://en.wikipedia.org/wiki/Silicon_dioxide, **accessed 15/09/2011**.

[47] a) W. Schnick, J. Lücke, F. Krumeich, *Chem. Mater.* **1996**, *8*, 281; b) S. Horstmann, E. Irran, W. Schnick, *Angew. Chem.* **1997**, *109*, 1938; *Angew. Chem., Int. Ed. Engl.* **1997**, *36*, 1873; c) S. Horstmann, E. Irran, W. Schnick, *Z. Anorg. Allg. Chem.* **1998**, *624*, 620.

[48] a) K. Landskron, H. Huppertz, J. Senker, W. Schnick, *Angew. Chem.* **2001**, *113*, 2713; *Angew. Chem., Int. Ed.* **2001**, *40*, 2643; K. Landskron, H. Huppertz, J. Senker, W. Schnick, *Z. Anorg. Allg. Chem.* **2002**, *628*, 1465.

[49] J. Ronis, B. Bondars, A. Vitola, T. Millers, J. Schneider, F. Frey, *J. Solid State Chem.* **1995**, *115*, 265.

[50] a) S. Horstmann, E. Irran, W. Schnick, *Angew. Chem.* **1997**, *109*, 2085; *Angew. Chem., Int. Ed. Engl.* **1997**, *36*, 1992; b) S. Horstmann, E. Irran, W. Schnick, *Z. Anorg. Allg. Chem.* **1998**, *624*, 221.

[51] L. Boukbir, R. Marchand, Y. Laurent, P. Bacher, G. Roult, *Ann. Chim. Fr.* **1989**, *14*, 475.

[52] J.-M. Léger, J. Haines, L. S. de Oliveira, C. Chateau, A. Le Sauze, R. Marchand, *J. Phys.: Condens. Matter* **1996**, *8*, L773.

[53] C. Chateau, J. Haines, J.-M. Léger, A. Le Sauze, R. Marchand, *Am. Mineral.* **1999**, *84*, 207.

[54] J. Haines, C. Chateau, J.-M. Léger, A. Le Sauze, N. Diot, R. Marchand, S. Hull, *Acta Crystallogr., Sect. B: Struct. Sci.* **1999**, *55*, 677.

[55] J.-M. Léger, J. Haines, L. Silva de Oliveira, C. Chateau, A. Le Sauze, R. Marchand, S. Hull, *J. Phys. Chem. Solids* **1999**, *60*, 145.

[56] W. Schnick, J. Lücke, *Z. Anorg. Allg. Chem.* **1992**, *610*, 121.

[57] A. F. Holleman, E. Wiberg, N. Wiberg, *Lehrbuch der Anorganischen Chemie*, de Gruyter, Berlin, 102nd edn., **2007**, p. 143.

[58] H. Huppertz, *Chem. Commun.* **2011**, *47*, 131.

[59] M. Pouchard, *Nature* **2006**, *442*, 878.

2.   Tl$_4$(PO$_2$NH)$_4 \cdot$ H$_2$O – A Commensurately Modulated Tetrametaphosphimate

Tri- and tetrametaphosphimates have been considered as optimal single-source precursors for condensed oxonitridophosphates. Although particularly *Stock*[†] and *Correll*[‡] have pursued synthesis strategy and described a huge number of compounds, until now no oxonitridophosphate resulted from them. The only exception exhibits Na(PO$_2$NH)$_3 \cdot$ H$_2$O, which could be transformed to Na$_4$P$_4$O$_8$(NH)N$_2$, an oxonitridophosphate including unusual chains with edge and corner linked tetrahedra. Insofar it is indeed worthwhile to characterize further phosphimates. Besides the original intension, the two described in this and in the following chapter include further exciting features, namely a challenging structure determination, where an elegant solution was chosen in one case and a material that exhibits a potential alternative material for bones in the other case.

ABSTRACT

Tetrathallium(I) tetra-μ-imidocyclotetraphosphate monohydrate, Tl$_4$(PO$_2$NH)$_4 \cdot$ H$_2$O, was obtained by evaporation of combined aqueous solutions of K$_4$(PO$_2$NH)$_4 \cdot$ 4H$_2$O and TlOOCCH$_3$ corresponding to the molar ratio of 1 : 4. The structure determination of Tl$_4$(PO$_2$NH)$_4 \cdot$ H$_2$O was performed by single-crystal X-ray diffraction methods. In addition to the basic structure ($P\overline{1}$ (no. 2), $a = 928.3(2)$, $b = 974.6(2)$, $c = 1018.0(2)$ pm, $\alpha = 74.47(3)$, $\beta = 64.68(3)$, $\gamma = 78.81(3)°$, Z = 2), satellite reflections indicate a fourfold superstructure ($A\overline{1}$, $a = 928.0(2)$, $b = 3897.1(8)$, $c = 2035.4(4)$, $\alpha = 74.47(3)$, $\beta = 64.68(3)$, $\gamma = 78.81(3)°$, Z = 16) that is described by an $a \times 4b \times 2c$, A-centered supercell which mainly concerns one thallium site of the basic structure. In order to reduce the number of parameters, this superstructure was handled as a commensurate occupancy modulation using the structural description in $(3 + 1)$-dimensional superspace ($P\overline{1}(\alpha\beta\gamma)$, q = 0.25b* + 0.5c*). The crystal structure of Tl$_4$(PO$_2$NH)$_4 \cdot$ H$_2$O consists of infinite columns of the cyclic [(PO$_2$NH)$_4$]$^{4-}$ anions (saddle conformation) which are interconnected by four N–H···O hydrogen bonds. By coordination to the Tl$^+$ ions the [(PO$_2$NH)$_4$]$^{4-}$ columns form a three-dimensional network with channels along [100] wherein the thallium ions that are mainly affected by the modulation are located. The commensurate occupancy modulation of these Tl$^+$ ions has been described with a single harmonic wave function. The modulation is verified by ^{31}P NMR spectroscopy. The thermal behavior of Tl$_4$(PO$_2$NH)$_4 \cdot$ H$_2$O and the FT-IR data are discussed as well.

[†] N. Stock, Doctoral Thesis, Univ. Bayreuth, **1998**.
[‡] S. Correll, Doctoral Thesis, Univ. München (LMU), **2006**.

2.1 INTRODUCTION

Silicate-analogous compound classes like P / O / N materials are of high research interest owing to interesting new zeolite-like framework structures with potential applications.

As phosphorus usually exhibits a high oxophily, nitrogen containing precursor compounds are required for the synthesis of framework structures built up from $P(O/N)_4$ tetrahedrons. With a molar ratio of $P : N : O = 1 : 1 : 2$ and a convenient cyclic structure which can occur as structural building units (SBUs) in zeolite structures, metaphosphimates (imidocyclophosphates) could be suitable starting materials.[1] In this connection we started a systematic investigation of this compound class, so recently, a number of metaphosphimates with a main focus on trimetaphosphimates were comprehensively investigated in our group.[2] In the last few years we intensified the research on tetrametaphosphimates as there is still a lack of knowledge in the structural chemistry of this class of compounds. However, due to the flexibility of the ring anion a large structural variety can be expected.

Since the discovery of the salts of the tetrametaphosphimic acid in 1896 by *Stokes*[3] for a long time the compounds have been characterized only by IR spectroscopy[4] and X-ray powder diffraction.[5] The first crystal structures of tetrametaphosphimates were reported by *Berking* and *Mootz*[6] concerning $K_4(PO_2NH)_4 \cdot 4H_2O$ and $Cs_4(PO_2NH)_4 \cdot 6H_2O$. Besides the crystal structures of $K_4(H_3O)\{Tm[(PO_2NH)_4]_2\} \cdot 17H_2O$[7] and $M^{II}_2(PO_2NH)_4 \cdot 8H_2O$ (M^{II} = Mg, Mn, Co, Zn, Ni)[8,9] mainly tetrametaphosphimates with monovalent cations ($Na_4(PO_2NH)_4 \cdot 2H_2O$, α/β-$Na_4(PO_2NH)_4 \cdot 3H_2O$,[10] $(NH_4)_4(PO_2NH)_4 \cdot 4H_2O$,[11] $(C(NH_2)_3)_4(PO_2NH)_4 \cdot 4H_2O$,[12] $Li_4(PO_2NH)_4 \cdot 4H_2O$[13]) have been described. These meta phosphimates exhibit three-dimensional network structures formed by extensive hydrogen bonding besides coordinative bonds from $[(PO_2NH)_4]^{4-}$ to the metal ions. Recently, we reported on $Na_2Cu(PO_2NH)_4 \cdot 7H_2O$ and $K_xNa_{2-x}Cu(PO_2NH)_4 \cdot 7H_2O$ which show a novel three-dimensional network with channels containing face-sharing chains of $[Na(H_2O)_6]^+$ polyhedrons.[14] In the course of the systematic investigation of the metaphosphimates and in order to find more compounds with interesting network structures we expanded the series of tetrametaphosphimates with monovalent cations to Tl^+. Except for an IR spectrum,[15] no detailed structural characterization of a thallium tetrametaphosphimate has been reported as yet. In this contribution we report on the synthesis, the commensurately modulated crystal structure and the properties of $Tl_4(PO_2NH)_4 \cdot H_2O$.

2.2   EXPERIMENTAL SECTION

2.2.1   Synthesis

$Tl_4(PO_2NH)_4 \cdot H_2O$ was obtained in aqueous solution according to Equation (1) using $K_4(PO_2NH)_4 \cdot 4H_2O$ (synthesized according to ref. [16]) and $TlOOCCH_3$ (Merck, $\geq 98 \%$).

$$K_4(PO_2NH)_4 \cdot 4H_2O + 4TlOOCCH_3 \rightarrow Tl_4(PO_2NH)_4 \cdot H_2O + 4KOOCCH_3 + 3H_2O \quad (1)$$

5 ml of a 0.01 M aqueous solution of $K_4(PO_2NH)_4 \cdot 4H_2O$ (27.0 mg, 50 μmol) and 5 ml of a 0.04 M aqueous solution of $TlOOCCH_3$ (52.7 mg, 200 μmol) were combined. After evaporation of the solvent at room temperature, 73.7 mg of a colorless powder remained. In order to remove $KOOCCH_3$ the powder was washed with methanol. Finally, 44.1 mg (38.4 μmol) phase-pure $Tl_4(PO_2NH)_4 \cdot H_2O$ were obtained as a crystalline, colorless, air-stable and water-soluble powder (yield 77 %). The composition of the product was confirmed by energy dispersive X-ray analysis (JSM 6500F scanning electron microscope, Jeol; detector model 7418, Oxford Instruments). All elements contained in the formula (except H) were detected and, within the accuracy of the method, the expected molar ratios were observed. The presence of potassium was excluded. The sample contained single crystals suitable for crystal structure investigation.

2.2.2   Thermal behavior

For TG (thermogravimetric) measurements a DTA-TG thermoanalytical balance TGA 92-2400 (Setaram) was used. A sample of $Tl_4(PO_2NH)_4 \cdot H_2O$ was heated under helium flow in an alumina crucible from room temperature up to 700 °C at a heating rate of 5 °Cmin^{-1}. The TG curve, together with its first derivative (dotted line), is represented in Figure 1.
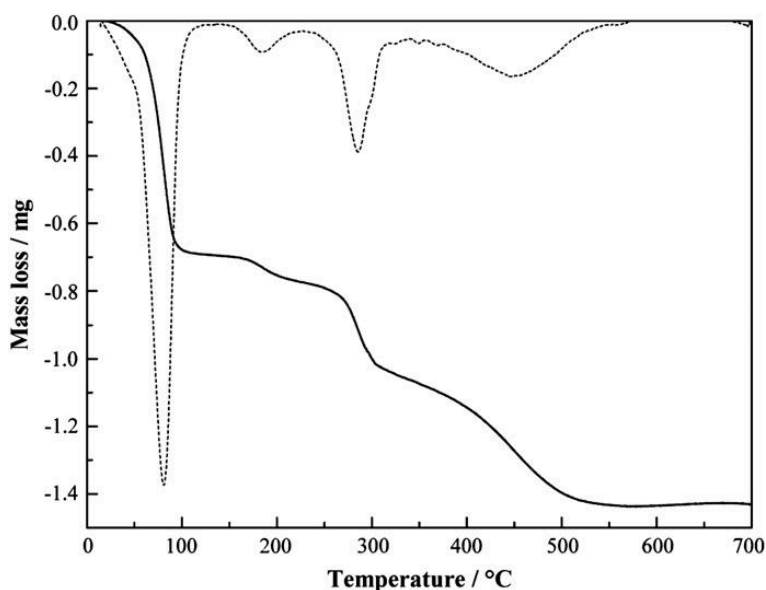
Figure 1. TG curve and its first derivative (dotted line) of $Tl_4(PO_2NH)_4 \cdot H_2O$, sample weight: 18.171 mg, heating rate: 5 °C min^{-1}.

Because all measured samples of $Tl_4(PO_2NH)_4 \cdot H_2O$ had some adherent water on their surface the first mass loss of 0.688 mg up to 100 °C is the drying step of the sample. Consequently this mass loss had been subtracted from the primary sample weight so that the reference for the decomposition is 17.483 mg.

The decomposition of $Tl_4(PO_2NH)_4 \cdot H_2O$ takes place in two steps between 100 and 550 °C with a maximum weight loss of 2.7 %. The first decomposition step between 100 and 300 °C includes a mass loss of 1.3 %, which nearly matches with the theoretical loss of the crystal water molecule (1.6 %). The second decomposition step up to 550 °C with 1.3 % could be assigned to the loss of one molecule of ammonia per formula (theoretical value: 1.5 %) so the total weight loss of 2.7 % approaches the theoretical value of 3.1 %. The decomposition product was a brown, hard, vitreous material.

2.2.3 Infrared spectroscopy

An FT-IR spectrum of $Tl_4(PO_2NH)_4 \cdot H_2O$ (Figure 2) was recorded in transmission geometry at room temperature in the range 4000–400 cm^{-1} with a Bruker IFS 66v/S spectrometer using the KBr pellet technique (2 mg sample, 300 mg dried KBr). Assignments of the observed bands (Table 1) were carried out by comparison with other tetrametaphosphimates. The characteristic bands for the NH-group (νNH, δNH) at 3041, 2686 and 1356 cm^{-1} show that the tetrametaphosphimate ion is existent in the imido form. The bands in the fingerprint region indicate lattice vibrations (νPO$_2$, δPO$_2$, νPN) of the ring anion whereby evidence for a saddle conformation is suggested.[17,18]
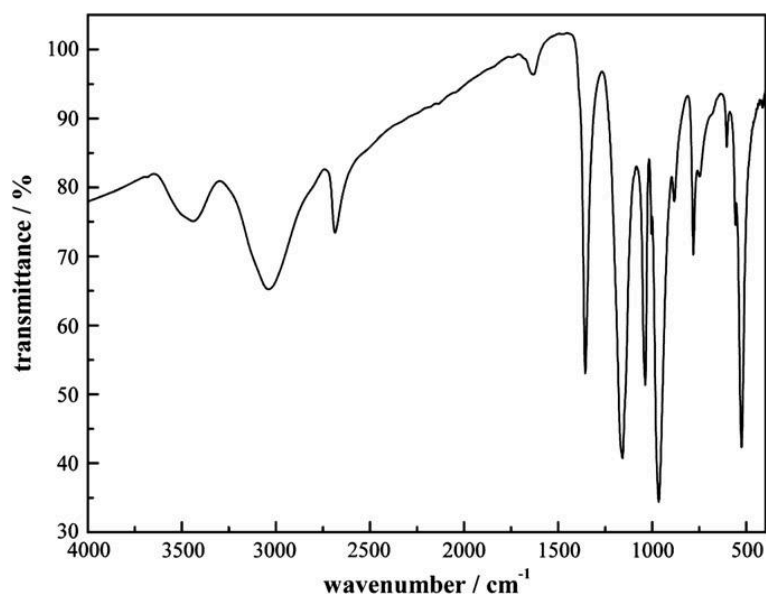
Figure 2. FT-IR spectrum of $Tl_4(PO_2NH)_4 \cdot H_2O$, KBr pellet.

Table 1. Vibrational frequencies/cm^{-1} of $Tl_4(PO_2NH)_4 \cdot H_2O$ as observed by FT-IR spectroscopy at room temperature and their assignments (ν = stretching, δ = in-plane deformation, γ = out-of-plane deformation, s = strong, m = medium, b = broad).

observed frequencies	assignment	observed frequencies	assignment
3441 m, b	$\nu \, H_2O$	966 s	$\nu_{as} \, PN$
3041 m, b	$\nu \, NH$	884 m	$\nu_s \, PN$
2686 m	$2\delta \, NH$	782 m	$\nu_s \, PN$
1630 w, b	$\delta \, H_2O$	749 m	$\gamma \, NH$
1356 s	$\delta \, NH$	603 w	$\delta \, PO_2$
1158 s	$\nu_{as} \, PO_2$	559 m	$\delta \, PO_2$
1038 s	$\nu_s \, PO_2$	525 s	$\delta \, PO_2$
1005 m	$\nu_s \, PO_2$		

2.2.4 X-ray diffraction

X-ray diffraction data of $Tl_4(PO_2NH)_4 \cdot H_2O$ were collected from a suitable single crystal enclosed in a glass capillary. The main reflections were indexed on the basis of a triclinic unit cell (a = 927.8(2), b = 974.2(2), c = 1017.5(2) pm, α = 74.46(3), β = 64.67(3), γ = 78.81(3)°). Considering only the main reflections, the basic structure model was determined using the SHELX programs.[19] During the refinement one of the five Tl sites turned out to be half occupied. After anisotropic refinement of all non-hydrogen atoms, the hydrogen atoms could be located by difference Fourier syntheses and refined with a riding model. The basic structure model yields R-factors of $R1$ = 0.0639 and $wR2$ = 0.0828 for all main reflections.
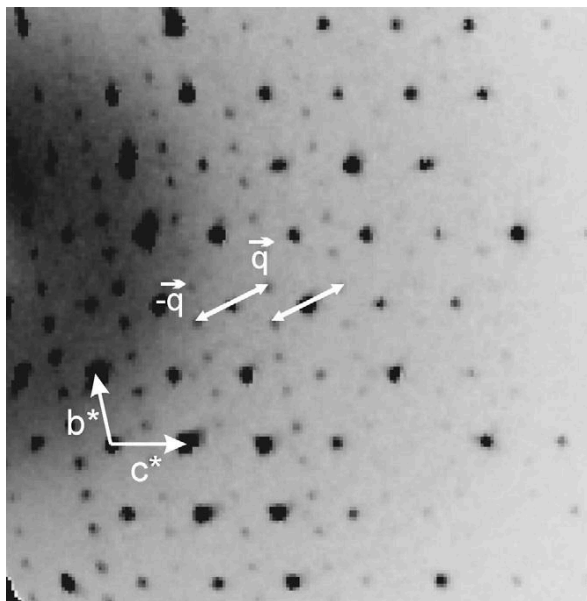
Figure 3. Representation of the reciprocal lattice layer (1kl) of $Tl_4(PO_2NH)_4 \cdot H_2O$ reconstructed from area detector data; the q vector and the axes b* and c* are indicated.

Besides the normal Bragg reflections, (first order) satellite reflections were found which could be indexed considering a commensurate modulation vector q = 0.25b* + 0.5c* (Figure 3). As Figure 3 indicates no second-order satellite reflections had been observed, which was expected as the first order satellites are of low intensity. The modulated structure was solved by charge-flipping[20] using Superflip[21,22] and EDMA.[23] The refinement in the superspace group $P\overline{1}(\alpha\beta\gamma)$ with anisotropic displacement parameters was performed using the JANA2000 package.[24] For the occupation-modulated Tl site both a crenel[25] and single harmonic wave (Figure 4a) function could be introduced. As for the harmonic wave the refinement leads to a better partial R-value for the satellite reflections (8.49 %, with crenel function: 13.62 %) the harmonic wave was used in the final refinement. With positional sinoidal modulation waves for the other atoms their relaxation with respect to the occupancy modulation has been considered. Without hydrogen atoms, the final refinement led to $R_{obs} = 0.035$ and $wR_{all} = 0.036$ for the main and the satellite reflections. A refinement in an $a \times 4b \times 2c$ supercell ($a = 928.0(2)$, $b = 3897.1(8)$, $c = 2035.4(4)$, $\alpha = 74.47(3)$, $\beta = 64.68(3)$, $\gamma = 78.81(3)°$) in the space group $A\overline{1}$ agrees with the structure model in (3 + 1)-dimensional superspace. However, the description in (3 + 1)-dimensional superspace (321 parameters) is preferable as more than twice the number of parameters are needed in the supercell refinement (782 parameters). Crystallographic data and details of the data collection and refinement in (3 + 1)-dimensional superspace are listed in Table 2. The atomic coordinates and displacement parameters are given in Tables 3 and 4.

In order to check the purity of $Tl_4(PO_2NH)_4 \cdot H_2O$ an X-ray powder diffraction pattern was recorded on a Stoe STADI P diffractometer using Cu-$K_{\alpha 1}$ radiation. The observed intensities of the reflections agree well with the reflections calculated from single-crystal

data. Moreover, all measured reflections have been indexed on the basis of the unit cell determined from single-crystal data.[†]
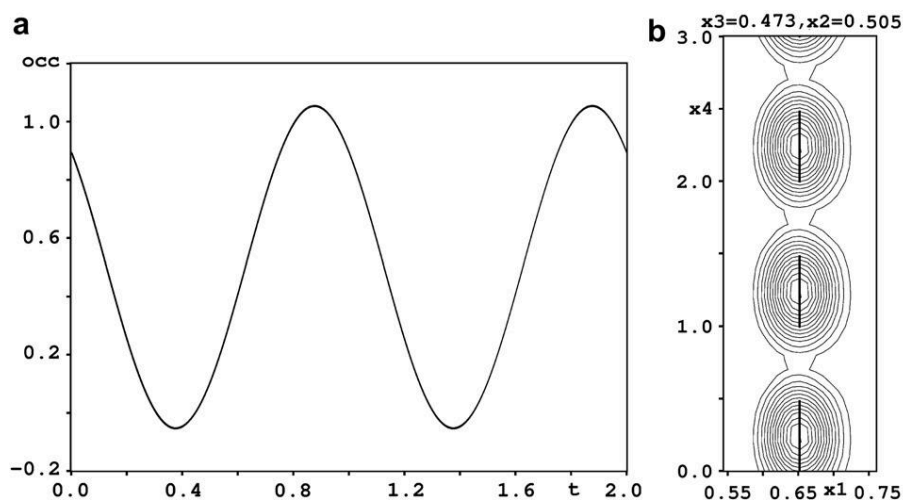
Figure 4. Tl(5) modulation function a) and F_o map b) showing the occupancy modulation of Tl(5) in Tl$_4$(PO$_2$NH)$_4$ · H$_2$O.

Table 2. Crystallographic data of Tl$_4$(PO$_2$NH)$_4$ · H$_2$O (esd's in parentheses).

Crystal Data		
formula	Tl$_4$(PO$_2$NH)$_4$ · H$_2$O	
formula mass / gmol^{-1}	1147.5	
temperature / K	293(2)	
crystal system	triclinic	
super space group	$P\bar{1}(\alpha\beta\gamma)$	
modulation vector	q = 0.25b* + 0.5c*	
cell parameters / pm, °	a = 928.3(2)	α = 74.44(3)
	b = 974.6(2)	β = 64.68(3)
	c = 1018.0(2)	γ = 78.78(3)
cell volume / 10^6 pm^3	798.57(3)	
formula units / cell	2	
crystal shape, color	block, colorless	
crystal size / mm^3	0.34 × 0.09 × 0.03	
x-ray density / g cm^{-3}	4.771	
abs. coefficient μ / mm^{-1}	40.677	
F(000)	968	

Data collection	
diffractometer	Stoe IPDS
radiation, monochromator	Mo-K_α (λ = 71.073 pm), graphite
θ range / °	2.8–30.4

[†] Further details of the crystal structure investigation may be obtained from the Fachinformationszentrum Karlsruhe, D-76344 Eggenstein-Leopoldshafen, Germany (e-mail: crysdata@fiz-karlsruhe.de) on quoting the depository number CSD-418498, the names of the authors and citation of the publication.

h, k, l	$-13 \leq h \leq 13, -12 \leq k \leq 12, -14 \leq l \leq 14$
m	$-1 \leq m \leq 1$
measured reflections	28030
absorption correction	numerical ($T_{min} = 0.215$, $T_{max} = 0.300$)

Solution and Refinement

structure solution	charge-flipping[20] using Superflip[21,22] and EDMA[23]
structure refinement	least square refinement on F using JANA2000[24]
independent reflections	13030
observed reflections	3286
refined parameters	321
GoF	1.13
R indices (main)	$R_{obs} = 0.032$, $wR_{all} = 0.0304$
R indices (satellite)	$R_{obs} = 0.085$, $wR_{all} = 0.269$
R indices (total)	$R_{obs} = 0.035$, $wR_{all} = 0.036$
weighting scheme	$w^{-1} = \sigma^2 F^2 + 0.000025 F^2$
max. / min. residual electron density / eÅ^{-3}	5.38 / −4.04

Table 3. Atomic coordinates and isotropic displacement parameters / 10^{-4} pm^2 for Tl$_4$(PO$_2$NH)$_4$ · H$_2$O; U_{eq} is defined as one third of the trace of the orthogonalized tensor U_{ij}; c.n. = coordination number (esd's in parentheses).

atom[c.n.]	Wyckoff Symbol	x	y	z	U_{eq}/U_{iso}	occupancy
Tl(1)[5+6]	2i	0.08232(3)	0.85034(4)	0.35907(3)	0.0344(2)	1
Tl(2)[5+4]	2i	0.54544(3)	0.56810(4)	0.13691(3)	0.0347(2)	1
Tl(3)[6+3]	2i	0.37228(3)	0.16008(4)	0.37794(3)	0.0384(2)	1
Tl(4)[8+2]	1a	½	0	0	0.0454(2)	1
Tl(5)[4+3]	2i	0.65246(7)	0.50452(8)	0.47332(6)	0.0399(3)	½
P(1)[4]	2i	0.8920(2)	0.7143(2)	0.1318(2)	0.0170(6)	1
P(2)[4]	2i	0.1389(2)	0.2430(2)	0.1593(2)	0.0159(6)	1
P(3)[4]	2i	0.7998(2)	0.1761(2)	0.3262(2)	0.0179(6)	1
P(4)[4]	2i	0.7650(2)	0.2167(2)	0.0348(2)	0.0184(6)	1
N(1)	2i	0.1631(5)	0.1911(6)	0.0055(5)	0.017(2)	1
N(2)	2i	0.9455(5)	0.2855(6)	0.2535(5)	0.016(2)	1
N(3)	2i	0.7915(6)	0.1203(6)	0.1889(5)	0.020(2)	1
N(4)	2i	0.9117(5)	0.3258(6)	0.9415(5)	0.018(2)	1
O(1)	2i	0.8431(5)	0.8106(5)	0.2382(4)	0.024(2)	1
O(2)	2i	0.8221(5)	0.5742(5)	0.1899(4)	0.026(2)	1
O(3)	2i	0.2001(5)	0.1144(5)	0.2458(4)	0.022(2)	1
O(4)	2i	0.2153(5)	0.3794(5)	0.1180(4)	0.021(2)	1
O(5)	2i	0.8409(5)	0.0431(5)	0.4232(4)	0.024(2)	1
O(6)	2i	0.6506(5)	0.2648(6)	0.3992(5)	0.030(2)	1
O(7)	2i	0.2206(5)	0.8917(5)	0.0507(4)	0.027(2)	1
O(8)	2i	0.6116(5)	0.3138(5)	0.0750(5)	0.025(2)	1
O(9)	2i	0.5105(6)	0.8775(8)	0.3086(6)	0.055(3)	1

Table 4. Anisotropic displacement parameters / 10^{-4} pm^2 for $Tl_4(PO_2NH)_4 \cdot H_2O$ (esd's in parentheses); c.n. = coordination number.

atom[c.n.]	U_{11}	U_{22}	U_{33}	U_{23}	U_{13}	U_{12}
Tl(1)[5+6]	0.0390(2)	0.0295(2)	0.0307(2)	0.0006(2)	–0.015(1)	–0.001(1)
Tl(2)[5+4]	0.0266(2)	0.0447(2)	0.0280(2)	–0.0072(2)	–0.003(1)	–0.011(1)
Tl(3)[6+3]	0.0339(2)	0.0482(2)	0.0390(2)	–0.0074(2)	–0.020(1)	–0.007(1)
Tl(4)[8+2]	0.0279(2)	0.0532(4)	0.0615(3)	–0.0013(2)	–0.019(1)	–0.022(1)
Tl(5)[4+3]	0.0494(3)	0.0445(4)	0.0237(2)	–0.0130(3)	–0.008(1)	–0.009(1)
P(1)[4]	0.0164(7)	0.016(1)	0.0164(6)	–0.0005(6)	–0.006(1)	–0.001(1)
P(2)[4]	0.0143(7)	0.017(1)	0.0176(6)	–0.0017(6)	–0.008(1)	–0.003(1)
P(3)[4]	0.0165(8)	0.020(1)	0.0155(7)	–0.0061(6)	–0.005(1)	–0.001(1)
P(4)[4]	0.0173(8)	0.021(1)	0.0186(7)	–0.0058(7)	–0.008(1)	–0.001(1)
N(1)	0.015(3)	0.019(3)	0.016(2)	–0.001(2)	–0.007(2)	–0.001(2)
N(2)	0.013(3)	0.019(4)	0.015(2)	0.000(3)	–0.006(2)	–0.001(2)
N(3)	0.024(3)	0.025(4)	0.014(3)	–0.009(2)	–0.007(2)	–0.003(2)
N(4)	0.012(3)	0.023(3)	0.015(2)	–0.003(2)	–0.006(2)	0.006(2)
O(1)	0.029(3)	0.024(3)	0.018(2)	0.006(2)	–0.011(2)	–0.006(2)
O(2)	0.026(2)	0.022(3)	0.023(2)	–0.007(2)	–0.005(2)	0.003(2)
O(3)	0.028(2)	0.021(3)	0.022(2)	–0.002(2)	–0.014(2)	–0.004(2)
O(4)	0.019(2)	0.025(3)	0.020(2)	–0.006(2)	–0.007(2)	–0.002(2)
O(5)	0.030(2)	0.026(3)	0.017(2)	–0.007(2)	–0.011(2)	0.002(2)
O(6)	0.013(2)	0.038(4)	0.034(3)	–0.003(2)	0.000(2)	–0.016(2)
O(7)	0.032(3)	0.031(3)	0.021(2)	–0.008(2)	–0.015(2)	–0.001(2)
O(8)	0.018(3)	0.024(3)	0.035(2)	0.001(2)	–0.014(2)	–0.003(2)
O(9)	0.035(3)	0.070(5)	0.036(3)	–0.002(3)	–0.001(2)	0.001(3)

2.2.5 ^{31}P MAS NMR spectroscopy

To verify the number of crystallographically independent P sites ^{31}P MAS NMR (solid state nuclear magnetic resonance with the magic angle spinning method) spectroscopic experiments were conducted on a conventional impulse spectrometer (Bruker DSX Avance 500 FT). A commercial double resonance probe (Bruker) and a ZrO_2 rotor (2.5 mm) were used with an external magnetic field of 11.7 T. The impulse length was 2.6 ms with 6 dB and a rotation frequency of 25 kHz (repetition time was 1 s). As reference 85 % H_3PO_4 was used.

The recorded ^{31}P MAS NMR spectrum of $Tl_4(PO_2NH)_4 \cdot H_2O$ (Figure 5) shows a very broad signal with two main maxima between 0 and –10 ppm. It consists of numerous single resonances which are in accordance with the modulation or the superstructure, respectively. Due to the coupling between the P and Tl nuclei the exact number of ^{31}P resonances could not be unambiguously resolved. However, apparently there are more than four resonances expected for the basic structure of $Tl_4(PO_2NH)_4 \cdot H_2O$. Therefore, the ^{31}P NMR measurements agree with the results of the crystal structure refinement.
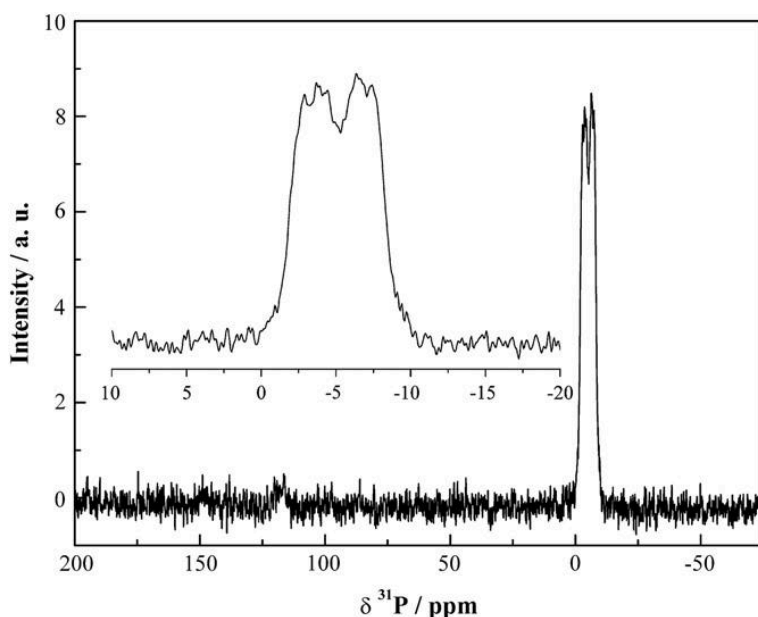
Figure 5. ^{31}P MAS NMR spectrum of $Tl_4(PO_2NH)_4 \cdot H_2O$.

2.3   STRUCTURAL STUDY AND DISCUSSION

2.3.1   Basic structure

The crystal structure of $Tl_4(PO_2NH)_4 \cdot H_2O$ consists of Tl^+ and $[(PO_2NH)_4]^{4-}$ ions as well as crystal water molecules. Whereas the cyclic anion $[(PO_2NH)_4]^{4-}$ in the imido form exhibits a chair conformation in most tetrametaphosphimates,[8,9,11–14] here, as in β-$Na_4(PO_2NH)_4 \cdot 3H_2O$,[10] the P_4N_4 ring shows a nearly ideal saddle conformation (symmetry $\overline{4}2m$). The bond lengths P–N and P–O as well as the angles in the ring, which are summarized in Table 5, are in typical ranges for metaphosphimates.[17,18]

As in the sodium tetrametaphosphimates (e.g. α- and β-$Na_4(PO_2NH)_4 \cdot 3H_2O$, $Na_4(PO_2NH)_4 \cdot 2H_2O$[10]) the $[(PO_2NH)_4]^{4-}$ ions are interconnected by eight N–H···O hydrogen bonds each forming infinite columns along [010]. The mode of the connection of $[(PO_2NH)_4]^{4-}$ pairs displaced against each other is displayed in Figure 6. Including hydrogen bonding with one crystal water molecule, the anionic columns are mainly interconnected by numerous coordinative bonds from O and N to the Tl^+ ions (Figure 7) so that a three-dimensional network with channels along [100] develops. The coordination numbers of the Tl^+ ions range between 7 and 11 with a very broad scattering of the distances Tl–(O,N) (Table 5) around the sum of the ionic radii (Tl–O: 300 pm, Tl–N: 311 pm).[26] The distances vary from very short ones (259.4 pm), which are well-known from other Tl(I) compounds (Tl_3PO_4,[27] TlOOCH,[28] Tl_2WO_4[29]), up to more than 400 pm. Larger voids in the coordination sphere of the Tl^+ ions that can be seen in Figure 8 can be

attributed to stereochemically active lone pairs. The coordination sphere of the half occupied Tl(5) site is presented in Figure 9. The Tl(5)–Tl(5) distance of 265.8(2) pm is much shorter than twice the ionic radius of Tl^+ (328 pm), which is consistent with the half occupancy of this Tl site and may explain the modulation of the structure. Consequently, one single Tl site causes the modulation of the structure of $Tl_4(PO_2NH)_4 \cdot H_2O$.
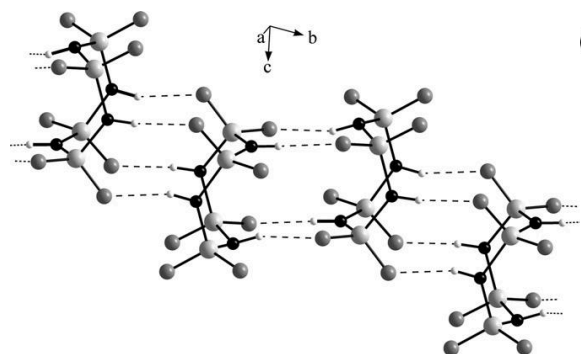
Figure 6. Connection of the $[(PO_2NH)_4]^{4-}$ ions in $Tl_4(PO_2NH)_4 \cdot H_2O$ (P: light gray; O: gray; N: black; H: white).
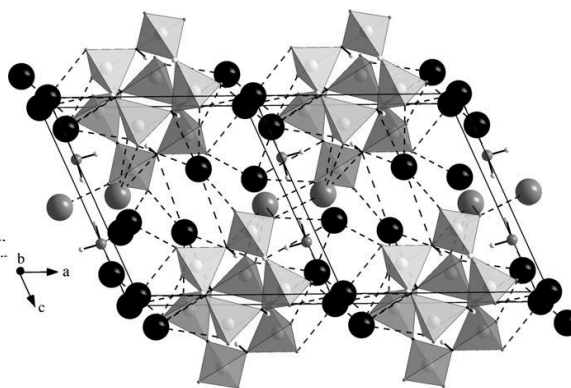
Figure 7. Representation of the basic structure of $Tl_4(PO_2NH)_4 \cdot H_2O$; view along the $[(PO_2NH)_4]^{4-}$ columns with Tl(5) in channels along [100] (Tl^+(1)–(4): black, large; Tl^+(5): dark gray, large; O: gray, small; H: white, small; PO_2N_2 tetrahedra are shown as closed polyhedrons).

2.3.2 Modulated structure

Considering the satellite reflections which can be described by the modulation vector q = 0.25b* + 0.5c* (Figure 3) both a crenel and a single harmonic wave (Figure 4a) function could be introduced for the half occupied Tl(5) site in the basic structure. With both functions the arrangement of the Tl^+ ions in the channels along [100] can be obtained. To illustrate this arrangement in the modulated structure of $Tl_4(PO_2NH)_4 \cdot H_2O$ a picture of the supercell is compared with eight unit cells of the basic structure in Figure 10. Half occupied Tl split positions in the basic structure (left) become fully occupied Tl sites (right). The structure remains centrosymmetric. As the refinement with the single harmonic wave function leads to a better fit to the data (see section 2.2.4) than the refinement with the crenel function this might indicate in addition to the occupancy modulation a small occupational disorder at the Tl(5) site. A contour plot of Tl(5) in Figure 4b shows its occupancy modulation in $Tl_4(PO_2NH)_4 \cdot H_2O$ together with its modulation function along the modulation period t. Positional sinoidal modulation waves were introduced for the other atoms considering their relaxations corresponding to the occupancy modulation of the Tl(5) position. Very small amplitudes for the waves indicate only a smooth adaptation

of neighboring atoms. Thus, except for Tl(5), the modulated structure of $Tl_4(PO_2NH)_4 \cdot H_2O$ is very similar to the basic structure.

Table 5. Selected interatomic distances / pm and angles / ° in $Tl_4(PO_2NH)_4 \cdot H_2O$ (values without consideration of modulation functions,[a] esd's in parentheses).

Tl(1)–O	259.7(4)–401.5(5)	8 times
Tl(1)–N	372.0(5)–400.0(5)	3 times
Tl(2)–O	259.4(3)–396.2(5)	7 times
Tl(2)–N	349.6(5)–383.4(5)	
Tl(3)–O	264.7(6)–370.0(7)	8 times
Tl(3)–N	352.2(5)	
Tl(4)–O	278.1(5)–376.5(6)	4 times (×2)
Tl(4)–N	330.0(5)	(×2)
Tl(5)–O	259.7(4)–399.6(7)	6 times
Tl(5)–N	347.3(5)	
P–O	148.9(4)–150.8(4)	8 times
P–N	165.7(5)–169.0(5)	8 times
P–N–P	126.3(4), 127.3(3), 129.4(4), 129.5(4)	
N–P–N	107.5(3), 107.8(3), 108.6(3), 109.4(3)	
O–P–O	116.5(4), 116.7(3), 117.0(3), 117.6(3)	
O–P–N	104.2(3)–112.6(3)	16 times

[a] values with consideration of modulation functions are less precise.
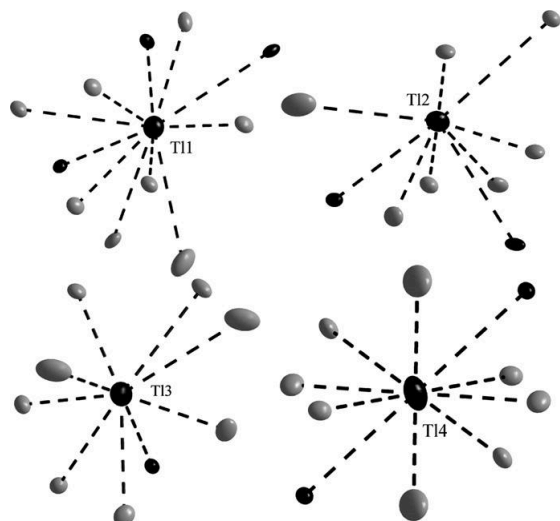
Figure 8. Representation of the environment of Tl(1)–Tl(4) in $Tl_4(PO_2NH)_4 \cdot H_2O$ (Tl^+: black, large; O: gray; N: black, small), the displacement ellipsoids represent 50 % probability.
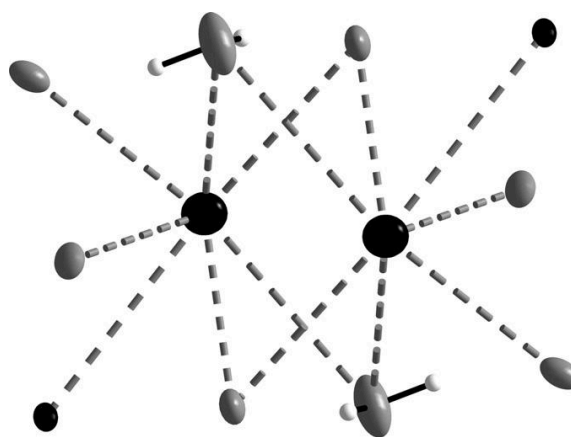
Figure 9. Representation of the Tl(5) environment in the basic structure of $Tl_4(PO_2NH)_4 \cdot H_2O$ (Tl^+: black, large; O: gray; H: white, small; N: black, small), the displacement ellipsoids represent 50 % probability.

Structures whose diffraction patterns show satellite reflection that can be indexed commensurately can be described as approximations in expanded unit cells. However, because of the reduced number of parameters in a superspace model with a small basic unit cell is the more elegant way to describe those structures. As a description in $3 + x$ dimensions can be confusing for non-specialists, the structure model for $Tl_4(PO_2NH)_4 \cdot H_2O$ is illustrated in Figure 11. Supercells, containing only $[(PO_2NH)_4]^{4-}$ anions and the Tl ions that are mainly affected by the modulation, are pictured. To understand the commensurate modulation, the Tl ions' arrangement in direction of the q vector in real space has to be considered. Along q, which is perpendicular to (012), bands of Tl ions above (bold atoms) as well as behind (thin atoms) the drawing plane are alternately existent. In the view parallel (012) (Figure 11b) the commensurate modulation of the concerning Tl ions is illustrated together with the single harmonic wave functions that describe their arrangement. A second harmonic wave function results from the inversion center. Consequently a clear structure model for the commensurately modulated $Tl_4(PO_2NH)_4 \cdot H_2O$ has been presented.
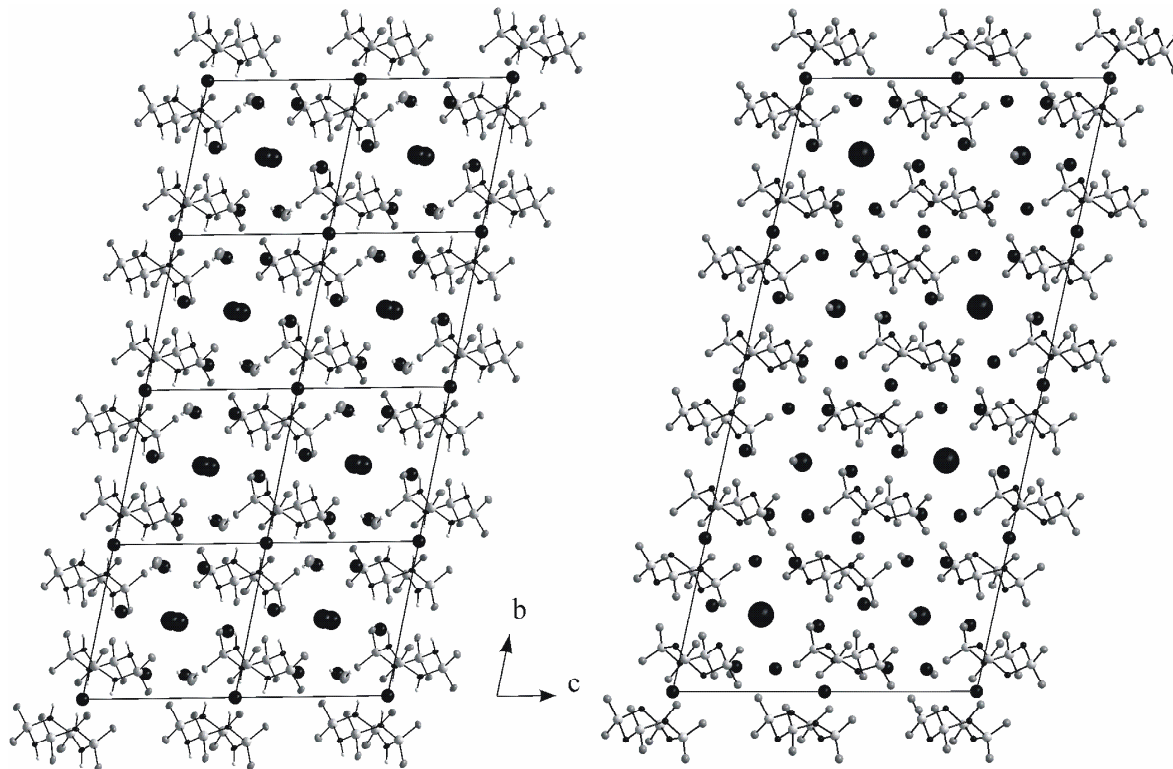
Figure 10. Comparison of eight unit cells of the basic structure (left) and the superstructure (right) of $Tl_4(PO_2NH)_4 \cdot H_2O$; the channels along [100] contain a Tl split position in the basic structure as fully occupied Tl sites exist in the superstructure (bold drawn Tl atoms are in the front).
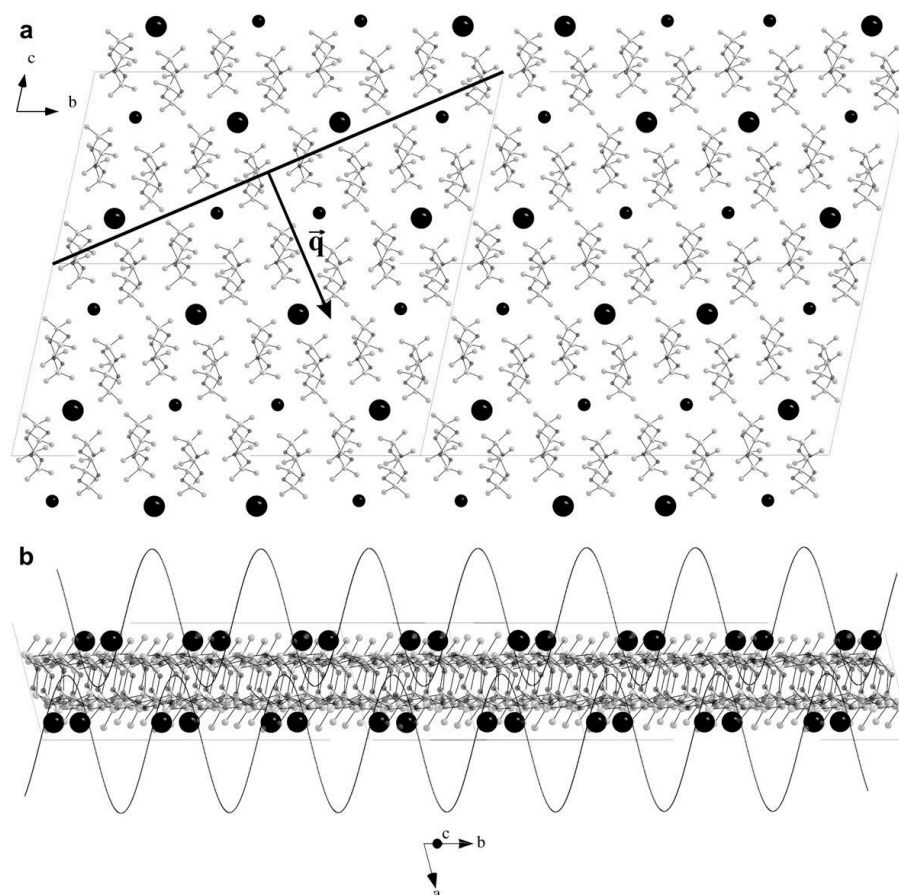
Figure 11. Representation of supercells containing only [(PO$_2$NH)$_4$]$^{4-}$ anions (shadowed) and the Tl ions that are mainly affected by the modulation; a) representation in [100] direction with the q vector perpendicular to (012), bold atoms are above, thin atoms behind the drawing plane; b) representation parallel (012) with single harmonic wave functions.

2.4 CONCLUSION

The new compound Tl$_4$(PO$_2$NH)$_4$ · H$_2$O has been phase purely synthesized from aqueous solution. Due to an occupancy modulation the structure elucidation from single-crystal data turned out to be challenging what probably prevented a comprehensive characterization of this thallium tetrametaphosphimate so far. By handling the commensurate occupancy modulation with the description in (3 + 1)-dimensional superspace we were able to elaborate a satisfying structure model for Tl$_4$(PO$_2$NH)$_4$ · H$_2$O and refine its superstructure with a minimum of structural parameters while a fourfold superstructure in an $a \times 4b \times 2c$, A-centered supercell could be avoided. Composed of infinite columns of the cyclic [(PO$_2$NH)$_4$]$^{4-}$ anions in the saddle conformation with coordinative bonds Tl–O and Tl–N and extensive hydrogen bonding a three-dimensional network structure with channels along [100] is formed. The occupancy modulation, which affects mainly one Tl site of the

basic structure was described with a single harmonic wave function. ^{31}P MAS NMR data are in accordance with the results from the X-ray structure determination.

2.5   REFERENCES

[1]   R. Marchand, W. Schnick, N. Stock, *Adv. Inorg. Chem.* **2000**, *50*, 193.

[2]   S. Correll, N. Stock, W. Schnick, *Phosphorus, Sulfur Silicon Relat. Elem.* **2001**, *168*, 321.

[3]   H. N. Stokes, *Am. Chem. J.* **1896**, *18*, 780.

[4]   D. E. C. Corbridge, E. J. Lowe, *J. Chem. Soc.* **1954**, 4555.

[5]   A. H. Herzog, M. L. Nielsen, *Anal. Chem.* **1958**, *30*, 1490.

[6]   B. Berking, D. Mootz, *Acta Crystallogr., Sect. B: Struct. Sci.* **1971**, *27*, 740.

[7]   V. I. Sokol, D. A. Murashov, I. A. Rozanov, M. A. Porai-Koshits, V. P. Nikolaev, L. A. Butman, *Zh. Neorg. Khim.* **1979**, *24*, 3385.

[8]   S. R. Römer, W. Schnick, *Z. Anorg. Allg. Chem.* **2005**, *631*, 31.

[9]   S. R. Römer, W. Schnick, *Z. Anorg. Allg. Chem.* **2005**, *631*, 1749.

[10]   N. Stock, H. Schmalz, W. Schnick, *Z. Anorg. Allg. Chem.* **1998**, *624*, 1777.

[11]   N. Stock, W. Schnick, *Acta Crystallogr., Sect. C: Cryst. Struct. Commun.* **1998**, *54*, 171.

[12]   N. Stock, B. Jürgens, W. Schnick, *Z. Naturforsch., B: J. Chem. Sci.* **1998**, *53*, 1115.

[13]   S. R. Römer, W. Schnick, *Z. Anorg. Allg. Chem.* **2006**, *632*, 59.

[14]   S. R. Römer, W. Schnick, *Solid State Sci.* **2007**, *9*, 644.

[15]   J. V. Pustinger, W. T. Cave, M. L. Nielsen, *Spectrochim. Acta* **1959**, *15*, 909.

[16]   M. L. Nielsen, T. J. Morrow, *Inorg. Synth.* **1960**, *6*, 99.

[17]   N. Stock, Doctoral Thesis, Univ. Bayreuth, **1998**.

[18]   S. Correll, Doctoral Thesis, Univ. Munich (LMU), **2006**.

[19]   G. M. Sheldrick, SHELX97, Univ. Göttingen, **1997**.

[20]   G. Oszlányi, A. Sütő, *Acta Crystallogr., Sect. A: Found. Crystallogr.* **2004**, *60*, 134.

[21]   L. Palatinus, *Acta Crystallogr., Sect. A: Found. Crystallogr.* **2004**, *60*, 604.

[22]   L. Palatinus, G. Chapuis, *J. Appl. Crystallogr.* **2007**, *40*, 786.

[23]   S. van Smaalen, L. Palatinus, M. Schneider, *Acta Crystallogr., Sect. A: Found. Crystallogr.* **2003**, *59*, 459.

[24]   V. Petricek, M. Dusek, L. Palatinus, *Jana2000*, Institute of Physics, Praha, Czech Republic, **2005**.

[25]   V. Petricek, A. van der Lee, M. Evain, *Acta Crystallogr., Sect. A: Found. Crystallogr.* **1995**, *51*, 529.

[26]   R. D. Shannon, C. T. Prewitt, *Acta Crystallogr., Sect. B: Struct. Sci.* **1969**, *25*, 925.

[27]   A. Zalkin, D.H. Templeton, *Acta Crystallogr., Sect. C: Cryst. Struct. Commun.* **1986**, *42*, 1686.

[28]   Y. Oddon, A. Tranquard, B. F. Mentzen, *Inorg. Chim. Acta* **1981**, *48*, 129.

[29]   K. Okada, J. Ossaka, S. Iwaii, *Acta Crystallogr., Sect. B: Struct. Sci.* **1979**, *35*, 2189.

3.   Synthesis and Characterization of $Ca_2(PO_2NH)_4 \cdot 8H_2O$

Stefan J. Sedlmaier, S. Rebecca Römer, Wolfgang Schnick

ABSTRACT

$Ca_2(PO_2NH)_4 \cdot 8H_2O$ was obtained as single-phase crystalline powder starting from aqueous solution of $K_4(PO_2NH)_4 \cdot 4H_2O$ and $Ca(NO_3)_2 \cdot 4H_2O$. A small fiber-like specimen has been used for single-crystal X-ray structure determination. In the structure of $Ca_2(PO_2NH)_4 \cdot 8H_2O$ (*Pbcn* (no. 60), $a = 1700.6(3)$, $b = 1069.3(2)$, $c = 963.2(2)$ pm, $Z = 4$) there are $(PO_2NH)_4^{4-}$ ions in saddle conformation which are interconnected by N-H⋯O hydrogen bonds forming infinite columns running along [001]. These columns are hold together by a complex hydrogen bonding network with crystal water molecules involved. The FT-IR spectrum of the title compound has been measured and the relevant bands were assigned. ^{31}P solid-state NMR investigations yielded three resolved resonances with chemical shift values of –3.1, –4.9 and –7.9 ppm. DTA / TG data are also discussed.

3.1 INTRODUCTION

Cyclic phosphazenes (PNCl$_2$)$_3$ and (PNCl$_2$)$_4$ can be synthesized by the reaction of PCl$_5$ and NH$_4$Cl at around 120 °C besides few short chain phosphazenes and little polymeric (PNCl$_2$)$_n$, known as inorganic caoutchouc.[1,2] By hydrolysis, the respective imidocyclophosphorus acids [PN(OH)$_2$]$_3$ and [PN(OH)$_2$]$_4$ (trimetaphosphimic and tetrametaphosphimic acid) result, whose salts were systematically investigated in our group.[3,4] Our interest in this compound class originates from their potential suitability as precursors for synthesis of oxonitridophosphates, the latter exhibiting a silicate analogous compound class. PO$_2$N$_2$-tetrahedra in [(PO$_2$NH)$_3$]$^{3-}$ and [(PO$_2$NH)$_4$]$^{4-}$ ions could possibly be thermally condensed to form three-dimensional frameworks while stabilizing cations are present during this process. Rings made up of tetrahedra are typical *secondary building units* (SBUs) of zeolite-like frameworks. And such rings are already preorganized in phosphimate anions. Accordingly, this compound class could be predestinated as precursors for synthesis of zeolite-like networks.[3,5] Possibly, tetrametaphosphimates are much more appropriate in this context than trimetaphosphimates because 4-rings are much more frequently found in zeolites than 3-rings.[6]

Tetrametaphosphimic acid has already been discovered as early as 1896.[7] However, there is still a considerable lack of knowledge concerning the salts of this 4-ring anion. In the literature, tetrametaphosphimates have been described with monovalent cations (Li$^+$,[8] Na$^+$,[9] K$^+$, Cs$^+$,[10] NH$_4^+$,[11] Tl$^+$,[12] C(NH$_2$)$_3^+$[13]). Tetrametaphosphimates with higher charged ions have only been described in case of K$_4$(H$_3$O){Tm[(PO$_2$NH)$_4$]$_2$} · 17 H$_2$O,[14] Na$_2$Cu(PO$_2$NH)$_4$ · 7H$_2$O and K$_x$Na$_{2-x}$Cu(PO$_2$NH)$_4$ · 7H$_2$O[15] and the series of M$^{II}_2$(PO$_2$NH)$_4$ · 8 H$_2$O (M^{II} = Mg, Mn, Co, Zn, Ni).[16,17] But keeping the higher conformeric flexibility for the eight-membered ring anion in mind (e.g. saddle-, tub-, twistboat-, chair-1-, chair-2-, twistchair-, crown-conformation),[4a] the structural diversity in this compound class could be significantly larger. Several tetrametaphosphimates beyond the ones mentioned above have been identified already quite early by IR spectroscopy.[18] But there, no information about the synthesis and least of all, even after analysis by X-ray powder diffraction,[19] no structural information emerged.

The alkali earth tetrametaphosphimates M$_2$(PO$_2$NH)$_4$ · 8H$_2$O (M = Ca, Sr) have already been synthesized by *Sakurai* and *Watanabe*,[20,21] but they only analyzed the thermal behavior. In this contribution, we report on the synthesis and the full characterization of Ca$_2$(PO$_2$NH)$_4$ · 8H$_2$O, which may also serve as a potential biomaterial.[22]

3.2   RESULTS AND DISCUSSION

3.2.1   Crystal structure

The crystal structure of $Ca_2(PO_2NH)_4 \cdot 8H_2O$ consists of Ca^{2+} and $[(PO_2NH)_4]^{4-}$ ions as well as crystal water molecules. Existent in the imido form, the cyclic anion $[(PO_2NH)_4]^{4-}$ exhibits a saddle conformation. As in β-$Na_4(PO_2NH)_4 \cdot 3H_2O$[9] and $Tl_4(PO_2NH)_4 \cdot H_2O$[12] the angles of torsion (-60.84, -61.14, 59.69, 59.69, -60.84, -61.14, 59.88, 59.88°; ideal sign sequence: -x/-x/x/x/-x/-x/x/x),[23] the displacement-asymmetry-parameters (Figure 1),[24] the puckering parameters ($q_2 = 1.481(1)$, $q_3 = 0.000(1)$, $q_4 = 0.000(1)$; ideal values: $q_2 \neq 0$,
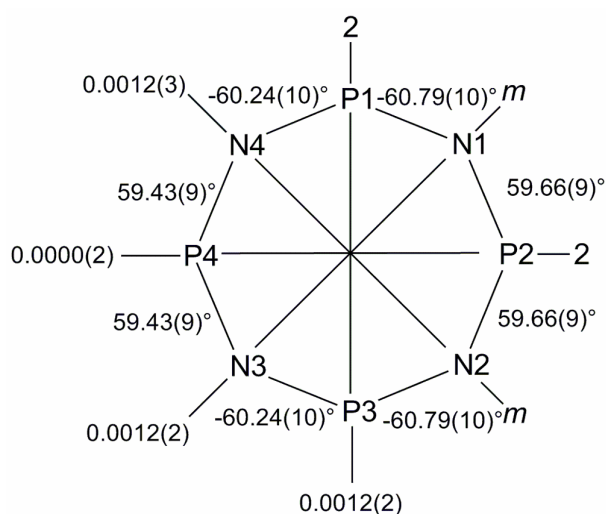
Figure 1. Symmetry of 8-membered P_4N_4 ring in the $[(PO_2NH)_4]^{4-}$ ion in $Ca_2(PO_2NH)_4 \cdot 8H_2O$; torsion angles /° and the displacement-asymmetry-parameter (DAP) for the mirror plane (*m*) and the twofold axes (2) are indicated (esd's in parentheses).

$q_3 = 0$, $q_4 = 0$)[25] and a phase angle $\varphi_2 = 90.00(3)°$ (ideal value: $\varphi_2 = \pi/4$) indicate a (nearly) regular $\overline{4}2m$ symmetry for the P_4N_4 ring.[26] The bond lengths P–N and P–O as well as the angles in the ring, which are summarized in Table 1, are in typical ranges for metaphosphimates.[3] The $[(PO_2NH)_4]^{4-}$ ions are interconnected by N-H···O hydrogen bonds forming infinite columns running along [001] (Figure 2), representing the shortest lattice parameter. Examples for this arrangement are the sodium tetrameta-

phosphimates (e.g. α- and β-$Na_4(PO_2NH)_4 \cdot 3H_2O$, $Na_4(PO_2NH)_4 \cdot 2H_2O$)[9] and $Tl_4(PO_2NH)_4 \cdot H_2O$.[12]
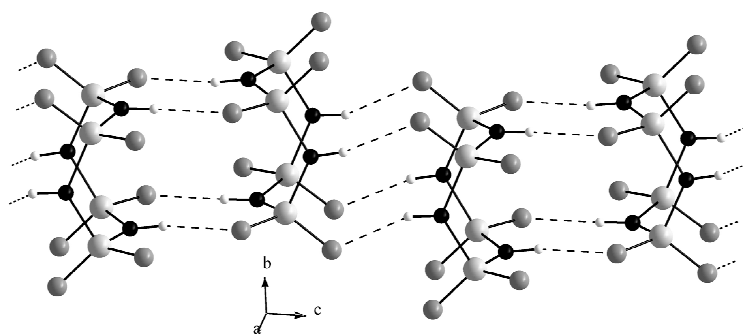
Figure 2. $[(PO_2NH)_4]^{4-}$ ions forming infinite columns along [001] in $Ca_2(PO_2NH)_4 \cdot 8H_2O$.

Table 1. Selected interatomic distances / pm and angles /° in $Ca_2(PO_2NH)_4 \cdot 8H_2O$ (esd's in parentheses).

Ca–O	234.0(2)–253.9(2)	7 times
P–O	149.6(2)–150.5(2)	4 times
P–N	165.3(2)–166.2(2)	4 times
P–N–P	126.64(4), 126.24(4)	
N–P–N	109.02(8), 106.69(12), 107.05(9)	
O–P–O	119.02(12), 119.5(2), 122.2(2)	
O–P–N	104.44(9)–109.44(8)	8 times
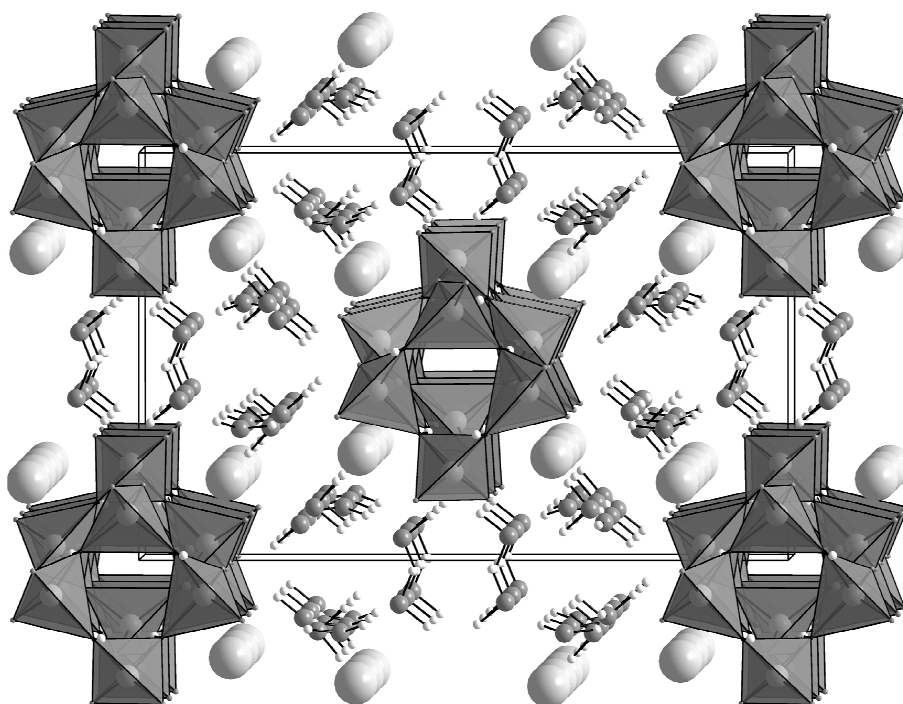
Figure 3. Representation of the crystal structure of $Ca_2(PO_2NH)_4 \cdot 8H_2O$ viewed along [001]; $[(PO_2NH)_4]^{4-}$ ions are drawn as ring of vertex-sharing PO_2N_2-tetrahedra; Ca^{2+}, O and H are pictured as light gray, dark gray and white balls, respectively.

The $[(PO_2NH)_4]^{4-}$ columns in $Ca_2(PO_2NH)_4 \cdot 8H_2O$ are surrounded by crystal water molecules and Ca^{2+} ions. Thus they are hold together by a complex hydrogen bonding system, which is indicated in Table 2, and with further coordinative bonds $Ca^{2+}\cdots O$ forming a sevenfold coordination sphere (see Figure 4, right) including distances Ca-O in the range of the sum of the respective ionic radii (Table 1).[27] Altogether, a three-dimensional network structure is generated (Figure 3). With the knowledge of the crystal structure, the fiber-like form of the crystals (Figure 4, left) can be understood.

Table 2. Hydrogen-bonding geometry (in pm and °) in Ca$_2$(PO$_2$NH)$_4$ · 8H$_2$O (D = proton donor, A = proton acceptor; esd's in parentheses).

D–H···A	D–H	D···A	H···A	D–H···A
N(1)-H(1)···O(3)	83.4(20)	290.0(3)	211.5(3)	156.94(9)
N(2)-H(2)···O(4)	82.5(20)	288.9(2)	208.5(2)	164.52(8)
Ow(1)-H(3)···O(4)	93.3(20)	291.3(2)	200.8(2)	162.96(10)
Ow(1)-H(4)···Ow(3)	93.7(20)	308.3(2)	217.1(2)	164.15(9)
Ow(2)-H(5)···O(2)	95.0(20)	280.5(3)	189.3(3)	160.28(11)
Ow(2)-H(6)···O(3)	94.0(20)	287.9(3)	198.7(3)	157.64(11)
Ow(3)-H(7)···Ow(2)	94.1(20)	296.1(2)	216.9(2)	141.11(10)
Ow(3)-H(8)···O(1)	94.5(20)	314.5(3)	236.2(3)	140.04(10)
Ow(4)-H(9)···Ow(2)	94.2(20)	270.2(2)	176.6(2)	171.72(10)
Ow(4)-H(10)···O(1)	94.5(20)	270.9(3)	178.0(3)	167.00(12)
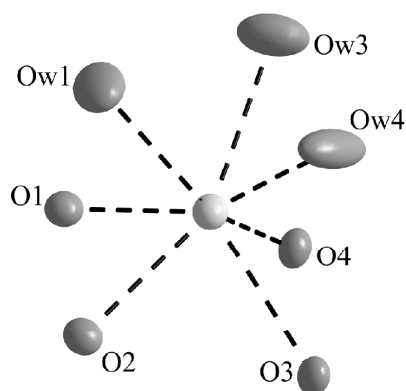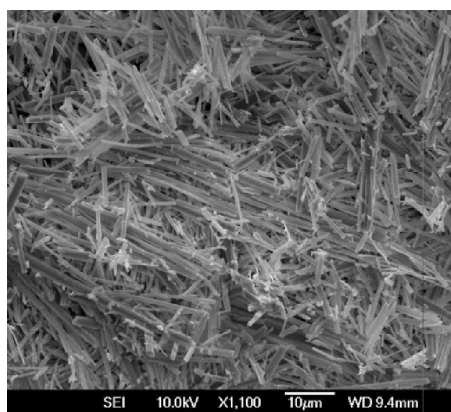
Figure 4. left: SEM image of fiber-like crystals of Ca$_2$(PO$_2$NH)$_4$ · 8H$_2$O; EDX results (Ca: 9.0, P: 19.8, O: 51.2, N: 18.6 atom-%) confirm the formula within the accuracy of the method; right: representation of the Ca^{2+} environment in Ca$_2$(PO$_2$NH)$_4$ · 8H$_2$O (Ca^{2+}: light gray, O: dark gray), the displacement ellipsoids represent 50 % probability.

3.2.2 Infrared Spectroscopy

The FT-IR spectrum of Ca$_2$(PO$_2$NH)$_4$ · 8H$_2$O is displayed in Figure 5. The strong absorption at high wavenumbers between 3183 and 3520 cm^{-1} results from stretching vibrations (νOH and νNH). With further deformation modes (δH$_2$O) at 1629 and (δNH) at 2670 and 1339 cm^{-1} both the crystal water molecules and their hydrogen bonding network as well as the imido form of the tetrametaphosphimate ion is indicated. The bands in the fingerprint region originate from lattice vibrations (νPO$_2$, δPO$_2$, νPN) of the ring anion whereby evidence for a saddle conformation is suggested. The assignments of all observed bands were carried out by comparison with other tetrametaphosphimates.[4a,c] They are presented in Table 3.
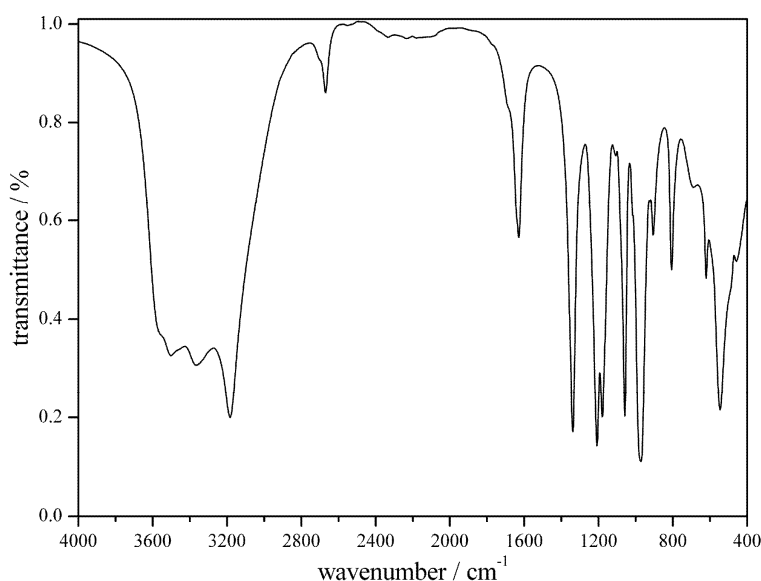
Figure 5. FT-IR vibrational spectrum of $Ca_2(PO_2NH)_4 \cdot 8H_2O$.

Table 3. Vibrational frequencies / cm^{-1} of $Ca_2(PO_2NH)_4 \cdot 8H_2O$ as observed by FT-IR spectroscopy at room temperature and their assignments (ν = stretching, δ = in-plane deformation, γ = out-of-plane deformation, s = strong, m = medium, b = broad).

observed frequencies	assignment	observed frequencies	assignment
3502 s, b	$\nu\, H_2O$	1180 s	$\nu_{as}\, PO_2$
3365 s, b	$\nu\, NH$	1059 s	$\nu_s\, PO_2$
3183 s, b	$\nu\, NH$	972 s	$\nu_{as}\, PN$
2670 w	$2\delta NH$	906 m	$\nu_s\, PN$
1629 m	δH_2O	806 m	$\nu_s\, PN$
1339 s	δNH	621 m	γNH
1208 s	$\nu_{as}\, PO_2$	546 s	δPO_2

3.2.3   Solid-State NMR Spectroscopy

The ^{31}P solid-state MAS NMR spectrum of $Ca_2(PO_2NH)_4 \cdot 8H_2O$ is shown in Figure 6. Three resonances with a mean FWHM of 1.0 ppm are observed at –3.1, –4.9 and –7.9 ppm which are corresponding to three crystallographic phosphorus sites. These values are in the typical range for PO_2N_2 groups in tri- and tetrametaphosphimates (e.g. 2.8, 2.1, –0.2 ppm in $Na_3(PO_2NH)_3 \cdot H_2O$;[4a,28] 4.5, 2.8, –4.6 ppm in $KCa(PO_2NH)_3 \cdot 4H_2O$;[4c] –1.4 ppm in $NaTl(PO_2NH)_3 \cdot 2H_2O$;[4c,29] 0 to –10 ppm in $Tl_4(PO_2NH)_4 \cdot H_2O$;[12] 2.1, –1.7 ppm in $Na_4(PO_2NH)_4 \cdot 2H_2O$).[9] They fit also in the range where PO_2N_2 tetrahedra have been assigned in N-doped phosphate glass.[30] After deconvolution and integration of the peaks an atomic ratio 2 : 1 : 1 became obvious according to the Wyckoff positions (P(1): 8d, P(2) and P(3): 4c). Therefore, the ^{31}P NMR measurements agree well with the results of the crystal structure refinement.
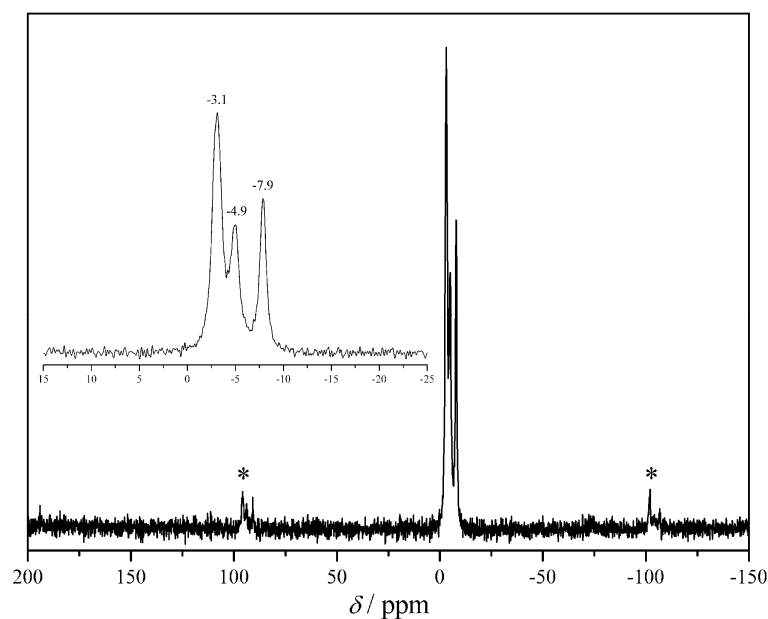
Figure 6. Solid-state ^{31}P MAS NMR spectrum of Ca$_2$(PO$_2$NH)$_4$ · 8H$_2$O at a spinning frequency of 20 kHz; spinning sidebands are marked with asterisks.

3.2.4 Differential Thermal Analysis and Thermogravimetry

TG and DTA curves of Ca$_2$(PO$_2$NH)$_4$ · 8H$_2$O recorded between room temperature and 800 °C are displayed in Figure 7. As already described by *Sakurai* and *Watanabe*,[20] the thermal behavior of this tetrametaphosphimate is characterized by a massive mass loss beginning already at 75 °C. Accompanied by a strong endothermic signal, the crystal water molecules are released in this step below 200 °C (–8 H$_2$O: mass loss *calculated*: 27 %; *observed*: 24(2) %). The weak mass loss running over an interval of around 500 °C (until at least 750 °C) could be assigned to the decomposition of the anhydrous calcium tetrametaphosphimate by releasing small amounts of ammonia. This was verified by analyses reported in ref. [20] where also further details concerning the decomposition products are described. The small and broad endothermic DTA signal around 700 °C probably means a slight reaction (e.g. further fragmentation of the anion) after the second mass loss (generating no DTA signal) is completed. A gray vitreous solid remains as final decomposition compound.
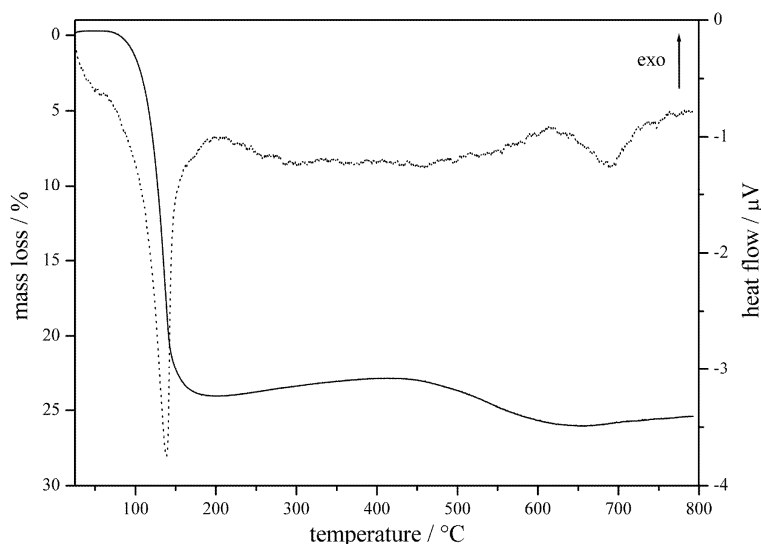
Figure 7. TG (solid) and DTA (dotted) curves of Ca$_2$(PO$_2$NH)$_4$ · 8H$_2$O; recorded with a heating rate of 5 °C min^{-1} (sample mass: 7.6 mg).

3.3   CONCLUSION

We were able to synthesize single-phase Ca$_2$(PO$_2$NH)$_4$ · 8H$_2$O. Although the compound crystallizes in form of very thin fibers, a suitable single crystal for X-ray structure determination could be found. According to the crystal structure, where infinite columns of saddle featured [(PO$_2$NH)$_4$]$^{4-}$ ions are held together by N-H···O hydrogen bonds along [001], this crystal shape is consequent. In total the structure is affected by a complex hydrogen bonding network that, besides coordinative Ca–O-bonds, connect the columns to a three-dimensional network.

The single-phase compound allowed recording of FT-IR and well resolved solid-state NMR spectra, which are in accordance with the structural model. The analysis of the thermal behavior of Ca$_2$(PO$_2$NH)$_4$ · 8H$_2$O showed that the compound can be completely dehydrated below 650 °C. From the resulting material, prospectively, it could be tried to crystallize a calcium oxonitridophosphate e.g. by tempering at a certain temperature or by a treatment under high-pressure conditions where oxonitridophosphates crystallize more easily.

3.4 EXPERIMENTAL SECTION

3.4.1 Syntheses

$K_4(PO_2NH)_4 \cdot 4H_2O$: Potassium tetra-μ-imidocyclotetraphosphate tetrahydrate has been synthesized according to ref. [31]. In a typical approach $H_4(PO_2NH)_4 \cdot 2H_2O$ (1.50 g, 4.26 mmol)[32,3a] is suspended in desalinated water (approx. 12 ml) at room temperature and potassium hydroxide (1.18 g, 21.0 mmol) is added. With an acetone/ethanol mixture a colorless precipitate is generated from the clear solution. After drying, $K_4(PO_2NH)_4 \cdot 4H_2O$ is obtained as a colorless and water-soluble powder (yield: 2.08 g, 3.85 mmol, 90.4 %).

$Ca_2(PO_2NH)_4 \cdot 8H_2O$: Calcium tetra-μ-imidocyclotetraphosphate octahydrate can be synthesized in aqueous solution using $K_4(PO_2NH)_4 \cdot 4H_2O$ and $Ca(NO_3)_2 \cdot 4H_2O$ (Sigma-Aldrich, 99 %) as starting materials. $Ca(NO_3)_2 \cdot 4H_2O$ (175 mg, 0.740 mmol) was dissolved in desalinated water (approx. 25 ml) and $K_4(PO_2NH)_4 \cdot 4H_2O$ (200 mg, 0.370 mmol) were added during stirring. After aging the emerging fine precipitate over night, it was filtered off, washed with ethanol and dried at air. Phase-pure $Ca_2(PO_2NH)_4 \cdot 8H_2O$ was obtained in form of a colorless, acicular microcrystalline powder. Larger fiber-like single crystals were grown by combining very diluted solutions of $Ca(NO_3)_2 \cdot 4H_2O$ and $K_4(PO_2NH)_4 \cdot 4H_2O$ in the respective molar ratio indicated above.

3.4.2 X-ray Diffraction

Single-crystal X-ray diffraction data of $Ca_2(PO_2NH)_4 \cdot 8H_2O$ were collected at 297 K from a suitable specimen mounted on the tip of a glass fiber on a Nonius Kappa CCD diffractometer using monochromated Mo-K_α radiation ($\lambda = 71.073$ pm). The diffraction intensities were scaled using the SCALEPACK software package[33] and no additional adsorption correction was applied. The crystal structure was solved (SHELXS-97) by direct methods in space group *Pbcn* (no. 60) and refined (SHELXL-97) against F^2 by applying the full-matrix least-squares method using the software package SHELX-97.[34] The hydrogen atoms have been located employing difference Fourier syntheses and were refined isotropically using constraints for nitrogen / oxygen-hydrogen distances with a riding model. The final refinement led to $R1 = 0.0680$ and $wR2 = 0.1127$ for all data. The relevant crystallographic data and further details of the data collection are summarized in Table 4. Tables 5 and 6 show the positional and displacement parameters for all atoms. The results from the single-crystal analysis were verified with a powder diffraction pattern (Huber G670, Cu-$K_{\alpha1}$, Figure 8). Besides phase-purity, it shows that all reflections could

be indexed with the known cell parameters and their observed intensities were in very good agreement with the calculated diffraction pattern based on single crystal data.[†]

Table 4. Crystallographic data for $Ca_2(PO_2NH)_4 \cdot 8H_2O$ (esd's in parentheses).

Crystal Data	
formula	$Ca_2(PO_2NH)_4 \cdot 8H_2O$
formula mass / gmol^{-1}	536.222
crystal system	orthorhombic
space group	*Pbcn* (no. 60)
cell parameters / pm	$a = 1700.6(3)$
	$b = 1069.3(2)$
	$c = 963.2(2)$
cell volume / 10^6 pm^3	$V = 1751.5(6)$
formula units Z / cell	4
crystal shape, color	needle, colorless
crystal size / mm^3	$0.08 \times 0.01 \times 0.01$
X-ray density ρ / gcm^{-3}	2.018
abs. coefficient μ / mm^{-1}	1.103
F(000)	1104

Data collection	
type of diffractometer	Nonius Kappa CCD
radiation, monochromator	Mo-K_α ($\lambda = 71.073$ pm), graphite
temperature / K	297(2)
θ range / °	3.7–27.7
h, k, l	$-22 \leq h \leq 22, -13 \leq k \leq 13, -10 \leq l \leq 12$
measured reflections	13396

Solution and Refinement	
structure solution method	direct methods using SHELXS-97[32]
structure refinement method	least square refinement on F^2 using SHELXL-97[32]
independent reflections	2023 ($R_{int} = 0.0693$)
observed reflections	1509 ($F_o^2 \geq 2\sigma (F_o)^2$)
refined parameters / constraints	101 / 10
R indices ($F_o^2 \geq 2\sigma (F_o)^2$)	$R1 = 0.0435$
	$wR2 = 0.1021$
R indices (all data)	$R1 = 0.0680$
	$wR2 = 0.1127$
GoF	1.066
weighting scheme	$w^{-1} = \sigma^2 F_o^2 + (0.0447P)^2 + 4.3891P$ with $P = (F_o^2 + 2F_c^2)/3$
max. / min. residual electron density / eÅ^{-3}	0.73 / –0.60

[†] Further details of the crystal structure investigation may be obtained from Fachinformationszentrum Karlsruhe, 76344 Eggenstein-Leopoldshafen, Germany (fax: (+49)7247-808-666; e-mail: crysdata@fiz-karlsruhe.de, http://www.fiz-karlsruhe.de/request_for_deposited_data.html) on quoting the depository number CSD-423118.

Table 5. Atomic coordinates and isotropic displacement parameters / 10^{-4} pm^2 for $Ca_2(PO_2NH)_4 \cdot 8H_2O$ (esd's in parentheses); U_{eq} is defined as one third of the trace of the orthogonalized tensor U_{ij}.

atom[c.n.]	Wyckoff position	x	y	z	U_{eq}/U_{iso}
Ca(1)[7]	8d	0.34903(4)	0.27687(7)	0.00108(7)	0.02235(19)
P(1)[4]	8d	0.38273(5)	0.55763(8)	0.19254(9)	0.0191(2)
P(2)[4]	4c	½	0.36021(11)	¼	0.0179(3)
P(3)[4]	4c	½	0.24350(10)	¾	0.0198(3)
N(1)	8d	0.4488(1)	0.66379(10)	0.1453(1)	0.0215(6)
H(1)	8d	0.461	0.6611	0.0616	0.026
N(2)	8d	0.4259(1)	0.45209(10)	0.2937(1)	0.0202(6)
H(2)	8d	0.4129	0.4585	0.3759	0.024
O(1)	8d	0.32294(14)	0.6193(2)	0.2846(2)	0.0240(5)
O(2)	8d	0.44461(15)	0.1759(2)	0.8445(3)	0.0243(5)
O(3)	8d	0.47740(14)	0.2894(2)	0.1211(2)	0.0228(5)
O(4)	8d	0.35579(8)	0.49610(13)	0.06074(14)	0.0242(5)
Ow(1)	8d	0.26724(8)	0.11850(13)	0.90002(14)	0.0542(9)
H(3)	8d	0.2279	0.0675	0.9368	0.065
H(4)	8d	0.2753	0.1133	0.8039	0.065
Ow(2)	8d	0.58022(8)	0.07710(13)	0.09215(14)	0.0464(8)
H(5)	8d	0.5596	0.9961	0.1096	0.056
H(6)	8d	0.5369	0.1316	0.0915	0.056
Ow(3)	8d	0.21388(8)	0.34420(13)	0.08441(14)	0.0550(9)
H(7)	8d	0.1729	0.3992	0.0603	0.066
H(8)	8d	0.1801	0.2806	0.1171	0.066
Ow(4)	8d	0.32686(8)	0.15024(13)	0.19528(14)	0.0631(12)
H(9)	8d	0.3624	0.1311	0.2673	0.076
H(10)	8d	0.2776	0.1414	0.2398	0.076

Table 6. Anisotropic displacement parameters / 10^{-4} pm^2 for $Ca_2(PO_2NH)_4 \cdot 8H_2O$ (esd's in parentheses).

atom[c.n.]	U_{11}	U_{22}	U_{33}	U_{23}	U_{13}	U_{12}
Ca(1)[7]	0.0225(4)	0.0228(4)	0.0218(3)	0.0012(3)	0.0003(3)	–0.0031(3)
P(1)[4]	0.0205(5)	0.0194(4)	0.0175(4)	–0.0002(3)	–0.0006(3)	0.0006(4)
P(2)[4]	0.0186(6)	0.0184(6)	0.0167(6)	0	0.0003(5)	0
P(3)[4]	0.0210(6)	0.0189(6)	0.0195(6)	0	0.0011(5)	0
N(1)	0.0245(15)	0.0242(15)	0.0159(13)	0.0023(12)	0.0024(12)	–0.003(2)
N(2)	0.0211(15)	0.0223(14)	0.0172(13)	0.0018(12)	0.0025(11)	0.0035(12)
O(1)	0.0221(13)	0.0255(13)	0.0245(12)	–0.0024(10)	0.0008(10)	0.0032(10)
O(2)	0.0261(13)	0.0213(12)	0.0254(13)	0.0015(10)	0.0031(10)	–0.003(1)
O(3)	0.0240(14)	0.0241(13)	0.0202(12)	–0.0048(10)	–0.001(1)	0.0004(10)
O(4)	0.0282(14)	0.0244(12)	0.0199(12)	–0.0018(10)	–0.004(2)	–0.001(2)
Ow(1)	0.056(2)	0.057(2)	0.0501(19)	–0.0108(16)	0.0051(16)	–0.033(2)
Ow(2)	0.0436(19)	0.0270(15)	0.068(2)	0.0010(14)	–0.010(2)	0.0020(14)
Ow(3)	0.0307(18)	0.051(2)	0.083(3)	0.0116(18)	0.0113(17)	0.0026(15)
Ow(4)	0.0288(17)	0.106(3)	0.055(2)	0.050(2)	–0.004(2)	–0.012(2)
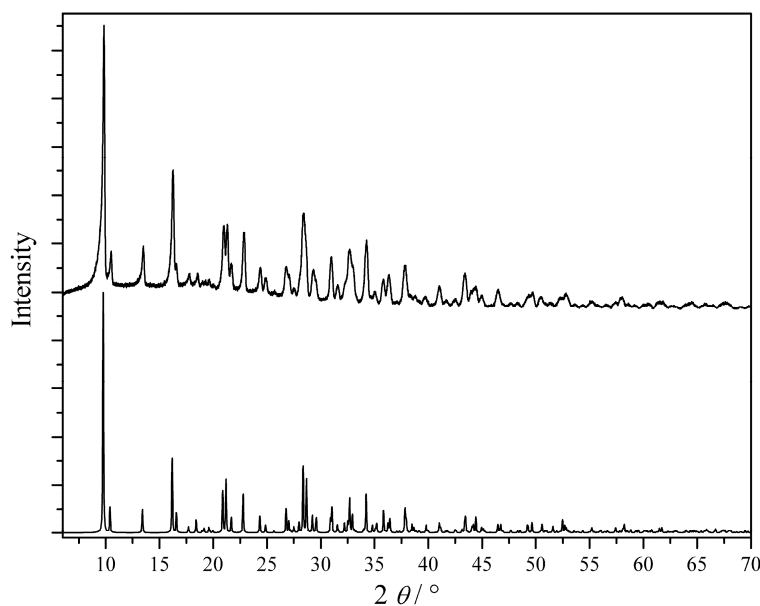
Figure 8. Observed (top, Huber G670, Cu-$K_{\alpha 1}$) and simulated (bottom) powder X-ray diffraction pattern of $Ca_2(PO_2NH)_4 \cdot 8H_2O$.

3.4.3 Infrared spectroscopy

An FT-IR spectrum of $Ca_2(PO_2NH)_4 \cdot 8H_2O$ was recorded in transmission geometry at room temperature in the range 4000–400 cm^{-1} with a Bruker IFS 66v/S spectrometer using the KBr pellet technique (2 mg sample, 300 mg dried KBr).

3.4.4 Solid-state NMR spectroscopy

A solid-state ^{31}P MAS NMR spectrum was carried out at ambient temperature on a Bruker Avance III spectrometer with an 11.75 T magnet. The sample was contained in a ZrO_2 rotor with outer diameters of 2.5 mm which was mounted in a commercial MAS double resonance probe. The rotation frequency was 20 kHz. The chemical shift values refer to a deshielding scale and 85 % H_3PO_4 used as an external reference.

3.4.5 Differential thermal analysis and thermogravimetry

Thermoanalytical measurements were performed with a Thermoanalyzer TG-DTA92 (Setaram) under inert gas atmosphere (He). A dried sample was heated in an alumina crucible from room temperature up to 800 °C with a heating rate of 5 °C min^{-1}.

3.5   REFERENCES

[1]   R. Schenck, G. Römer, *Chem. Ber.* **1924**, *57B*, 1343.

[2]   M. L. Nielsen, G. Cranford, *Inorg. Synth.* **1960**, *6*, 94.

[3]   R. Marchand, W. Schnick, N. Stock, *Adv. Inorg. Chem.* **2000**, *50*, 193.

[4]   a) N. Stock, Doctoral Thesis, Univ. Bayreuth **1998**; b) S. Correll, Doctoral Thesis, Univ. Munich (LMU) **2006**; c) S. Sedlmaier, Master Thesis, Univ. Munich (LMU) **2006**.

[5]   S. Correll, N. Stock, W. Schnick, *Phosphorus, Sulfur Silicon* **2001**, *168*, 321.

[6]   C. Baerlocher, L. B. McCusker, *Database of Zeolites Structures*: http://www.iza-structure.org/databases/.

[7]   H. N. Stokes, *Am. Chem. J.* **1896**, *18*, 780.

[8]   S. R. Römer, W. Schnick, *Z. Anorg. Allg. Chem.* **2006**, *632*, 59.

[9]   N. Stock, H. Schmalz, W. Schnick, *Z. Anorg. Allg. Chem.* **1998**, *624*, 1777.

[10]   B. Berking, D. Mootz, *Acta Crystallogr., Sect. B: Struct. Sci.* **1971**, *27*, 740.

[11]   N. Stock, W. Schnick, *Acta Crystallogr., Sect. C: Cryst. Struct. Commun.* **1998**, *54*, 171.

[12]   S. J. Sedlmaier, O. Oeckler, W. Schnick, *Solid State Sci.* **2008**, *10*, 1150.

[13]   N. Stock, B. Jürgens, W. Schnick, *Z. Naturforsch., B: J. Chem. Sci.* **1998**, *53*, 1115.

[14]   V. I. Sokol, D. A. Murashov, I. A. Rozanov, M. A. Porai-Koshits, V. P. Nikolaev, L. A. Butman, *Zh. Neorg. Khim.* **1979**, *24*, 3385.

[15]   S. R. Römer, W. Schnick, *Solid State Sci.* **2007**, *9*, 644.

[16]   S. R. Römer, W. Schnick, *Z. Anorg. Allg. Chem.* **2005**, *631*, 31.

[17]   S. R. Römer, W. Schnick, *Z. Anorg. Allg. Chem.* **2005**, *631*, 1749.

[18]   D. E. C. Corbridge, E. J. Lowe, *J. Chem. Soc.* **1954**, 4555.

[19]   A. H. Herzog, M. L. Nielsen, *Anal. Chem.* **1958**, *30*, 1490.

[20]   M. Sakurai, M. Watanabe, *Phos. Res. Bull.* **1995**, *5*, 161.

[21]   M. Sakurai, M. Watanabe, *Phos. Res. Bull.* **1996**, *6*, 141.

[22]   A. Bertoluzza, C. Fagnano, O. Francioso, M. Vasina, *Spectroscopy of Biological Molecules, 6th European Conference on the Spectroscopy of Biological Molecules, Villeneuve d'Ascq,* **1995**, 515.

[23]   R. Bucourt, *"Topics in Stereochemistry"*, Wiley, New York, **1974**, *8*, 159.

[24]   M. Nardelli, *Acta Crystallogr., Sect. C: Cryst. Struct. Commun.* **1983**, *39*, 1141.

[25]   D. Cremer, J. A. Pople, *J. Am. Chem. Soc.* **1975**, *97*, 1354.

[26]   all values were calculated with M. Nardelli, *PARST97*, Univ. Parma, **1997**.

[27]   R. D. Shannon, C. T. Prewitt, *Acta Crystallogr., Sect. B: Struct. Sci.* **1969**, *25*, 925.

[28]   N. Stock, W. Schnick, *Acta Crystallogr., Sect. C: Cryst. Struct. Commun.* **1997**, *53*, 532.

[29]   S. J. Sedlmaier, D. Johrendt, O. Oeckler, W. Schnick, *Z. Anorg. Allg. Chem.* **2007**, *633*, 2217.

[30]   B. C. Bunker, D. R. Tallant, C. A. Balfe, R. J. Kirkpatrick, G. L. Turner, M. R. Reidmeyer, *J. Am. Ceram. Soc.* **1987**, *70*, 675.

[31]   K. Lunkwitz, E. Steger, *Z. Anorg. Allg. Chem.* **1968**, *358*, 111.

[32]   E. Steger, K. Lunkwitz, *Z. Anorg. Allg. Chem.* **1962**, *313*, 262.

[3^3]   Z. Otwinowski, W. Minor, *Methods Enzymol.* **1997**, *276*, 307.

[34]   a) G. M. Sheldrick, *SHELX97,* Univ. Göttingen, **1997**; b) G. M. Sheldrick, *Acta Crystallogr., Sect. A: Cryst. Found. Crystallogr.* **2008**, *64*, 112.

4.   New Synthesis and Crystal Structure of Ammonium *Catena*-polyphosphate IV [NH$_4$PO$_3$]$_x$

To synthesize compounds like e.g. silicates usually the respective boundary phases or parent compound are used as starting materials—for oxosilicates SiO$_2$, for borates B$_2$O$_3$ and for the synthesis of nitridophosphates P$_3$N$_5$. Consequently, for the synthesis of oxonitridophosphates the compound PON is required and of course it was tried to prepare it. However, experiments performed according to the most frequently cited method in the literature serves up a surprise.

ABSTRACT

Phase-pure ammonium *catena*-polyphosphate IV [NH$_4$PO$_3$]$_x$ was synthesized by heating NH$_4$H$_2$PO$_4$ in a tube furnace under an ammonia gas flow. The product contained single crystals of [NH$_4$PO$_3$]$_x$ IV appropriate for X-ray structure determination enabling structure refinement of this compound. The pseudo-merohedrally twinned crystals of [NH$_4$PO$_3$]$_x$ crystallize in the monoclinic crystal system (*P*2$_1$/*c* (no. 14), *a* = 2270.3(5), *b* = 458.14(9), *c* = 1445.1(3) pm, *β* = 108.56(3)°, Z = 4, 2264 data, *R*1 = 0.076). In the unit cell the *catena*-polyphosphate chain anions run parallel [010] with a chain-periodicity *P* = 2 and a stretching factor *f*$_s$ = 0.94. The chain anions are interconnected through extensive hydrogen bonding towards the ammonium ions. Due to 'chemical twinning' a novel *catena*-polyphosphate structure type is realized in [NH$_4$PO$_3$]$_x$ IV. The vibrational spectra of [NH$_4$PO$_3$]$_x$ IV are reported as well.

4.1   INTRODUCTION

Alkali *catena*-polyphosphates (MPO$_3$)$_x$, known as Kurrol's salts, have been thoroughly investigated due to their interesting applications (e.g. paper fabrication[1] or fermentation process of yeast[2,3]). However, there is still a lack of structural information on ammonium *catena*-polyphosphate that is used as an important flame resistant in the paper and wood industry.[4] Already in the 1960s, five modifications of [NH$_4$PO$_3$]$_x$ have been reported by *Shen* et al.[5] However, a detailed crystal structure analysis has been only described for one modification of this compound so far. *Jansen* et al. reported on a crystal structure determination and refinement of [NH$_4$PO$_3$]$_x$ II based on X-ray powder diffraction data.[6] Its orthorhombic structure can be derived from that of rubidium *catena*-polyphosphate. However, it has not been possible to obtain phase-pure products or single crystals large enough for a structure determination from the other modifications so far. This shortcoming results from difficulties that occur in the synthesis of highly condensed crystalline ammonium *catena*-polyphosphates (e.g. thermal condensation of ammonium orthophosphates yields only amorphous mixtures of polyphosphates with a minor content of ammonium). Other synthetic methods lead to phosphates with lower condensation degrees or even to metaphosphates. *Shen* et al. synthesized modification I of ammonium *catena*-polyphosphate by heat-treating of mixtures of ammonium orthophosphate with urea.[5] From these products all other modifications have been obtained by thermal annealing of [NH$_4$PO$_3$]$_x$ I at different temperatures. In spite of a thorough analysis of the thermodynamic and kinetic stability of all modifications [NH$_4$PO$_3$]$_x$ IV has only been obtained with glassy impurities. *Shen* et al. assumed that for synthesis of a phase-pure modification IV a quite high ammonia pressure would be necessary.[5]

Taking these reports into consideration we were able to obtain a phase-pure product of modification IV of [NH$_4$PO$_3$]$_x$ containing large single crystals by applying an elevated ammonia partial pressure during the synthesis. Thereby we can present the first structure elucidation of an ammonium *catena*-polyphosphate based on single-crystal X-ray diffraction methods.

4.2   SYNTHESIS AND CHARACTERIZATION

$[NH_4PO_3]_x$ IV was obtained according to Equation 1 by heating $NH_4H_2PO_4$ in an ammonia flow at 530 °C.

$$NH_4H_2PO_4 \xrightarrow[\text{530°C}]{\text{NH}_3\text{-flow}} [NH_4PO_3]_x \text{ IV} + H_2O \qquad (1)$$

$NH_4H_2PO_4$ (Grüssing GmbH, 99 %) was ground and transferred into an alumina boat. After placing the latter into a silica glass tube in the centre of a tube furnace an ammonia gas flow with an ammonia partial pressure of approximately 950 Pa over atmospheric pressure was adjusted. After heating slowly to 530 °C crystalline $[NH_4PO_3]_x$ IV is formed in feather-type morphology at the cold regions of the silica glass tube. The typical morphology of the product is displayed as a REM-image in Figure 1.
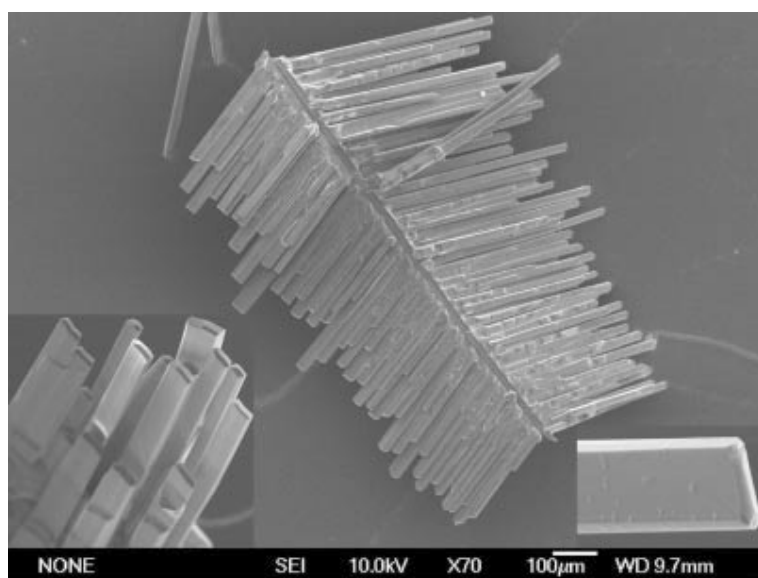
Figure 1. REM pictures of single crystals of $[NH_4PO_3]_x$ IV.

The purity of the product was checked by energy dispersive X-ray analysis (JSM 6500F scanning electron microscope, JEOL; detector model 7418, Oxford Instruments). No elements except P, O and N were detected. Other ammonium phosphate phases were excluded by measuring an X-ray powder diffraction pattern on a Stoe Stadi P diffractometer using Cu-$K_{\alpha1}$ radiation. No impurity reflections were detected.

Fractionary rods from the feathers (Figure 1) turned out to be suitable for an X-ray structure determination. Is has not been possible to break the rods perpendicular to the growing axis [010]. By mechanical treatment the rods split into thin fibers. This splitting has also been observed after exposure $[NH_4PO_3]_x$ IV to water.

4.3 CRYSTAL STRUCTURE

4.3.1 X-ray diffraction

X-ray diffraction data of [NH$_4$PO$_3$]$_x$ were collected from a single crystal enclosed in a glass capillary. The diffraction pattern indicated orthorhombic metrics. As the structure turned out to be monoclinic ($a = 2270.3(5)$, $b = 458.14(9)$, $c = 1445.1(3)$ pm, $\beta = 108.56(3)°$) a case of pseudomerohedral twinning is likely to occur. The domains are related by the matrix (1 0 1, 0 1 0, 0 0 –1) which corresponds to a mirror plane *m* that is present in the orthorhombic lattice but not in the structure. The structure of [NH$_4$PO$_3$]$_x$ was solved by direct methods (SHELX97)[7] in the centrosymmetric space group $P2_1/c$ (no. 14). After anisotropical refinement of the non-hydrogen atoms, the hydrogen atoms have been located employing difference Fourier syntheses. Idealized positions for the H atoms of the tetrahedral NH$_4$ groups were generated by constraints in combination with a riding model. The relevant crystallographic data and further details of the data collection are summarized in Table 1. Table 2 and 3 show the positional and displacement parameters for all atoms.[†]

Table 1. Crystallographic data of [NH$_4$PO$_3$]$_x$ IV (esd's in parentheses).

Crystal Data	
formula	(NH$_4$PO$_3$)$_4$
formula mass / gmol^{-1}	388.05
crystal system	monoclinic
space group	$P2_1/c$ (no. 14)
cell parameters / pm, °	$a = 2270.3(5)$
	$b = 458.14(9)$ $\beta = 108.56(3)°$
	$c = 1445.1(3)$
cell volume / 10^6 pm^3	$V = 1424.9(5)$
formula units Z / cell	4
crystal shape, color	rod, colorless
crystal size / mm^3	$0.64 \times 0.06 \times 0.04$
X-ray density ρ / gcm^{-3}	1.809
abs. coefficient μ / mm^{-1}	0.595
F(000)	800
twin matrix	(1 0 1, 0 1 0, 0 0 -1)
twin ratio	0.45

---

† Futher details of the crystal structure investigation may be obtained from the Fachinformationszentrum Karlsruhe, D-76344 Eggenstein-Leopoldshafen, Germany (e-mail: crysdata@fiz-karlsruhe.de) on quoting the depository number CSD-419184, the names of the authors and citation of the publication.

Data collection	
type of diffractometer	Nonius Kappa CCD
radiation, monochromator	Mo-K_α (λ = 71.073 pm), graphite
temperature / K	297(2)
θ range / °	3.1–26.0
h, k, l	-28 ≤ h ≤ 27, -5 ≤ k ≤ 5, -17 ≤ l ≤ 17
measured reflections	5369

Solution and Refinement	
structure solution method	direct methods using SHELXS-97[7]
structure refinement method	least square refinement on F^2 using SHELXL-97[7]
independent reflections	2799 (R_{int} = 0.0497)
observed reflections	2264 ($F_o^2 \geq 2\sigma\,(F_o)^2$)
refined parameters / constraints	195 / 40
R indices ($F_o^2 \geq 2\sigma\,(F_o)^2$)	$R1$ = 0.0567 $wR2$ = 0.1308
R indices (all data)	$R1$ = 0.0759 $wR2$ = 0.1397
GooF	1.145
weighting scheme	$w^{-1} = \sigma^2 F_o^2 + (0.0327P)^2 + 7.4401P$ with $P = (F_o^2 + 2F_c^2)/3$
max. / min. residual electron density / eÅ^{-3}	0.67 / –0.45

Table 2. Atomic coordinates and isotropic displacement parameters / 10^{-4} pm^2 for [NH$_4$PO$_3$]$_x$ IV (esd's in parentheses); all atoms are on Wyckoff position 4*e*; U_{eq} is defined as one third of the trace of the orthogonalized tensor U_{ij}.

atom	x	y	z	U_{eq}/U_{iso}
N(1)	0.4678(3)	0.211(2)	0.8295(6)	0.019(2)
H(1)	0.4390	0.2110	0.8575	0.023
H(2)	0.4926	0.0698	0.8506	0.023
H(3)	0.4868	0.3767	0.8430	0.023
H(4)	0.4500	0.1967	0.7674	0.023
N(2)	0.0331(4)	0.725(2)	0.8619(8)	0.041(2)
H(5)	0.043	0.786	0.812	0.049
H(6)	0.9992	0.811	0.863	0.049
H(7)	0.063	0.768	0.915	0.049
H(8)	0.027	0.541	0.858	0.049
N(3)	0.2071(4)	0.277(2)	0.0303(7)	0.028(2)
H(9)	0.1786	0.3986	0.0300	0.033
H(10)	0.2434	0.3466	0.0617	0.033
H(11)	0.2018	0.1167	0.0588	0.033
H(12)	0.2060	0.2354	0.9713	0.033
N(4)	0.2951(4)	0.742(2)	0.3269(7)	0.029(2)
H(13)	0.2934	0.7528	0.2661	0.035
H(14)	0.2738	0.8814	0.3404	0.035
H(15)	0.2803	0.5759	0.3372	0.035
H(16)	0.3333	0.7558	0.3633	0.035

P(1)	0.3906(1)	0.3110(4)	0.0321(2)	0.0176(5)
O(11)^{term}	0.3745(3)	0.241(2)	0.9279(5)	0.024(2)
O(12)^{term}	0.4533(3)	0.290(2)	0.1033(5)	0.029(2)
O(1)^{br}	0.3443(2)	0.131(1)	0.0764(4)	0.018(2)
P(2)	0.3500(1)	0.8128(4)	0.1221(2)	0.0167(5)
O(21)^{term}	0.4032(3)	0.791(2)	0.2110(5)	0.027(2)
O(22)^{term}	0.2852(3)	0.743(2)	0.1251(6)	0.026(2)
O(2)^{br}	0.3633(2)	0.634(1)	0.0355(3)	0.020(2)
P(3)	0.1508(2)	0.2084(5)	0.7723(2)	0.0221(6)
O(31)^{term}	0.2122(3)	0.274(2)	0.8392(6)	0.025(2)
O(32)^{term}	0.0967(3)	0.230(2)	0.8083(6)	0.031(2)
O(3)^{br}	0.1580(2)	0.613(1)	0.2294(4)	0.025(2)
P(4)	0.1106(1)	0.7938(5)	0.1418(2)	0.0223(6)
O(41)^{term}	0.1199(3)	0.727(2)	0.0465(5)	0.030(2)
O(42)^{term}	0.0455(3)	0.772(2)	0.1422(5)	0.029(2)
O(4)^{br}	0.1397(2)	0.388(2)	0.6720(4)	0.025(2)

Table 3. Anisotropic displacement parameters / 10^{-4} pm^2 for [NH$_4$PO$_3$]$_x$ IV (esd's in parentheses).

atom	U_{11}	U_{22}	U_{33}	U_{23}	U_{13}	U_{12}
N(1)	0.028(4)	0.019(3)	0.015(4)	−0.006(3)	0.012(3)	−0.002(3)
N(2)	0.032(4)	0.015(3)	0.073(7)	−0.001(4)	0.014(5)	0.000(3)
N(3)	0.036(5)	0.021(3)	0.030(5)	−0.001(3)	0.015(5)	−0.004(3)
N(4)	0.033(4)	0.026(4)	0.026(5)	0.004(3)	0.007(4)	0.007(3)
P(1)	0.023(1)	0.010(2)	0.021(2)	0.0001(9)	0.0083(9)	−0.0024(8)
O(11)^{term}	0.034(4)	0.020(3)	0.023(4)	−0.004(2)	0.015(3)	0.003(2)
O(11)^{term}	0.032(3)	0.017(3)	0.037(4)	−0.002(2)	0.009(3)	0.002(2)
O(1)^{br}	0.023(2)	0.011(2)	0.023(3)	0.003(2)	0.010(2)	0.003(2)
P(2)	0.022(2)	0.010(2)	0.018(2)	0.0011(8)	0.0067(9)	0.0007(8)
O(21)^{term}	0.047(4)	0.024(3)	0.009(3)	0.001(2)	0.009(3)	−0.001(2)
O(22)^{term}	0.028(3)	0.021(3)	0.032(5)	−0.001(2)	0.015(4)	−0.002(2)
O(2)^{br}	0.026(3)	0.016(2)	0.014(2)	−0.003(2)	0.003(2)	0.001(2)
P(3)	0.022(2)	0.020(2)	0.025(2)	0.0013(9)	0.0080(9)	0.0000(9)
O(31)^{term}	0.027(3)	0.025(3)	0.023(4)	0.000(2)	0.006(3)	0.001(2)
O(32)^{term}	0.024(3)	0.020(3)	0.054(5)	0.002(3)	0.020(4)	0.001(2)
O(3)^{br}	0.022(2)	0.017(2)	0.033(3)	−0.001(3)	0.004(2)	0.002(2)
P(4)	0.022(2)	0.015(2)	0.029(2)	−0.002(1)	0.006(1)	−0.0027(8)
O(41)^{term}	0.035(4)	0.032(3)	0.017(3)	−0.004(2)	0.000(3)	−0.005(3)
O(42)^{term}	0.015(3)	0.024(3)	0.045(5)	0.005(3)	0.007(3)	0.002(2)
O(4)^{br}	0.039(3)	0.012(2)	0.023(3)	0.001(2)	0.009(2)	0.000(2)

All reflections detected by X-ray powder diffraction (Stoe Stadi P) of [NH$_4$PO$_3$]$_x$ IV have been indexed and their observed intensities are in good agreement with the calculated diffraction pattern based on single-crystal data.

The unit cell obtained does not agree with that assumed by *Shen* et al. ($a = 14.5$,

$b = 4.62$, c = 11.0 Å, $\beta = 100°$).[5] Furthermore, due to a smaller monoclinic angle, the lattice parameter c (here: a) is doubled in [NH$_4$PO$_3$]$_x$. Concerning this doubling it has been verified (with Platon[8]) that no additional symmetry is present. The assumption from *Shen et al.* that the unit cell of [NH$_4$PO$_3$]$_x$ might be nearly identical with of potassium Kurrol's salt is subsequently also not correct as well.[9]

4.3.2   The Crystal Structure

In the solid, ammonium *catena*-polyphosphate IV [NH$_4$PO$_3$]$_x$ contains infinite chains of corner-sharing PO$_4$ tetrahedra $^1_\infty$[PO$_2$O$_{2/2}$]$^-$ as well as NH$_4^+$ ions. In the unit cell the two crystallographically independent polyphosphate chain anions with a chain-periodicity $P = 2$ and a stretching factor[10] $f_s = 0.94$ run parallel [010], representing the shortest lattice parameter (Figure 2). As expected the bond lengths P–O^{term} to the terminal oxygen atoms of the PO$_4$ tetrahedra (145.2(7)–152.1(8) pm) are significantly shorter than the bond lengths P–O^{br} to the bridging O atoms (159.0(6)–162.4(6) pm) being typical for *catena*-polyphosphate chains.[9,11,12] Bond lengths and angles inside the chains are summarized in Table 4. The values agree very well with the respective values observed in other *catena*-polyphosphates.[9,11,12] The angles O–P–O show an average value of 109.1°, which is close to the ideal tetrahedral angle.
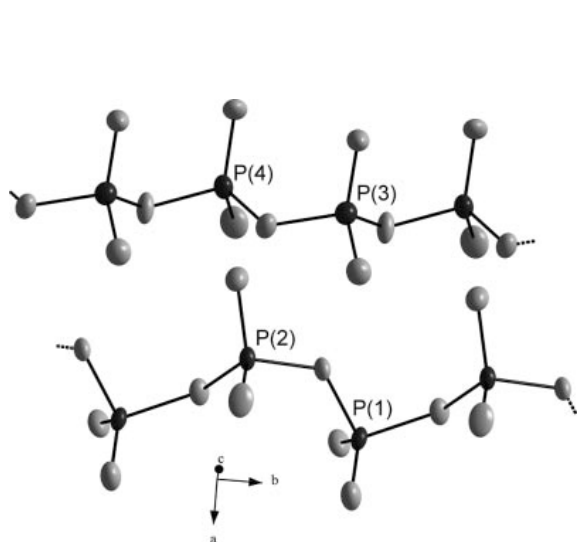
Figure 2. View of the *catena*-polyphosphate anions in [NH$_4$PO$_3$]$_x$ IV, the displacement ellipsoids represent 50 % probability.
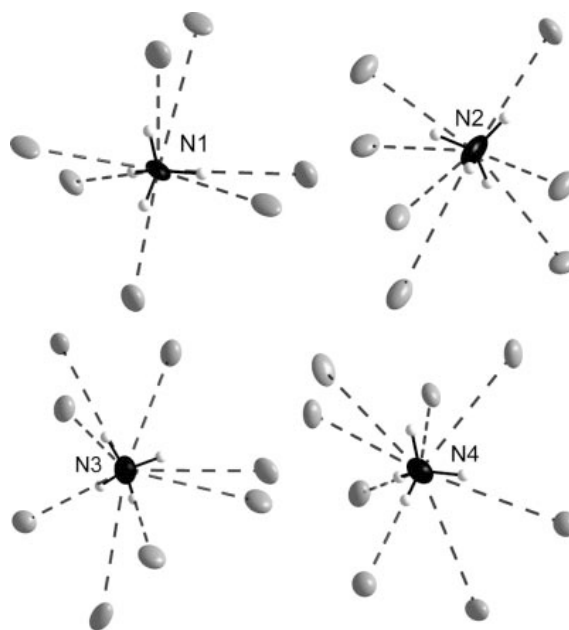
Figure 3. Representation of the environment of the ammonium ions (N1–N4) in [NH$_4$PO$_3$]$_x$ IV (N: black; H: white; O: light gray), the displacement ellipsoids represent 50 % probability.

The cohesion of the *catena*-polyphosphate anions are provided by extensive hydrogen bonding between the O atoms and the ammonium ions. Hence, the four crystallographically independent nitrogen atoms are mostly coordinated by terminal O^{term} and fewer bridging O^{br} atoms. The coordination numbers count seven or eight, respectively (Figure 3). The distances N–O range between 276.7(12) and 339.1(11) pm (Table 4) and thus represent both stronger and weaker hydrogen bonding. All hydrogen bonds of the network are listed in Table 5. The orientation of the *catena*-polyphosphate chains is displayed in Figure 4A. Considering the axes P-P of single chains in the (010) plane, the chains' orienttation is pairwise alternating along [100]. Thus, formally double layers of equally oriented chains are followed by double-layers with the second orientation. The two orientations can be transformed into each other by a rotation about 57.181(6) and 122.819(6)°, respectively. Thus, the crystal structure of [NH$_4$PO$_3$]$_x$ IV is characterized by 'chemical twinning'[13] involving two different orientated *catena*-polyphosphate chain double-layers.

Table 4. Selected interatomic distances / pm and angles / ° in [NH$_4$PO$_3$]$_x$ IV (esd's in parentheses).

N(1)–O	287.8(9)–317.9(12)	7 times
N(2)–O	276.7(12)–327.5(15)	7 times
N(3)–O	280.1(14)–339.0(14)	8 times
N(4)–O	285.3(14)–339.0(14)	8 times
P–O^{term}	145.2(7)–152.1(8)	8 times
P–O^{br}	159.0(6)–162.4(6)	8 times
O^{term}–P–O^{term}	115.1(5), 118.7(5), 119.8(5), 125.0(5)	
O^{br}–P–O^{br}	97.1(3), 98.1(3), 98.6(3), 99.0(3)	
O^{br}–P–O^{br}	104.4(4)–112.9(4)	16 times
P–O^{br}–P	129.8(4), 130.2(4), 130.8(4), 131.6(4)	

Table 5. Hydrogen-bonding geometry (in pm and °) in [NH$_4$PO$_3$]$_x$ IV (D = proton donor, A = proton acceptor; esd's in parentheses).

D–H···A	D–H	D···A	H···A	D–H···A
N(1)-H(1)···O(11)^{term}	87.0(2)	290.6(12)	203.6(8)	175.6(6)
N(1)-H(2)···O(12)^{term}	84.9(2)	288.1(9)	203.5(6)	175.7(5)
N(1)-H(3)···O(12)^{term}	86.4(2)	287.8(9)	202.9(6)	166.9(5)
N(1)-H(4)···O(12)^{term}	86.1(2)	317.9(12)	239.7(8)	151.2(6)
···O(21)^{term}	86.1(2)	296.3(9)	249.8(6)	114.7(5)
N(2)-H(5)···O(42)^{term}	86.9(2)	327.5(15)	248.7(5)	151.7(4)
···O(32)^{term}	86.9(2)	295.6(12)	238.0(7)	124.3(5)
N(2)-H(6)···O(42)^{term}	86.6(2)	290.3(10)	215.4(6)	144.2(5)
N(2)-H(7)···O(41)^{term}	86.2(2)	276.7(12)	193.7(4)	159.0(5)
N(2)-H(8)···O(42)^{term}	85.8(2)	288.3(10)	218.2(6)	139.1(3)
···O(32)^{term}	85.8(2)	292.4(12)	240.3(7)	119.8(2)

N(3)-H(9)···O(41)^{term}	85.3(2)	292.0(11)	207.4(7)	171.1(6)
N(3)-H(10)···O(22)^{term}	86.5(2)	283.4(10)	211.7(6)	139.9(6)
···O(1)^{br}	86.5(2)	304.5(10)	244.0(5)	127.4(7)
N(3)-H(11)···O(41)^{term}	86.9(2)	325.7(11)	254.2(7)	140.2(5)
···O(4)^{br}	86.9(2)	301.6(13)	247.6(6)	120.9(7)
···O(22)^{term}	86.9(2)	307.6(9)	250.7(6)	123.8(5)
N(3)-H(12)···O(31)^{term}	86.5(2)	280.1(14)	196.6(9)	161.4(7)
N(4)-H(13)···O(22)^{term}	86.8(2)	285.3(14)	198.7(9)	174.8(7)
N(4)-H(14)···O(31)^{term}	86.0(2)	295.0(11)	210.6(7)	167.1(6)
N(4)-H(15)···O(31)^{term}	86.5(2)	306.2(11)	223.3(7)	160.6(5)
N(4)-H(16)···O(2)^{br}	86.2(2)	297.2(10)	241.5(5)	122.9(7)

4.3.3   Comparison with potassium Kurrol's salt and [NH$_4$PO$_3$] II

Due to very similar ionic radii[14] K- and NH$_4$-compounds are frequently isostructural. And this has also been erroneously assumed for [KPO$_3$]$_x$ and [NH$_4$PO$_3$]$_x$.[5] The main reason for this misconception is the 'chemical twinning' found in [NH$_4$PO$_3$]$_x$ IV leading to a doubling of the lattice parameter *c* (in [KPO$_3$]$_x$: *a*).[9] Although the conformation of the *catena*-polyphosphate chain in [KPO$_3$]$_x$ is very similar to the one in [NH$_4$PO$_3$]$_x$ IV ($P = 2$; $f_s = 0.94$) no 'chemical twinning' has been observed (Figure 4B). In [NH$_4$PO$_3$]$_x$ IV the distinctive network of hydrogen bonds might be responsible for this 'chemical twinning' effect. The physical properties of [KPO$_3$]$_x$ (e.g. exposure to water) has been described identical with [NH$_4$PO$_3$]$_x$ IV (see chapter 4.2).[9] Comparison of [NH$_4$PO$_3$]$_x$ IV with modification II[6] reveals major structural differences. Besides a different metric (orthorhombic, $a = 1207.9$, $b = 648.87$, $c = 426.20$ pm) the chain anions in [NH$_4$PO$_3$]$_x$ II ($P = 2$) are less stretched ($f_s = 0.82$). As pictured in Figure 4C these single chains are alternating with two different orientations regarding the axes P–P in the (001) plane (see chapter 4.3.2) along [100] similar to [NH$_4$PO$_3$]$_x$ IV (there: pairwise alternation). Furthermore comparisons of the two [NH$_4$PO$_3$]$_x$ modifications with their corresponding alkali catena-polyphosphates show that [NH$_4$PO$_3$]$_x$ II differs only marginally from [RbPO$_3$]$_x$ whereas [NH$_4$PO$_3$]$_x$ IV and [KPO$_3$]$_x$ have a greater structural discrepancy. This consequently points out the novelty of the *catena*-polyphosphate structure of [NH$_4$PO$_3$]$_x$ IV.

A)

B)   C)
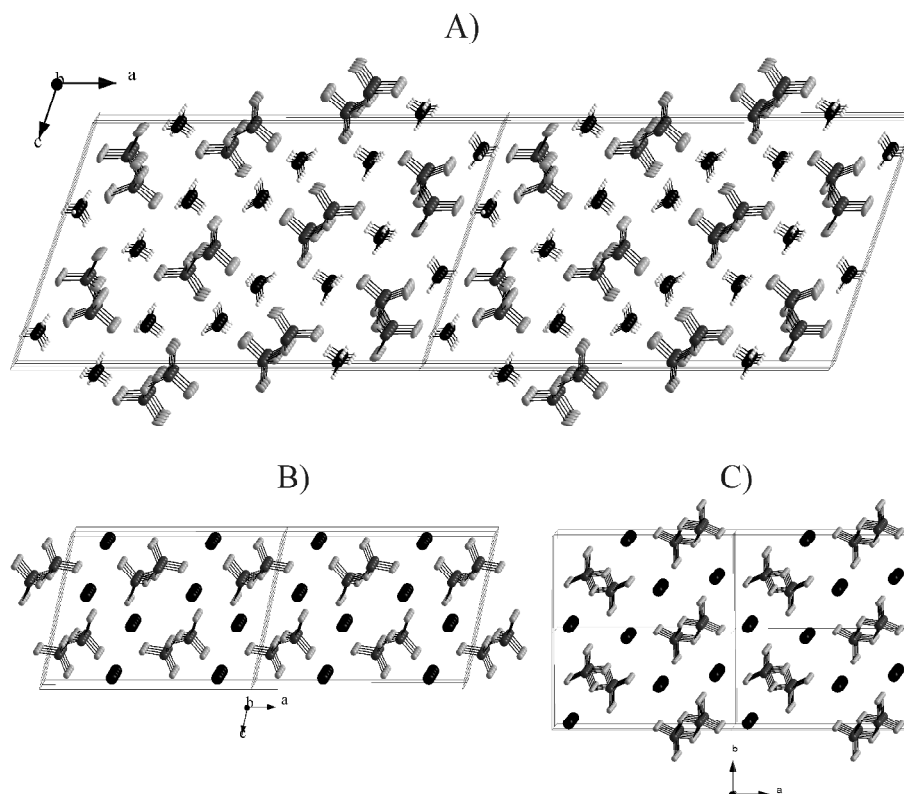
Figure 4. Perspective view of the crystal structures of [NH$_4$PO$_3$]$_x$ IV (A), [KPO$_3$]$_x$ (B) and [NH$_4$PO$_3$]$_x$ II (C) (N / K: black; H: white; P: dark gray; O: light gray).

4.4   VIBRATIONAL SPECTROSCOPY

An FT-IR spectrum of [NH$_4$PO$_3$]$_x$ IV was recorded in transmission geometry at room temperature in the range 4000–400 cm^{-1} with a Bruker IFS 66v/S spectrometer using the KBr pellet technique (2 mg sample, 300 mg dried KBr). A Raman spectrum was obtained by using a FRA 106/S Raman module operating with a Nd:YAG laser system ($\lambda = 1064$ nm). Figure 5 shows the vibrational spectra of the title compound [NH$_4$PO$_3$]$_x$ IV. In the IR spectrum intensive ν NH bands (maximum at 3243 cm^{-1}) with a δ NH frequency at 1692 cm^{-1} are visible.[15] Besides a couple of bands between 1750 and 2400 cm^{-1} that indicates the network of hydrogen bonds, a typical spectrum for a *catena*-polyphosphate is observed.[16] The characteristic frequencies such as ν_{as} PO$_2$ between 1350 and 1170 cm^{-1} with a maximum at 1251 cm^{-1} and the ν_{as} POP and the ν PO^{term} ranging from 780 to 1145 cm^{-1} with several maxima are detected with a very high intensity. In addition, the Raman spectrum shows strong vibrations in the region around 1139 cm^{-1} that unambiguously can be assigned with ν_s PO^{term}. In the region between 800 and 650 cm^{-1} the number of bands should correspond to the periodicity P of the phosphate chain.[16] With

maxima at 684 and 645 cm^{-1} ($\rightarrow P = 2$) the vibrational data agree well with the results from the crystal structure determination.
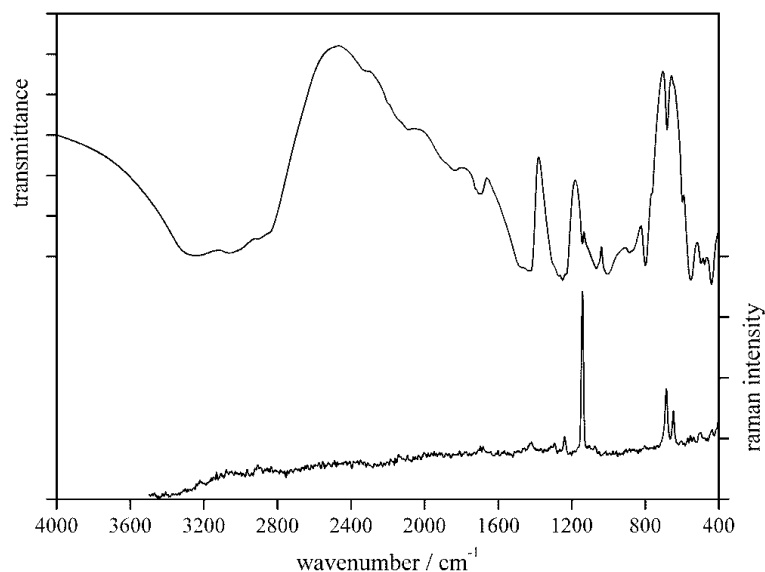
Figure 5. Infrared and Raman vibrational spectra of [NH$_4$PO$_3$]$_x$ IV.

4.5   CONCLUSION

In this contribution the single-crystal structure determination of ammonium catena-polyphosphate [NH$_4$PO$_3$]$_x$ IV, a compound that is known since the 1960s, is presented. A new synthesis method, namely heating NH$_4$H$_2$PO$_4$ in an ammonia gas flow with an elevated ammonia partial pressure enabled this investigation. [NH$_4$PO$_3$]$_x$ IV has been obtained phase-pure with an interesting feather-type morphology. The crystal structure of [NH$_4$PO$_3$]$_x$ IV turned out to be a novel *catena*-polyphosphate structure which is characterized by 'chemical twinning'. With extensive N-H···O hydrogen bonding and two different oriented chain anions $^1_\infty$[PO$_2$O$_{2/2}$]$^-$ ($P = 2$, $f_s = 0.94$) that run parallel [010], this 'chemical twinning' is realized. Double-layers of equally orientated chains are followed by double-layers with the second orientation. The measured vibrational spectra of [NH$_4$PO$_3$]$_x$ IV correspond well with the expected values for *catena*-polyphosphates and are in accordance with the results from the X-ray structure determination. By solving the synthetic challenge of synthesizing phase-pure [NH$_4$PO$_3$]$_x$ IV we were able to present the first single crystal structure elucidation of one of the five modifications of ammonium *catena*-polyphosphate, a multi-applicable compound.

4.6   REFERENCES

[1]   E. J. Griffith, T. M. Ngo, US Patent, US 4909902, **1990**.

[2]   E. J. Griffith, T. M. Ngo, US Patent, US 5362639, **1994**.

[3]   E. J. Griffith, T. M. Ngo, M. Veiderma, *Eesti Teaduste Akadeemia Toimetised*, *Keemia* **1993**, *42*, 113.

[4]   T. Futterer, *Speciality Chemicals Magazine* **2006**, *26*, 34.

[5]   C. Y. Shen, N. E. Stahlheber, D. R. Dyroff, *J. Am. Chem. Soc.* **1969**, *91*, 62.

[6]   B. Brühne, M. Jansen, *Z. Anorg. Allg. Chem.* **1994**, *620*, 931.

[7]   G. M. Sheldrick, SHELX97, Univ. Göttingen, **1997**.

[8]   A. L. Spek, *PLATON – A Multipurpose Crystallographic Tool*, Univ. Utrecht, **2003**.

[9]   K. H. Jost, *Acta Crystallogr.* **1963**, *16*, 623.

[10]   F. Liebau, *Structural Chemistry of Silicates*, Springer-Verlag, Berlin, **1985**, p. 80.

[11]   D. W. Cruickshank, *Acta Crystallogr.* **1964**, *17*, 681.

[12]   A. Immirzi, W. Porzio, *Acta Crystallogr., Sect. B: Struct. Sci.* **1982**, *38*, 2788.

[13]   S. Andersson, *Angew. Chem.* **1983**, *95*, 67; *Angew. Chem., Int. Ed. Engl.* **1983**, *22*, 69.

[14]   R. D. Shannon, C. T. Prewitt, *Acta Crystallogr., Sect. B: Struct. Sci.* **1969**, *25*, 925.

[15]   J. Weidlein, U. Müller, K. Dehnicke, *Schwingungsfrequenzen I*, Thieme, Stuttgart, **1981**.

[16]   A. Rulmont, R. Cahay, M. Liegeois-Duyckaerts, P. Tarte, *Eur. J. Solid State Inorg. Chem.* **1991**, *28*, 207.

5. High-pressure Synthesis and Structural Investigation of $H_3P_8O_8N_9$: A New Phosphorus(V) Oxonitride Imide with an Interrupted Framework Structure

As the experiments to synthesize PON as starting material according to literature methods yielded no satisfying results but instead moist and contaminated samples and a prominent flame retardant (see last chapter), it was decided to develop a new PON preparation method. The foundation of this synthesis strategy is i.e. illustrated in this contribution.

ABSTRACT

The first crystalline phosphorus oxonitride imide $H_3P_8O_8N_9$ $(=P_8O_8N_6(NH)_3)$ has been synthesized under high-pressure and high-temperature conditions. To this end, a new, highly reactive phosphorus oxonitride imide precursor compound was prepared and treated at 12 GPa and 750 °C by using a multianvil assembly. $H_3P_8O_8N_9$ was obtained as a colorless, microcrystalline solid. The crystal structure of $H_3P_8O_8N_9$ was solved *ab initio* by powder X-ray diffraction analysis, applying the charge-flipping algorithm, and refined by the Rietveld method ($C2/c$ (no. 15), $a = 1352.11(7)$, $b = 479.83(3)$, $c = 1820.42(9)$ pm, $\beta = 96.955(4)°$, $Z = 4$). $H_3P_8O_8N_9$ exhibits a highly condensed ($\kappa = 0.47$), 3D, but interrupted network that is composed of all-side vertex-sharing (Q^4) and only threefold-linking (Q^3) $P(O,N)_4$ tetrahedra in a Q^4/Q^3 ratio of 3:1. The structure, which includes 4-ring assemblies as the smallest ring size, can be subdivided into alternating open-branched zweier double layers $\{oB,2^2_\infty\}[^2P_3(O,N)_7]$ and layers containing pairwise-linked Q^3 tetrahedra parallel (001). Information on the hydrogen atoms in $H_3P_8O_8N_9$ was obtained by ^1D ^1H MAS, 2D homo- and heteronuclear (together with ^{31}P) correlation NMR spectroscopy, and a ^1H spin-diffusion experiment with a hard-pulse sequence designed for selective excitation of a single peak. Two hydrogen sites with a multiplicity ratio of 2:1 were identified and thus the formula of $H_3P_8O_8N_9$ was unambiguously determined. The protons were assigned to Wyckoff positions $8f$ and $4e$, the latter located within the Q^3 tetrahedra layers.

amorphous precursor   12 GPa, 750 °C   →   8 PON · NH₃
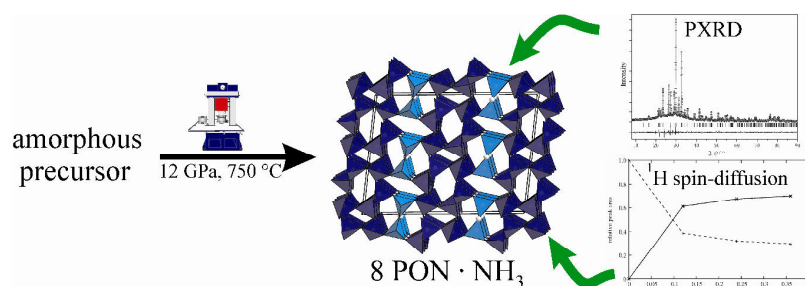
5.1   INTRODUCTION

Silica, one of the most abundant solid compounds on earth, occurs in a multitude of crystalline and amorphous forms and has different important industrial applications, for example, as a raw material for glasses, ceramics, and silicon, and as high-tech products such as quartz oscillators or optical waveguides.[1] Phosphorus oxonitride (PON) is isolobal and isoelectronic (valence electron concentration $VEC_{SiO2,PON}$=16/3) and consequently structurally and chemically analogous. Although known since 1846,[2] detailed information concerning PON was rather sparse for a long time due to difficulties in preparing crystalline samples. In addition, a large structural variety, comparable to SiO_2, has still not been achieved. With PON in the β-cristobalite,[3,4] moganite,[5,6] and quartz forms,[7] three crystalline polymorphs have been discovered so far.[8,9] Nevertheless, with the presence of nitrogen, there should exist a structural flexibility beyond the already huge number of theoretical possibilities connecting tetrahedra just by their vertices to form 3D networks. A (not verified) example would be an interrupted PON structure consisting of only PON_3 tetrahedra in which all nitrogen atoms are three-binding and the oxygen atoms are exclusively bound terminally.[10] With increasing nitrogen content, the diversity should further increase, however, most notably, more condensed framework structures can be generated while simultaneously causing a positive impact on properties (e.g., stability and hardness). Besides HPN_2, which crystallizes in the above-mentioned β-cristobalite- type structure,[11] in this respect, the phosphorus nitride imide HP_4N_7 and the phosphorus oxonitride P_4N_6O have been verified.[12,13] They both adopt two different structures with the motif of edge-sharing tetrahedra PN_4 and $P(NH)N_3$ or PON_3, respectively, in addition to simple vertex connections. Further increase of the content of nitrogen ultimately leads to the phosphorus nitride polymorphs of P_3N_5, α-P_3N_5,[14] in which edge-sharing PN_4 tetrahedra are also integrated, and γ-P_3N_5,[15] in which the network is built up of vertex-sharing PN_4 tetrahedra and also of distorted PN_5 square pyramids.

For the syntheses of these phosphorus (oxo)nitrides (imides), special procedures are often necessary. Although HP_4N_7 and highly crystalline α-P_3N_5, for example, are pre-pared by the thermal treatment of special single-source precursor compounds $(NH_2)_2P(S)NP(NH_2)_3$ and $P(NH_2)_4I$,[16,17] respectively, most of the others require extreme high-pressure and high-temperature conditions (e.g., 11 GPa and 1500 °C for γ-P_3N_5). The complexity of the syntheses, which results from the fact that crystallization and decomposition temperatures are usually rather close (around 750 °C at normal pressure),[18] and challenging analytical aspects (localization of H, O/N differentiation) may be the

reasons for the small number of compounds known within this compound class. As the synthesis, identification, and structural characterization of new phosphorus (oxo)nitrides (imides) seem to be a challenge, an innovative synthetic approach combined with sophisticated analysis is demanded.

Solid-state NMR spectroscopy is a convenient quantitative element-selective analytical technique that has proven its potential for the characterization of oxonitridophosphates before.[19,20] However, as often no phase-pure samples are available in the P/O/N system, one faces the problem that the ^1H and ^{31}P NMR peaks partially overlap with peaks from different side phases. 2D correlation spectroscopy is one time-consuming option to achieve unambiguous peak assignment under these conditions. A poor signal-to-noise ratio and probe background may make 1D ^1H spin-diffusion experiments based on homonuclear zero-quantum dipolar recoupling experiments such as RFDR,[21] fpRFDR,[22] RIL,[23] or supercycled R sequences[24] the better choice, however. 1D spin-diffusion experiments require selective excitation of individual peaks for which many solutions exist in liquid-state NMR spectroscopy.[25] Selective pulses in solid-state 1H NMR spectroscopy often suffer from relaxation and high-order multiquantum generation the longer the applied pulse sequence, which makes application of typical liquid schemes difficult, even though soft Gaussian pulses[26] have been shown to be efficient in some cases. A good alternative could be composite pulses comprising short, hard pulses and short periods of free evolution,[24,27,28] which prove to be efficient even when $T_{1\rho}$ is short. The extreme case is the DANTE[29] sequence, which often, however, turns out to be too long for efficient selective excitation.

In this contribution, we report on the synthesis and structural investigation of the first crystalline PON imide $H_3P_8O_8N_9$, which exhibits an interrupted, but highly condensed framework structure. Besides *ab initio* structure solution from powder X-ray diffraction data and analysis of the hydrogen content by solid-state ^1H NMR spectroscopy, this contribution also includes the preparation of a new, highly reactive PON imide precursor compound that is comprehensively well suited to the high-pressure synthesis of highly condensed P/O/N/(H) compounds. Similar systems are currently being investigated for their catalytic properties. In the last few years, related polymeric C/N/H compounds have proved to be effective photocatalysts with visible light.[30] Nowadays, phosphorus-doped C/N/H systems[31] or even P/O/N/H compositions are also the focus of the catalysis research community. In this respect, the performance of materials is predominantly investigated without gathering any detailed structural information (systems are rather

undefined). However, we can now provide an idea of how structural features could look in complex P/O/N/H compounds. Thus, deeper insights into the mechanisms of catalysis, for example, could possibly be acquired.

5.2   RESULTS AND DISCUSSION

5.2.1   Synthesis

Diverse synthetic approaches have been reported in the literature for the synthesis of PON.[3,32–34] Some of these methods are rather specific and thus difficult to perform, some yield quite humid samples, and many of them are rather susceptible to contamination. The most defined procedure for obtaining PON, however, is the thermal decomposition of water-sensitive phosphoryl triamide $(PO(NH_2)_3)$.[35] However, this demands the phase-pure synthesis of this molecule,[36] which requires a laborious purification procedure. For a more simple access to pure and dry PON, we have developed a route starting from a mixture of $PO(NH_2)_3$ and NH_4Cl, which is obtained from the reaction of $POCl_3$ with ammonia and subsequently used without any further purification. By heating this mixture in a continuous flow of ammonia at 300 and 620 °C, respectively [Eq. (1)], the condensation of $PO(NH_2)_3$ towards PON (but right before its crystallization at around 700 °C) and the complete removal of NH_4Cl is achieved simultaneously in a single step.

$$PO(NH_2)_3 + 3\ NH_4Cl \xrightarrow[\text{-2NH}_3\ \text{-3NH}_4\text{Cl}]{\text{NH}_3\text{-flow, 620°C}} \text{``}PO_{0.88}N_{1.24}H_{0.56}\text{''} \qquad (1)$$
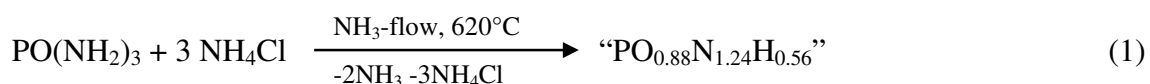
An amorphous and slightly nitrogen-enriched (by reaction with NH_3) phosphorus oxonitride imide is obtained in the form of a dry, colorless powder, which is a basic precursor for P/O/N chemistry. With a higher reactivity than crystalline PON, it has proved its worth as a starting material for the synthesis of the oxonitridophosphates $AE_3P_6O_6N_8$ (AE = Sr, Ba).[19,37] Furthermore, this P/O/N/H powder is also an excellent precursor for the fabrication of crystalline PON polymorphs. By tempering at 750 °C in an evacuated silica glass ampoule, the condensation reaction is easily completed and highly crystalline cristobalite PON is obtained. Quartz-type PON can be generated from it at 6 GPa and 750 °C.

The impact of our amorphous P/O/N/H precursor also becomes apparent in the synthesis of the first crystalline PON imide, namely $H_3P_8O_8N_9$, presented in this contribution. This compound, which can be formulated as $8PON·NH_3$, is formed under

extreme conditions at 12 GPa and around 750 °C. At such a high pressure, the elimination of any remaining ammonia within the precursor, and thus complete condensation to crystalline PON, is suppressed. As observed with other compounds in which decomposition was prevented,[38] this is a big advantage of high-pressure chemistry. Thus, under these conditions, we were able to crystallize the precursor material [Eq. (2)]. Under ambient pressure the synthesis of $H_3P_8O_8N_9$ is not yet feasible.

$$9.09\ ``PO_{0.88}N_{1.24}H_{0.56}" \longrightarrow H_3P_8O_8N_9 + ``H_{2.09}P_{1.09}N_{2.27}" \tag{2}$$
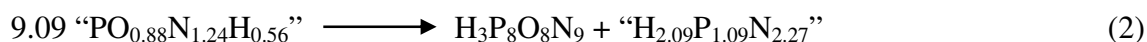
5.2.2 Powder X-ray diffraction

Powder X-ray diffraction data were recorded from a powdered sample enclosed in a glass capillary (for details see the Experimental Section). All the observed reflections were indexed on the basis of monoclinic unit cell parameters ($a = 1351.18$, $b = 479.46$, $c = 1818.98$ pm, $\beta = 96.918°$) and thus $H_3P_8O_8N_9$ turned out to be the only crystalline phase. A P/N/H-containing side-product obtained from the formal reaction in Equation (2) is amorphous, as is indicated by the elevated background in the diffractogram (cf. Figure 10) and additional signals in the ^1H NMR spectrum (see the solid-state NMR study section).

In accord with the systematic extinction conditions hkl ($h+k \neq 2n$) and $00l$ ($l \neq 2n$), which correspond to a C-centering and a c glide plane, respectively, the space groups Cc (no. 9) and $C2/c$ (no. 15) were considered. During *ab initio* structure solution and refinement the centrosymmetric space group turned out to be the correct one. In $C2/c$, a Rietveld refinement was performed with a structure model that included four phosphorus and nine oxygen and nitrogen atoms in the asymmetric unit. However, this structure model was incomplete in terms of the hydrogen positions as they cannot be detected by X-ray diffraction due to their low scattering power. Information about the hydrogen atoms in $H_3P_8O_8N_9$ is included in the following solid-state NMR study section.

Detailed information concerning data collection, structure solution, and refinement, and further crystal data are presented in the Experimental Section and in Tables 3 and 4.

5.2.3 Solid-state NMR study

The synthesized material is a multiphase mixture that contains both amorphous and crystalline contributions. It was not possible to clarify the number of hydrogen sites and their relative frequency from the diffraction study. To this end we performed ^{1}H and ^{31}P MAS NMR experiments. In a first step, we identified peaks belonging to the crystalline phase in the 1D MAS and 2D homo- and heteronuclear correlation spectra. In a second step, we probed the ^{1}H resonances of the crystalline title compound through a ^{1}H spin-diffusion experiment, which starts with the polarization of a single resonance. We chose a resonance that we unambiguously identified as belonging to $H_3P_8O_8N_9$. For long mixing times, the spin-diffusion experiment gives rigorous constraints for the number and relative frequency of hydrogen sites.
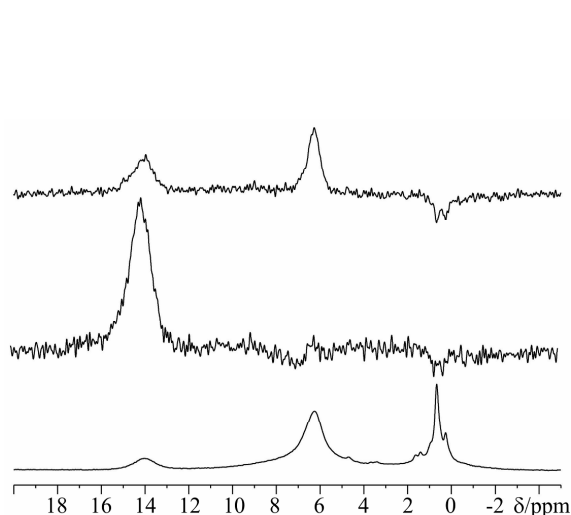
Figure 1. ^{1}H NMR spectra of the $H_3P_8O_8N_9$; bottom: spectrum obtained by direct excitation, middle: selective excitation with pulse sequence B (see Figure 4) of the peak at 14.6 ppm (H_A), top: selective excitation followed by longitudinal magnetization transfer and a mixing time τ_{mix} of 120 μs; Redistribution of magnetization can be observed on H_B at 6.8 ppm.
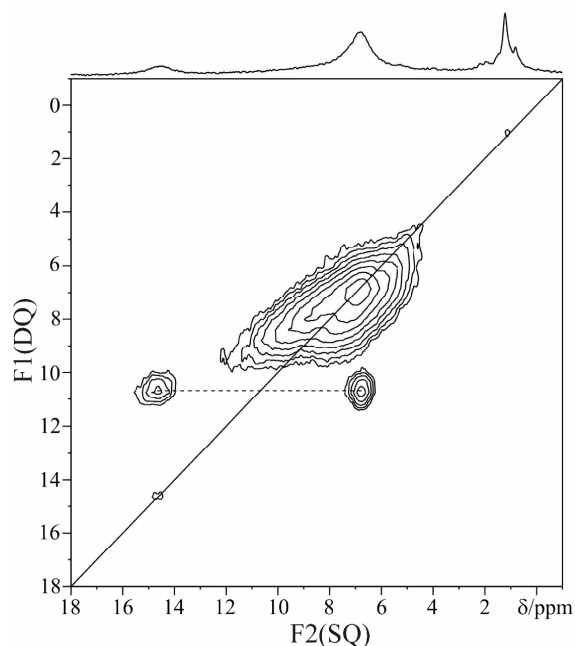
Figure 2. ^{1}H MAS NMR DQ-SQ correlation spectrum of the synthesized material; the solid diagonal line indicates the position of DQ coherence of two isochronous ^{1}H nuclei; the dashed line connects the two peaks arising from H_A and H_B in the crystalline phase.

First, 1D ^{1}H MAS (Figure 1) and 2D double-quantum (DQ) single-quantum (SQ) correlation (Figure 2) MAS NMR spectra were acquired. Because the linewidths of resonances from well-ordered commensurate crystalline materials are supposed to be significantly smaller than those of peaks from amorphous matter, we assigned the broad resonance at 5–12 ppm (see Figure 2) to an amorphous contribution and the sharp peaks at

14.6 and 6.8 ppm (peaks H_A and H_B, respectively; see Figures 1 and 2) were assigned to crystalline $H_3P_8O_8N_9$. The sharp peaks below 1 ppm were assigned to silicon grease. Although the peak at 6.8 ppm, caused by $H_3P_8O_8N_9$, strongly overlaps the amorphous contribution, the peak at 14.6 ppm is well resolved. This circumstance turns out to be useful in the following: A selective $^{31}P\{^1H\}$ CP-RAMP experiment[39] (see Figure 3) indicates that the resonance at 0.8 ppm in the ^{31}P MAS NMR spectrum belongs to the crystalline phase. The broad contribution from the amorphous component was only observed in a nonselective $^{31}P\{^1H\}$ CP-RAMP experiment.
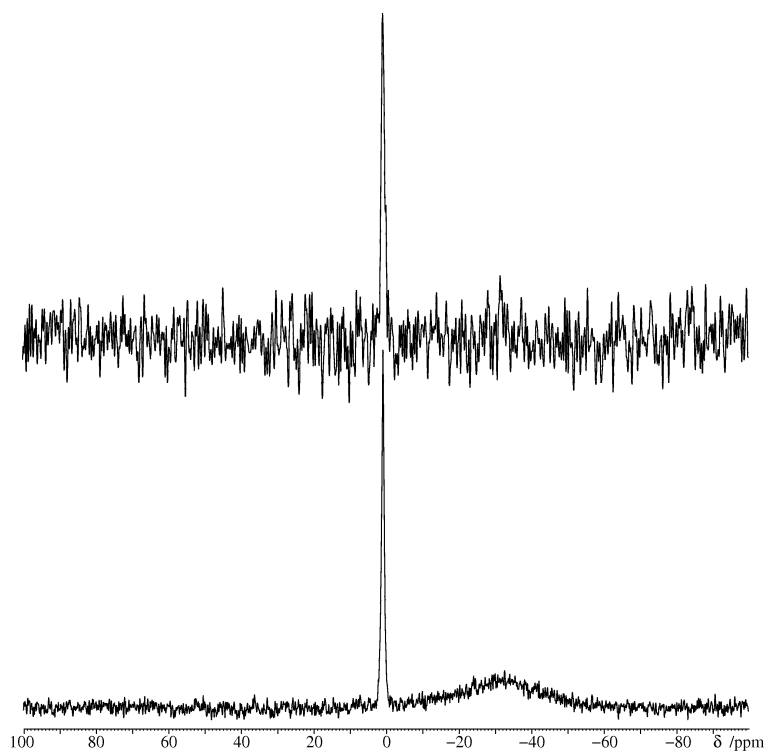
Figure 3. Non-selective $^{31}P\{^1H\}$ CP-RAMP experiment (bottom); selective $^{31}P\{^1H\}$ CP-RAMP experiment (top); contribution from the broad amorphous component can only be observed in the non-selective experiment;
Recycle delays for both experiments were set to 4 s; The non-selective CP-RAMP experiment was recorded with a contact time of 5 ms and accumulated 128 transients using an 8-step phase cycle. The selective CP-RAMP experiment had a contact time of 4 ms and accumulated 2048 transients. It used a 512-step phase cycle.

After assigning the peaks at 14.6 and 6.8 ppm in the 1D ^1H MAS NMR spectrum to the $H_3P_8O_8N_9$ it was still not clear whether additional ^1H peaks of the crystalline phase exist that could not be resolved in the 2D DQ–SQ correlation spectrum. To this end we prepared for polarization on the peak at 14.6 ppm with the help of a series of three pairs of pulses with a flip angle of 90° (see pulse sequence A in Figure 4). The pulses were on-resonance with respect to peak H_A and the three delays were optimized to achieve a good suppression of all peaks between 2 and 12 ppm.[27] We selectively prepared for polarization on the peak at 14.6 ppm and spin diffusion was driven with the help of supercycled $R6_6^2$ with the R-element $90_{180}270_0$,[24] which generates a zero-quantum Hamiltonian, so that the polarization is redistributed between all ^1H atoms in the crystalline phase. Variable mixing times

(τ_{mix}) are generated by repeating full R cycles. Clearly, at long mixing times, only the already observed sharp component H_B gains in intensity. We conclude that only the peaks H_A and H_B can be assigned to the crystalline phase and no other hidden signals exist. The sum of all the I_z operators over all the coupling spins is a constant of motion because it commutes with the Hamilton operator provided by $SR6_6^2$.[24] Therefore we plotted the relative peak area for the two observed peaks as a function of mixing time τ_{mix} (Figure 5). At long mixing times, spin diffusion is close to the equilibrium value, which reflects the relative frequency of the hydrogen sites in the crystal structure. The peak area ratio of $0.66 : 0.33$ for H_B/H_A indicates that two hydrogen sites with a multiplicity ratio of $2 : 1$ exist in the crystal structure. This permits the calculation of an empirical formula.

Starting first with $P_8O_a(NH)_bN_c$, one can easily calculate the correct formula consulting the edge conditions of the number of anion sites [Eq. (3)] and the charge balance [Eq. (4)].

$$(a + b) + c = 17 \qquad (3)$$

$$2(a + b) + 3c = 40 \qquad (4)$$

By entering Equation (3) solved for c into Equation (4), with the result for $(a + b) = 11$, the single indices a, b and c are determinable to be $a = 8$, $b = 3$ (from the hydrogen site ratio $2 : 1$, see above) and $c = 6$. Consequently, the formula has to read $P_8O_8(NH)_3N_6$ (=

Figure 4. NMR pulse sequences used for site-selective preparation of polarization on peak H_A (sequence B) and selective preparation followed by spin diffusion (sequence A);[24] the sample rotation period and the mixing time for spin diffusion are denoted as τ_r and τ_{mix}, respectively; spin-diffusion was driven by supercycled $R6_6^2$ ($SR6_6^2$);[24] a variable number of $SR6_6^2$ blocks defines distinct mixing times τ_{mix}; delays τ_1, τ_2 and τ_3 were chosen so as to suppress unwanted peaks; for a detailed description of the $SR6_6^2$ sequence see ref. [24], we applied the basic R-element $90_{180}270_0$, the supercycling scheme consists of a phase inversion step, that is, $R6_6^2$ followed by $R6_6^{-2}$ and additional two steps in which all pulse phases of $R6_6^2R6_6^{-2}$ are incremented by 120 and 240°, that is, $R6_6^2(120)R6_6^{-2}(120)$ and $R6_6^2(240) R6_6^{-2}(240)$.

$H_3P_8O_8N_9$). Within the accuracy of the method, this was confirmed by semi-quantitative EDX analyses (calcd ratio N/O = 1.1, exptl ratio N/O = 1.3).
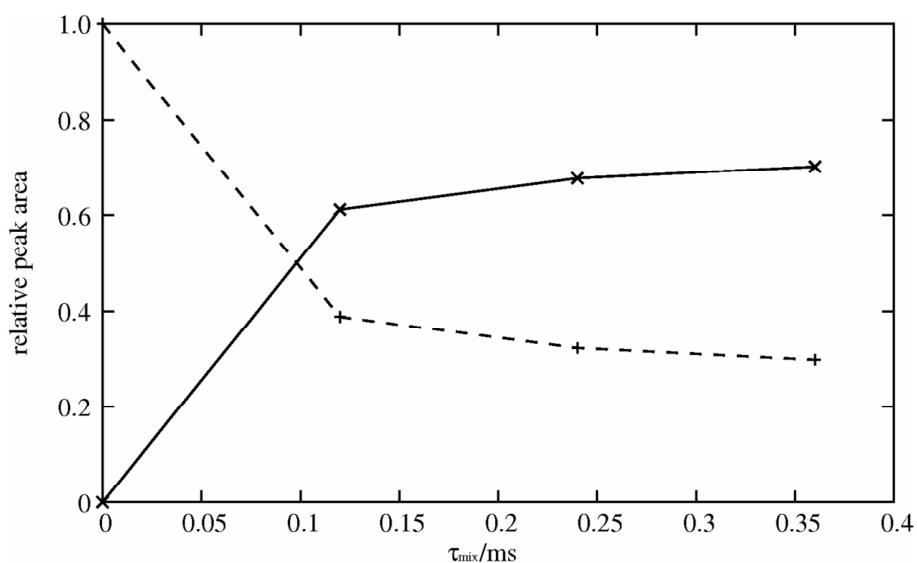
Figure 5. Relative peak areas of the ^1H NMR resonance at 14.6 (dashed line) and 6.8 ppm (solid line) observed after a homonuclear dipolar mixing time τ_{mix}; lines serve only as a guide to the eye; homonuclear dipolar interactions were recoupled with $SR6_6^2$; the peak area ratio 0.66 : 0.33 for H_B/H_A indicates two distinct hydrogen sites in the crystal structure with a ratio in multiplicity of 2 : 1.

5.2.4   Structure Description and Discussion

Despite a formula unlike TX_2 and a corresponding degree of condensation $\kappa < ½$, which is defined as the atomic ratio of tetrahedral centers and bridging atoms, the new phosphorus oxonitride imide $H_3P_8O_8N_9$ exhibits a 3D network of vertex-sharing $P(O,N)_4$-tetrahedra (Figure 6). According to the formula $_{\infty}^{3}\left[\left(P_8^{[4]}O_2^{[1]}O_6^{[2]}N_9^{[2]}\right)^{3-}\right]$, which includes terminal oxygen atoms, in addition to all-side-bridging Q^4-type tetrahedra, this network also consists of only threefold-bridging Q3-type tetrahedra, which interrupt the framework. With a 3:1 molar ratio of Q^4/Q^3 tetrahedra and a corresponding high framework density (FD = 27.3 T-atoms 1000 $Å^{-3}$), $H_3P_8O_8N_9$ is quite exceptional among the small group of known "interrupted frameworks". Of these few compounds, mainly consisting of (alumino)silicates,[40–46] the proportion of Q^3 tetrahedra is usually rather high, with framework densities comparable to zeolite-type materials (FD < 21 T-atoms 1000 $Å^{-3}$).[47] A very complex interrupted open framework that also includes Q^2 tetrahedra is present in the nitridosilicate $M_7Si_6N_{15}$ (M = La, Ce, Pr).[48] The reason for the high density of the framework of the title compound may lie in the fact that it is a cation-free interrupted network, the first crystalline cation-free interrupted network to our knowledge. Within

phosphorus (oxo)nitride(s) (imides) and the Si/(O)/N/(H) system, no crystalline interrupted 3D network has been observed so far. These compounds are rather more highly condensed with structural motifs of edge-sharing tetrahedra in P_4N_6O[13] or HP_4N_7[12] and three-binding nitrogen atoms in Si_2N_3H[49] or Si_2N_2O.[50] The sparsity in the class of interrupted tetrahedra frameworks, also with cations, is due to the fact that less condensed frameworks (with $\kappa \leq 1/2$), primarily silicates,[51] tend to form layered or lesscondensed structures instead. Consequently the highly condensed network of $H_3P_8O_8N_9$ is unique in this respect and has to be classified, with $\kappa = 0.47$, directly before a 3D TX_2 tetrahedra framework.
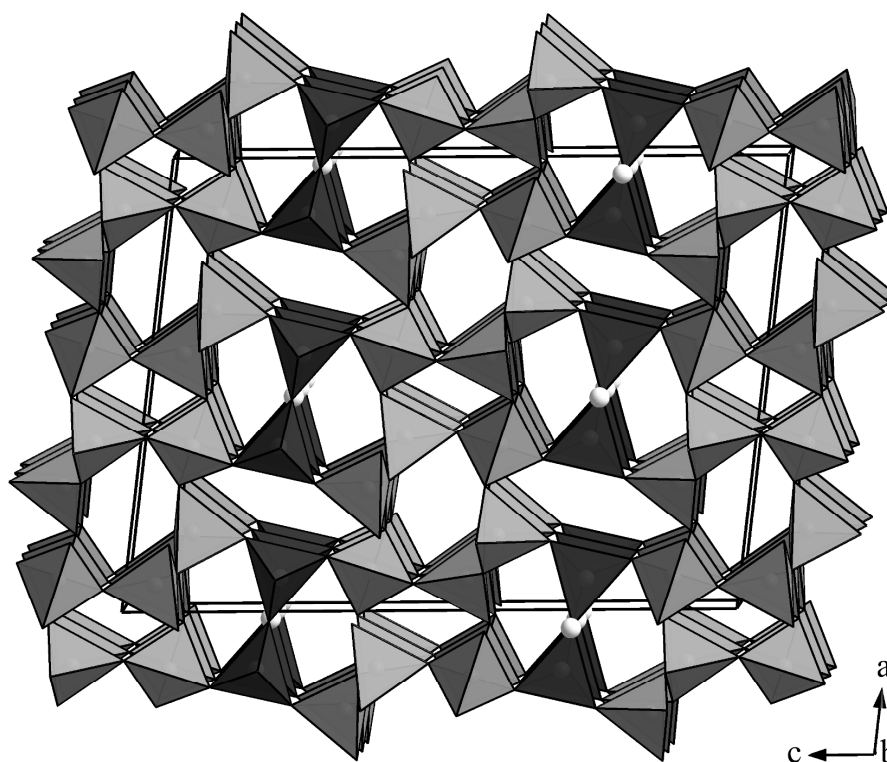
Figure 6. Crystal structure of $H_3P_8O_8N_9$, view along [010]; the interrupted 3D network of vertex-sharing $P(O,N)_4$-tetrahedra is composed of Q^4 (light gray) and Q^3 tetrahedra (dark gray), the hydrogen atoms (white balls) are placed on the $4e$ position within the Q^3 tetrahedra layer.

The crystal structure of $H_3P_8O_8N_9$ is shown in Figure 6. As indicated by differently shaded tetrahedra, the topology can be subdivided into two different layerlike sections parallel to (001). Condensed double layers composed of Q^4 tetrahedra (light gray) and layers containing Q^3 tetrahedra (dark gray) alternate along [001]. The double layers consist of two 8-ring single layers, which are connected to each other by a rotation of 180° (Figure 7). According to Liebau,[51] the 8-ring single layers can be described as open-branched zweier single layers $\{oB,1^2_\infty\}[^2P_3(O,N)_7]$ built of zweier single chains with single tetrahedra as side-chains running parallel to [010] (Figure 7, left). This kind of chain is in-

corporated as a substructure in HP_4N_7[12] and in the silicate chain astrophyllite.[52] The entire double layer is described as an openbranched zweier double layer $\{oB,2^2_\infty\}[^2P_3(O,N)_7]$ (Figure 7, right).
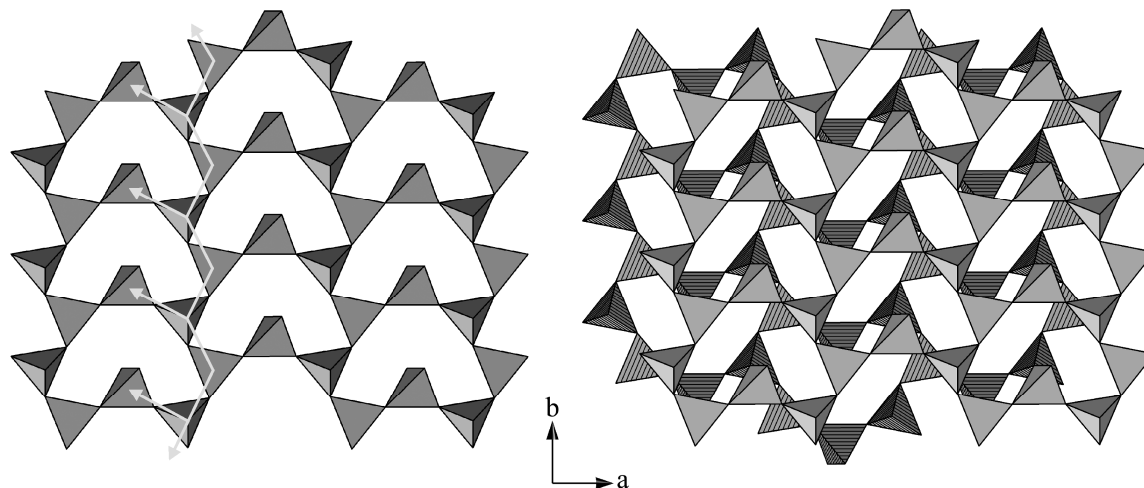
Figure 7. Left: An 8-ring single-layer and right: an 8-ring double-layer parallel to (001) as substructures in $H_3P_8O_8N_9$; the light gray arrow marks the open-branched zweier single-chain.

The layer containing the Q^3 tetrahedra is shown in Figure 8, left. The Q^3-tetrahedra are linked pairwise and all point, in each layer, with their terminally bound oxygen atoms in the same direction. As the space group $C2/c$ is a nonpolar space group, for balance, the pointing direction alternates ([010] and [0-10]) from layer to layer. Altogether the 8-ring double layers and the Q^3 tetrahedra-pair layers form the interrupted network of $H_3P_8O_8N_9$. The coordination sequences and the vertex symbols for the framework are given in Table 1.
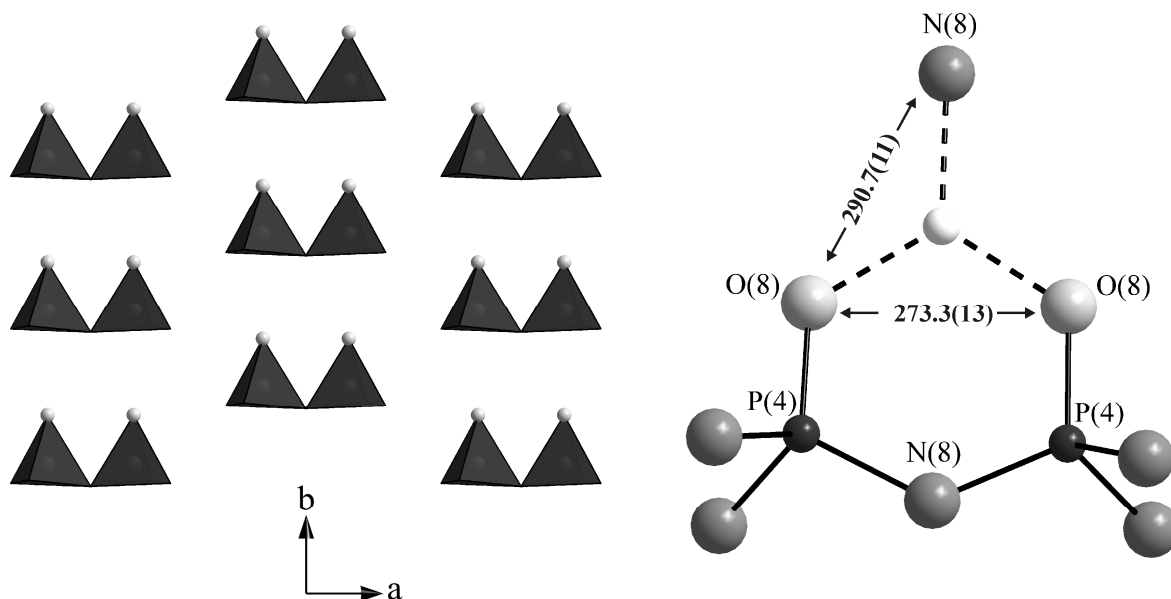
Figure 8. Left: Layer of pairwise linked Q^3-tetrahedra in $H_3P_8O_8N_9$; right: a Q^3 tetrahedra pair with a hydrogen atom placed at the $4e$ position between the terminal oxygen atoms O(8) and bridging nitrogen N(8) resulting in a bifurcated hydrogen bridge.

Table 1. Coordination Sequence and Vertex symbols for the framework in $H_3P_8O_8N_9$ (analyzed with the program TOPOPOL[†]).

atom, Wyckoff symbol	Coordination Sequence	Vertex Symbol
P(1), 8f	1 4 10 23 44 72 99 135 179 222 274 345 385 470 550 611 708	$4.8_2.5.6_2.8_2$
P(2), 8f	1 4 11 24 45 68 100 136 174 225 275 335 400 466 534 628 702	$5.6.6.9_3.8.8_5$
P(3), 8f	1 4 11 24 45 70 102 134 172 226 283 324 405 464 536 628 707	$4.8_2.5.6.6.8_3$
P(4), 8f	1 3 8 19 44 58 96 132 171 216 271 319 397 456 529 607 704	$5.5.8_2$

The described topology of $H_3P_8O_8N_9$ is reflected in the observed $P_n(N/O)_n$ ring sizes and their relative frequency, that is, the cycle class sequence according to Klee.[53] The cycle class sequences for the frameworks of several phosphorus (oxo)nitride(s) (imides) and one of the highest condensed interrupted networks (in $M_6Si_{10}O_{23}$ (M = Rb, Cs)) are listed in Table 1 (calculated with the program TOPOLAN).[54] In contrast to $M_6Si_{10}O_{23}$ (M = Rb, Cs) and the three polymorphs of PON, with the exception of 2- and 3-rings, all ring sizes exist in $H_3P_8O_8N_9$. The smaller four, five, and six rings are visible in Figure 6. More small rings, as well as edge-sharing tetrahedra (= 2-rings), are present in highly condensed networks, such as P_4N_6O,[13] HP_4N_7,[12] and α-P_3N_5.[14]

† M. M. J. Treacy, S. Srivilliputhur, M. D. Foster, K. Randall, *TOTOPOL – A Topological Analysis Tool*, Version 1.68, **2010**: http://www.hypotheticalzeolites.net/NEWDATABASE/TOPO/upload_cif.html.

Table 2. Cycle class sequence of the interrupted framework of $H_3P_8O_8N_9$ in comparison to that of frameworks of $M_6Si_{10}O_{23}$ (M = Rb, Cs), cristobalite, moganite, and quartz PON, P_4N_6O, HP_4N_7 and α-P_3N_5.

$P_n(O,N)_n$-rings	2	3	4	5	6	7	8	9	10
$M_6Si_{10}O_{23}$ (M=Rb, Cs)	-	-	-	-	9	-	-	-	42
$H_3P_8O_8N_9$	-	-	2	4	4	4	30	32	88
cristobalite PON	-	-	-	-	4	-	6	-	48
moganite PON	-	-	2	-	4	-	32	-	108
quartz PON	-	-	-	-	3	-	21	-	30
P_4N_6O	2	-	2	8	16	40	132	296	852
HP_4N_7	4	-	4	16	60	72	252	520	1752
α-P_3N_5	2	-	2	8	26	52	168	416	1302

In the Rietveld refinement, the bond lengths P–(O,N) were constrained to 157 pm, the mean value of P–(O,N) distances in the polymorphs of PON, which have an atomic ratio O/N most comparable to that in $H_3P_8O_8N_9$. With a certain permitted deviation, the distances P–(O,N) vary between 154.4 and 162.5 pm, with the shortest distance in the Q^3 tetrahedron between P(4) and the nonbridging O(9). The shortening of the bond lengths to terminal O,N atoms compared with bridging O,N atoms is typical of both phosphate[55] and silicate chemistry.[51] The angles (O,N)–P–(O,N) ranging between 101.5 and 116.4° are on average (109.4°) similar to the angle of a regular tetrahedron. The angles P–(O,N)–P between 127.7 and 144.4° are also typical of P/O/N networks. Selected bond lengths and angles are given in Table 2.

Table 3. Selected interatomic distances / pm and angles / ° in $H_3P_8O_8N_9$ (esd's in parentheses).

P(1)–(O,N)	156.2(6), 160.0(6), 160.1(6), 162.5(6)	
P(2)–(O,N)	156.2(5), 157.1(6), 157.7(5), 159.1(4)	
P(3)–(O,N)	157.3(5), 159.9(5), 160.3(6), 160.4(6)	
P(4)–(O,N)	154.4(5), 157.4(6), 158.6(7), 161.2(6)	
P–(O,N)–P	127.7(2)–144.4(3)	8 times
(O,N)–P(1)–O,N)	105.5(4)–111.8(4)	6 times
(O,N)–P(2)–(O,N)	105.1(3)–116.4(3)	6 times
(O,N)–P(3)–(O,N)	106.1(3)–112.8(3)	6 times
(O,N)–P(4)–O,N)	101.5(3)–114.3(3)	6 times

From the structure solution and solid-state NMR study, the empirical formula of $H_3P_8O_8N_9$ was unambiguously determined. To establish the formula of this oxonitride directly by X-ray diffraction is impossible as differentiation between oxygen and nitrogen is not feasible due to their similar scattering factors. In general we assume a statistical O/N

distribution in the network of $H_3P_8O_8N_9$. This assumption is reasonable because in PON polymorphs and other oxonitridic TX_2 networks[3,6,7,56,57] no O/N ordering was experimentally observed by neutron diffraction. However, in the Rietveld refinement, we occupied the terminal and bridging positions by linking the Q^3 tetrahedra (three-binding situation with hydrogen, see below) exclusively with oxygen and nitrogen, respectively, as such an assignment is chemically reasonable by taking into account Pauling's rules and experiences with other oxonitridic compounds.[19,58] For the other twofold bridging positions, mixed positions with 4/7 N and 3/7 O were assumed to guarantee the O/N ratio of 8 : 9 in the formula. Other ordered or disordered models may also be possible. Acquiring information on the O/N distribution by lattice energy calculations (MAPLE)[59] has so far not been successful.

The charge on the polymeric anion $[P_8O_8N_9]^{3-}$ is balanced by the incorporation of protons into the structure. According to the solid-state NMR study, per formula unit, there are three protons separated over two sites with a multiplicity ratio of 2 : 1. As only eight and fourfold positions exist in space group $C2/c$, one can assign the hydrogen atoms to the corresponding Wyckoff positions 8f and 4a to 4e, respectively. Although an unambiguous, chemically reasonable localization of the hydrogen atom in the general 8f position is not successful because of too many possibilities in the large unit cell, for the hydrogen atom in the fourfold position, however, there is a predestined position (4e) in the structure. This probable hydrogen position is located in the Q^3 tetrahedra pair layer between the terminal O(8) and the bridging N(8) atoms. As shown in Figure 8, right, in this location, a bifurcated asymmetric hydrogen bridge with proton donor–acceptor distances of 273.3 and 290.7 pm, respectively, can be formed. With the determined amount of incorporated hydrogen, $H_3P_8O_8N_9$ exhibits ammonia molecules and PON in a ratio of 1 : 8 ($P_8O_8N_8 \cdot NH_3$). A comparable compound in this respect, in which the TX_2 network to ammonia ratio is 1 : 4, is the phosphorus nitride imide $P_4N_4(NH)_4 \cdot NH_3$.[60] However, in this case, as this compound is a nitridic clathrate, the ammonia molecules are not incorporated into the structure with an effect of interruption, but encapsulated within $4^2 8^4$ cages.

5.3   CONCLUSION

Herein we have presented the high-pressure synthesis and structural elucidation of the first phosphorus oxonitride imide $H_3P_8O_8N_9$. It was prepared by a new synthetic strategy based on an activated amorphous P/O/N/H phase obtained by thermal precondensation of a mixture of $PO(NH_2)_3$ and NH_4Cl. Note that this synthetic strategy provides various possibilities for the preparation of P/O/N compounds in general. It allows the chemist to create differently modified precursor compounds depending on the intended product.

With its highly condensed, 3D, but interrupted framework structure, $H_3P_8O_8N_9$ is an unexpected and very exceptional compound among the huge class of tetrahedra-based networks, which is now significantly expanded. Although the crystal structure was solved *ab initio* from powder X-ray diffraction data, information concerning the hydrogen content in the structure was obtained from ^1H and ^{31}P MAS NMR experiments. ^1H spin-diffusion experiments combined with spectral editing techniques may generally prove useful because of the high sensitivity of 1H NMR spectroscopy. In this case a few milligrams of a heterogeneous mixture were sufficient for all experiments and allowed ^1H NMR peaks to be assigned to particular Wyckoff positions and thus the localization of protons in the structure. These protons can possibly become mobile at elevated temperatures (up to the decomposition temperature of about 700 °C) and travel on pathways through, for example, the more open Q^3 tetrahedra layers. Verification of whether $H_3P_8O_8N_9$ is a potential proton conductive material[61] is the subject of ongoing investigations.

Unexpectedly, by treating a P/O/N/H-containing precursor under conditions of 12 GPa and 750 °C we observed the crystallization of $H_3P_8O_8N_9$ instead of a PON polymorph. We thus anticipate that at higher synthesis temperatures, full condensation with elimination of the remaining ammonia may be achieved, and so possibly unprecedented PON polymorphs with a structure beyond those known for SiO_2 could form. Moreover, under high pressure, there is the chance to realize increased coordination numbers at phosphorus (CN = 5 or 6); this would give a material with extreme hardness even if three-binding nitrogen atoms are also involved. By performing experiments in diamond anvil cells (DAC), in which pressures of up to 200 GPa are feasible,[62] the potential for a stishovit polymorph of PON, for example, should be unequivocally improved.

5.4   EXPERIMENTAL SECTION

5.4.1   Synthesis

The synthesis of $H_3P_8O_8N_9$ is tripartite. In the first step, a mixture of phosphoryl triamide ($PO(NH_2)_3$) and ammonia chloride (NH_4Cl) in a molar ratio 1 : 3 was prepared in a modified version of a procedure described by Klement and Koch.[36] In a flame-dried three-necked 1 L flask excess ammonia (ca. 250 mL; Messer Griessheim, Sulzbach, Germany, 3.8), previously piped through a gas purifier (SAES Pure Gas, Inc., San Luis Obispo, USA), was condensed at −78 °C. Freshly distilled $POCl_3$ (20 mL; Acros Organics, Geel, Belgium) was added directly and slowly over 4 h through a syringe under vigorous stirring. After further stirring for 2 h at −78 °C, the suspension was warmed to room temperature and then excess NH_3 was removed. The colorless and water-sensitive product mixture ($PO(NH_2)_3/3NH_4Cl$; 20.4 g, 100% conversion) was stored in a glovebox (MBraun, Garching, Germany) filled with dry argon.

In the second step, a finely ground portion of the mixture (ca. 2.5 g) was transferred into a silica glass boat and placed in a silica glass tube in the center of a tube furnace. The sample was heated at 300 and 620 °C for 5 and 12 h, respectively (heating rate 5 °Cmin^{-1}) under a continuous flow of ammonia gas (0.125 mLs^{-1}). A dry and colorless powder was obtained (theoretical yield: 24.7; found: 26.1%). X-ray diffraction, elementary analysis (Co. Pascher, Remagen, Germany: P 47.9, O 21.8, N 26.8, H 0.9%), and FT-IR spectroscopy (cf. Figure 9) revealed a chlorine free, amorphous phosphorus oxonitride imide with formula sum $PO_{0.88}N_{1.24}H_{0.56}$.
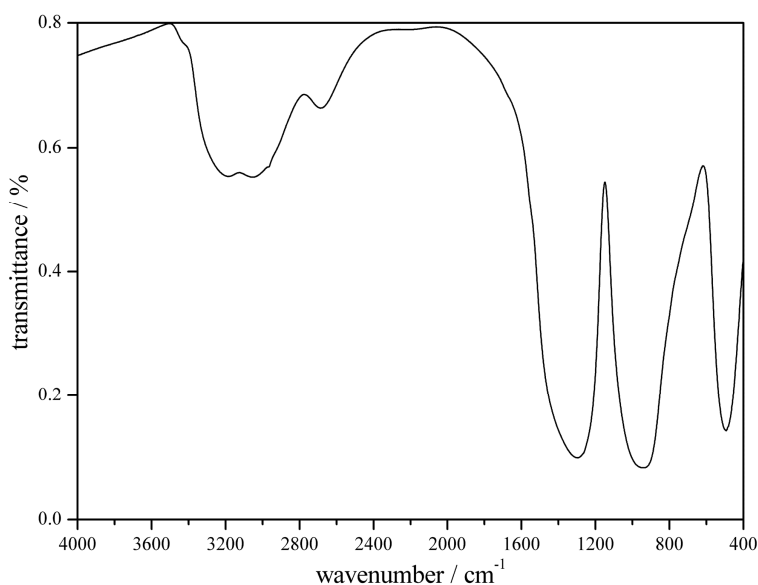
Figure 9. FT-IR spectrum of the amorphous phosphorus oxonitride imide with the composition $PO_{0.88}N_{1.24}H_{0.56}$ (KBr pellet technique; 300 mg dried KBr and 2 mg sample);
The FT-IR spectrum shows that the amorphous phosphorus oxonitride contains a stoichiometric amount of hydrogen. The strong signals around 3200 cm^{-1} indicate stretching vibrations [ν(OH)] and [ν(NH)].

$H_3P_8O_8N_9$ was synthesized under high-pressure and high-temperature conditions of 12 GPa and approx. 750 °C by using the multianvil technique and a 1000 t hydraulic press (Voggenreiter, Mainleus, Germany). $PO_{0.88}N_{1.24}H_{0.56}$ (ca. 7 mg) was ground thoroughly in the glovebox, filled and precompressed in a boron nitride crucible (Henze BNP GmbH, HeBoSint® S10, Kempten, Germany), and centered into a 14/8 assembly. A detailed description of the assembly and its preparation can be found in refs. [63–67]. The assembly was integrated into the center of eight truncated tungsten carbide cubes (TSM-10, Ceratizit, Reutte, Austria) and embedded in a Walker-type module. The assembly was compressed up to 12 GPa at room temperature within 5 h and kept at this pressure for the heating period. The sample was heated to 750 °C in 10 min, maintained at this temperature for 30 min, and then cooled to room temperature in 10 min. Subsequently, the pressure was released over a period of 16 h and the pressure medium were recovered. After removing the surrounding boron nitride, the product (ca. 5 mg) was isolated in the form of a light-gray, cylindrical solid. Powdered $H_3P_8O_8N_9$ (accompanied by an undefined amount of amorphous side-product) was obtained as a material that is stable in air. Semi-quantitative EDX analyses gave a P/O/N atomic ratio of 0.8 : 1.0 : 1.3.

5.4.2 Powder X-ray diffraction, Structure Solution, Rietveld Refinement

A powder X-ray diffraction pattern of $H_3P_8O_8N_9$ was recorded at 298 K on a STOE Stadi P powder diffractometer (STOE, Darmstadt, Germany) in Debye–Scherrer geometry (capillary inner diameter: 0.28 mm) by using Ge(111)-monochromated Cu$K_{\alpha 1}$ radiation (154.0596 pm) and a position sensitive detector. Extraction of the peak positions, pattern indexing, structure solution, Fourier calculations, and Rietveld refinement were carried out by using the TOPAS package.[68] Indexing by using the SVD method[69] unambiguously yielded a monoclinic unit cell with parameters $a = 1351.18$, $b = 479.46$, $c = 1818.98$ pm and $\beta = 96.9188$ (Gof = 31.2). The *ab initio* structure solution was achieved by using the charge-flipping algorithm[70] and subsequent difference Fourier syntheses. Rietveld refinement of the final structure model was carried out by applying the fundamental parameter approach (direct convolution of source emission profiles, axial instrument contributions, and crystallite size and microstrain effects).[71] The preferred orientation of the crystallites was described with eighth-order spherical harmonics. A capillary absorption correction was applied by taking the capillary diameter and linear absorption coefficient into account. To describe peak-broadening and shape-anisotropy effects, the approach of Le Bail and

Jouanneaux[72] was implemented. Overall displacement parameters were used for atoms N/O(1)–N/O(7). Except for N(8) and O(9) with full nitrogen and oxygen occupancy, respectively, the O/N positions were equally occupied with nitrogen and oxygen in a ratio of 4 : 3 guaranteeing the electroneutrality of the formula. The P–(O,N) distances were constrained to 157 pm (mean distance P–(O,N) in PON phases). The crystallographic data and further details of the data collection are summarized in Table 3.† Table 4 shows the positional and displacement parameters for all atoms. The Rietveld fit is displayed in Figure 10.

Table 4. Crystallographic data (esd's in parentheses) for $H_3P_8O_8N_9$ and details of data collection and relative structure solution and refinement.

Crystal Structure Data	
formula	$H_3P_8O_8N_9$
formula mass / g mol^{-1}	504.8707
crystal system	monoclinic
space group	$C2/c$ (no. 15)
	$a = 1352.11(7)$
cell parameters / pm, °	$b = 479.83(3)$
	$c = 1820.42(9)$
	$\beta = 96.955(4)$
cell volume / Å^3	$V = 1172.37(10)$
formula units Z / cell	4
X-ray density ρ / g cm^{-3}	2.84(1)

Data collection	
diffractometer	Stoe Stadi P
radiation, monochromator	Cu-$K_{\alpha 1}$, $\lambda = 154.06$ pm, Ge(111)
detector, internal step width / °	linear PSD ($\Delta 2\theta = 5°$), 0.01
temperature / K	298(2)
2θ range / °	8.0–90.0
step width / °	0.2
data points	8200
number of observed reflections	492

Structure Solution and Refinement	
structure solution method	charge-flipping[70]
structure refinement method	fundamental parameters model[71]
program used	TOPAS-Academic 4.1[68]
background function / parameters	shifted Chebyshev / 40
number of atomic parameters	43

† Further details of the crystal structure investigation(s) can be obtained from the Fachinformationszentrum Karlsruhe, 76344 Eggenstein-Leopoldshafen, Germany (fax: (+49) 7247-808-666; e-mail: crysdata@fizkarlsruhe.de, http://www.fiz-karlsruhe.de/request_for_deposited_data.html) on quoting the depository number CSD-423298.

number of profile and other parameters	71
constraints / restaints	16 / 1
χ^2	1.648
	$R_p = 0.03018$
R indices	$wR_p = 0.03996$
	$R_{Bragg} = 0.00833$

Table 5. Wyckoff symbols, atomic coordinates, and isotropic displacement parameters (B_{iso}) for the atoms in $H_3P_8O_8N_9$ (space group $C2/c$, esd's in parentheses); occupancy of N(1)–N(7) and O(1)–O(7) is 4/7 and 3/7, respectively.

atom	Wyckoff symbol	x	y	z	B_{iso}
P(1)	8f	0.6066(2)	0.5445(6)	0.0955(2)	2.40(12)
P(2)	8f	0.3021(2)	0.7525(6)	0.1096(2)	1.86(13)
P(3)	8f	0.9073(2)	0.7563(6)	0.0625(2)	1.78(12)
P(4)	8f	0.3985(2)	0.1630(6)	0.7613(2)	1.47(10)
N/O(1)	8f	0.6941(3)	0.3485(10)	0.0803(5)	
N/O(2)	8f	0.9907(3)	0.8607(12)	0.3916(5)	
N/O(3)	8f	0.9164(6)	0.7681(14)	0.9773(2)	
N/O(4)	8f	0.6835(5)	0.7193(18)	0.3028(2)	1.72(10)[a]
N/O(5)	8f	0.6844(4)	0.5502(8)	0.9214(4)	
N/O(6)	8f	0.3890(4)	0.9475(7)	0.0910(4)	
N/O(7)	8f	0.3556(9)	0.7302(13)	0.3336(2)	
N(8)	4e	½	0.6924(22)	¼	
O(8)	8f	0.9000(7)	0.6578(8)	0.2551(4)	2.60(25)

[a] the value applies to all atoms N/O(1)–N/O(7) and N(8).
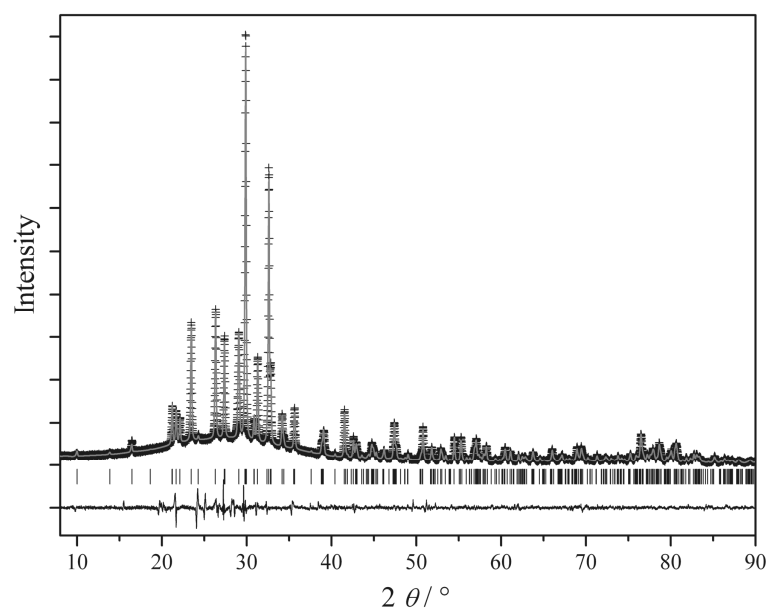
Figure 10. Observed (crosses) and calculated (gray line) powder diffraction pattern of $H_3P_8O_8N_9$ (Cu-$K_{\alpha1}$, 154.06 pm) as well as difference profile of the Rietveld refinement; peak positions are marked by vertical lines.

5.4.3 Solid-state NMR spectroscopy

MAS NMR experiments were carried out on a Bruker Avance III spectrometer, equipped with a commercial 1.3 mm MAS NMR double-resonance probe (filled with 4–5 mg of powder sample) at a spinning frequency of 50 kHz. The magnetic field strength was 11.75 T, which corresponds to a ^{1}H NMR resonance frequency of 500.25 MHz. A commercially available pneumatic control unit was used to limit MAS frequency variations to 5 Hz for the duration of the experiment. ^{1}H and ^{31}P chemical shift values are reported by using the d scale and are referenced to 1% TMS in $CDCl_3$ and 85% H_3PO_4, used as an external reference, respectively.[73] Saturation combs were used prior to relaxation delays in every experiment, except for direct excitation. Rectangular, resonant radio-frequency pulses are denoted as ξ_ϕ, with ξ as the flip angle and ϕ the phase (both in degrees). A recycle delay of 4 s was used for the direct excitation experiment and 256 transients were accumulated. A four-step phase cycle was implemented.

The ^{1}H NMR DQ–SQ correlation spectrum was obtained with the BABA pulse sequence as described in the literature.[74] The recycle delay was set to 74 s and 12 transients were accumulated; four rotor periods were used for DQ excitation. Absorptive sign-sensitive spectra were acquired by using the method of States et al.[75]

We tried different schemes to prepare longitudinal magnetization on H_A, for example, DANTE[29] and soft Gaussian-shaped pulses.[24,26] However, strong polarization losses were observed due to relaxation effects and multiquantum coherence generation. To minimize these losses, we designed a selective pulse sequence from three pairs $90_0-\tau-90_{180}$ of hard 90° pulses, each pair of pulses separated by a specific delay τ, which implements a chemical-shift-selective filter.[24,27] When the transmitter frequency was set to the to-be-selected peak, its magnetization vector in a simple Bloch picture would return to the z direction of the rotating frame after each pulse pair. The magnetization vectors of other peaks could be forced to remain in the xy plane of the rotating frame by making an appropriate choice for the delay τ. The sequence became more selective as more pulse pairs were used. In our case, three pairs were sufficient. We used a two-step, nested, phase cycle[76] for each 90° pulse of each pulse pair to cancel out artifacts and a four-step cycle on the read pulse to select the coherence pathways indicated in the coherence pathway diagram in Figure 4B, which overall amounts to a 256-step cycle. For the time intervals, we optimized $\tau 1$, $\tau 2$, and $\tau 3$ as 75.8, 34.0, and 59.5 μs.

Longitudinal magnetization transfer was achieved by the rotor-synchronized zero-quantum recoupling sequence $SR6_6^2$ with the R-element $90_{180}270_0$, which was used as

previously described in detail (Figure 4A).[24] The recycle delay was set to 4 s and 256 transients were accumulated. Peak areas were determined by deconvolution of the experimental spectra with mixed Gaussian/Lorentzian line shapes.

5.5   REFERENCES

[1]   G. H. Beall, *Rev. Mineral./Geochem.* **1994**, *29*, 469.

[2]   M. C. Gerhardt, *Ann. Chim. Phys.* **1846**, *18*, 188.

[3]   L. Boukbir, R. Marchand, Y. Laurent, P. Bacher, G. Roult, *Ann. Chim.* **1989**, *14*, 475.

[4]   J.-M. Léger, J. Haines, L. S. de Oliveira, C. Chateau, A. Le Sauze, R. Marchand, *J. Phys. Condens. Matter* **1996**, *8*, L773.

[5]   C. Chateau, J. Haines, J.-M. Léger, A. Le Sauze, R. Marchand, *Am. Mineral.* **1999**, *84*, 207.

[6]   J. Haines, C. Chateau, J.-M. Léger, A. Le Sauze, N. Diot, R. Marchand, S. Hull, *Acta Crystallogr., Sect. B: Struct. Sci.* **1999**, *55*, 677.

[7]   J.-M. Léger, J. Haines, L. S. de Oliveira, C. Chateau, A. Le Sauze, R. Marchand, S. Hull, *J. Phys. Chem. Solids* **1999**, *60*, 145.

[8]   J.-M. Léger, J. Haines, C. Chateau, R. Marchand, *J. Phys. Chem. Solids* **2000**, *61*, 1447.

[9]   J.-M. Léger, J. Haines, C. Chateau, G. Bocquillon, M. W. Schmidt, S. Hull, F. Gorelli, A. Le Sauze, R. Marchand, *Phys. Chem. Miner.* **2001**, *28*, 388.

[10]   a) E. Guéguen, Doctoral Thesis, University of Rennes (France), **1994**; b) R. Marchand, W. Schnick, N. Stock, *Adv. Inorg. Chem.* **2000**, *50*, 193.

[11]   W. Schnick, J. Lücke, *Z. Anorg. Allg. Chem.* **1992**, *610*, 121.

[12]   a) S. Horstmann, E. Irran, W. Schnick, *Angew. Chem.* **1997**, *109*, 2085; *Angew. Chem., Int. Ed. Engl.* **1997**, *36*, 1992; b) S. Horstmann, E. Irran, W. Schnick, *Z. Anorg. Allg. Chem.* **1998**, *624*, 221.

[13]   J. Ronis, B. Bondars, A. Vitola, T. Millers, J. Schneider, F. Frey, *J. Solid State Chem.* **1995**, *115*, 265.

[14]   S. Horstmann, E. Irran, W. Schnick, *Angew. Chem.* **1997**, *109*, 1938-1940; *Angew. Chem., Int. Ed. Engl.* **1997**, *36*, 1873; b) S. Horstmann, E. Irran, W. Schnick, *Z. Anorg. Allg. Chem.* **1998**, *624*, 620.

[15]   a) K. Landskron, H. Huppertz, J. Senker, W. Schnick, *Angew. Chem.* **2001**, *113*, 2713; *Angew. Chem., Int. Ed.* **2001**, *40*, 2643; b) K. Landskron, H. Huppertz, J. Senker, W. Schnick, *Z. Anorg. Allg. Chem.* **2002**, *628*, 1465.

[16]   S. Horstmann, W. Schnick, *Z. Naturforsch., B: J. Chem. Sci.* **1997**, *52*, 490.

[17]   S. Horstmann, W. Schnick, *Z. Naturforsch., B: J. Chem. Sci.* **1994**, *49*, 1381.

[18]   F. Tessier, A. Navrotsky, A. Le Sauze, R. Marchand, *Chem. Mater.* **2000**, *12*, 148.

[19]   S. J. Sedlmaier, J. Schmedt auf der Günne, W. Schnick, *Dalton Trans.* **2009**, 4081.

[20]   S. J. Sedlmaier, M. Döblinger, O. Oeckler, J. Weber, J. Schmedt auf der Günne, W. Schnick, *J. Am Chem. Soc.* **2011**, *133*, 12069.

[21]   A. E. Bennett, R. G. Griffin, J. H. Ok, S. Vega, *J. Chem. Phys.* **1992**, *96*, 8624.

[22]   Y. Ishii, *J. Chem. Phys.* **2001**, *114*, 8473.

[23]   M. Baldus, M. Tomaselli, B. H. Meier, R. R. Ernst, *Chem. Phys. Lett.* **1994**, *230*, 329.

[24]   A. Brinkmann, J. Schmedt auf der Günne, M. H. Levitt, *J. Magn. Reson.* **2002**, *156*, 79.

[25]   H. Kessler, S. Mronga, G. Gemmecker, *Magn. Reson. Chem.* **1991**, *29*, 527.

[26]   S.-J. Huang, Y.-H. Tseng, Y. Mou, S.-B. Liu, S.-H. Huang, C.-P. Lin, J. C. C. Chan, *Solid State Nucl. Magn. Reson.* **2006**, *29*, 272.

[27]   C. L. Dumoulin, *Magn. Reson. Med.* **1985**, *2*, 583.

[28]   M. Carravetta, J. Schmedt auf der Günne, M. H. Levitt, *J. Magn. Reson.* **2003**, *162*, 443.

[29]   G. A. Morris, R. Freeman, *J. Magn. Reson.* **1978**, *29*, 433.

[30]   a) X. Wang, K. Maeda, A. Thomas, K. Takanabe, G. Xin, J. M. Carlsson, K. Domen, M. Antonietti, *Nat. Mat.* **2009**, *8*, 76; b) F. Su, S. C. Mathew, L. Möhlmann, M. Antonietti, X. Wang, S. Blechert, *Angew. Chem.* **2011**, *123*, 683; *Angew. Chem., Int. Ed.* **2011**, *50*, 657.

[31]   Y. Zhang, T. Mori, J. Ye, M. Antonietti, *J. Am. Chem. Soc.* **2010**, *132*, 6294.

[32]   K. Sommer, German Patents No. 23 17 282.9 and 23 55 575.1, **1973**.

[33]   K. R. Waerstad, J. M. Sullivan, *J. Appl. Crystallogr.* **1976**, *9*, 411.

[34]   A. Vitola, V. Avotins, J. Ronis, D. Schweitz, *Latv. PSR Zinat. Akad. Vestis Kim. Ser.* **1986**, *3*, 299.

[35]   E. Steger, G. Mildner, *Z. Anorg. Allg. Chem.* **1964**, *332*, 314.

[36]   R. Klement, O. Koch, *Chem. Ber.* **1954**, *87*, 333.

[37]   S. J. Sedlmaier, D. Weber, W. Schnick, *Z. Kristallogr.-NCS* **2012**, *227*, in press.

[38] S. J. Sedlmaier, M. Eberspächer, W. Schnick, *Z. Anorg. Allg. Chem.* **2011**, *637*, 362.

[39] G. Metz, X. L. Wu, S. O. Smith, *J. Magn. Reson. A* **1994**, *110*, 219.

[40] V. Kahlenberg, B. Marler, J. C. Muñoz Acevedo, J. Patarin, *Solid State Sci.* **2002**, *4*, 1285.

[41] S. M. Haile, B. J. Wuensch, *Acta Crystallogr., Sect. B: Struct. Sci.* **2000**, *56*, 773.

[42] O. G. Karpov, E. A. Pobedimskaya, N. V. Belov, *Kristallografiya*, **1977**, *22*, 382.

[43] H. Schichl, H. Völlenkle, A. Wittmann, *Monatsh. Chem.* **1973**, *104*, 854.

[44] B. H. W. S. de Jong, H. T. J. Supèr, A. L. Spek, N. Veldman, G. Nachtegaal, J. C. Fischer, *Acta Crystallogr., Sect. B: Struct. Sci.* **1998**, *54*, 568.

[45] V. Tazzoli, M. C. Domeneghetti, F. Mazzi, E. Cannillo, *Eur. J. Mineral.* **1995**, *7*, 1339.

[46] S. Merlino, *Acta Crystallogr., Sect. B: Struct. Sci.* **1974**, *30*, 1262.

[47] G. O. Brunner, W. M. Meier, *Nature* **1989**, *337*, 146.

[48] C. Schmolke, O. Oeckler, D. Bichler, D. Johrendt, W. Schnick, *Chem. Eur. J.* **2009**, *15*, 9215.

[49] D. Peters, H. Jacobs, *J. Less Common Met.* **1989**, *146*, 241.

[50] I. Idrestedt, C. Brosset, *Acta Chem. Scand.* **1964**, *18*, 1879.

[51] F. Liebau, *Structural Chemistry of Silicates*, Springer, Berlin, **1985**.

[52] P. J. Woodrow, *Acta Crystallogr.* **1967**, *22*, 673.

[53] W. E. Klee, *Z. Kristallogr.* **1987**, *179*, 67.

[54] G. Thimm, S. Schumacher, W. Uhr, W. E. Klee, *TOPOLAN, Topological Analysis of Crystal Structures*, Univ. Karlsruhe, **1993**.

[55] A. Durif, *Crystal Chemistry of Condensed Phosphates*, Springer, Berlin, **1995**.

[56] N. Stock, E. Irran, W. Schnick, *Chem. Eur. J.* **1998**, *4*, 1822.

[57] S. Correll, N. Stock, O. Oeckler, J. Senker, T. Nilges, W. Schnick, *Z. Anorg. Allg. Chem.* **2004**, *630*, 2205.

[58] H. A. Höppe, F. Stadler, O. Oeckler, W. Schnick, *Angew. Chem.* **2004**, *116*, 5656; *Angew. Chem., Int. Ed.* **2004**, *43*, 5540.

[59] a) R. Hoppe, *Angew. Chem.* **1966**, *78*, 52; *Angew. Chem., Int. Ed. Engl.* **1966**, *5*, 95; b) R. Hoppe, *Angew. Chem.* **1970**, *82*, 7; *Angew. Chem., Int. Ed. Engl.* **1970**, *9*, 25.

[60] F. Karau, W. Schnick, *Angew. Chem.* **2006**, *118*, 4617; *Angew. Chem., Int. Ed.* **2006**, *45*, 4505.

[61] K.-D. Kreuer, *Chem. Mater.* **1996**, *8*, 610.

[62] A. Zerr, G. Serghiou, R. Boehler in *Handbook of Ceramics and Hard Materials*, Vol. 1 (Ed: R. Riedel), Wiley-VCH, Weinheim, **2000**, 41.

[63] H. Huppertz, *Z. Kristallogr.* **2004**, *219*, 330.

[64] N. Kawai, S. Endo, *Rev. Sci. Instrum.* **1970**, *41*, 1178.

[65] D. Walker, M. A. Carpenter, C. M. Hitch, *Am. Mineral.* **1990**, *75*, 1020.

[66] D. Walker, *Am. Mineral.* **1991**, *76*, 1092.

[67] D. C. Rubie, *Phase Transitions* **1999**, *68*, 431.

[68] A. A. Coelho, *TOPAS-Academic,* Version 4.1, Coelho Software, Brisbane, **2007**.

[69] A. A. Coelho, *J. Appl. Crystallogr.* **2003**, *36*, 86.

[70] G. Oszlányi, A. Sütő, *Acta Crystallogr., Sect. A: Found. Crystallogr.* **2004**, *60*, 134.

[71] J. Bergmann, R. Kleeberg, A. Haase, B. Breidenstein, *Mater. Sci. Forum* **2000**, *347-349*, 303.

[72] A. Le Bail, A. Jouanneaux, *J. Appl. Crystallogr.* **1997**, *30*, 265.

[73] R. K. Harris, E. D. Becker, *J. Magn. Reson.* **2002**, *156*, 323.

[74] M. Feike, D. E. Demco, R. Graf, J. Gottwald, S. Hafner, H. W. Spiess, *J. Magn. Reson. A* **1996**, *A122*, 214.

[75] D. J. States, R. A. Haberkorn, D. J. Ruben, *J. Magn. Reson.* **1982**, *48*, 286.

[76] G. Bodenhausen, H. Kogler, R. R. Ernst, *J. Magn. Reson.* **1984**, *58*, 370.

6.   An Unprecedented AB$_2$ Tetrahedra Network Structure Type in a High-Pressure Phase of Phosphorus Oxonitride (PON)

Already in the last chapter, the potential of the synthesis strategy with the self-developed PON starting material is indicated—the first phosphorus oxonitride imide with an exceptional framework structure resulted. The original intention, however, was to use precondensed PON as single-source precursor under high-pressure, high-temperature conditions to prepare possibly unknown PON polymorphs, perhaps even stishovite-PON with coordination number six for P. By DFT calculations, *Römer* has showed that a stability range for PON in the stishovite structure-type exists. According to the enthalpy-pressure diagram (Figure 0), stishovite-PON might be feasible at pressures above around 9 GPa. As known from the last chapter, at 12 GPa and 750 °C full condensation of the PON precursor is prevented. The logical next step to achieve PON is to increase the temperature. If stishovite-PON or another PON polymorph resulted is described in this contribution.
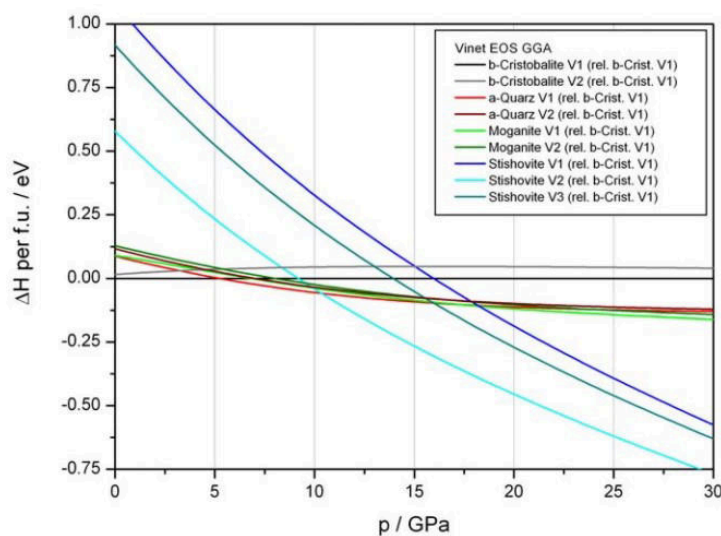
Figure 0. Enthalpy-pressure (*H-p*) diagram for the transition of β-cristobalite PON into stishovite PON ($p_t \approx 9$, 14, 16 GPa, dependent on different O/N ordered models); derived from the evaluation of the *E-V* data by the Vinet EOS).[source: Dr. S. R. Römer]

                        Dominik Baumann, Stefan J. Sedlmaier, Wolfgang Schnick

ABSTRACT

Restructuring: An unprecedented framework structure made up of tetrahedral has been discovered in a novel high-pressure polymorph of the phosphorus oxonitride PON by treating a single-source precursor at 12 GPa and 1250 °C. It is the first polymorph of PON which does not crystallize in a structure type known from SiO$_2$.

6.1   INTRODUCTION WITH RESULTS AND DISCUSSION

Compounds exhibiting AB_2-type tetrahedral network structures are versatile materials and of great technical importance. First of all microporous zeolites are known for their outstanding absorption properties and catalytic behavior and are therefore extensively used in industrial, agricultural, and laboratory environments.[1] However, the importance of dense AB_2 networks should not be underestimated. SiO_2 and to a minor extent $GaPO_4$ are applied in piezoelectric devices, such as pressure sensors and microbalances,[2] while quartz-like compounds in general, including phosphates such as $AlPO_4$ and BPO_4, can also be used for second-harmonic generation (SHG) purposes.[3,4] Owing to the variety of applications, widespread research into novel AB_2-type structures was conducted, including the prediction of more than two million unique prospective crystal structures for zeolites.[5] However, only a minute subset of possible structures has been realized to date. In this search for new structure types, we have directed our attention to the system P-O-N, which is isoelectronic to silica. The inclusion of nitrogen provides additional structural flexibility, which theoretically opens up an even wider range of possible structure types. The few known compounds in this system include the first nitridic zeolites NPO[6] and $Ba_{19}P_{36}O_{6+x}N_{66-x}Cl_{8+x}$ ($x \approx 4.54$)[7] as well as the nitridic clathrate $P_4N_4(NH)_4(NH_3)$[8] and the polymorphs of PON exhibiting cristobalite-,[9] quartz-,[10] and moganite-type[11] structures. Glassy compounds in the system Li-Ca-P-N also exhibit desirable properties, such as a high hardness and refractive index.[12] The great potential for novel structure types in this system is offset by difficulties in preparation, such as thermal decomposition, low reactivity, and a low degree of crystallinity. To circumvent the mentioned problems, we developed a novel synthetic approach, utilizing an amorphous single-source precursor. Herein, we report on a new high-pressure phase of phosphorus oxonitride PON. Since this is the fourth known polymorph of PON, we propose the name δ-PON. Unlike the quartz and moganite polymorphs, it is not directly accessible by treating cristobalite-type PON under high-pressure/high-temperature conditions. This result hints at the possibility of δ-PON being thermodynamically metastable at these conditions. Instead, we prepared δ-PON by carrying out the final thermal condensation step of an amorphous phosphorus oxonitride imide under high pressure by employing the multianvil technique.[13] The starting material was subjected to a temperature of around 1350 °C at 12 GPa for 120 min in a Walker-type module. The product could be obtained as a hard, colorless solid.

The crystal structure of δ-PON was elucidated *ab initio* with X-ray powder diffraction data in space group $P2_1/c$ (no. 14).[†] Final refinement was carried out by employing the Rietveld method (Figure 1). Energy-dispersive X-ray spectroscopy showed the presence of P, O, and N, while no other elements were detected. The product was further characterized by FT-IR and solid-state NMR spectroscopy.
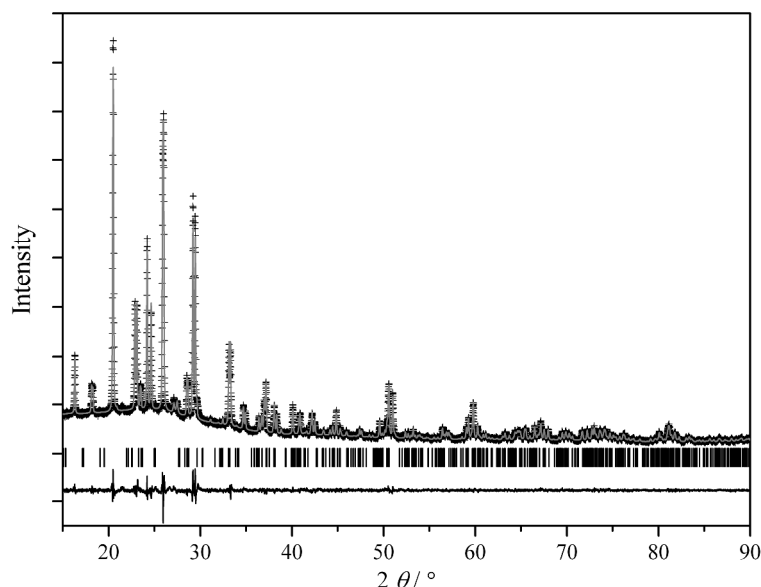
Figure 1. Observed (crosses) and calculated (gray line) powder diffraction pattern of δ-PON as well as position of Bragg reflections (vertical lines) and difference profile below (dark gray line); Cu-$K_{\alpha1}$-radiation.

The crystal structure of δ-PON exhibits a three-dimensional network composed of all-side vertex sharing P(O,N)$_4$- tetrahedra representing an unprecedented topology (Figure 2). The arrangement of the tetrahedra is characterized of condensed 4-, 6-, and 8-rings, which is expressed by the cycle class sequence according to *Klee*[14] (Table 1). The comparison with the cycle class sequences of the other polymorphs shows that δ-PON is not topologically equivalent to any of the known phases. The arrangement of P(O,N)$_4$-tetrahedra into 4- and 6-rings is reminiscent of that of moganite PON, but owing to the difference in framework topologies no crystallographic group–subgroup relation between the two phases exists. One type of the two crystallographically independent 4-rings forms ladder-like chains along [010] (Figure 3), which are surrounded by 6-rings.

---

† Further details on the crystal structure investigations may be obtained from the Fachinformationszentrum Karlsruhe, 76344 Eggenstein-Leopoldshafen, Germany (fax: (+49) 7247-808-666; e-mail: crysdata@fiz-karlsruhe.de), on quoting the depository number CSD-423589.

Table 1. Cycle class sequence of the network of δ-PON in comparison with the networks of the other PON polymorphs showing the prevalence of the $P_n(O/N)_n$-rings.

n	2	3	4	5	6	7	8
δ-PON	0	0	6	0	12	0	68
cristobalite-PON	0	0	0	0	4	0	6
quartz PON	0	0	0	0	3	0	21
moganite-PON	0	0	2	0	4	0	32
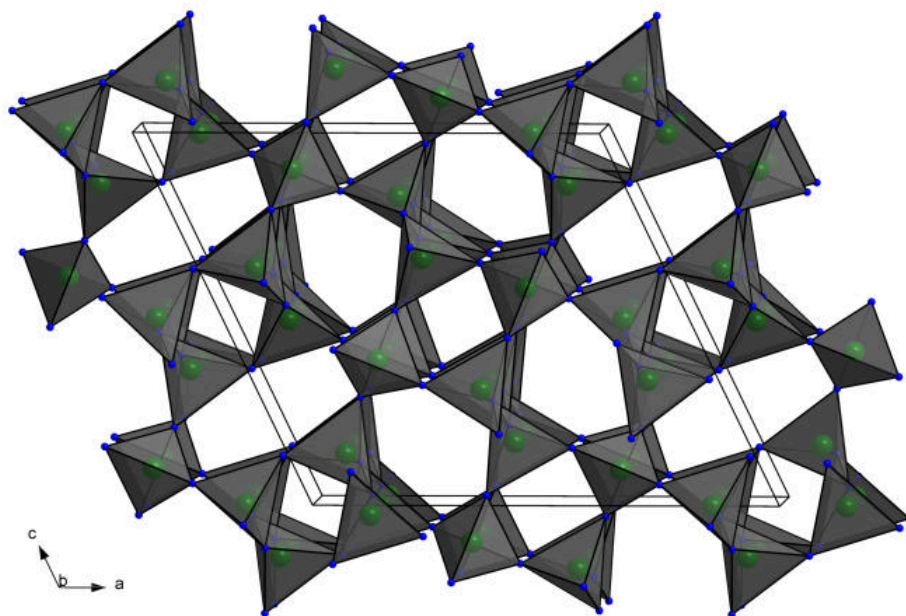
Figure 2. Crystal structure of δ-PON; view along [010] (P: green, O/N: blue).
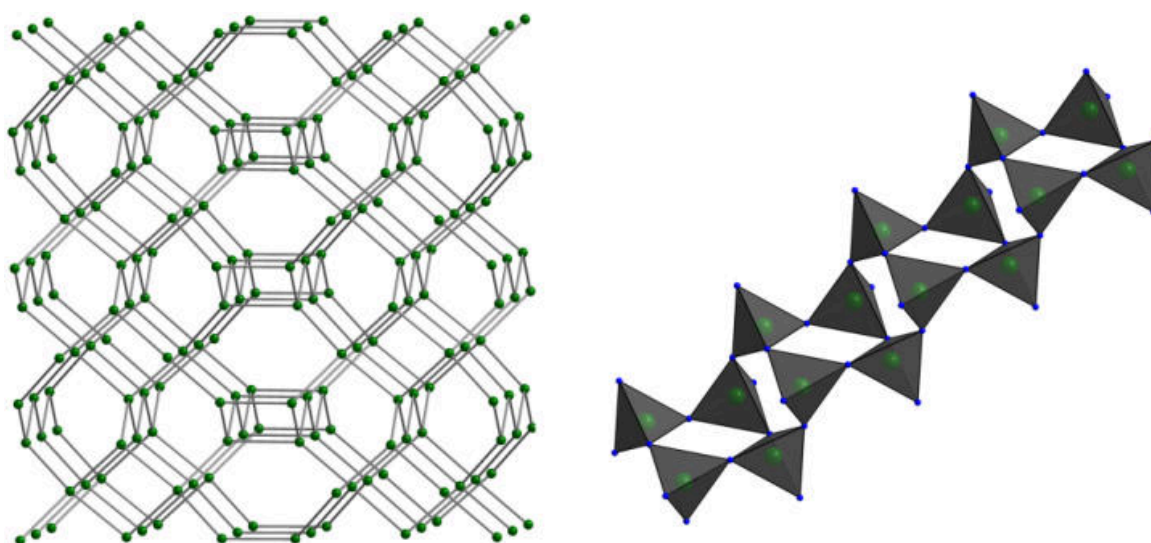
Figure 3. Left: Topological representation of the crystal structure of δ-PON; right: section from the crystal structure showing the ladder-like arrangement of 4-rings.

The topology of this framework (Figure 3) indicated by the vertex symbol $(4_16_28_3)(4_16_48_1)(4_26_38)_2$ (determined by the TOPOS Software)[15] is different from those of all other PON polymorphs and has not been found in any other known compound as yet. Therefore, δ-PON can be considered a truly novel structure type and correspondingly supplements the few known AB_2 structure types. However, a SiO_2 modification with the same topology in space group *Aea*2 has been predicted and can be found in the Predicted Crystallography Open Database (PCOD; entry 3102887).[16] Both compounds are related through a common aristotype in space group *Cmce*. The corresponding *Bärnighausen* tree,[17] illustrating the symmetry reduction to the two hettotypes is shown in Figure 4. The space groups of both structures are *translationengleiche* subgroups of index 2 of the space group of the aristotypes space group *Cmce*.

Cmce (64)

TX₂

T:8f	T:16g	T:8d	X:8f	X:16g	X:16g	X:8e	X:16g
m..	1	2..	m..	1	1	.2.	1
0	0.816	0.098	0	0.824	0.863	¾	0.942
0.827	0.827	½	0.713	0.711	0.932	0.108	0.906
0.600	0.223	0	0.7874	0.407	0.274	¾	0.670

t2

t2

½(a-b), -c, b

½x−0.25, −½x+z−0.25, −y

Bbe2 (41)

SiO₂

Si:8b	Si:8b	Si:8b	Si:8b
1	1	1	1
0.001	0.186	0.824	0.099
0.819	0.830	0.332	0.985
0.282	0.460	0.407	0.206
O:8b	O:8b	O:8b	O:8b
1	1	1	1
0.984	0.830	0.839	0.857
0.706	0.726	0.229	0.950
0.096	0.249	0.619	0.417
O:8b	O:8b	O:8b	O:8b
1	1	1	1
0.864	0.754	0.960	0.929
0.455	0.133	0.930	0.354
0.440	0.938	0.162	0.792

P2₁/c (14)

δ-PON

P:4e	P:4e	P:4e	P:4e
1	1	1	1
0.499	0.131	0.697	0.134
0.400	0.778	0.006	0.224
0.327	0.144	0.098	0.492
O/N:4e	O/N:4e	O/N:4e	O/N:4e
1	1	1	1
0.497	0.152	0.224	0.004
0.216	0.588	0.719	0.234
0.211	0.040	0.299	0.360
O/N:4e	O/N:4e	O/N:4e	O/N:4e
1	1	1	1
0.228	0.380	0.144	0.612
0.233	0.336	0.099	0.177
0.937	0.340	0.113	0.968

Figure 4. *Bärnighausen* tree showing the symmetry relation between δ-PON and the predicted SiO_2 phase from the PCOD database.

P–(O,N) bond lengths vary between 152 and 165 pm, and their variance and the mean bond length are slightly larger than in the other known polymorphs of PON. The bonding angles at the bridging atoms range from 128 to 147°, which is comparable to other PON

phases. Deviations from the regular tetrahedral angle vary slightly with values between 104 and 118°. Detailed information on bond lengths and angles can be found in Table 2. The electrostatic plausibility of the crystal structure was assessed by using the MAPLE (Madelung part of lattice energy) concept.[18] The partial MAPLE values of the atomic sites (O/N = 4460–4778, P = 13941–14878 kJmol^{-1}) as well as the overall MAPLE value (23809 kJmol^{-1}) are in good agreement with those calculated for the other PON polymorphs. Notably, the partial MAPLE values of the anion sites are between the literature values for nitrogen (4600–6000 kJmol^{-1}) and oxygen (2400–2800 kJmol^{-1}),[19] giving a strong indication for anion disorder.

Table 2. Selected interatomic distances / pm and angles / ° in δ-PON (esd's in parentheses).

P(1)–(O,N)	152.5(9), 156.0(11), 159.2(10), 159.3(8)	
P(2)–(O,N)	156.8(10), 159.2(9), 161.0(11), 164.7(11)	
P(3)–(O,N)	152.5(9), 157.5(9), 160.1(9), 162.2(10)	
P(4)–(O,N)	152.5(10), 152.8(9), 157.7(10), 161.2(9)	
P–(O,N)–P	128.3(5)–146.7(6)	8 times
(O,N)–P(1)–(O,N)	106.0(5)–111.2(5)	6 times
(O,N)–P(2)–(O,N)	104.7(5)–112.8(5)	6 times
(O,N)–P(3)–(O,N)	103.2(5)–113.8(5)	6 times
(O,N)–P(4)–(O,N)	103.9(5)–118.2(5)	6 times

Since neutron diffraction studies on the known polymorphs of PON by *Marchand* et al.[9,11] did not show any evidence for O/N-order, we assume similar disorder in δ-PON. To corroborate this hypothesis, δ-PON was characterized further by recording a ^{31}P solid-state NMR spectrum. The chemical shift of $\delta_{iso} = -32.1$ ppm is close to those found for cristobalite-PON ($\delta_{iso} = -26.3$ ppm, see Figures 5 and 6) and $H_3P_8O_8N_9$ ($\delta_{iso} = -31.9$ ppm).[20] As expected for a phase with statistical O/N distribution, the full width at half maximum (FWHM) of the signal is so high that the four individual signals expected for the four crystallographically distinct P atoms cannot be resolved. To rule out the possibility of δ-PON being in fact a phosphorus oxonitride imide, the absence of stoichiometric amounts of hydrogen was confirmed by ^{1}H solid-state NMR spectroscopy as well as FT-IR spectroscopy (FT-IR spectrum see Figure 7).
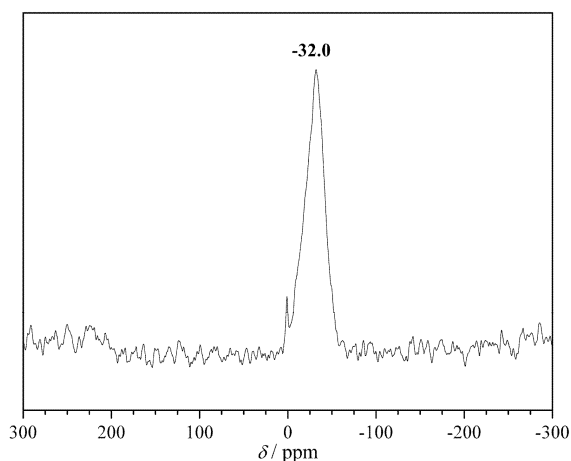
Figure 5. ^{31}P solid-state NMR spectrum of δ-PON; the small peak at δ = 0 ppm results from small amounts of hydrolysis products.
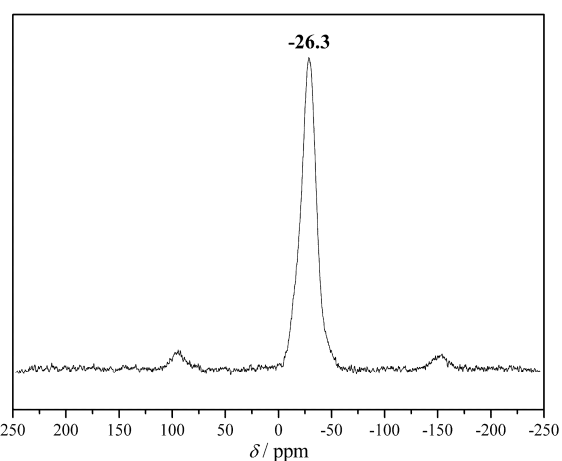
Figure 6. ^{31}P solid-state NMR spectrum of cristobalite-PON.
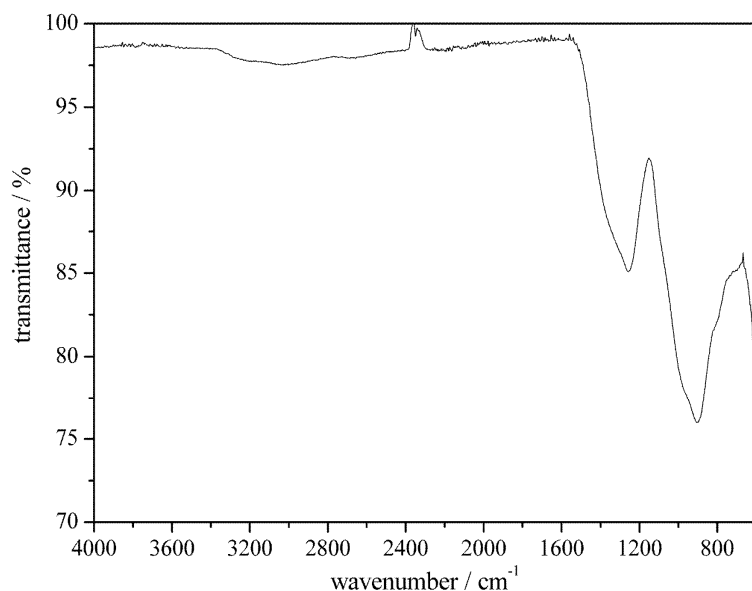
Figure 7: FT-IR spectrum of δ-PON.

With δ-PON, we have found the first polymorph of PON that does not crystallize in a structure type known from SiO_2. This novel AB_2 structure type had only been predicted theoretically so far. With the high-pressure high-temperature condensation of a newly developed amorphous phosphorus oxonitride imide precursor, a powerful synthetic approach towards new high-pressure phases of PON has been established. This method could lead to further high-pressure polymorphs of PON, allowing a structural diversity approaching that of SiO_2. This promising synthesis approach could also be applied to many other systems, possibly facilitating the discovery of a range of novel networks with interesting properties. The high-pressure approach in combination with the inclusion of

nitrogen in the framework allows an even wider range of possible frameworks, even including triply coordinated nitrogen atoms or edge-sharing tetrahedra.[21] Even the synthesis of stishovite-like polymorphs with interesting materials properties showing higher coordination numbers of P may be possible.

6.2   EXPERIMENTAL SECTION

6.2.1   Synthesis and Energy dispersive X-ray analysis

Amorphous phosphorus oxonitride imide with composition $PO_{0.88}N_{1.24}H_{0.56}$ has been prepared by heating a mixture of phosphoryl triamide $PO(NH_2)_3$ and NH_4Cl (ratio 1 : 3) in a fused silica boat at 300 and 620 °C in a continuous ammonia flow for 12 h. The mixture can be obtained by the reaction of $POCl_3$ (99% Acros Organics, Geel, Belgium) with liquid NH_3 (5.0, Linde, Pullach, Germany) as described in the literature.[22] δ-PON has been synthesized by high-pressure high-temperature treatment of $PO_{0.88}N_{1.24}H_{0.56}$ in a 1000 t hydraulic press (Voggenreiter, Mainleus, Germany) using a Walker-type multianvil assembly. Further information concerning the assembly can be found in the literature.[13] Inside a glovebox (Unilab, MBraun, Garching, Germany) the starting material was tightly packed into a hexagonal boron nitride capsule. The capsule was placed inside two graphite tubes, which themselves were placed inside a Crdoped MgO-octahedron with an edge length of 14 mm (Ceramic Substrates and Components, Isle of Wight, UK). The octahedron was compressed between eight tungsten carbide cubes (Hawedia, Marklkofen, Germany) with a truncation edge length of 8 mm. The pressure on the sample was raised to 12 GPa and the sample was heated to approximately 1350 °C within 15 min. The temperature was held for 120 min and subsequently lowered to room temperature within 30 min. After decompression, the product was isolated.

Energy dispersive X-ray analyses were performed using a JSM 6500F scanning electron microscope (Jeol, Tokyo, Japan) with an Oxford Instruments 7418 X-ray detector.

6.2.2   Powder X-ray diffraction, infrared and solid-state NMR spectroscopy

Powder diffraction measurements were conducted in parafocusing Debye-Scherrer geometry using a StadiP-diffractometer (Stoe & Cie, Darmstadt, Germany) using Ge(111) monochromated Cu-$K_{\alpha 1}$-radiation and a position sensitive detector. Structure elucidation was carried using TOPAS Academic4.1.[23] Reflections were indexed using the SVD-

algorithm[24] and their intensities extracted with the Pawley-method. The full structural model was obtained using the charge-flipping-algorithm.[25] Final refinement was carried out using the Rietveld method, employing the fundamental parameters approach (direct convolution of source emission profiles, axial instrument contributions and crystallite size and microstrain effects).[26] The anion positions were occupied equally with 0.5 for both O and N applying a common atomic displacement parameter. 3% of moganite-type PON was additionally refined as side-phase. Capillary absorption correction (inner diameter 0.28 mm) was carried out using the calculated absorption coefficient.

The FT-IR spectrum was collected on a Spectrum BX II-spectrometer (Perkin Elmer, Waltham MA, USA).

Solid-state MAS-NMR-experiments were carried out on an Avance III Spectrometer (500 MHz, 4.7 T, Bruker, Bellerica, USA). The chemical shift values refer to a deshielding scale. 85% H_3PO_4 was used as an external reference.

Table 2. Crystallographic data of δ-PON (esd's in parentheses) and details of the data collection and relative structure solution and refinement.

Crystal Structure Data	
formula	PON
formula mass / g mol^{-1}	60.98
crystal system	monoclinic
space group	$P2_1/c$ (no. 14)
cell parameters / pm, °	$a = 1224.72(2)$
	$b = 483.618(6)$
	$c = 1086.04(2)$
	$\beta = 115.8026(8)$
cell volume / Å^3	$V = 579.12(2)$
formula units Z / cell	16
X-ray density ρ / g cm^{-3}	2.7976

Data collection	
diffractometer	Stoe Stadi P
radiation, monochromator	Cu-$K_{\alpha 1}$, $\lambda = 154.06$ pm, Ge(111)
detector, internal step width / °	linear PSD ($\Delta 2\theta = 5°$), 0.01
temperature / K	298(2)
2θ range / °	15.0–90.0
step width / °	0.2
data points	7500
number of observed reflections	474

Structure Solution and Refinement	
structure solution method	charge-flipping[25]
structure refinement method	fundamental parameters model[26]
program used	TOPAS-Academic 4.1[23]
background function / parameters	shifted Chebyshev / 32
number of atomic parameters	41
number of profile and other parameters	17
constraints	8
χ^2	1.447
R indices	$R_p = 0.03806$ $wR_p = 0.0491$ $R_{Bragg} = 0.01213$

Table 3. Atomic coordinates, Wyckoff symbols, and isotropic displacement parameters B_{eq} / Å^2 for the atoms in δ-PON (space group $P2_1/c$, esd's in parentheses); occupancy of N(1)–N(8) and O(1)–O(8) is ½, respectively.

atom	Wyckoff symbol	x	y	z	B_{eq}
P(1)	4e	0.4993(4)	0.3996(6)	0.3269(3)	2.02(9)
P(2)	4e	0.1306(3)	0.7784(9)	0.1439(3)	2.10(10)
P(3)	4e	0.6966(3)	0.0061(10)	0.0977(3)	2.00(8)
P(4)	4e	0.1342(3)	0.2235(9)	0.4920(3)	2.38(10)
N/O(1)	4e	0.4967(9)	0.2163(14)	0.2114(8)	
N/O(2)	4e	0.1520(7)	0.588(2)	0.0396(8)	
N/O(3)	4e	0.2235(7)	0.7188(18)	0.2985(8)	
N/O(4)	4e	0.0043(8)	0.234(2)	0.3603(7)	3.17(9)[a]
N/O(5)	4e	0.2278(7)	0.2332(19)	0.9364(8)	
N/O(6)	4e	0.3799(7)	0.3362(14)	0.3400(8)	
N/O(7)	4e	0.1436(7)	0.099(2)	0.1126(8)	
N/O(8)	4e	0.6116(8)	0.1768(15)	0.9677(9)	

[a] the value applies to all atoms N/O(1) to N/O(8)

6.3   REFERENCES

[1]   F. A. Mumpton, *Proc. Natl. Acad. Sci. USA* **1999**, *96*, 3463.

[2]   H. Thanner, P. W. Krempl, W. Wallnöfer, P. M. Worsch, *Vacuum* **2002**, *67*, 687.

[3]   S. Defregger, G. F. Engel, P.W. Krempl, *Phys. Status Solidi B* **1990**, *162*, 311.

[4]   Z. Li, Z. Lin, Y.Wu, P. Fu, Z.Wang, C. Chen, *Chem. Mater.* **2004**, *16*, 2906.

[5]   a) M. M. J. Treacy, I. Rivin, E. Balkovsky, K. H. Randall, M. D. Foster, *Micropor. Mesopor. Mater.* **2004**, *74*, 121; b) M. D. Foster, M. M. J. Treacy, *Database of Hypothetical Zeolite Structures*: http://www.hypotheticalzeolites.net, accessed March **2012**.

[6]   a) S. Correll, O. Oeckler, N. Stock, W. Schnick, *Angew. Chem.* **2003**, *115*, 3674; *Angew. Chem., Int. Ed.* **2003**, *42*, 3549; b) S. Correll, N. Stock, O. Oeckler, J. Senker, T. Nilges, W. Schnick, *Z. Anorg. Allg. Chem.* **2004**, *630*, 2205.

[7]   S. J. Sedlmaier, M. Döblinger, O. Oeckler, J. Weber, J. Schmedt auf der Günne, W. Schnick, *J. Am. Chem. Soc.* **2011**, *133*, 12069.

[8]   F. Karau, W. Schnick, *Angew. Chem.* **2006**, *118*, 4617; *Angew. Chem., Int. Ed.* **2006**, *45*, 4505.

[9]   J. M. Léger, J. Haines, C. Chateau, G. Bocquillon, M. W. Schmidt, S. Hull, F. Gorelli, A. Lesauze, R. Marchand, *Phys. Chem. Miner.* **2001**, *28*, 388.

[10]   J. M. Léger, J. Haines, L. S. de Oliveira, C. Chateau, A. Le Sauze, R. Marchand, S. Hull, *J. Phys. Chem. Solids* **1999**, *60*, 145.

[11]   J. Haines, C. Chateau, J. M. Léger, A. Le Sauze, N. Diot, R. Marchand, S. Hull, *Acta Crystallogr., Sect. B: Struct. Sci.* **1999**, *55*, 677.

[12]   a) T. Grande, J. R. Holloway, P. F. McMillan, C. A. Angell, *Nature* **1994**, *369*, 43; b) T. Grande, S. Jacob, J. R. Holloway, P. F. McMillan, C. A. Angell, *J. Non-Cryst. Solids* **1995**, *184*, 151.

[13]   a) N. Kawai, S. Endo, *Rev. Sci. Instrum.* **1970**, *41*, 1178; b) D. Walker, M. A. Carpenter, C. M. Hitch, *Am. Mineral.* **1990**, *75*, 1020; c) D.Walker, *Am. Mineral.* **1991**, *76*, 1092; d) D. C. Rubie, *Phase Transitions* **1999**, *68*, 431; e) H. Huppertz, *Z. Kristallogr.* **2004**, *219*, 330.

[14]   a) W. E. Klee, *Z. Kristallogr.* **1987**, *179*, 67; b) A. Beukemann, W. E. Klee, *Z. Kristallogr.* **1994**, *209*, 709.

[15]   a) V. A. Blatov, M. O'Keeffe, D. M. Proserpio, *CrystEngComm* **2010**, *12*, 44; b) V. A. Blatov, *IUCr CompComm Newsletter* **2006**, *7*, 4.

[16]   A. Le Bail, *Phys. Chem. Chem. Phys.* **2010**, *12*, 8521.

[17]   a) H. Bärnighausen, *MATCH, Commun. Math. Chem.* **1980**, *9*, 139; b) U. Müller, *Z. Anorg. Allg. Chem.* **2004**, *630*, 1519.

[18]   a) R. Hoppe, *Angew. Chem.* **1966**, *78*, 52; *Angew. Chem., Int. Ed. Engl.* **1966**, *5*, 95; b) R. Hoppe, *Angew. Chem.* **1970**, *82*, 7; *Angew. Chem., Int. Ed. Engl.* **1970**, *9*, 25.

[19]   M. Zeuner, S. Pagano, W. Schnick, *Angew. Chem.* **2011**, *123*, 7898; *Angew. Chem., Int. Ed.* **2011**, *50*, 7754.

[20]   S. J. Sedlmaier, V. R. Celinski, J. Schmedt auf der Günne, W. Schnick, *Chem. Eur. J.* **2012**, *18*, 4358.

[21]   W. Schnick, *Angew. Chem.* **1993**, *105*, 846; *Angew. Chem., Int. Ed. Engl.* **1993**, *32*, 806.

[22]   R. Klement, O. Koch, *Chem. Ber.* **1954**, *87*, 333.

[23]   A. A. Coelho, *TOPAS-Academic*, Version 4.1, Coelho Software, Brisbane (Australia), **2007**.

[24]   A. A. Coelho, *J. Appl. Crystallogr.* **2003**, *36*, 86.

[25]   a) G. Oszlányi, A. Sütő, *Acta Crystallogr., Sect. A: Found. Crystallogr.* **2004**, *60*, 134; b) G. Oszlányi, A. Sütő, *Acta Crystallogr., Sect. A: Found. Crystallogr.* **2008**, *64*, 123; c) A. A. Coelho, *Acta Crystallogr., Sect. A: Found. Crystallogr.* **2007**, *63*, 400.

[26]   J. Bergmann, R. Kleeberg, A. Haase, B. Breidenstein., *Mater. Sci. Forum* **2000**, *347-349*, 303.

7.   Sr$_3$P$_6$O$_6$N$_8$ – A Highly Condensed Layered Phosphate

The newly developed amorphous PON starting material has proved to be an excellent precursor for unprecedented phosphorus oxonitride imides and phosphorus oxonitrides (see last two chapters). As it seems to be highly reactive, it could also be an optimal starting material for the synthesis of oxonitridophosphates. And this synthesis can be performed according to the synthesis strategy developed by *Landskron* for the synthesis of nitridophosphates—the so-called azide route (treating P$_3$N$_5$ and metal azides in a high-pressure press). Whether or not the transfer of this strategy to the synthesis of oxonitridophosphates was successful by simply replacing the starting material P$_3$N$_5$ by the precondensed amorphous PON, can be read in this chapter.
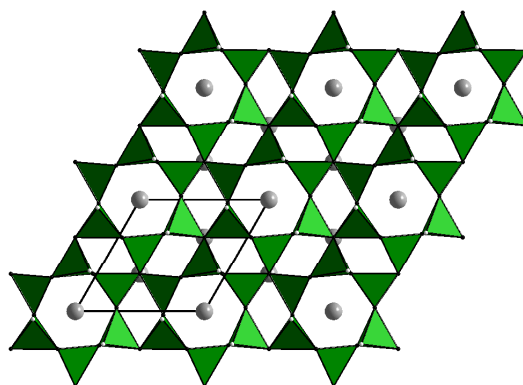
7.1   INTRODUCTION WITH RESULTS AND DISCUSSION

We describe the synthesis and the structure elucidation of $Sr_3P_6O_6N_8$, a novel, highly condensed layered phosphate.

During the last decades, inorganic phosphates have emerged from chemical commodities to advanced materials. Classical application areas of these basic inorganic compounds include usage as water softeners, fertilizers and coating materials.[1] Nowadays, phosphates are being used as ionic conductors,[2] catalysts in organic syntheses[3] and even as modern optical materials.[4–6] For example, KH_2PO_4 and $KTiOPO_4$ represent famous non-linear optical (NLO) materials used for frequency doubling (second harmonic generation, SHG), while ultraphosphates and phosphate glass (e.g. REP_4O_{11} and REP_5O_{14} where RE = lanthanide, and Nd^{3+}-doped vitreous phosphates) find applications as powerful laser materials.

The structural chemistry of inorganic phosphates has been widely studied in the past.[7] Classical representatives consist predominantly of orthophosphates, finite and infinite chain-phosphates, as well as ring-phosphates. Here Q^0 (non-linking) up to Q^2-type (double linking) PO_4-tetrahedra occur. Band-, layer- or framework-structures with Q^3 or even Q^4-type tetrahedra (comparable to silicates) have barely been identified. For higher condensed phosphates (exhibiting a degree of condensation (i.e. the molar ratio P : O = κ > 1/3)), only a few examples in the group of ultra-phosphates have been described. Moreover, the maximum degree of condensation for oxophosphates is $\kappa = 0.40$.[8] A further increase of cross-linking in phosphates, and thereby higher condensed structures, can be achieved in nitridophosphates or oxonitridophosphates by full or partial substitution O/N. With the integration of three-fold linking nitrogen, the structural diversity is significantly enhanced resulting in silicate-analogous networks, the latter being a consequence of the isolobal relation between P–N and Si–O which is further corroborated, for example, by HPN_2 (= PN(NH)) and PON that are isosteric to SiO_2. By variation of the molar ratio O:N, thus changing the framework charge, network structures with different topologies similar to silicate structures can be achieved. Complete substitution of O for N, yields nitridophosphates like MP_4N_7 with M = K, Rb, Cs[9] which adopt a network of corner-sharing PN_4-tetrahedra. The silicate analogy has further been demonstrated by the class of nitridosodalites[10] and related oxonitridosodalites.[11] However, complementing the diverse and rich structural chemistry of oxosilicates, new framework-types have been realized in (oxo-)nitridophosphates,[12] e.g. the first nitridic zeolite NPO.[13] Recently, this novel framework-type containing large 12-ring channels was paralleled by its nitridosilicate

analogue.[14] Another novel porous compound was obtained under high-pressure conditions—$P_4N_4(NH)_4(NH_3)$[15]—the first nitridic clathrate that traps ammonia molecules in an unique cage structure that had been previously predicted as a possible silica framework.[16,17] Highly condensed layer structures had not been realized so far; this includes oxophosphates and nitridophosphates, although the layered *O'*-form of $(P_2O_5)_x$ was discovered in the late 1940s.[18]

In this contribution we communicate the synthesis and structural characterization of a novel oxonitridophosphate, namely $Sr_3P_6O_6N_8$. Its P–O–N substructure exhibits a degree of condensation of $\kappa = 0.43$ thus representing the most condensed layer structure in phosphate chemistry so far. A few known oxonitridophosphates (e.g. $M^I_3M^{III}P_3O_9N$ or $M^I_2M^{II}_2P_3O_9N$)[19,20] have been synthesized by conventional solid-state reactions.[21] By contrast, the preparation of $Sr_3P_6O_6N_8$ demands high-pressure conditions. Thereby, the so-called "azide approach", that is well established for the preparation of diverse nitridophosphates,[15,22,23] was transferred to the synthesis of oxonitridophosphates (see chapter 7.2.1). Employing a modified Walker module (multi-anvil assembly), $Sr_3P_6O_6N_8$ was obtained by heating a mixture of strontium azide $Sr(N_3)_2$ and phosphorus oxonitride PON at ca. 920 °C and 6 GPa (Equation (1)). Accordingly, the metal azide features a double role in the synthesis.

$$3Sr(N_3)_2 + 6PON \rightarrow \text{"}Sr_3N_2\text{"} + 8N_2 + 6PON \rightarrow Sr_3P_6O_6N_8 + 8N_2 \qquad (1)$$

With the thermolysis of the azide in a closed system, a high N_2 partial pressure is generated and the dissociation of PON is suppressed at temperatures above 850 °C which are necessary for the crystallization of the product.[24] Simultaneously, the metal nitride that may be formulated as an intermediate (Equation (1)) is provided in situ for the reaction. Marginal amounts of amorphous, black phosphorus occurring during the synthesis of $Sr_3P_6O_6N_8$ coming from partial decomposition of the product can be removed by sublimation *in vacuo*. The elemental composition of the product was confirmed by energy dispersive X-ray analysis. All elements contained in the formula were detected and, within the accuracy of the method, the expected molar ratios were observed.

The crystal structure of $Sr_3P_6O_6N_8$ was solved on the basis of powder X-ray diffraction data by direct methods (EXPO)[25] and refined by the Rietveld method (GSAS;[26] Figure 1).[27]
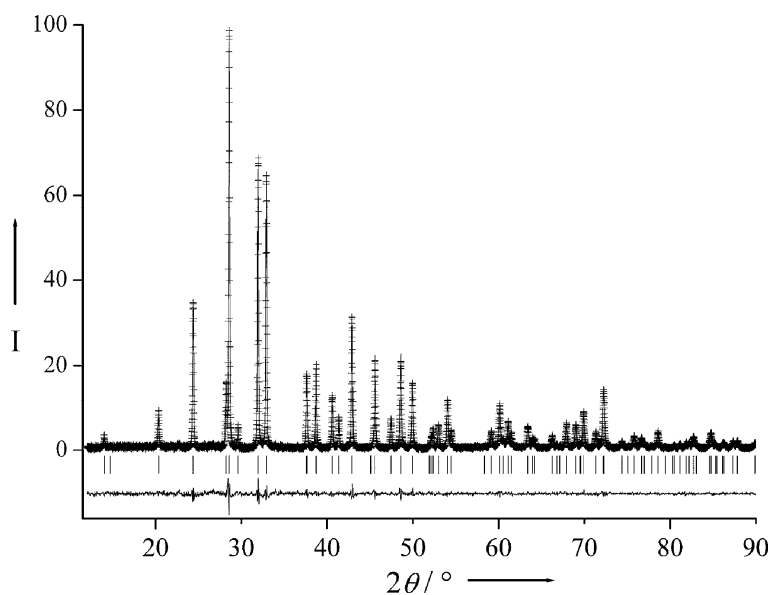
Figure 1. Observed (crosses) and calculated (line) X-ray powder diffraction pattern (Cu-$K_{\alpha 1}$-radiation) as well as the difference profile of the Rietveld refinement of $Sr_3P_6O_6N_8$; allowed peak positions are marked by vertical lines; background is subtracted.

$Sr_3P_6O_6N_8$ exhibits an unprecedented phosphate layer resembling those of oxonitridosilicates (Figure 2).[28] It is made up of Q^3-type PON_3-tetrahedra leading to a degree of condensation $\kappa = n(P) : n(O,N) = 0.43$ for the $[P_6O_6N_8]^{6-}$ structure. According to $\{uB,3,1_{\infty}2\}[(P_6^{[4]}O_6^{[1]}N_6^{[2]}N_{6/3}^{[3]})^{6-}]$,[29,30] the N atoms bridge two and three P atoms, respectively, whereas the O atoms are exclusively terminally bound to P. In contrast to nitridosilicates, $N^{[3]}$-connections are quite rare in nitridophosphate chemistry. The only examples yet known are P_3N_5,[31] HP_4N_7 (= P_4N_6NH),[32] P_4N_6O,[33] $Na_3P_6N_{11}$,[34] and $K_3P_6N_{11}$.[35]
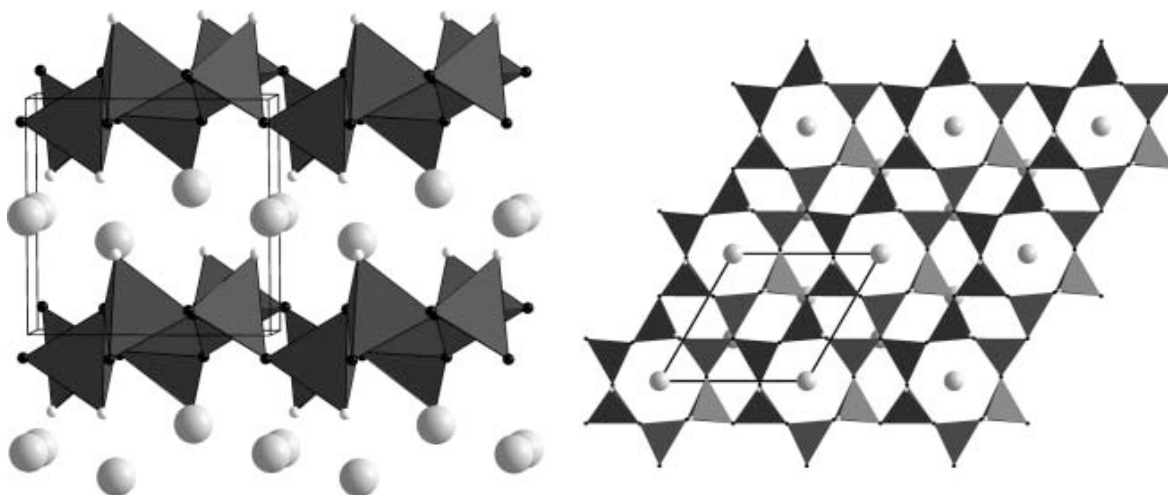
Figure 2. Crystal structure of $Sr_3P_6O_6N_8$, left: view along [010], right: view perpendicular to one single layer along [001] (Sr^{2+} light gray, O^{2-} white, N^{3-} black).

Due to similar scattering factors, a direct experimental differentiation between O and N is impossible by X-ray methods. However, in the case of $Sr_3P_6O_6N_8$ complete O/N

ordering is most probable as evidenced by ^{31}P solid-state NMR investigations, lattice energy calculations (MAPLE),[36] and P–O and P–N bond length differences. In the ^{31}P solid-state NMR spectrum of $Sr_3P_6O_6N_8$ (Figure 3) a single resonance at $\delta_{iso} = 2.6$ ppm (principle components: –23, 2, 29 ppm) was observed agreeing with the single P site and its point group symmetry (1). According to ^{31}P chemical shift data of other P–O–N-compounds in the literature,[37–39] this resonance is indicative of a condensed PON_3-tetrahedra. The calculated partial MAPLE values (O^{2-}: 2526, N^{3-}: 6786–6410, Sr^{2+}: 1977–2111, P^{5+}: 14608 kJ mol^{-1})[40] suggest that N atoms bridge the P atoms ($N^{[2]}$ and $N^{[3]}$ respectively) within the layerand the O atoms are bound terminally (Figure 1). The MAPLE values vary in a range typical for these ions.[28,41] The presence of hydrogen atoms bound to the $N^{[2]}$ atoms has been excluded by solid-state NMR employing a [31]P{[1]H} C-REDOR[42] experiment. Consequently, the bond length distribution in the N-bridges (158 and 164 pm) is according to P–$N^{[2]}$=P. The longest distance P–N (173 pm) was found at $N^{[3]}$. The shorter P–O bond lengths (153 pm) also corroborate the existence of exclusively PON_3-tetrahedra in $Sr_3P_6O_6N_8$. A similar O/N ordering was found in the layered oxonitridosilicates $M^{II}Si_6O_9N_4$[43] and $M^{II}Si_2O_2N_2$.[44]
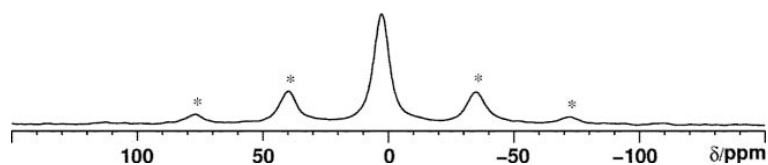
Figure 3. ^{31}P MAS NMR spectrum of $Sr_3P_6O_6N_8$ at a spinning frequency of 3 kHz; spinning sidebands are marked with asterisks.

The Sr^{2+}-ions along the channels (cf. Figure 2) are coordinated distorted octahedrally by six O at a distance of 261 pm(Figure 4, Sr2). In a longer distance (334 pm), these ions are further surrounded by six N atoms also in a distorted octahedral way. Around the second Sr site (Figure 4, Sr1), six O (267–286 pm) and four N (281–322 pm) coordinate predominantly from different sides. The Sr–O and Sr–N distances range in the interval of the sum of their ionic radii.[45]
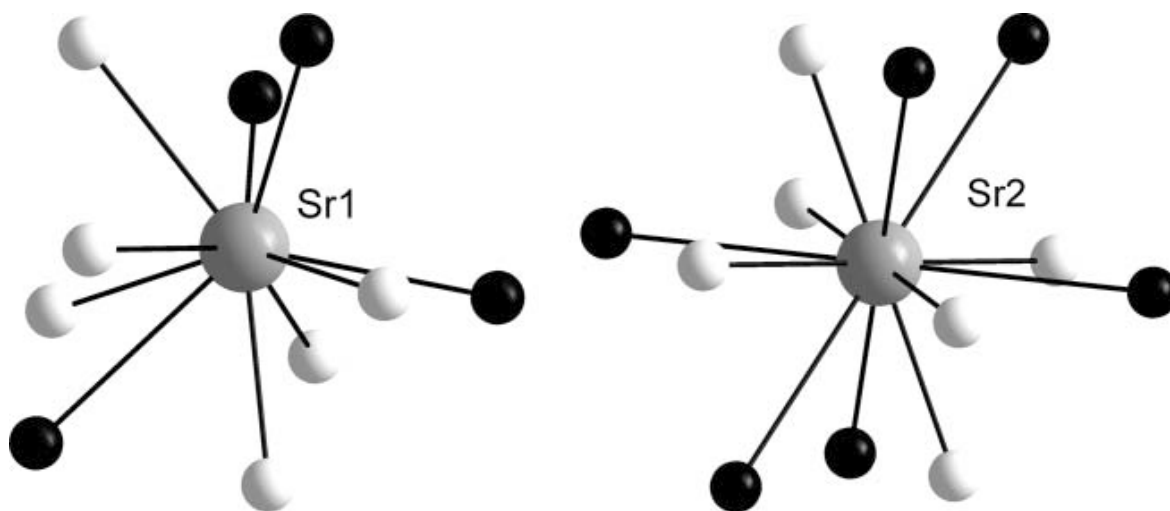
Figure 4. Coordination of the Sr sites in $Sr_3P_6O_6N_8$ (Sr^{2+} gray, O^{2-} white, N^{3-} black).

The $[P_6O_6N_8]^{6-}$-layers in $Sr_3P_6O_6N_8$ are built up of condensed 6-rings and 4-rings (Figure 2). These fundamental building units (FBUs) occur in other layered phosphates, but not simultaneously. In ultraphosphates (e.g. compositions like $M^{II}P_4O_{11}$ or $M^{III}P_5O_{14}$), besides small rings, there are always other rings with up to 16 tetrahedra resulting in large pore size layers.[8] Comparable layers can only be found within silicates,[29] whereas in purely oxidic silicates isostructural layers are prevented because oxygen usually avoids three-fold bridging positions. The oxonitridosilicates $M^{II}Si_6O_9N_4$[43] exhibit a related structure which, however, contain different 6-rings and additional 3-rings. However, an analogous structural motif can be identified in the structure of β-Si_3N_4.[46] There, isosteric Si_6N_{14}-layers are linked in the third dimension through SiN_4-tetrahedra (Figure 5). A formal derivation of the structure of $Sr_3P_6O_6N_8$ from the β-Si_3N_4-structure can be achieved by a separation of the Si_6N_{14}-layers and intercalating Sr^{2+}-ions, disregarding the atom assignment (P–Si, O–N). A compound that might be isostructural to $Sr_3P_6O_6N_8$, namely $Ba_3Si_6O_{12}N_2$, has been mentioned recently in a patent for a new green luminescent material for phosphor-converted white light (pc)LED applications. However a detailed crystallographic structure solution and refinement for the latter compound has not been communicated as yet.[47]
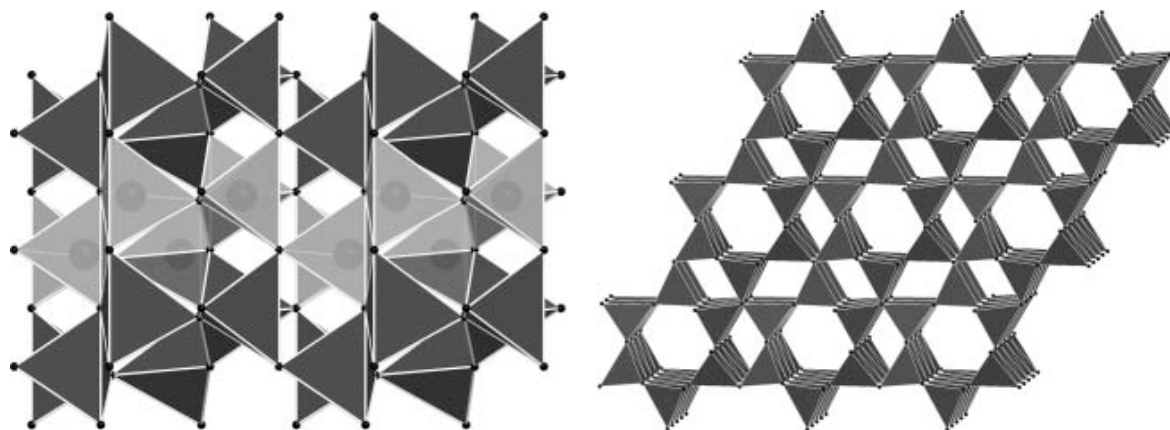
Figure 5. Crystal structure of β-Si_3N_4, left: view along [010]. By removing every second layer (gray) and substituting the emerging terminal N by O atoms (besides a Si / P-replacement) results in topological similar layers as found in $Sr_3P_6O_6N_8$; right: view along [001]; (Si^{4+} dark gray, N^{3-} black).

In conclusion, with $Sr_3P_6O_6N_8$ this class of phosphates gains a remarkable expansion of its structural chemistry. The highly condensed layered structure of $Sr_3P_6O_6N_8$, containing 6- and 4-rings of PON_3-tetrahedra, represents the first closed layer structure in phosphate chemistry. Layer structures with such a high degree of condensation were hitherto only known in silicate chemistry. The fact that the title compound is probably isostructural with a new green phosphor suggests an analogous application for $Sr_3P_6O_6N_8$. By doping it with lanthanides (e.g. Eu^{2+}) we are currently investigating the potential of $Sr_3P_6O_6N_8$ as a phosphor material. Consequently the substance class of the oxonitridophosphates could be developed to a new substance class for luminous applications. Prospectively, it would be interesting to access denser layer structures in oxonitridophosphates by a stepwise increase of the nitrogen ratio.

7.2   EXPERIMENTAL SECTION

7.2.1   Synthesis and Energy dispersive X-ray analysis

$Sr_3P_6O_6N_8$ was synthesized from $Sr(N_3)_2$[48] and PON[49,50] by a high-pressure, high-temperature reaction in a Walker-type multi-anvil[51,52] assembly. In a glovebox (Unilab, MBraun, filled with dry Ar, O_2 < 0.1 ppm, H_2O < 0.1 ppm) a finely ground mixture of the starting materials (approx. 50 mg) was placed into a capsule made of hexagonal boron nitride (Henze, Kempten) and compressed in an MgO-octahedron with an edge length of 18 mm (Ceramic Substrates, Isle of Wight). At 6 GPa the sample was heated over 15 min to about 920 °C, this temperature was maintained for 15 min, and finally the sample was cooled down to room temperature over 30 min. Further details concerning the assembly are

described in the literature.[53] A crude product in the form of a black, cylindrical solid was isolated. To purify $Sr_3P_6O_6N_8$ from small amounts of black, amorphous phosphorus the product was pulverized and heated *in vacuo* at 680 °C for 5 d. $Sr_3P_6O_6N_8$ was obtained as a gray, air- and water stable, microcrystalline powder.

Energy dispersive X-ray analysis measurements were performed on a JSM 6500F scanning electron microscope (Jeol; detector model 7418, Oxford Instruments). At 14 measuring points the ratios P : Sr = 2.5 (theoretical value according to the formula: 2.0) and N : O = 1.3 (theoretical value according to the formula: 1.3) were determined. These values are located within the accuracy of measurement for the method.

7.2.2   Solid state NMR spectroscopy

$^{31}P\{^1H\}$ MAS NMR experiments were carried out on a BRUKER Avance II spectrometer equipped with a commercial 2.5 mm MAS NMR double resonance probe at a magnetic field strength of 4.7 T. The chemical shift values refer to a deshielding scale and 85 % H_3PO_4 used as an external reference. The C-REDOR experiment and the determination of the principle components were carried out as described in the literature.[54,55] Up to 1.2 ms on the unified dephasing scale, no dephasing was observed in the C-REDOR curves (see Figure 6). Hence ^1H-^{31}P spin pairs at a distance smaller than approximately 1 pm can be ruled out at the noise level of the experiment. Together with half the maximum P–P distance in the unit cell, this proves the absence of H atoms in $Sr_3P_6O_6N_8$.
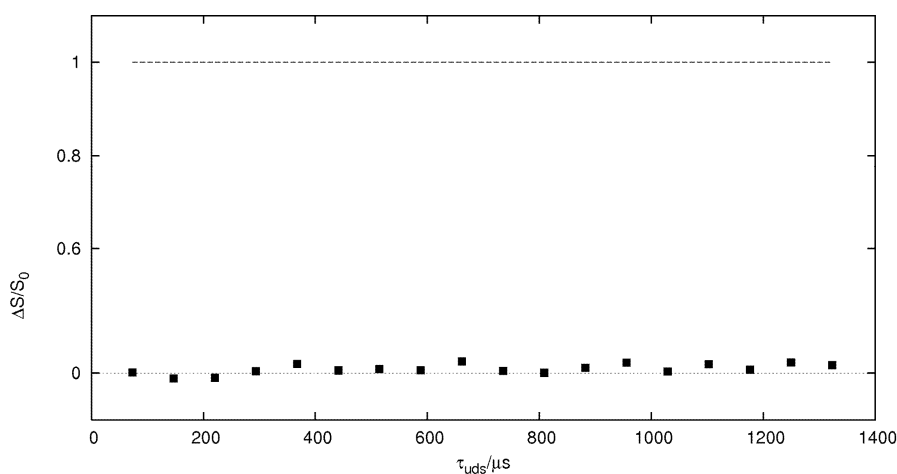
Figure 6. $^{31}P\{^1H\}$-CREDOR curve of the ^{31}P resonance of $Sr_3P_6O_6N_8$; the experimental conditions are the same as those used in reference [54].

7.3   REFERENCES

[1]   A. F. Holleman, E. Wiberg, N. Wiberg, *Lehrbuch der Anorganischen Chemie*, de Gruyter, Berlin, 102nd edn., **2007**, pp. 798.

[2]   A. R. West, *Basic Solid State Chemistry*, John Wiley & Sons Ltd, Chichester, UK, **1999**, pp. 336.

[3]   P. T. Nguyen, A. W. Sleight, N. Roberts, W. W. Warren, *J. Solid State Chem.* **1996**, *122*, 259.

[4]   C. N. R. Rao, J. Gopalakrishnan, *New directions in solid state chemistry*, Cambridge University Press, Cambridge, **1986**.

[5]   J. D. Bierlein, H. Vanherzeele, *J. Opt. Soc. Am. B* **1989**, *6*, 622.

[6]   M. J. Weber, *J. Non-Cryst. Solids* **1990**, *123*, 208; R. K. Brow, *J. Non-Cryst. Solids* **2000**, *263–264*, 1; J. H. Campbell, T. I. Suratwala, *J. Non-Cryst. Solids* **2000**, *263–264*, 318.

[7]   A. Durif, *Crystal Chemistry of Condensed Phosphates*, Plenum Press, New York and London, **1995**.

[8]   R. Glaum, habilitation treatise, Univ. Gießen, **1999**.

[9]   K. Landskron, E. Irran, W. Schnick, *Chem. Eur. J.* **1999**, *5*, 2548.

[10]   W. Schnick, J. Lücke, *Angew. Chem.* **1992**, *104*, 208; W. Schnick, J. Lücke, *Angew. Chem., Int. Ed. Engl.* **1992**, *31*, 213; W. Schnick, J. Lücke, *Z. Anorg. Allg. Chem.* **1994**, *620*, 2014; W. Schnick, N. Stock, J. Lücke, M. Volkmann, M. Jansen, *Z. Anorg. Allg. Chem.* **1995**, *621*, 987; F. Wester, W. Schnick, *Z. Anorg. Allg. Chem.* **1996**, *622*, 1281.

[11]   N. Stock, E. Irran, W. Schnick, *Chem. Eur. J.* **1998**, *4*, 1822.

[12]   S. Correll, N. Stock, O. Oeckler, W. Schnick, *Angew. Chem.* **2003**, *115*, 3674; S. Correll, N. Stock, O. Oeckler, W. Schnick, *Angew. Chem., Int. Ed.* **2003**, *42*, 3549.

[13]   C. Baerlocher, L. B. McCusker, *Database of Zeolites Structures*, http://www.iza-structure.org/databases/.

[14]   A. J. D. Barnes, T. J. Prior, M. G. Francesconi, *Chem. Commun.* **2007**, 4638.

[15]   F. Karau, W. Schnick, *Angew. Chem.* **2006**, *118*, 4617; F. Karau, W. Schnick, *Angew. Chem., Int. Ed.* **2006**, *45*, 4505.

[16]   M. D. Foster, O. D. Friedrichs, R. G. Bell, F. A. A. Paz, J. Klinowski, *J. Am. Chem. Soc.* **2004**, *126*, 9769.

[17]   M. M. J. Treacy, K. H. Randall, S. Raho, J. A. Perry, D. J. Chadi, *Z. Kristallogr.* **1997**, *212*, 768.

[18]   C. H. MacGillavry, H. C. J. de Decker, L. M. Nijland, *Nature* **1949**, *164*, 448.

[19]   W. Feldmann, *Z. Chem.* **1987**, *27*, 100.

[20]   R. Conanec, W. Feldmann, R. Marchand, Y. Laurent, *Solid State Chem.* **1996**, 121, 418.

[21]   R. Marchand, W. Schnick, N. Stock, *Adv. Inorg. Chem.* **2000**, *50*, 193.

[22]   F.W. Karau, W. Schnick, *J. Solid State Chem.* **2005**, *178*, 135.

[23]   F. Karau, W. Schnick, *Z. Anorg. Allg. Chem.* **2006**, *632*, 231.

[24]   F. Tessier, A. Navrotsky, A. Le Sauze, R. Marchand, *Chem. Mater.* **2000**, *12*, 148.

[25]   A. Altomare, M. C. Burla, M. Camalli, B. Carrozzini, G. L. Cascarano, C. Giacovazzo, A. Guagliardi, A. G. G. Moliterni, G. Polidori, R. Rizzi, *J. Appl. Crystallogr.* **1999**, *32*, 339.

[26]   A. C. Larson, R. B. Von Dreele, *Los Alamos National Laboratory Report LAUR*, **2000**, 86; B. H. Toby, *J. Appl. Crystallogr.* **2001**, *34*, 210.

[27]   Crystal data for $Sr_3P_6O_6N_8$ (M_r = 656.8 g mol^{-1}): trigonal, space group $P\bar{3}$ (no. 147), a = 7.29667(5), c = 6.02603(5) Å, V = 277.851(5) Å^3, Z = 1; Stoe Stadi P diffractometer (Debye-Scherrer geometry), Cu-$K_{\alpha1}$ (λ = 1.5406 Å), T = 298(2) K, step width of 2θ = 0.1°, N_{obs} = 159; 8 profile parameters (pseudo-Voigt), 17 atomic parameters, background function: shifted Chebyshev (20 coefficients), $R(F^2)$ = 0.0229, wR_p = 0.0263, R_p = 0.0202.[†]

[28]   a) H. A. Höppe, Doctoral Thesis, Univ. Munich (LMU), **2003**; b) F. Stadler, Doctoral Thesis, Univ. Munich (LMU), **2006**.

[29]   F. Liebau, *Structural Chemistry of Silicates*, Springer, Berlin, **1985**.

[30]   H.-J. Klein, F. Liebau, *J. Solid State Chem.* **2008**, *181*, 2412.

[31]   W. Schnick, J. Lücke, F. Krumeich, *Chem. Mater.* **1996**, *8*, 281; S. Horstmann, E. Irran, W. Schnick, *Angew. Chem.* **1997**, *109*, 1938; S. Horstmann, E. Irran, W. Schnick, *Angew. Chem., Int. Ed. Engl.* **1997**, *36*, 1873; S. Horstmann, E. Irran, W. Schnick, *Z. Anorg. Allg. Chem.* **1998**, *624*, 620.

[32]   S. Horstmann, E. Irran, W. Schnick, *Angew. Chem.* **1997**, *109*, 2085; S. Horstmann, E. Irran, W. Schnick, *Angew. Chem., Int. Ed. Engl.* **1997**, *36*, 1992; S. Horstmann, E. Irran, W. Schnick, *Z. Anorg. Allg. Chem.* **1998**, *624*, 221.

[33]   J. Ronis, B. Bondars, A. Vitola, T. Millers, J. Schneider, F. Frey, *J. Solid State*

---

† Further details of the crystal structure investigation may be obtained from Fachinformationszentrum Karlsruhe, 76344 Eggenstein-Leopoldshafen, Germany (fax: (+49)7247-808-666; e-mail: crysdata@fiz-karlsruhe.de, http://www.fiz-karlsruhe.de/request_for_deposited_data.html) on quoting the depository number CSD-419864.

Chem. **1995**, *115*, 265.

[34]   A. Vitola, J. Ronis, T. Millers, *Latv. PSR Zinat. Akad. Vestis, Kim. Ser.* **1990**, *1*, 35.

[35]   H. Jacobs and R. Nymwegen, *Z. Anorg. Allg. Chem.* **1997**, *623*, 429.

[36]   R. Hoppe, *Angew. Chem.* **1966**, *78*, 52; R. Hoppe, *Angew. Chem., Int. Ed. Engl.* **1966**, *5*, 95; R. Hoppe, *Angew. Chem.* **1970**, *82*, 7; R. Hoppe, *Angew. Chem., Int. Ed. Engl.* **1970**, *9*, 25.

[37]   N. Stock, E. Irran, W. Schnick, *Chem. Eur. J.* **1998**, *4*, 1822.

[38]   A. Le Sauze, L. Montagne, G. Palavit, R.Marchand, *J. Non-Cryst. Solids* **2001**, *293–295*, 81.

[39]   S. Correll, N. Stock, O. Oeckler, J. Senker, T. Nilges, W. Schnick, *Z. Anorg. Allg. Chem.* **2004**, *630*, 2205.

[40]   Lattice energy calculations were carried out with R. Hübenthal, MAPLE, *Programm zur Berechnung des Madelunganteils der Gitterenergie*, Version 4, Univ. Gießen, **1993**.

[41]   a) K. Landskron, Doctoral Thesis, Univ. Munich (LMU), **2001**; b) K. Köllisch, Doctoral Thesis, Univ. Munich (LMU), **2001**.

[42]   J. C. C. Chan, H. Eckert, *J. Chem. Phys.* **2001**, *115*, 6095.

[43]   F. Stadler, W. Schnick, *Z. Anorg. Allg. Chem.* **2006**, *632*, 949.

[44]   H. A. Höppe, F. Stadler, O. Oeckler, W. Schnick, *Angew. Chem.* **2004**, *116*, 5656; H. A. Höppe, F. Stadler, O. Oeckler, W. Schnick, *Angew. Chem., Int. Ed.* **2004**, *43*, 5540; F. Stadler, O. Oeckler, H. A. Höppe, M. H. Möller, R. Pöttgen, B. D. Mosel, P. Schmidt, V. Duppel, A. Simon, W. Schnick, *Chem. Eur. J.* **2006**, *12*, 6984; O. Oeckler, F. Stadler, T. Rosenthal, W. Schnick, *Solid State Sci.* **2007**, *9*, 205; J. A. Kechele, O. Oeckler, F. Stadler, W. Schnick, *Solid State Sci.* **2009**, *11*, 537.

[45]   R. D. Shannon, C. T. Prewitt, *Acta Crystallogr., Sect. B: Struct. Sci.* **1969**, *25*, 925.

[46]   R. Grün, *Acta Crystallogr., Sect. B: Struct. Sci.* **1979**, *35*, 800.

[47]   S. Shimooka, K. Uheda, M. Mikami, N. Kijima, H. Imura and K. Horibe, Mitsubishi Chemical Corporation, PCT Int. Appl., WO088966, A1, **2007**.

[48]   a) P. Remy-Genneté, *Ann. Chim.* **1933**, *19*, 263; b) P. Ehrlich, H. J. Seifert, *Handbuch der Präparativen Anorganischen Chemie*, G. Brauer (ed.), Ferdinand Enke Verlag, vol. 2, Stuttgart, **1987**, p. 930.

[49]   L. Boukbir, R. Marchand, Y. Laurent, P. Bacher, G. Roult, *Ann. Chim. Fr.* **1989**, *14*, 475.

[50]   Amorphous PON was obtained by heating a mixture of one part $PO(NH_2)_3$ and

three parts NH_4Cl in a ZrO_2-crucible in a continuous nitrogen flow at 680 °C for 48 h according to the equation $PO(NH_2)_3 + 3NH_4Cl \rightarrow PON + 3NH_4Cl + 2NH_3$. The mixture results from the reaction of $POCl_3$ with liquid NH_3 described by R. Klement, O. Koch, *Chem. Ber.* **1954**, *87*, 333.

[51] D. Walker, M. A. Carpenter, C. M. Hitch, *Am. Mineral.* **1990**, *75*, 1020.

[52] D. Walker, *Am. Mineral.* **1991**, *76*, 1092.

[53] H. Huppertz, *Z. Kristallogr.* **2004**, *219*, 330.

[54] M. Roming, C. Feldmann, Y. S. Avadhut, J. Schmedt auf der Günne, *Chem. Mater.* **2008**, *20*, 5787.

[55] J. Schmedt auf der Günne, *J. Magn. Reson.* **2003**, *165*, 18.

8.   High-Pressure Synthesis and Crystal Structure of Ba$_3$P$_6$O$_6$N$_8$

The potential of Sr$_3$P$_6$O$_6$N$_8$ as well as of Ba$_3$P$_6$O$_6$N$_8$, described in this chapter, as luminescent material was investigated in a series of experiments by doping the compounds with Eu^{2+}. In contrast to the green phosphor M$_3$Si$_6$O$_{12}$N$_2$:Eu^{2+} (M = Sr, Ba) the oxonitridophosphates did not show any luminescent properties. The reason for the absence of a visible emission may be a band gap which is smaller than the excitation energy. This could worked out by determination of the band gap of M$_3$P$_6$O$_6$N$_8$ (M = Sr, Ba) by e.g. X-ray absorption near edge spectroscopy (XANES) or DFT calculations. Possibly, by doping with other activator ions than Eu^{2+}, e.g. Sn^{2+},[†] emission could be generated.

ABSTRACT

Ba$_3$N$_8$O$_6$P$_6$, hexagonal, $P\bar{3}$ (no. 147), $a = 740.2270(89)$, $b = 631.436(11)$ pm, $V = 299.633(9)$ Å^3, Z = 1, $R_p = 0.041$, $wR_p = 0.054$, T = 297 K.

[†] R. C. Ropp, R. W. Mooney, *J. Electrochem. Soc.* **1960**, *107*, 15.

8.1   SOURCE OF MATERIAL

$Ba_3P_6O_6N_8$ was synthesized by a high-pressure, high-temperature reaction from $Ba(N_3)_2$ and amorphous PON in a Walker-type multi-anvil assembly. A finely ground mixture (ratio $Ba(N_3)_2$: PON = 1 : 2; approx. 50 mg) was placed into a capsule made of hexagonal boron nitride and compressed in a MgO-octahedron with an edge length of 18 mm. At 6 GPa the sample was heated over 15 min to about 920 °C, this temperature was maintained for 15 min, and finally the sample was cooled down to room temperature over 30 min. Further details concerning the assembly are described in ref. [1]. $Ba_3P_6O_6N_8$ was obtained as a light gray, air- and water stable, microcrystalline solid.

8.2   EXPERIMENTAL

A Rietveld refinement was performed with the TOPAS package starting from the atomic parameters of isotypic $Sr_3P_6O_6N_8$. Preferred orientation of the crystallites was described with a spherical harmonics function of 4th order. Displacement parameters of atoms N/O have been constraint to one common value.

8.3   DISCUSSION

A few years ago, the $Ba_3Si_6O_{12}N_2$: Eu^{2+} and its solid solution series $Ba_{3-x}Sr_xSi_6O_{12}N_2$ have been discovered as efficient green phosphors for phosphor-converted light-emitting diodes.[2,3] Just short before, the structure type of this silicate compound, however, was elucidated for the oxonitridophosphate $Sr_3P_6O_6N_8$.[4] It exhibits a highly condensed layered structure. $Sr_3P_6O_6N_8$ was successfully synthesized by transferring the so-called azide high-pressure synthesis route to the P/O/N system. This synthesis route was originally applied for the preparation of pure nitridophosphates in combination with P_3N_5.[5] The benefits of transforming a metal azide with P_3N_5 in the closed system of a high-pressure press are that the respective metal nitride is generated *in-situ* while simultaneously the decomposition of P_3N_5 is suppressed with the high nitrogen partial pressure. By employing this method using amorphous PON as starting material, we were able to synthesize $Sr_3P_6O_6N_8$ and by now also $Ba_3P_6O_6N_8$. According to the pressure-homologue rule, the higher homologue $Ba_3P_6O_6N_8$ can also be generated at lower pressures such as 4 GPa. Like for the oxonitridosilicate system, evidence for a calcium homogogue ($Ca_3P_6O_6N_8$) however, is not

existent, even not at higher pressures. The crystal structure of $Ba_3P_6O_6N_8$ consists of two-dimensional layer anions $[P_6O_6N_8]^{6-}$ parallel (001) and Ba^{2+} ions in-between (Figure 1). The anions are composed of vertex-sharing Q^3-type PON_3 tetrahedra, which form condensed 4- and 6-rings with twofold and threefold N atoms involved within the layer. The O atoms are bound terminally. The bond length P–N were determined to 159.1 and 166.4 pm ($N^{[2]}$ involved) and 172.5 pm ($N^{[3]}$ involved). As expected the bond length P–$O^{[1]}$ is with 144.9 pm significantly shorter. The Ba^{2+} ions are coordinated 10-fold by four N [Ba-N: 295.4, 297.3 pm] and six O atoms [283.0, 293.1 pm], and 12-fold by 6 N [272.2 pm] and 6 O atoms [345.0 pm], respectively.
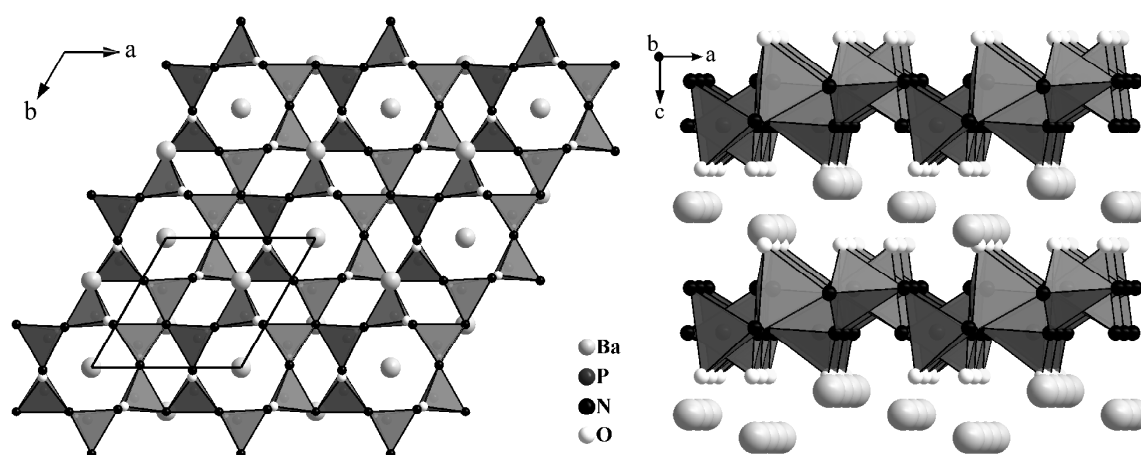
Figure 1. Crystal structure of $Ba_3P_6O_6N_8$, left: view perpendicular to one single layer along [001], right: view along [010], (Ba^{2+} light gray, O^{2-} white, N^{3-} black).

Table 1. Data collection and handling.

material:	colorless powder
wavelength:	Mo-K_α (71.069 pm)
μ:	9.7 mm^{-1}
diffractometer:	Stoe Stadi P
2θ range:	2–60°
N(hkl):	604
N(param):	68
programs:	TOPAS-Academic 4.1,[6] Diamond 3.0[7]

Table 2. Atomic coordinates, Wyckoff symbols and isotropic displacement parameters U_{iso} / $\mathring{A}^2$.

atom	Wyckoff symbol	x	y	z	U_{iso}
Ba(1)	2d	2/3	1/3	0.38528(23)	0.0101(5)
Ba(2)	1b	0	0	1/2	0.0129(6)
P	6g	0.77473(54)	0.17468(56)	0.89670(54)	0.0053(8)
N(1)	2d	2/3	1/3	0.9175(19)	0.0058(13)
N(2)	6g	0.6860(17)	0.0193(13)	0.1073(16)	0.0058(13)
O	6g	0.7094(14)	0.0721(11)	0.6840(12)	0.0058(13)

8.4   REFERENCES

[1]   H. Huppertz, *Z. Kristallogr.* **2004**, *219*, 330.

[2]   S. Shimooka, K. Uheda, M. Mikami, N. Kijima, H. Imura and K. Horibe, Mitsubishi Chemical Corporation, PCT Int. Appl., WO088966, A1, **2007**.

[3]   C. Braun, M. Seibald, S. L. Börger, O. Oeckler, T. D. Boyko, A. Moewes, G. Miehe, A. Tücks, W. Schnick, *Chem. Eur. J.* **2010**, *16*, 9646.

[4]   S. J. Sedlmaier, J. Schmedt auf der Günne, W. Schnick, *Dalton Trans.* **2009**, 4081.

[5]   a) K. Landskron, Doctoral Thesis, Univ. Munich (LMU), **2001**; b) F. Karau, Doctoral Thesis, Univ. Munich (LMU), **2007**.

[6]   A. A. Coelho, *TOPAS-Academic*, Version 4.1, Coelho Software, Brisbane, **2007**.

[7]   K. Brandenburg, *DIAMOND – Visual Crystal Structure Information System*, Version 2.0f, Crystal Impact, Bonn, Germany **1998**.

9.   High-Pressure Synthesis, Crystal Structure, and Characterization of Zn₂PN₃ – A New *Catena*-Polynitridophosphate

The compounds presented in the last chapters have all been synthesized under high pressure. Hence, the parameter pressure seems to be essential for P/O/N chemistry. In this chapter the value of high-pressure conditions is impressively pointed out for solid-state chemistry in general and (oxo)nitridophosphate chemistry in particular. Already 1986, directly after the idea of a silicate-analogous compound class of nitridophosphates was born, it has been tried to synthesize Zn_2PN_3. At that time the classical approach employing solid-state reactions starting from the binary nitrides at high temperatures has been applied—without success. The reason can be found out here:

ABSTRACT

Phase-pure zinc *catena*-polynitridophosphate Zn_2PN_3 was synthesized by means of high-pressure high-temperature conditions (1200 °C, 8 GPa) starting from Zn_3N_2 and P_3N_5 utilizing a multianvil assembly. It was obtained as a colorless, microcrystalline powder. The crystal structure of Zn_2PN_3 ($Cmc2_1$ (no. 36), $a = 937.847(6)$, $b = 547.696(4)$, $c = 492.396(3)$ pm, $Z = 4$, $Rp = 0.0110$, $wRp = 0.0141$) has been refined from powder X-ray diffraction data by the Rietveld method using the atomic parameters of isotypic Mg_2PN_3 as starting values. Interconnected by N-coordinated Zn^{2+} ions, the *catena*-polynitridophosphate chain anions run parallel [001] with a chain periodicity $P = 2$ and a stretching factor $f_s = 0.88$. FT-IR and Raman spectra of Zn_2PN_3 were recorded and relevant bands were assigned. The solid-state ^{31}P MAS NMR spectrum yielded a single resonance at $\delta = 42.8$. In addition an account of the thermal behavior of Zn_2PN_3 is given.

9.1   INTRODUCTION

Advances in modern materials chemistry often depend on developments in synthetic solid-state chemistry. A technique, becoming more and more important, is the high-pressure / high-temperature approach. Usage of diamond anvil cells (DACs) make very high pressures accessible ($\leq 500\,\text{GPa}$), however due to very small sample sizes, this method is predominantly employed for in situ studies on evolution of physical properties under pressure. For high-pressure synthesis up to 25 GPa targeting preparative amounts the multianvil technique is the method of choice.[1] Besides stabilization of higher coordination numbers, high-pressure synthesis may also have the great advantage that thermally labile precursors are stabilized when high temperatures are applied, which are typically used in solid-state reactions for kinetic activation.[2–4] This approach has been intensively utilized in our investigation of phosphorus (oxo)nitrides and (oxo)nitridophosphates, where the crystallization temperature often lies near or even above the decomposition temperature of the phases.[5] With the so-called azide-route, where P_3N_5 or PON react with respective metal azides, we succeeded to synthesize a variety of highly condensed (oxo)nitridophosphates with diverse structure types. Among these there are interesting networks like the first closed layer phosphate $Sr_3P_6O_6N_8$[6] or the first nitridic clathrate $P_4N_4(NH)_4 \cdot NH_3$[7] that has been discussed, amongst others, as gas storage material.[8] Furthermore, with this method, a series of alkaline earth nitridophosphates with composition $M^{II}P_2N_4$ are well-established, which exhibit a megakalsilite (for M^{II} = Sr, Ba(/Ca))[9] and a phenakite (for M^{II} = Be)[10] structure type, respectively. With $M^I_3P_6N_{11}$ (with M^I = Na–Cs)[11] and $M^IP_4N_7$ (M^I = Na–Cs),[12] even networks with a degree of condensation $\kappa > 0.5$ were realized by the high-pressure multianvil approach. In contrast, the number of compounds yet synthesized by classical solid-state reactions at ambient pressure is limited in the field of (oxo)nitridophosphates. Besides some nitridic open-framework structures (nitridosodalites,[13] oxonitridosodalites[14] and *NPO*-type zeolites[15]) only few less condensed compounds like Li_7PN_4[16] with isolated PN_4^{7-} ions, $Li_{10}P_4N_{10}$[17] containing the phosphorus(V) oxide related anion $P_4N_{10}^{10-}$, or the *catena*-polynitridophosphates $M^{II}_2PN_3$ (Mg, Ca)[18] could be obtained starting from the binary nitrides. However, if thermally unstable nitrides like Zn_3N_2 are involved in the synthesis, the multianvil high-pressure technique is the method of choice.

In this contribution we report on the high-pressure synthesis, crystal structure, vibrational spectra, NMR spectrum and thermal behavior of the new nitridophosphate Zn_2PN_3.

9.2   RESULTS AND DISCUSSION

9.2.1   Synthesis

The azide-route proved to be specifically useful for the synthesis of highly condensed nitridophosphates.[5] In this approach, phosphorus(V) nitride P_3N_5[19] or phosphorus oxonitride PON[20] react with respective metal azides under high-pressure conditions. Thereby, through the thermolysis of the azide in a closed system a high N_2 partial pressure is generated to suppress dissociation of P_3N_5 / PON at temperatures above 800 to 850 °C (Equation (1)), which are necessary for the crystallization of the compounds. Simultaneously, the respective metal nitride is provided in situ for the reaction.

$$P_3N_5 \rightarrow 3PN + N_2 \; \rightarrow \; 0.75P_4 + 2.5N_2 \tag{1}$$

$$P_3N_5 + Zn_3N_2 \rightarrow 3\,Zn_2PN_3 \tag{2}$$

In case of the synthesis of Zn_2PN_3, zinc nitride Zn_3N_2 that was used instead of zinc azide due to explosion hazard, had to be stabilized in the first instance, besides P_3N_5. At ambient pressure Zn_3N_2 exhibits a decomposition temperature of $T_d = 400$ °C (under oxygen atmosphere) and 600 °C (under nitrogen atmosphere), respectively.[21] However, by applying high-pressure conditions of 8 GPa we succeeded to prevent the decomposition of both starting materials and synthesized Zn_2PN_3 at around 1200 °C (Equation (2)).

9.2.2   Crystal Structure

The crystal structure of Zn_2PN_3 is isotypic with that of Mg_2PN_3[18a] and Li_2SiO_3,[22] respectively. It is made up of Zn^{2+} ions besides infinite chains of corner-sharing PN_4 tetrahedra $^1_\infty[PN_2N_{2/2}]^{4-}$, thus representing a *catena*-polynitridophosphate. The nitridic polyphosphate chain anions with a chain periodicity $P = 2$ (Zweiereinfach-Kette) and a stretching factor[23] $f_s = 0.88$ run parallel [001], corresponding with the shortest lattice parameter (Figure 1). Due to an enhanced bond order,[24] the bond lengths P–N[1] to the terminal nitrogen atoms of the PN_4 tetrahedra (162.2(4) pm) are significantly shorter than the bond lengths P–N[2] to the bridging nitrogen atoms (170.2(6), 171.8(7) pm). This is typical for chain- and ring-type structures both in phosphate[25] and silicate chemistry.[26] The values for bond lengths and angles concerning the chain, which are summarized in Table 1, agree well with the values in $M^{II}_2PN_3$ (M^{II} = Mg, Ca),[18] with other chain-type

silicates and in a minor degree with other *catena*-polyoxophosphates.[27] The angles N–P–N have values close to the regular tetrahedral angle.
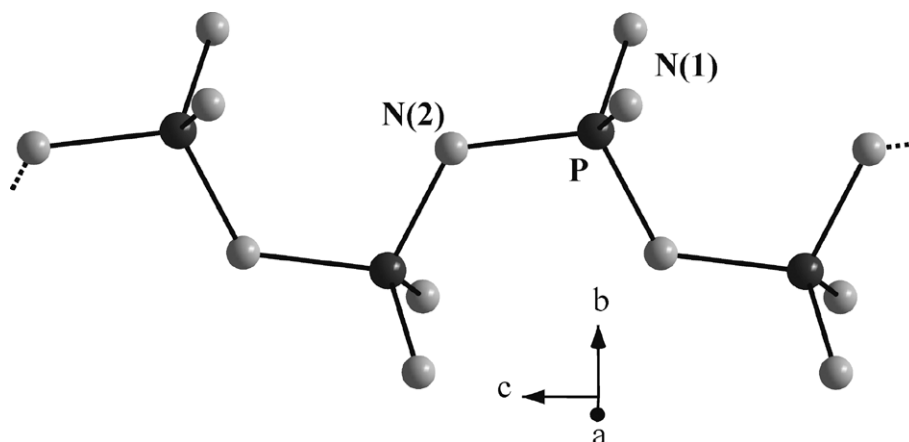
Figure 1. *Catena*-polynitridophosphate anion in Zn_2PN_3.

Table 1. Selected interatomic distances / pm and angles / ° in Zn_2PN_3 (esd's in parentheses).

Zn–N(1)^{term}	199.9(4), 200.5(4), 204.0(3)
Zn–N(2)^{br}	212.7(4)
P–N(1)^{term}	162.2(4)
P–N(2)^{br}	170.2(6), 171.8(7)
N(1)^{term}–P–N(1)^{term}	113.9(2)
N(2)^{br}–P–N(2)^{br}	109.2(3)
N(1)^{term}–P–N(2)^{br}	107.3(1), 109.5(2)
P–N(2)^{br}–P	123.8(3)

As already reported for Li_2SiO_3[22] and later for Mg_2PN_3,[28,18a] this structure can be described as a superstructure of the wurtzite structure type. In case of Zn_2PN_3 the Zn^{2+} ions together with the phosphorus atoms (in a molar ratio of 2 : 1) occupy half of the tetrahedral voids of a hexagonal closed pack arrangement of nitrogen atoms in an ordered manner. The pseudo-hexagonal symmetry is illustrated in Figure 2. Although for both magnesium and zinc *catena*-polynitridophosphates this consideration can be carried out, a minor difference concerning the coordination spheres of the cations exists. After the first four nitrogen atoms surrounding Zn^{2+} in a distance ranging from 199.9(4) to 212.7(4) pm (Table 1), which corresponds with the sum of the ionic radii,[29,30] the fifth nitrogen atom in the coordination sphere of Zn^{2+} (N5) is located at a distance of 291.5(3) pm. In Mg_2PN_3, however, the fifth nitrogen atom (N5) around the Mg^{2+} ion is situated significantly closer (257.7(4) pm). To decide whether this fifth nitrogen atom has to be considered to belong to the respective coordination sphere, the contributions ΔE for each N ligand (summing the

partial effective coordination number ECoN) were calculated using the CHARDI concept (charge density in solids; Tables 2 and 3).[31,32] With a contribution $\Delta E(N5 \cdots Mg^{2+}) \neq 0$ for ECoN, a [4+1] coordination is given in Mg_2PN_3. As no ECoN contribution $\Delta E(N5 \cdots Zn^{2+})$ is evident, thus the Zn^{2+} coordination is exclusively fourfold in Zn_2PN_3. All comparable structural parameters of Zn_2PN_3 (distances, angles, coordination) are also in well agreement with that of $Zn_6[P_{12}N_{24}]$[33] and $Zn_8[P_{12}N_{24}]O_2$,[34] respectively, the other Zn/P/(O)/N containing compounds.
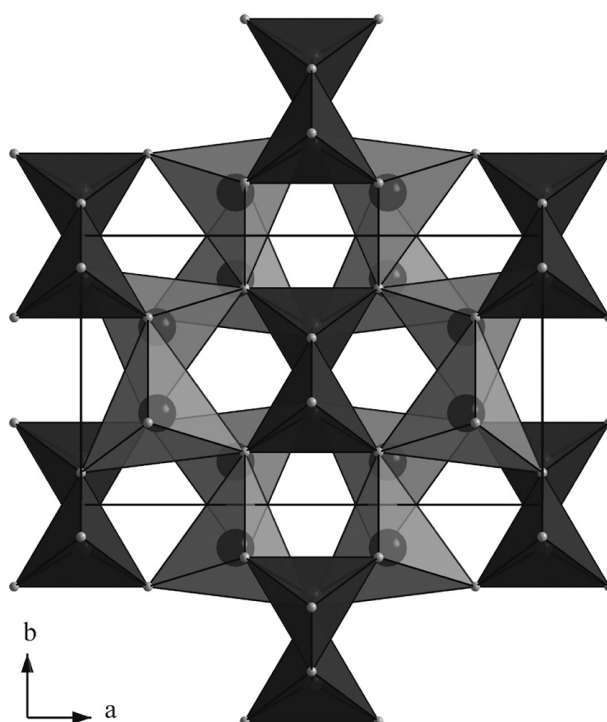
Figure 2. Representation of the crystal structure of Zn_2PN_3 viewed along [001]; PN_4 tetrahedra are dark, ZnN_4 tetrahedra are light gray.

Table 2. Results of the calculation of ECoN concerning the coordination sphere of Mg^{2+} in Mg_2PN_3.

ligand no.	atom	x	y	z	distance / pm	ΔE
	Mg	0.1653	0.3331	0.9667		
1	N1	0.3552	0.1940	0.9244	201.686	1.197
2	N1	0.1448	0.6940	0.9244	205.606	1.083
3	N2	0	0.1173	0.8510	208.983	0.985
4	N1	0.1448	0.3060	1.4244	217.955	0.736
5	N1	0.1448	0.3060	0.4244	257.747	0.076
6	N2	0	−0.1173	1.3510	351.414	0.000

ECoN: 4.0786
coordination number: 5

Table 3. Results of the calculation of ECoN concerning the coordination sphere of Zn^{2+} in Zn$_2$PN$_3$.

ligand no.	atom	x	y	z	distance / pm	ΔE
	Zn	0.1651	0.3400	0.9667		
1	N1	0.3550	0.1955	0.8773	199.799	1.110
2	N1	0.1450	0.6955	0.8773	200.508	1.088
3	N1	0.1450	0.3045	1.3773	203.983	0.985
4	N2	0	0.1191	0.8012	212.729	0.737
5	N1	0.1450	0.3045	0.3773	291.479	0.000

ECoN: 3.9206
coordination number: 4

9.2.3 Vibrational Spectroscopy

The IR and Raman spectra of Zn$_2$PN$_3$ are shown in Figure 3. Similarly with M$^{II}_2$PN$_3$ (M^{II} = Mg, Ca),[18a] there are no absorption bands at high wavenumbers (> 3000 cm^{-1}), which proves the absence of hydrogen in the sample in form of amide- or imide-groups. Furthermore, between 1050 and 400 cm^{-1} the spectrum looks very similar to that of the other *catena*-polynitridophosphates. The characteristic *catena*-polyphosphate frequencies ν_{as} NPN, ν_{as} PNP, ν_s PNP and ν PN^{term} cause very intensive absorption bands in the range between 1040 and 870 cm^{-1} just as the vibrations δ PNP and δ NPN in the range between 730 and 470 cm^{-1}. In the Raman spectrum one single strong signal is present at 989 cm^{-1}, which can be assigned with ν_s PN^{term}. Compared to ν_s PO^{term}[35,36] its value is significantly lower (around 200 cm^{-1}) according to the weaker character of the P–N bond. In Raman spectra of *catena*-phosphates the periodicity of the chain is often indicated by the number of bands below 800 cm^{-1}.[37] In the case of Zn$_2$PN$_3$, due to a low signal-to-noise ratio, two signals (corresponding with $P = 2$) can only be assumed between 385 and 415 cm^{-1}.
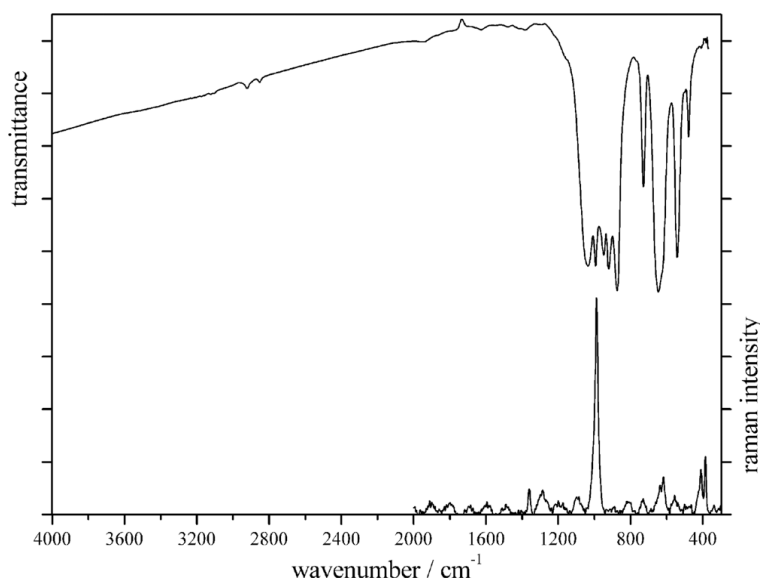
Figure 3. FT-IR and Raman spectra of Zn_2PN_3.

9.2.4   Solid-state NMR Spectroscopy

The ^{31}P solid-state MAS NMR spectrum of a phase-pure sample of Zn_2PN_3 is shown in Figure 4. Corresponding to one crystallographic phosphorus site, one single resonance is observed at $\delta = 42.8$ with FWHM = 1.0 ppm. This value is indeed not in the range, where most of the phosphorus (oxo)nitrides and (oxo)nitridophosphates have their chemical shift (101.7 (in γ-P_3N_5[38]) to +6.5 (in *NPO*-zeolite[15b])). But besides the influence of the cation the low degree of condensation could be the reason why the signal appears in a complete different region. With Li_7PN_4 (49.2 and 54.6 ppm)[39] and Mg_2PN_3 ($\delta = 22.8$),[40] there are definitely two examples of less condensed nitridophosphates that have ^{31}P resonances strongly shifted in the downfield region relative to 85 % H_3PO_4.
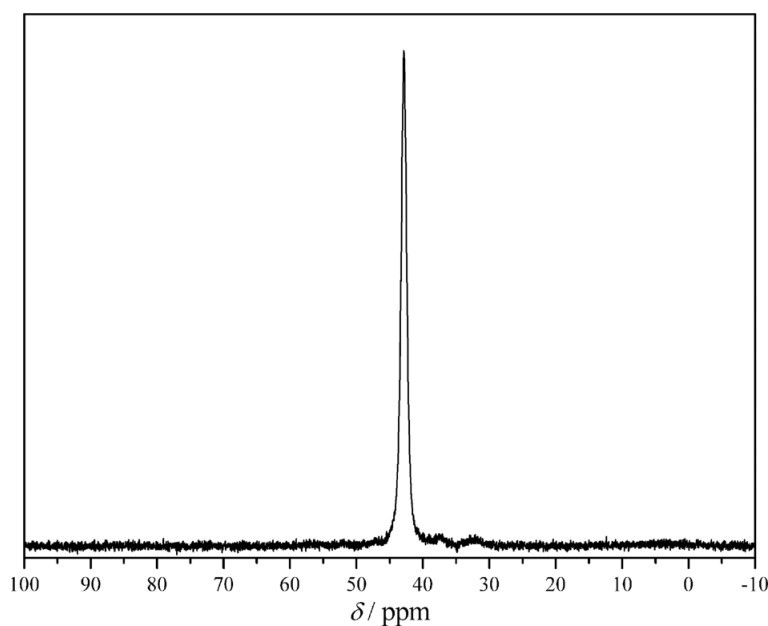
Figure 4.   Solid-state ^{31}P MAS NMR spectrum of Zn_2PN_3.

9.2.5 Thermal Behavior

The temperature-dependent X-ray powder diffraction patterns of Zn_2PN_3 are shown (in the range $5° \leq 2\theta \leq 35°$) in Figure 5. Besides two reflections at 11.3 and 32.1 $°2\theta$, which are originating from the furnace and become more intensive with increasing temperature, the diffraction patterns are hardly changing, even in their intensities. This observation strongly suggests that Zn_2PN_3 is no quenched high-pressure modification but stable at ambient pressure until at least 1100 °C. Contrary to our experience, this value is unexpectedly high for phosphorus nitrides and nitridophosphates that often already decompose at temperatures around 850 °C.
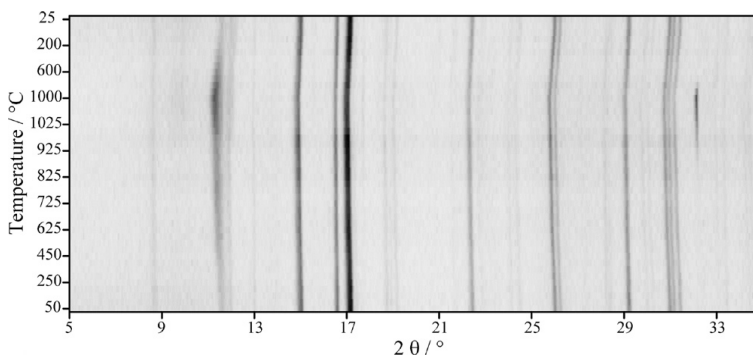
Figure 5. Temperature-dependent X-ray powder diffraction patterns (Mo-$K_{\alpha 1}$) of Zn_2PN_3.

For further thermal characterization of Zn_2PN_3 the average thermal expansion coefficient $\overline{\alpha}$. has been determined according to Equation (3). The values are given in Table 4.

Table 4. Average thermal expansion coefficients.

lattice parameter / cell volume	$\alpha / 10^{-6}\ K^{-1}$
a	8.7
b	9.3
c	4.9
V	23.0

$$\overline{\alpha} = \frac{1}{X_0}\left(\frac{\partial X}{\partial T}\right)_p \text{ with} \qquad \begin{array}{l} X \equiv \text{lattice parameter / cell volume} \\ T \equiv \text{temperature} \end{array} \qquad (3)$$

All cell parameters increase linearly with increasing temperature. The average thermal expansion is anisotropic occurring more strongly in directions [100] and [010] than in [001], the direction of the polyphosphate chain. It seems that the stretched P–N chain is transversally displaced with increasing temperature. If we would classify Zn_2PN_3 into the

three categories for ceramics,[41] with its expansion coefficient of [$\alpha(V)$] it belongs to the high expansion materials ($\alpha > 8 \times 10^{-6}$ K^{-1}). The value is more comparable with metallic materials like aluminum ($\alpha = 22 \times 10^{-6}$ K^{-1}), brass ($\alpha = 19 \times 10^{-6}$ K^{-1}), or magnesium ($\alpha = 26 \times 10^{-6}$ K^{-1}).[42]

9.3   CONCLUSION

In this contribution the synthesis and full characterization of Zn$_2$PN$_3$ is presented. By applying the high-pressure high-temperature approach using a multianvil apparatus, we were able to stabilize the respective nitrides Zn$_3$N$_2$ and P$_3$N$_5$ at 8 GPa so that we could obtain Zn$_2$PN$_3$ at 1200 °C. The crystal structure turned out to be isotypic with that of Mg$_2$PN$_3$ containing *catena*-polynitridophosphate anions $^1_\infty$[PN$_2$N$_{2/2}$]$^{4-}$ ($P = 2$, $f_s = 0.88$) running parallel [001] that are connected by tetrahedral coordination of the N atoms to Zn^{2+}-ions. The phase-pure powder could be used to record vibrational spectra of Zn$_2$PN$_3$ which correspond well with the expected vibrations for *catena*-polyphosphates and are in accordance with the structure model. A further confirmation for the refined structure is afforded by the ^{31}P solid-state NMR spectrum. The thermal analysis of thermodynamic stable Zn$_2$PN$_3$ resulted a thermal stability until at least 1100 °C and an average expansion coefficient of $\overline{\alpha} = 23.0 \times 10^{-6}$ K^{-1}. Thus, the reaction product of Zn$_3$N$_2$ and P$_3$N$_5$ which decompose above 400 and 850 °C, respectively, has a much higher thermal stability than the starting materials.

The presented example of Zn$_2$PN$_3$ reveals that the high-pressure technique gives important impulses for the materials chemistry by realizing compounds that could not be synthesized so far. Furthermore, it points out that the high-pressure approach in combination with multianvil technique is a powerful synthetic tool for P/(O)/N chemistry.

9.4   EXPERIMENTAL SECTION

9.4.1   Synthesis

Zn$_2$N$_3$: Zinc nitride was synthesized, based on the method reported by *Hahn et al.*,[21] by heating zinc powder (Merck KGaA, Darmstadt, Germany, 99.9 %) in a continuous ammonia gas flow at 600 °C (rate of heating and cooling: 2 °C min^{-1}) for a period of 24 h. To avoid Zn(OH)$_2$ / ZnO the plug-flow reactor has been previously annealed in vacuo

(10^{-3} mbar), ammonia gas (Messer Griessheim, Sulzbach, Germany, 3.8) was piped through a gas purifier (SAES Pure Gas, Inc., San Luis Obispo, USA) and all operations were performed under inert gas atmosphere. The purity of Zn_2N_3 as black powder has been checked by powder X-ray diffractometry (good crystallinity and no impurity reflections) and IR spectroscopy (no signals for imide or amide).

P_3N_5: Phosphorus(V) nitride was obtained by the reaction of hexachlorocyclotriphosphazene $(PNCl_2)_3$ (Sigma–Aldrich, Inc., St. Louis, USA, 99 %) with purified ammonia gas (see above) at 950 °C following the procedure given in the literature.[18a,19]

Zn_2PN_3: The synthesis was carried out under high-pressure / high-temperature conditions of 8 GPa and approx. 1200 °C using the multianvil technique and a 1000 t hydraulic press (Voggenreiter, Mainleus, Germany). In an argon filled glovebox (MBraun, Garching, Germany) a stoichiometric mixture of Zn_2N_3 and P_3N_5 according to Equation (2) was ground thoroughly, filled in a boron nitride crucible (Henze BNP GmbH, HeBoSint. S10, Kempten, Germany) and centered into an 18/11 assembly. A detailed description of the assembly and its preparation can be found in references [3,43–46]. The assembly was integrated into the center of eight truncated tungsten carbide cubes (TSM-10, Ceratizit, Reutte, Austria) and embedded into a Walker-type module as fast as possible to minimize the exposure time to air. The assembly was compressed up to 8 GPa at room temperature within 3 h and kept at this pressure for the heating period. The sample was heated to 1200 °C in 10 min, kept there for 10 min and cooled down to room temperature in 30 min. Subsequently, the pressure was released over a period of 9 h and the pressure media was recovered. After removing the surrounding boron nitride a crude product in form of a dark gray, cylindrical solid was isolated. To purify Zn_2PN_3 from traces of zinc phosphides a powdered sample was treated with an aqueous solution of HCl (2 M). Zn_2PN_3 was obtained as a colorless, air- and water stable, microcrystalline powder.

9.4.2 Crystal Structure Analysis

The crystal structure of Zn_2PN_3 was determined on the basis of powder X-ray diffraction data. The powder X-ray diffraction pattern was recorded with a STOE Stadi P powder diffractometer (STOE, Darmstadt, Germany) in Debye–Scherrer geometry using Ge(111) monochromated Mo-$K_{\alpha 1}$-radiation (70.93 pm). The indexing resulted unambiguously in an orthorhombic unit cell with $a = 937.632(6)$, $b = 547.649(3)$,

$c = 492.109(3)$ pm. A Rietveld refinement (Figure 6) was performed with the TOPAS package[47] using the structure of Mg_2PN_3 as starting model. The reflection profiles were determined using the fundamental parameters approach[48] by convolution of appropriate source emission profiles with axial instrument contributions and crystalline microstructure effects. Preferred orientation of the crystallites was described with a spherical harmonics function of 4th order. The z-parameter of zinc has been fixed to define the origin of the unit cell. The relevant crystallographic data and further details of the data collection are summarized in Table 5. Table 6 shows the positional and displacement parameters for all atoms.[†]
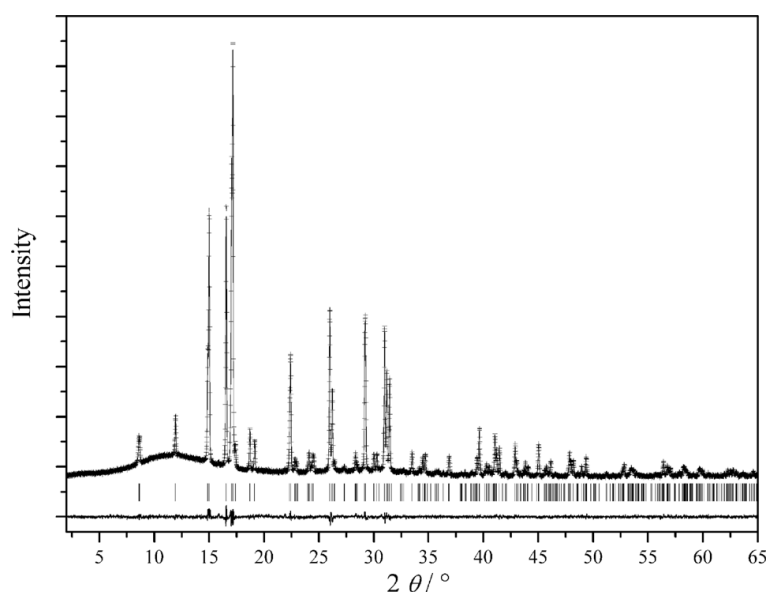
Figure 6. Observed (crosses) and calculated (line) X-ray powder diffraction pattern (Mo-$K_{\alpha1}$) as well as the difference profile of the Rietveld refinement of Zn_2PN_3; Allowed peak positions are marked by vertical lines.

Table 5. Crystallographic data for Zn_2PN_3 (esd's in parentheses).

Crystal Structure Data	
formula	Zn_2PN_3
formula mass / g mol^{-1}	203.775
crystal system	orthorhombic
space group	$Cmc2_1$ (no. 36)
cell parameters / pm	$a = 937.847(6)$
	$b = 547.696(4)$
	$c = 492.396(3)$
cell volume / 10^6 pm^3	$V = 252.922(3)$
formula units Z / cell	4
X-ray density ρ / gcm^{-3}	5.351(1)
abs. coefficient μ / mm^{-1}	19.28

---

† Further details of the crystal structure investigation may be obtained from Fachinformationszentrum Karlsruhe, 76344 Eggenstein-Leopoldshafen, Germany (Fax: +49-7247-808-666; E-Mail: crysdata@fiz-karlsruhe.de, http://www.fiz-karlsruhe.de/request_for_deposited_data.html) on quoting the depository number CSD-422150.

Data collection	
type of diffractometer	Stoe Stadi P
radiation, monochromator	Mo-$K_{\alpha 1}$ ($\lambda = 70.93$ pm), Ge(111)
temperature / K	297(2)
detector	linear PSD ($\Delta 2\theta = 5°$)
internal step width of 2θ /°	0.01
2θ range /°	2.0–65.0
step width /°	0.2
data points	6300
number of observed reflections	271

Structure analysis and Refinement	
method of refinement	fundamental parameters model[48]
program used	TOPAS-Academic[47]
atomic parameters	12
profile parameters	8
background function / parameters	shifted Chebyshev / 20
other parameters	7
	GoF(χ^2) = 1.149
R indices	$R_p = 0.0110$
	$wR_p = 0.0141$

Table 6. Atom coordinates, Wyckoff symbols and isotropic displacement parameters B_{iso} / $Å^2$ for the atoms in Zn_2PN_3.

atom	Wyckoff symbol	x	y	z	B_{iso}
Zn	8b	0.1651(1)	0.3400(1)	0.9667	0.70(2)
P	4a	0	0.1591(4)	0.4553(10)	0.39(4)
N(1)[term]	8b	0.1450(4)	0.3045(7)	0.3773(5)	0.14(6)
N(2)[br]	4a	0	0.1191(10)	0.8012(8)	0.14(6)

9.4.3 Vibrational Spectroscopy

An FT-IR spectrum of Zn_2PN_3 was recorded in transmission geometry at room temperature in the range 4000–400 cm^{-1} with a Bruker IFS 66v/S spectrometer using the KBr pellet technique (2 mg sample, 300 mg dried KBr). A Raman spectrum was recorded by using a Bruker MultiRAM FT-Raman spectrometer with an Nd-YAG laser ($\lambda = 1064$ nm) scanning a range from 2000 to 300 cm^{-1}.

9.4.4   Solid-state NMR Spectroscopy

A solid-state ^{31}P MAS NMR spectrum was recorded at room temperature with a Bruker DSX Avance 500 FT spectrometer equipped with a commercial 2.5 mm MAS NMR double-resonance probe at a magnetic field of 11.7 T, the rotation frequency was 25 kHz. The chemical shift values refer to a deshielding scale and 85 % H_3PO_4 was used as an external reference.

9.4.5   Temperature-dependent *in situ* X-ray Diffractometry

In situ X-ray powder diffraction experiments were done with a STOE Stadi P powder diffractometer (Mo-$K_{\alpha 1}$-radiation (70.93 pm)) equipped with a computer controlled STOE resistance graphite furnace. Enclosed in a silica glass capillary under argon, the sample was heated from room temperature to 1100 °C (heating/cooling rate: 25 °C min^{-1}) in steps of 50 °C (up) and 100 °C (down), respectively. At each heating step (after holding the temperature for 1 min), a diffraction pattern was recorded with an IP-PSD in the range of $2° \leq 2\theta \leq 80°$. To determine the cell parameters at different temperatures accurately for all diffraction patterns a Rietveld refinement has been performed for every temperature step.

9.5   REFERENCES

[1]   a) H. Huppertz, B. von der Eltz, *J. Am. Chem. Soc.* **2002**, *124*, 9376; b) H. Emme, H. Huppertz, *Chem. Eur. J.* **2003**, *9*, 3623; c) H. Emme, H. Huppertz, *Acta Crystallogr., Sect. C: Cryst. Struct. Commun.* **2005**, *61*, i29; d) H. Emme, H. Huppertz, *Phys. Chem. Glasses: Eur. J. Glass Sci. Technol.* **2006**, *B47*, 364; e) J. S. Knyrim, F. Roeßner, S. Jakob, D. Johrendt, I. Kinski, R. Glaum, H. Huppertz, *Angew. Chem.* **2007**, *119*, 9256; *Angew. Chem., Int. Ed.* **2007**, *46*, 9097.

[2]   G. Demazeau, *Chem. Scr.* **1988**, *28*, 21.

[3]   H. Huppertz, *Z. Kristallogr.* **2004**, *219*, 330.

[4]   G. Demazeau, H. Huppertz, J. A. Alonso, R. Pöttgen, E. Moran, J. P. Attfield, *Z. Naturforsch.* **2006**, *61b*, 1457.

[5]   a) K. Landskron, Doctoral Thesis, Univ. Munich (LMU) **2001**; b) F. Karau, Doctoral Thesis, Univ. Munich (LMU) **2007**.

[6]   S. J. Sedlmaier, J. Schmedt auf der Gu□nne, W. Schnick, *Dalton Trans.* **2009**, 4081.

[7]   F. Karau, W. Schnick, *Angew. Chem.* **2006**, *118*, 4617; *Angew. Chem., Int. Ed.* **2006**, *45*, 4505.

[8]   M. Pouchard, *Nature* **2006**, *442*, 878.

[9]   a) F. Karau, W. Schnick, *Z. Anorg. Allg. Chem.* **2006**, *632*, 231; b) F. W. Karau, L. Seyfarth, O. Oeckler, J. Senker, K. Landskron, W. Schnick, *Chem. Eur. J.* **2007**, *13*, 6841.

[10]   F. J. Pucher, S. R. Römer, F. W. Karau, W. Schnick, *Chem. Eur. J.* **2010**, *16*, 7208.

[11]   K. Landskron, W. Schnick, *J. Solid State Chem.* **2001**, *156*, 390.

[12]   K. Landskron, E. Irran, W. Schnick, *Chem. Eur. J.* **1999**, *5*, 2548.

[13]   a) W. Schnick, J. Lu☐cke, *Angew. Chem.* **1992**, *104*, 208; *Angew. Chem., Int. Ed. Engl.* **1992**, *31*, 213; b) W. Schnick, J. Lücke, *Z. Anorg. Allg. Chem.* **1994**, *620*, 2014; c) W. Schnick, N. Stock, J. Lücke, M. Volkmann, M. Jansen, *Z. Anorg. Allg. Chem.* **1995**, *621*, 987; d) F. Wester, W. Schnick, *Z. Anorg. Allg. Chem.* **1996**, *622*, 1281.

[14]   N. Stock, E. Irran, W. Schnick, *Chem. Eur. J.* **1998**, *4*, 1822.

[15]   a) S. Correll, N. Stock, O. Oeckler, W. Schnick, *Angew. Chem.* **2003**, *115*, 3674; *Angew. Chem., Int. Ed.* **2003**, *42*, 3549; b) S. Correll, N. Stock, O. Oeckler, J. Senker, T. Nilges, W. Schnick, *Z. Anorg. Allg. Chem.* **2004**, *630*, 2205.

[16]   W. Schnick, J. Lücke, *J. Solid State Chem.* **1990**, *87*, 101.

[17]   W. Schnick, U. Berger, *Angew. Chem.* **1991**, *103*, 857; *Angew. Chem., Int. Ed. Engl.* **1991**, *30*, 830.

[18]   a) V. Schultz-Coulon, W. Schnick, *Z. Anorg. Allg. Chem.* **1997**, *623*, 69; b) W. Schnick, V. Schultz-Coulon, *Angew. Chem.* **1993**, *105*, 308; *Angew. Chem., Int. Ed. Engl.* **1993**, *32*, 280.

[19]   J. Lücke, Doctoral Thesis, Univ. Bonn **1994**.

[20]   L. Boukbir, R. Marchand, Y. Laurent, P. Bacher, G. Roult, *Ann. Chim. Fr.* **1989**, *14*, 475.

[21]   R. Juza, A. Neuber, H. Hahn, *Z. Anorg. Allg. Chem.* **1938**, *239*, 273.

[22]   a) K.-F. Hesse, *Acta Crystallogr., Sect. B* **1977**, *33*, 901; b) H. Völlenkle, *Z. Kristallogr.* **1981**, *154*, 77.

[23]   F. Liebau, *Structural Chemistry of Silicates*, Springer, Berlin, **1985**, p. 80.

[24]   D. W. J. Cruickshank, *J. Chem. Soc.* **1961**, 5486.

[25]   A. Durif, *Crystal Chemistry of Condensed Phosphates*, Springer, Berlin, **1995**.

[26]   F. Liebau, *Structural Chemistry of Silicates*, Springer, Berlin, **1985**.

[27]   D. W. J. Cruickshank, *Acta Crystallogr.* **1964**, *17*, 671.

[28]   a) R. Marchand, Y. Laurent, *Mater. Res. Bull.* **1982**, *17*, 399; b) R. Marchand, Y. Laurent, *Eur. J. Solid State Inorg. Chem.* **1991**, *28*, 57.

[29]   R. D. Shannon, *Acta Crystallogr., Sect. A* **1976**, *32*, 751.

[30]   W. H. Baur, *Crystallogr. Rev.* **1987**, *1*, 59.

[31]   a) R. Hoppe, *Z. Kristallogr.* **1979**, *150*, 23; b) R. Hoppe, S. Voigt, H. Glaum, J. Kissel, H. P. Müller, K. Bernet, *J. Less-Common Met.* **1989**, *156*, 105.

[32]   R. Hübenthal, *MAPLE – Program for the Calculation of MAPLE Values*, Version 4, Univ. Giessen **1993**.

[33]   J. Weitkamp, S. Ernst, F. Cubero, F. Wester, W. Schnick, *Adv. Mater.* **1997**, *9*, 247.

[34]   F. Karau, O. Oeckler, F. Schäfers, R. Niewa, W. Schnick, *Z. Anorg. Allg. Chem.* **2007**, *633*, 1333.

[35]   H. A. Höppe, S. J. Sedlmaier, *Inorg. Chem.* **2007**, *46*, 3467.

[36]   S. J. Sedlmaier, W. Schnick, *Z. Anorg. Allg. Chem.* **2008**, *634*, 1501.

[37]   A. Rulmont, R. Cahay, M. Liegeois-Duyckaerts, P. Tarte, *Eur. J. Solid State Inorg. Chem.* **1991**, *28*, 207.

[38]   a) K. Landskron, H. Huppertz, J. Senker, W. Schnick, *Angew. Chem.* **2001**, *113*, 2713; *Angew. Chem., Int. Ed.* **2001**, *40*, 2643; b) K. Landskron, H. Huppertz, J. Senker, W. Schnick, *Z. Anorg. Allg. Chem.* **2002**, *628*, 1465.

[39]   R. Lauterbach, Diploma Thesis, Univ. Bayreuth **1996**.

[40]   S. J. Sedlmaier, W. Schnick, unpublished.

[41]   R. Roy, D. K. Agrawal, H. A. McKinstry, *Ann. Rev. Mater. Sci.* **1989**, *19*, 59.

[42]   D. R. Lide, *Handbook of Chemistry and Physics*, 88th ed., CRC Press, Boca Raton **2008**, pp. 12–215.

[43]   N. Kawai, S. Endo, *Rev. Sci. Instrum.* **1970**, *41*, 1178.

[44]   D. Walker, M. A. Carpenter, C. M. Hitch, *Am. Mineral.* **1990**, *75*, 1020.

[45]   D. Walker, *Am. Mineral.* **1991**, *76*, 1092.

[46]   D. C. Rubie, *Phase Transitions* **1999**, *68*, 431.

[47]   A. A. Coelho, *TOPAS-Academic*, Version 4.1, Coelho Software, Brisbane, **2007**.

[48]   J. Bergmann, R. Kleeberg, A. Haase, B. Breidenstein, *Mater. Sci. Forum* **2000**, *347–349*, 303.

10. Unprecedented Zeolite-Like Framework Topology Constructed from Cages with 3-rings in a Barium Oxonitridophosphate

Thermal condensation of molecules PO(NH$_2$)$_3$ and PS(NH$_2$)$_3$ has formerly proved to be a good synthesis strategy for oxonitridophosphates. Nevertheless, in complex starting material systems difficulties (too small crystals, multiple products) can arise for identification of new compounds. Whether it was with numerous experiments and despite failed attempts to measure mounted microcrystals successful in this case, can be found out in this chapter.

ABSTRACT

A novel oxonitridophosphate, Ba$_{19}$P$_{36}$O$_{6+x}$N$_{66-x}$Cl$_{8+x}$ (x ≈ 4.54), has been synthesized by heating a multicomponent reactant mixture consisting of phosphoryl triamide OP(NH$_2$)$_3$, thiophosphoryl triamide SP(NH$_2$)$_3$, BaS, and NH$_4$Cl enclosed in an evacuated and sealed silica glass ampoule up to 750 °C. Despite the presence of side phases, the crystal structure was elucidated *ab initio* from high-resolution synchrotron powder diffraction data (λ = 39.998 pm) applying the charge-flipping algorithm supported by independent symmetry information derived from electron diffraction (ED) and scanning transmission electron microscopy (STEM). The compound crystallizes in the cubic space group $Fm\overline{3}c$ (no. 226) with a = 2685.41(3) pm and Z = 8. As confirmed by Rietveld refinement, the structure comprises all-side vertex sharing P(O,N)$_4$ tetrahedra forming slightly distorted 3^{8}4^{6}8^{12} cages representing a novel composite building unit (CBU). Interlinked through their 4-rings and additional 3-rings, the cages build up a 3D network with a framework density FD = 14.87 T / 1000 Å^3 and a 3D 8-ring channel system. Ba^{2+} and Cl$^-$ as extra-framework ions are located within the cages and channels of the framework. The structural model is corroborated by ^{31}P double-quantum (DQ) / single-quantum (SQ) and triple-quantum (TQ) /single-quantum (SQ) 2D correlation MAS NMR spectroscopy. According to ^{31}P{^{1}H} C-REDOR NMR measurements, the H content is less than one H atom per unit cell.

10.1   INTRODUCTION

Classical zeolites, such as aluminosilicates and aluminophosphates, are well-established in fundamental industrial processes, e.g., substance separation, air and water conditioning, or catalysis. As they have the potential for further applications in future technologies (e.g., sensors, electronic, or optical systems), inorganic open-framework materials emerged as a research area with a multitude of compound classes in the last decades. In addition to diverse metal phosphates, germanates, and borates, there are sulfates, arsenates, or phosphonates as well as organic-inorganic hybrid compounds with porous networks.[1,2] However, many microporous structures are thermally and chemically not sufficiently stable to make their way toward advanced materials. Consequently, it is worthwhile to synthesize novel open-framework materials that exhibit three-dimensional, rigid framework structures based on vertex-sharing tetrahedra. Since the discovery of the aluminophosphates by *Flanigen* et al.[3] in the 1980s, it has been attempted with great creativity and effort to access new stable frameworks with different pore sizes and shapes combined with varying chemical and physical properties. Different synthesis conditions (temperature, reaction time, pH), many different structure-directing agents (SDA), as well as a broad spectrum of solvents, including ionic liquids, were employed. The fluoride route[4] has been utilized, and other tetrahedra centers (e.g., B, Ga, Zn) were included, resulting in new zeotypes in compound classes like silicoaluminophosphates (SAPOs) and metal-containing versions (e.g., MeAPO, MeAPSO) thereof.[2,5] Thus, the field of zeolite chemistry seems quite mature which means that the search for new framework types becomes increasingly challenging.

The exchange of oxygen by nitrogen in the anionic substructure is an innovative but rarely realized expansion of zeolite chemistry. Nitrido-zeolites promise beneficial chemical and physical properties (e.g., higher thermal stability or adjustable acidity / basicity) and a huge structural diversity. As compared with oxygen, nitrogen atoms are more common in three-binding situations, and they provide more flexibility as bridging atoms in networks by occasionally realizing smaller angles T–X–T (X = O, N). Consequently, both large rings as well as rare 3-rings can be stabilized so that novel zeolite-like frameworks become possible.

This nitride concept became reality in (oxo-)nitridosilicates and (oxo-)nitride-phosphates. After the proof of concept with nitridosodalites[6] and related oxonitrido-sodalites,[7] the benefits of nitrogen in zeolite-like framework structures have been demonstrated only for very few examples. Besides a zeolite-like Si–N framework in

$Ba_2Nd_7Si_{11}N_{23}$ with a notable thermal stability up to 1600 °C,[8] the flexibility of N bridging resulted in $Li_xH_{12-x-y+z}[P_{12}O_yN_{24-y}]X_z$ for X = Cl, Br with a new zeolite topology, namely, *NPO* (*n*itrido*p*hosphate *o*ne).[9] The typical (ring-)strain in such an extended 3-ring system could only be realized with that framework type material and the related nitridic compounds $Ba_3Si_3N_5OCl$, $Ba_3Ta_3N_6Cl$, $Ba_{15}Ta_{15}N_{33}Cl_4$, and $Ba_6Si_6N_{10}O_2(CN_2)$ so far.[10,11] The clathrate $P_4N_4(NH)_4 \cdot (NH_3)$[12] with its 4^28^4 cages encapsulating ammonia molecules could be synthesized because rather small angles T–X–T can be realized in phosphorus nitride networks. Taking into account the high thermal and chemical stability and further proposed applications like, e.g., the clathrate as gas storage or membrane reactor material,[13] these examples show the potential of the nitride chemistry in the field of open-framework structures.

In this contribution, we describe the synthesis and structure elucidation of the oxonitridophosphate $Ba_{19}P_{36}O_{6+x}N_{66-x}Cl_{8+x}$ (x ≈ 4.54), which exhibits a novel zeolite-like framework topology involving a new composite building unit (CBU).

10.2   EXPERIMENTAL SECTION

10.2.1 Synthesis of $Ba_{19}P_{36}O_{6+x}N_{66-x}Cl_{8+x}$ (x ≈ 4.54)

Phosphoryl triamide $OP(NH_2)_3$ and thiophosphoryl triamide $SP(NH_2)_3$ were synthesized according to the literature[14,15] similar to procedures described by *Correll*.[16] First, 10-20 mL of freshly distilled $POCl_3$ (Acros Organics, Geel, Belgium, 99 %) and $PSCl_3$ (Acros Organics, 98 %), respectively, were added directly and slowly to liquid ammonia in a flame-dried Schlenk-type 1 L flask. In the second step, the elimination of NH_4Cl from the products was carried out performing a Soxhlet extraction with distilled Et_2NH (Grüssing GmbH, Filsum, Germany, 99 %) in dry CH_2Cl_2 for three days. After drying *in vacuo*, $OP(NH_2)_3$ and $SP(NH_2)_3$ are available as starting materials in the form of colorless, water-sensitive powders. Their purity was verified with powder X-ray diffraction.

$Ba_{19}P_{36}O_{6+x}N_{66-x}Cl_{8+x}$ (x ≈ 4.54) has been synthesized employing a multicomponent reactant system. In a typical procedure, BaS (57.9 mg, 0.342 mmol; Sigma-Aldrich, 99.9 %), $OP(NH_2)_3$ (10.3 mg, 0.108 mmol), $SP(NH_2)_3$ (60.0 mg, 0.540 mmol), and NH_4Cl (23.1 mg, 0.432 mmol; Fluka, puriss. p.a.) were thoroughly mixed and ground in a glovebox (MBraun, Garching, Germany) and subsequently transferred into a silica glass ampoule (wall thickness 2 mm, inner diameter 11 mm). The evacuated and sealed ampoule (length around 110 mm) was heated to 200 and 750 °C in a tube furnace with dwell times

of 12 and 48 h (heating rate, 1 K min^{-1}; cooling rate, 0.25 K min^{-1}), respectively. The emerging condensation products NH_3 and H_2S partially are deposited as $(NH_4)_2S$ together with excess NH_4Cl at the cooler zones of the ampoule. After breaking the ampoules, the samples were washed with water and DMF to remove the remaining NH_4Cl and BaS. $Ba_{19}P_{36}O_{6+x}N_{66-x}Cl_{8+x}$ (x ≈ 4.54) was obtained as a colorless, water- and air-resistant, microcrystalline powder containing small amounts of various crystalline and amorphous byproducts that could not be removed by washing. Besides the starting materials named above, $BaCl_2$ or other P/N/O/Cl containing chemicals like $P(NH_2)_4Cl$,[17] $[PN(NH)_2]_3$[18] or $(NH_2)_2(O)PNP(NH_2)_3$[19] can also be used in the synthesis. The purest product, however, was obtained with the combination named at the beginning of the paragraph.

10.2.2 Powder X-ray Diffraction (PXRD), Structure Solution, and Rietveld Refinement

High-resolution synchrotron PXRD data of different samples were collected at 298 K at beamline ID31 (ESRF, Grenoble, France), using a Debye-Scherrer setup (with spinning glass capillaries, 1 mm diameter) with monochromatic radiation (λ = 39.998 pm) and a nine-crystal multianalyzer detector.[20]

Extraction of the peak positions, pattern indexing, structure solution, Fourier calculations, and Rietveld refinements was carried out with the TOPAS package.[21] By evaluation of all measured patterns, the reflections of $Ba_{19}P_{36}O_{6+x}N_{66-x}Cl_{8+x}$ (x ≈ 4.54) have been identified unequivocally. Indexing by the SVD method[22] yielded cubic unit cells, either cP with a = 1341.62 pm or—taking into account some additional weak reflections—cF with a = 2683.24 pm. For the further process, the pattern with the lowest amount of impurity reflections was selected. After evaluation of scanning transmission electron microscopy (STEM) images recorded in high-angle annular dark field (HAAF) mode and selected-area electron diffraction (SAED) patterns (see below), the space group $Fm\bar{3}c$ (no. 226) was unambiguously identified. The structure solution succeeded *ab initio* using the charge flipping algorithm[23] and subsequent difference Fourier syntheses and placing bridging atoms at reasonable positions. Rietveld refinement of the final structure model was carried out applying the fundamental parameters approach (direct convolution of source emission profiles, instrument contributions, and crystallite size and microstrain effects).[24] The preferred orientation of the crystallites was described with fourth-order spherical harmonics. As far as possible, regions containing parasitic reflections from

byproducts have been excluded. Remaining misfits indicated by the difference profile originate from regions where impurity reflections are overlapping with those of the target compound (cf. Figure 1). Overall displacement parameters have been used for Cl^- and N/O, respectively. A common O/N ratio on all bridging atom positions was derived by constraining the occupancy to be 100 % and guaranteeing charge neutrality by taking the partially occupied Cl^- positions into account. For an optimized tetrahedral geometry, distance constraints (165 pm for P–(N/O), 269 pm for (N/O)–(N/O)) have been included. Furthermore, absorption as well as a cylindrical 2θ correction[25] was applied. Crystallographic data and further details of the data collection are summarized in Table 1. Table 2 shows the positional and displacement parameters for all atoms. Due to a step width of 0.002 °2θ, severe serial correlation occurs. Consequently, the estimated standard derivations are underestimated.[26,27] The Rietveld fit is displayed in Figure 1.[†]

A refinement in space group $Pm\overline{3}m$ (no. 221) was performed as well in the same way as described above (Figure 2). The results of this refinement are given in Tables 3 und 4.
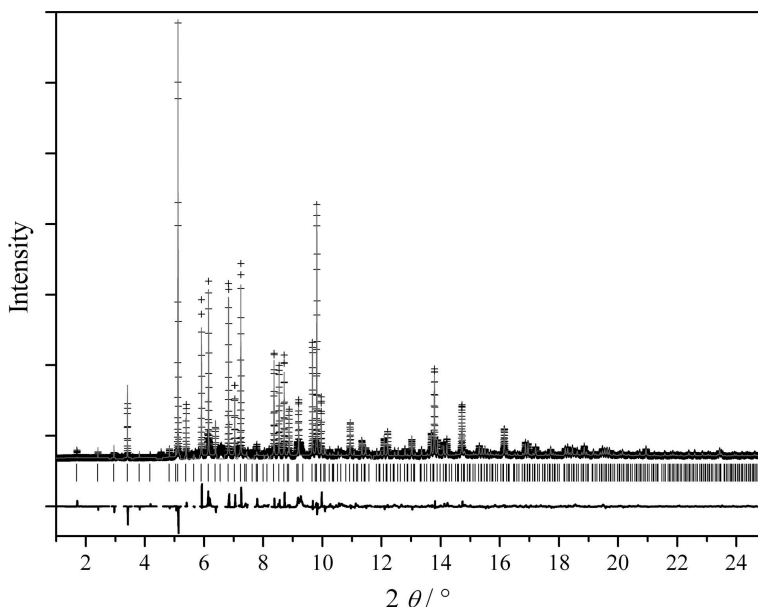
Figure 1. Observed (crosses) and calculated (gray line) powder diffraction pattern as well as difference profile of the Rietveld refinement performed in $Fm\overline{3}c$; peak positions are marked by vertical lines; regions with impurity reflections have been excluded (wherever applicable, see text).

Table 1. Crystallographic data for $Ba_{19}P_{36}O_{6+x}N_{66-x}Cl_{8+x}$ ($x \approx 4.54$) in $Fm\overline{3}c$ (esd's in parentheses).

Crystal Structure Data	
formula	$Ba_{19}P_{36}O_{10.54}N_{61.46}Cl_{12.54}$
formula mass / g mol^{-1}	5198.4143
crystal system	cubic
space group	$Fm\overline{3}c$ (no. 226)
cell parameter / pm	$a = 2685.41(3)$
cell volume / 10^6 pm^3	$V = 19365.6(6)$
formula units / cell	$Z = 8$
X-ray density / g cm^{-3}	$\rho = 3.566(2)$
FD / T 10^{-3} Å^{-3}	14.87
Data Collection	
radiation	Synchrotron (beamline ID31, ESRF, Grenoble), $\lambda = 39.998$ pm)
temperature / K	298(2)
2θ range /°	1.0–45.5
data points	22000
number of observed reflections	3211
Structure Refinement	
method of refinement	fundamental parameters model[24]
program used	TOPAS-Academic 4.1[21]
atomic parameters	27
profile parameters	9
background function / parameters	shifted Chebyshev / 40
other parameters	4
restraints	3
constraints	15
fwhm (reflection at 3.424 °2θ)/°	0.008
R indices	$\chi^2 = 5.172$ $R_p = 0.0906$ $wR_p = 0.1215$ $R_{Bragg} = 0.0770$

Table 2. Atom coordinates, Wyckoff symbols and isotropic displacement parameters B_{iso} / Å^2 for the atoms in $Ba_{19}P_{36}O_{6+x}N_{66-x}Cl_{8+x}$ ($x \approx 4.54$) in $Fm\overline{3}c$ (esd's in parentheses are underestimated due to severe serial correlation).

| atom	Wyckoff symbol	x	y	z	occupancy	B_{iso}
Ba(1)	48f	0.1055(1)	¼	¼	1	2.28(5)
Ba(2)	96i	0	0.1402(1)	0.1334(1)	1	3.06(5)
Ba(3)	8b	0	0	0	1	1.56(13)
P(1)	192j	0.6238(2)	0.6182(1)	0.6962(1)	1	0.58(8)
P(2)	96h	¼	0.9441(1)	y	1	1.81(16)
Cl(1)	64g	0.0689(2)	x	x	1	1.14(11)
Cl(2)	96i	0.2969(5)	0	0.7593(7)	0.378(5)	
N(1)	96i	0	0.9331(2)	0.7337(2)	0.854(5)	
O(1)					0.146(5)	
N(2)	192j	0.3334(2)	0.3291(2)	0.4025(2)	0.854(5)	
O(2)					0.146(5)	2.56(20)
N(3)	96h	¼	0.8591(2)	y	0.854(5)	
O(3)					0.146(5)	
N(4)	192j	0.5840(2)	0.5712(2)	0.6984(2)	0.854(5)	
O(4)					0.146(5)	
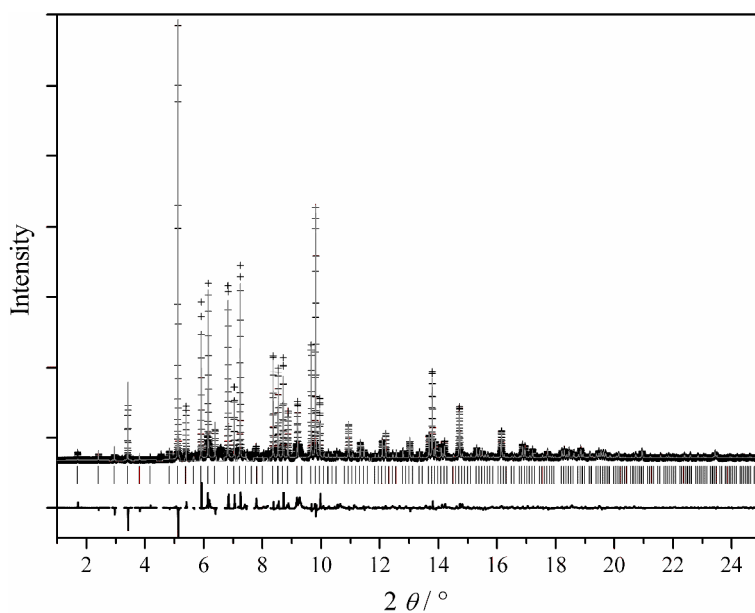
Figure 2. Observed (crosses) and calculated (gray line) powder diffraction pattern as well as difference profile of the Rietveld refinement performed in $Pm\overline{3}m$; peak positions are marked by vertical lines; regions with impurity reflections have been excluded (wherever applicable, see text).

Table 3. Crystallographic data for $Ba_{19}P_{36}O_{6+x}N_{66-x}Cl_{8+x}$ (x ≈ 4.36) in $Pm\bar{3}m$ (esd's in parentheses).

Crystal Structure Data	
formula	$Ba_{19}P_{36}O_{12.36}N_{61.64}Cl_{12.36}$
formula mass / g mol^{-1}	5191.6742
crystal system	cubic
space group	$Pm\bar{3}m$ (no. 221)
cell parameter / pm	$a = 1342.95(2)$
cell volume / 10^6 pm^3	$V = 2422.0(2)$
formula units / cell	$Z = 1$
X-ray density / g cm^{-3}	$\rho = 3.559(2)$
FD / T 10^{-3} Å^{-3}	14.87

Data Collection	
radiation	Synchrotron (beamline ID31, ESRF, Grenoble), λ = 39.998 pm)
temperature / K	298(2)
2θ range /°	1.0–45.5
data points	22000
number of observed reflections	1862

Structure Refinement	
method of refinement	fundamental parameters model[24]
program used	TOPAS-Academic 4.1[21]
atomic parameters	21
profile parameters	9
background function / parameters	shifted Chebyshev / 40
other parameters	4
restraints	3
constraints	11
fwhm (reflection at 3.424 °2θ)/°	0.008
R indices	$\chi^2 = 5.457$ $R_p = 0.0974$ $wR_p = 0.1282$ $R_{Bragg} = 0.0807$

Table 4. Atom coordinates, Wyckoff symbols and isotropic displacement parameters B_{iso} / Å^2 for the atoms in $Ba_{19}P_{36}O_{6+x}N_{66-x}Cl_{8+x}$ ($x \approx 4.36$) in $Pm\overline{3}m$ (esd's in parentheses are underestimated due to severe serial correlation).

atom	Wyckoff symbol	x	y	z	occupancy	B_{iso}
Ba(1)	6e	0.2886(2)	0	0	1	2.23(6)
Ba(2)	12j	0.7739(1)	½	0.2261(1)	1	3.59(6)
Ba(3)	1b	½	½	½	1	1.39(14)
P(1)	24m	0.7426(2)	x	0.8912(2)	1	0.89(8)
P(2)	12i	0.3871(3)	0	1–x	1	1.81(17)
Cl(1)	8g	0.3621(3)	x	x	1	1.41(13)
Cl(2)	12h	0.0912(10)	0	½	0.363(5)	
N(1) O(1)	12h	0.6408(3)	½	0	0.856(5) 0.144(5)	
N(2) O(2)	24m	0.1614(3)	x	0.3042(3)	0.856(5) 0.144(5)	2.90(21)
N(3) O(3)	12i	0	0.2196(4)	1–y	0.856(5) 0.144(5)	
N(4) O(4)	24m	0.6561(2)	x	0.8932(3)	0.856(5) 0.144(5)	

10.2.3 Electron Microscopy

SAED and STEM measurements were carried out on a transmission electron microscope FEI Titan 80-300 equipped with a field emission gun operating at 300 kV. STEM-HAADF images were recorded using a Fischione model 3000 ADF detector, and diffraction patterns were recorded with a Gatan UltraScan 1000 (2k × 2k) CCD camera. The samples were finely dispersed in ethanol by sonication, and a small amount of the suspension was subsequently dispersed on copper grids coated with holey carbon film. The grids were mounted on a double tilt holder with a maximum tilt angle of 30°. Simulations of electron diffraction patterns were carried out with the online version of the EMS program package (Electron Microscopy Image Simulation).[28]

Scanning electron microscopy (SEM) and energy dispersive X-ray analysis (EDX) were performed using a JSM-6500F electron microscope (JEOL Ltd., Tokyo, Japan) with a field emission source equipped with an EDX detector model 7418 (Oxford Instruments, Oxfordshire, UK). Powders were placed on a brass sample carrier fixed with self-adhesive carbon plates (Plano GmbH, Wetzlar, Germany). The samples were sputtered with carbon (sputter device: BAL-TEC MED 020, BAL-TEC AG, Balzers, Netherlands). EDX data collection and evaluation was carried out with the aid of the INCA program package.

10.2.4 Solid-state MAS (*m*agic *a*ngle *s*pinning) NMR (*n*uclear *m*agnetic *r*esonance) methods

^1H and ^{31}P solid-state MAS NMR spectra of $Ba_{19}P_{36}O_{6+x}N_{66-x}Cl_{8+x}$ (x ≈ 4.54) were recorded at ambient temperature on a Bruker Avance III spectrometer with an 11.75 T magnet. The powdered samples were contained in ZrO_2 rotors with outer diameters of 2.5 or 1.3 mm which were mounted in commercial MAS probes (Bruker). The rotors were spun at rotation frequencies ν_{MAS} between 8 and 20 (2.5 mm), and 50 kHz (1.3 mm), respectively. Chemical shifts are given relative to the respective reference compounds (^1H: 1 % tetramethylsilane (TMS) in $CDCl_3$; ^{31}P: 85 % H_3PO_4, T = 298 K) as external standards. The calibration of the spectrometer was done with TMS under MAS conditions using the unified scale Ξ and the chemical shift definitions in the literature.[29] Quantitative ^1H spectra and ^{31}P spectra were obtained by a rotor-synchronized spin-echo sequence at ν_{MAS} = 20 kHz with a repetition delay of 32 s in the case of ^1H and of 1500 s in the case of ^{31}P.

A ^{31}P 2D double-quantum (DQ) single-quantum (SQ) correlation MAS NMR spectrum was obtained using PostC7[30] with a conversion period of 0.8 ms and rotor-synchronized data sampling of the indirect dimension. A ^{31}P 2D triple-quantum (TQ) single-quantum (SQ) correlation MAS NMR spectrum[31] was obtained with a conversion period of 1.6 ms and rotor-synchronized data sampling of the indirect dimension. A $^{31}P\{^1H\}$ PostC3_3^1-REDOR[32] curve was recorded to determine the effective dipolar coupling constant and estimate limits for the interatomic P–H distances. The experimental data are compared with simulated curves for different effective dipolar couplings on the universal dephasing scale.[33]

10.3   RESULTS AND DISCUSSION

10.3.1 Synthesis

Oxonitridophosphates are isolobal and isoelectronic with silicates. However, the variety of silicate structures is far from being emulated with P/O/N chemistry. This suggests great potential, but the reaction and crystallization temperatures are often close to the decomposition temperature of the starting materials (e.g., PON and P_3N_5 decompose from 800 °C) or the (oxo-)nitridophosphate phases themselves.[34] To prevent this decomposition,[35] high-pressure synthesis[36] has been used for most known P/(O)/N phases. However, high-pressure obviously favors materials with a high density and is not the method of choice to obtain porous open-framework oxonitridophosphates. Therefore,

suitable starting materials and reaction conditions are required, e.g., P/(O)/N/H-containing molecular compounds in the closed system of evacuated silica glass ampoules in the presence of metal salts and NH_4X (X = halogen) as mineralizer.[6,7,9]

Besides other starting materials like $(NH_2)_2(O)PNP(NH_2)_3$,[19] a convenient approach for synthesis of oxonitridophosphate frameworks is the joint thermal condensation of phosphoryl triamide $OP(NH_2)_3$ and thiophosphoryl triamide $SP(NH_2)_3$. While the latter allows a controlled addition of oxygen, the ammonia partial pressure emerging during the condensation in a closed system offers the conditions necessary for the crystallization process which can further be adjusted by adding a respective amount of NH_4X (X = halogen). The metal salts act as structure-stabilizing agents.

In the case of $Ba_{19}P_{36}O_{6+x}N_{66-x}Cl_{8+x}$ ($x \approx 4.54$), the combination of BaS, $OP(NH_2)_3$, $SP(NH_2)_3$, and NH_4Cl (cf. Experimental Section) led to the best result after a series of experiments with different starting materials (e.g., $BaCl_2$ or $P(NH_2)_4Cl$) in different molar ratios, and different temperature programs had been carried out to optimize the yield of the title compound. Although $Ba_{19}P_{36}O_{6+x}N_{66-x}Cl_{8+x}$ ($x \approx 4.54$) is routinely obtained by different approaches, it turned out that the reactant system is very sensitive concerning the appearance

Figure 3. SEM images of $Ba_{19}P_{36}O_{6+x}N_{66-x}Cl_{8+x}$ ($x \approx 4.54$) as cuboidal microcrystals and the Ba/P/O/N side phase as nanometer-sized platelets (bright areas in the big image and small SEM image).

and type of impurities. This is an intrinsic problem as at least four starting materials react at high temperatures. Many parameters such as the NH_3 partial pressure and the amount of Cl^- ions are simultaneously affected and cannot be fully controlled, so far impeding the phase-pure synthesis of $Ba_{19}P_{36}O_{6+x}N_{66-x}Cl_{8+x}$ ($x \approx 4.54$). However, the title compound is typically obtained as the most prominent crystalline phase with more than 90 % yield (estimated from the intensity ratio of strongest Bragg peaks of the title compound and side phase(s)). Figure 3 shows the title compound as cuboidal microcrystals with a mean edge length of 3–5 μm together with the most significant side phase, an unknown Ba/P/O/N compound in the form of nanometer-sized platelets.

10.3.2 Indexing and Structure Solution

As no single crystals of adequate dimensions were available, it was a challenge to solve the structure from PXRD data obtained from multiphase samples of $Ba_{19}P_{36}O_{6+x}N_{66-x}Cl_{8+x}$ ($x \approx 4.54$). Starting with data from conventional laboratory diffractometers, indexing was not possible due to low resolution (with Mo-K_α-radiation) or a bad signal-to-noise ratio (with Cu-$K_{\alpha1}$-radiation). An unambiguous determination of the unit cell was additionally impeded by several reflections with low intensity at low angles; it was unclear whether the latter are superstructure reflections or due to unknown side phases. Indexing became possible and fairly unambiguous after evaluating of high-resolution synchrotron PXRD data from different samples. As each sample contains different impurity phases, the reflections of the main phase $Ba_{19}P_{36}O_{6+x}N_{66-x}Cl_{8+x}$ ($x \approx 4.54$) could be clearly identified. While initially a cP unit cell with a = 1341.62 pm had been considered, a cF unit cell with a doubled lattice parameter was suggested by reflections that could be superstructure reflections ($h, k, l = 2n + 1$). Although the doubling of a results in an 8-fold cell volume due to the F-centering, this, however, exhibits a 2-fold superstructure. To exclude the possibility that these reflections are due to unknown impurities, the 2-fold superstructure was subsequently confirmed by SAED. Figure 4 compares the experimental diffraction pattern of the [0–15] zone axis with respective simulations on the basis of structure models in the primitive (a = 1342.95 pm) and in the F-centered (a = 2685.41 pm) cell. The appearances of reflections on odd lines, e.g., reflections with indices $h15$, require the doubled lattice parameter. A further comparison of a simulated and an experimental electron diffraction pattern is indicated in Figure 5.
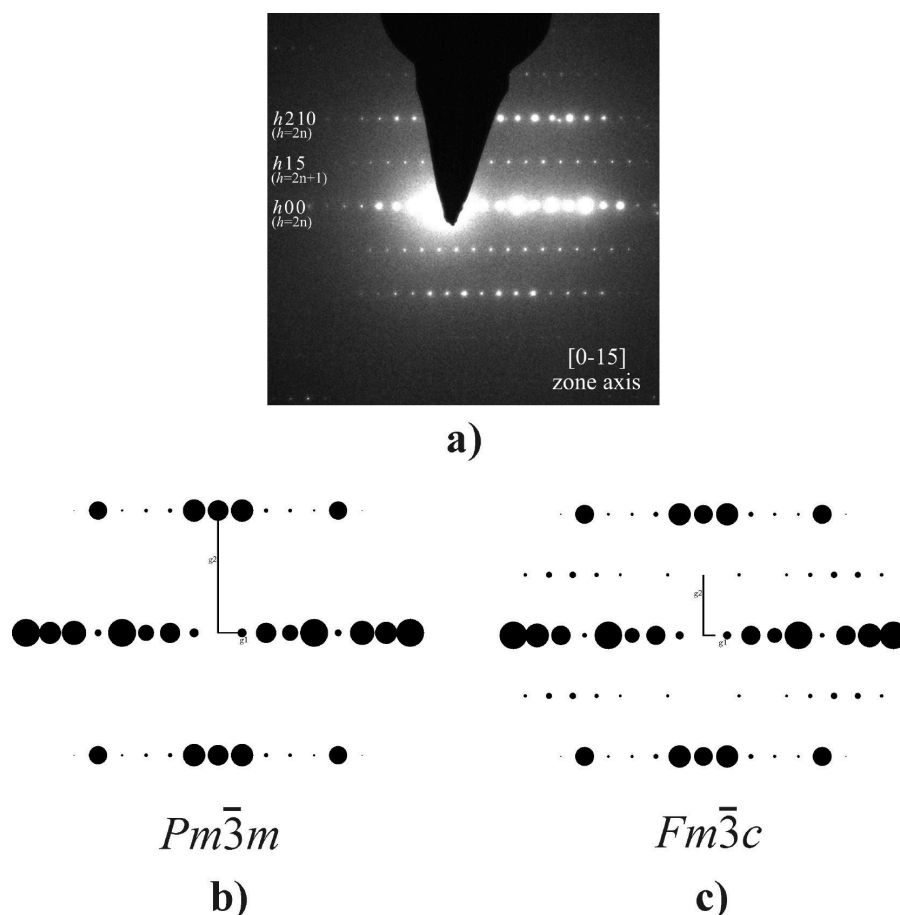
Figure 4. (a) SAED pattern of a cuboidal microcrystal of $Ba_{19}P_{36}O_{6+x}N_{66-x}Cl_{8+x}$ (x ≈ 4.54) (top) and corresponding kinematic simulations of electron diffraction patterns in the [0–15] zone axis for structure models refined in space groups $Pm\overline{3}m$ (b) and $Fm\overline{3}c$ (c).

Figure 5. SAED pattern of a cuboidal microcrystal of $Ba_{19}P_{36}O_{6+x}N_{66-x}Cl_{8+x}$ (x ≈ 4.54) (left) and simulation from the crystal structure in space group $Fm\overline{3}c$ (right) of zone axis [100].
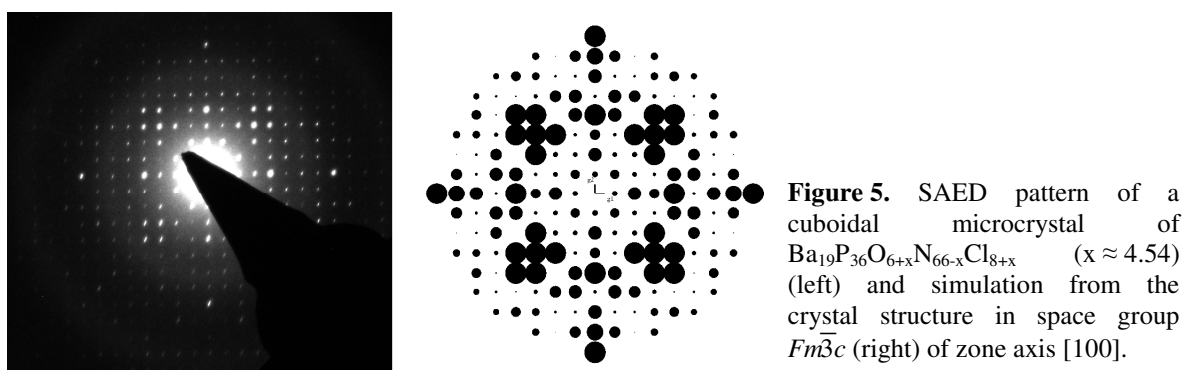
As some *cF* space groups are indistinguishable by means of reflection conditions, STEM-HAADF images along [100] and [110] (Figure 6, left) have been used to derive the correct space group. Comparison of their plane groups (*p4mm* (top) and *p2mm* (bottom)) with the symmetry of the special projections leaves only two options ($Fm\overline{3}c$, $Fd\overline{3}c$). As $Fd\overline{3}c$ is not consistent with the extinction conditions analyzed in the PXRD pattern, $Fm\overline{3}c$ is unambiguously the correct space group.

Structure solution succeeded *ab initio* by applying the charge-flipping algorithm.[23] Initially, the Ba, P, and fully occupied Cl positions have been located. The correctness of the heavy-atom positions was corroborated by the STEM-HAADF images. Incorrect solutions regarding heavy atom positions could be directly identified because of the atomic number sensitivity of the STEM-HAADF in [100] and [110]. Figure 6 depicts the match of the heavy-atom structure with the STEM images. The final crystal structure has been elucidated by evaluation of difference Fourier maps generated after refinements of fragmentary structure models and placing additional bridging atoms at reasonable positions. The final Rietveld refinement of the complete structure model was performed in space group $Fm\bar{3}c$. This is reasonable as almost all superstructure reflections are observed, although they are rather weak. Additionally, refinement of the basic structure in space group $Pm\bar{3}m$ was done as well. The results are given in Tables 3 and 4.
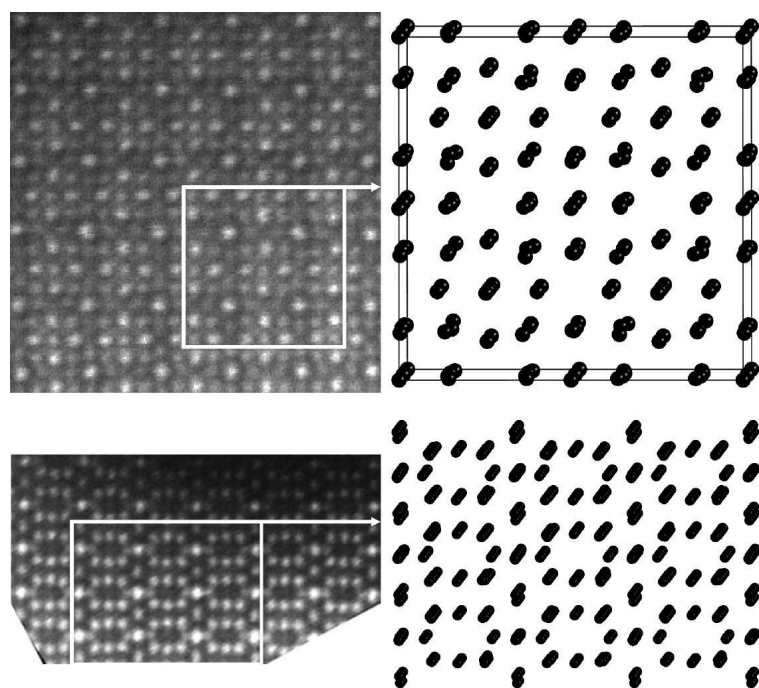
Figure 6. STEM-HAADF images (left) indicating the heavy atom structure (right) of $Ba_{19}P_{36}O_{6+x}N_{66-x}Cl_{8+x}$ (x ≈ 4.54); top: image along [100] with plane group *p4mm*; bottom: image along [110] with plane group *p2mm*.

10.3.3 NMR Study

In addition to the X-ray / electron diffraction data, solid-state NMR spectroscopic investigations have been performed. These experiments can add further information about the structure, for example, if hydrogen is present in the title compound. Thereby, additional evidence for the structural model of $Ba_{19}P_{36}O_{6+x}N_{66-x}Cl_{8+x}$ (x ≈ 4.54) has been obtained by an independent method.

A quantitative ^{31}P NMR spectrum is shown at the top of the 2D spectrum in Figure 7. Two peaks are observed at –4.6 and –17.7 ppm. These shift values agree well with NMR data of most other nitridophosphates[36] and oxonitridophosphates (oxonitridosodalite, -8.7 ppm;[7] *NPO* type material, 6.5, –0.1 ppm;[9] $Sr_3P_6O_6N_8$, 2.6 ppm).[37] With the resolution power of a ^{31}P double-quantum filtered 2D spectrum, several independent resonances can be revealed (see Figure 7). The two sharp resonances, labelled A and B, are assigned to the two P sites of the title compound, which lead to the double-quantum coherences B–B and A–B. They can clearly be distinguished from a broad contribution, which is probably due to an amorphous impurity. It is much broader and has its center of gravity in the range of peak A of the crystalline title compound. The ^{31}P peaks were assigned according to their peak areas and according to the different frequency of the P sites in the unit cell (Wyckoff positions 192*j* (P(1)) and 96*h* (P(2)), Table 5). To obtain reliable results, the line shape parameters were first constrained on the sum projection of the A–B DQ resonance in the 2D spectrum. Subsequently, the quantitative spin-echo spectrum was deconvoluted which resulted in a 5.2 : 10.0 peak area ratio for peaks A and B, respectively. The deconvolution data in Table 5 also show that—besides P-containing impurities—a high proportion of the sample is amorphous or heavily disordered. In agreement with the SEM image (Figure 3), we conclude that during the reaction first amorphous particles are formed and later crystallization sets in from the particle surface.
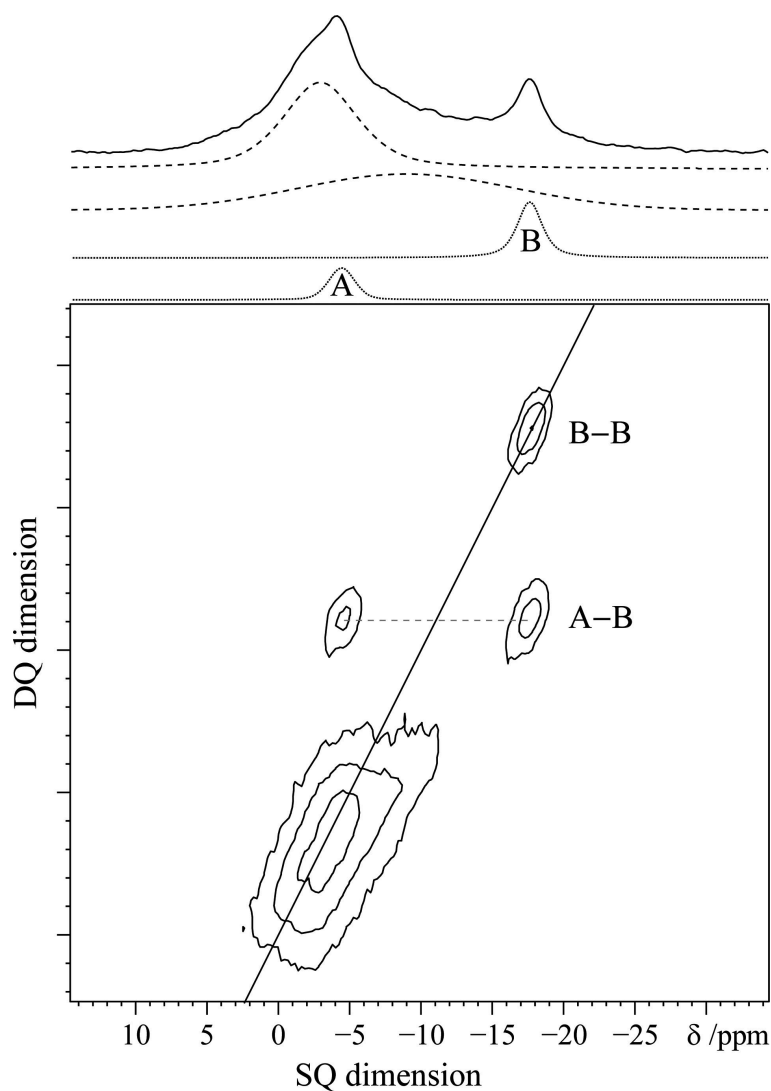
Figure 7. ^{31}P-MAS NMR double-quantum (DQ) single-quantum (SQ) correlation spectrum of $Ba_{19}P_{36}O_{6+x}N_{66-x}Cl_{8+x}$ ($x \approx 4.54$); the quantitative 1D spectrum (top) was obtained by direct excitation, and below are the individual line shapes of the four Gaussian / Lorentzian profiles which were obtained by constrained line shape deconvolution (dashed lines, amorphous; dotted lines, crystalline). The diagonal is indicating the position of DQ coherences of two isochronous nuclei. The sharp DQ coherences of two crystalline ^{31}P sites are visible next to a broad autocorrelated DQ peak which is assigned to an amorphous impurity.

Table 5. Peak assignment in the quantitative spin-echo ^{31}P NMR spectrum of $Ba_{19}P_{36}O_{6+x}N_{66-x}Cl_{8+x}$ ($x \approx 4.54$).

δ_{iso} / ppm	peak area / a.u.	T_1 / s	assignment
−17.7	10.0	13	P(1), peak B
−4.6	5.2	4	P(2), peak A
−9.1	42.9	48	amorphous
−3.1	44.1	67	amorphous
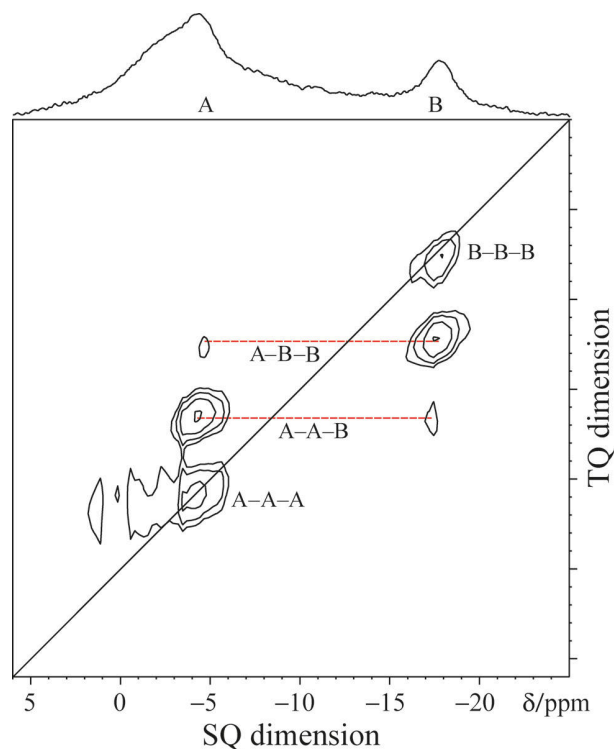
Figure 8. ^{31}P-MAS NMR triple-quantum (TQ) single-quantum (SQ) correlation spectrum of $Ba_{19}P_{36}O_{6+x}N_{66-x}Cl_{8+x}$ (x ≈ 4.54); the 1D spectrum (top) was obtained by direct excitation; the diagonal is indicating the position of TQ coherences of three isochronous nuclei; and the peaks labeled with A–A–A, A–A–B, A–B–B, and B–B–B belong to the title compound. The amorphous impurity is almost perfectly suppressed.

To clarify whether the sharp and broad peaks originate from the same phase, for example, in the form of a crystal with regions of heavy and weak N/O disorder, a ^{31}P triple-quantum filtered 2D spectrum (Figure 8) was acquired. This cannot be concluded from the ^{31}P double-quantum filtered 2D spectrum because of the spectral overlap of peak A with the broad features. ^{31}P triple-quantum coherences, which are expected for the crystalline title compound, are only observed between peaks A and B, while the broad contributions centered around –3 and –9 ppm are reduced in intensity. It is noteworthy that the triple-quantum coherences involving phosphorus atoms P(1) and P(2) are not related to the broad features. Hence, the description of the sample as a heterogeneous mixture of the title compound and an amorphous impurity is consistent with the triple-quantum filtered 2D correlation spectrum (Figure 8). Furthermore, the signal pattern of the spectrum with its linking schemes A–A–A, A–A–B, A–B–B, and B–B–B corroborates the refined structure model. In the *NPO* $Li_xH_{12-x-y+z}[P_{12}O_yN_{24-y}]X_z$ (X = Cl, Br) or the oxonitridosodalithes $M_{8-m}H_m[P_{12}N_{18}O_6]Cl_2$ (M = Cu, Li), hydrogen atoms are bound to the bridging nitrogen atoms forming imide groups. The occurrence of hydrogen in $Ba_{19}P_{36}O_{6+x}N_{66-x}Cl_{8+x}$ (x ≈ 4.54) is difficult to prove or disprove with diffraction techniques on an inhomogeneous mixture and because of the oxygen and nitrogen site disorder. NMR however is rather sensitive to small amounts of hydrogen in the structure. The $^{31}P\{^1H\}$ C-REDOR experiment can be used to investigate the stoichiometric occurrence of hydrogen in the structure. The experimental REDOR curve of the deconvoluted peak B is shown in Figure 9 together with three calculated curves for different dipolar coupling constants of –60, –70, and –80 Hz which refer to internuclear distances P–H of 933, 886, and 847 pm, respectively. There is no point in the unit cell

which has such a large distance from atom P(1). Hence, the REDOR curves prove that small amounts of hydrogen are incorporated into the structure; however, the observed slow dephasing effects are indicative of substoichiometric hydrogen content (H atoms / unit cell <1) only. Similar observations have been made previously for many zeolites.[38]
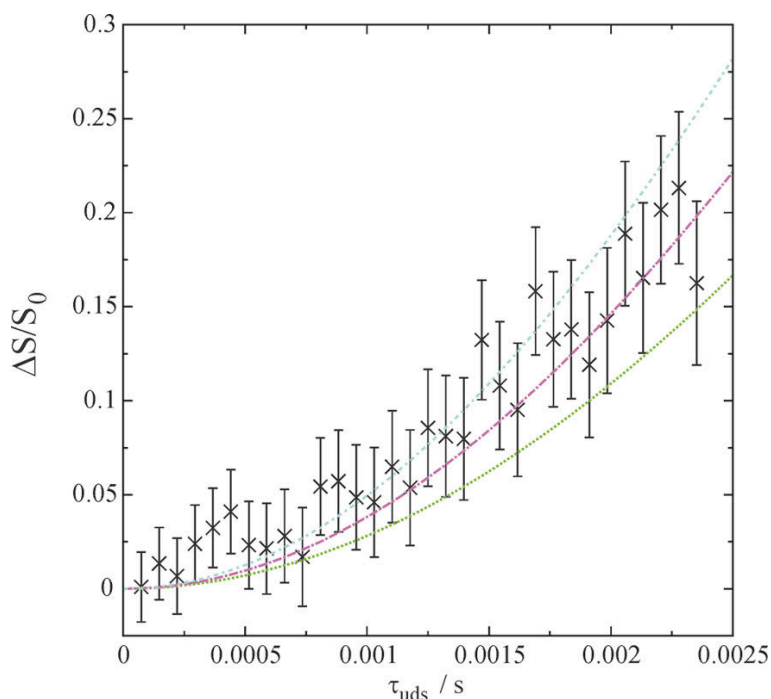
Figure 9. $^{31}P\{^1H\}$ REDOR curve of $Ba_{19}P_{36}O_{6+x}N_{66-x}Cl_{8+x}$ (x ≈ 4.54) (in black); the plotted lines in green, cyan, and magenta indicate simulated REDOR curves calculated with dipolar coupling constants of –60, –70, and –80 Hz, respectively; the REDOR experiment proves a small, nonstoichiometric (H atoms / unit cell < 1) contamination with hydrogen atoms, which is often observed in zeolites.[38]

10.3.4 Structure Description and Discussion

The crystal structure of $Ba_{19}P_{36}O_{6+x}N_{66-x}Cl_{8+x}$ (x ≈ 4.54) (Figure 10) consists of Ba^{2+} ions, Cl^- ions, and a framework of all-side vertex-sharing $P(O/N)_4$ tetrahedra representing an unprecedented topology that has been predicted by *Foster* and *Treacy* as a hypothetical zeolite structure on the SiO_2 basis.[39]
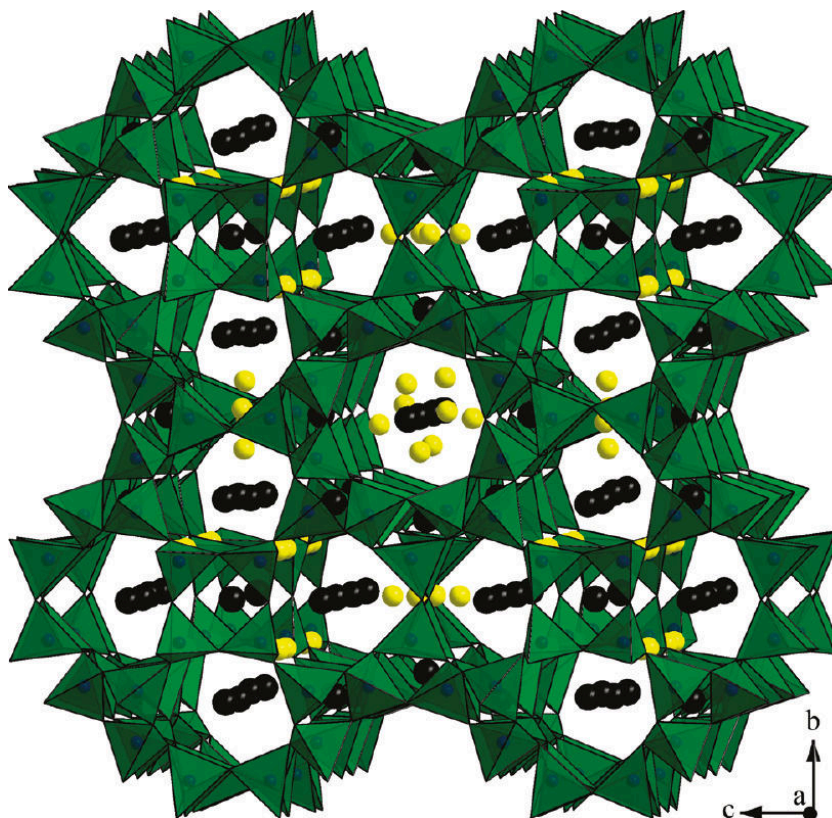
Figure 10. Crystal structure of $Ba_{19}P_{36}O_{6+x}N_{66-x}Cl_{8+x}$ (x ≈ 4.54). View along [100] (Ba^{2+} black, Cl^- yellow, $P(O,N)_4$ tetrahedra green).

According to the IUPAC[40] formula $|Ba_{19}^{2+}Cl_{8+x}^-|[P_{36}^{+V[4]}O_{6+x}^{-II[2]}N_{66-x}^{-III[2]}]_h\{3[3^84^68^{12}]\}_p\{3[3^88^6]<100>(8\text{-ring})\}(Fm\overline{3}c)$, the tetrahedra build up 3-, 4-, and 8-rings forming $3^84^68^{12}$ cages that exhibit a CBU (Figure 11) that is not included in the current pool of CBU types so far.[41] The idealized solid body corresponds to the RCSR symbol *rdo-a*.[42] It can be derived from the Catalan polyhedron of a rhombic dodecahedron by grinding off all vertices. Interconnecting the novel CBUs via their 4-rings (forming additional 3-rings) yields 8-ring channels along <100> with a free diameter of 292 pm (calculation considering r(N) = 147 pm). The coordination sequences and the vertex symbols for the framework (RCSR symbol *fuv*)[42] are given in Table 6.
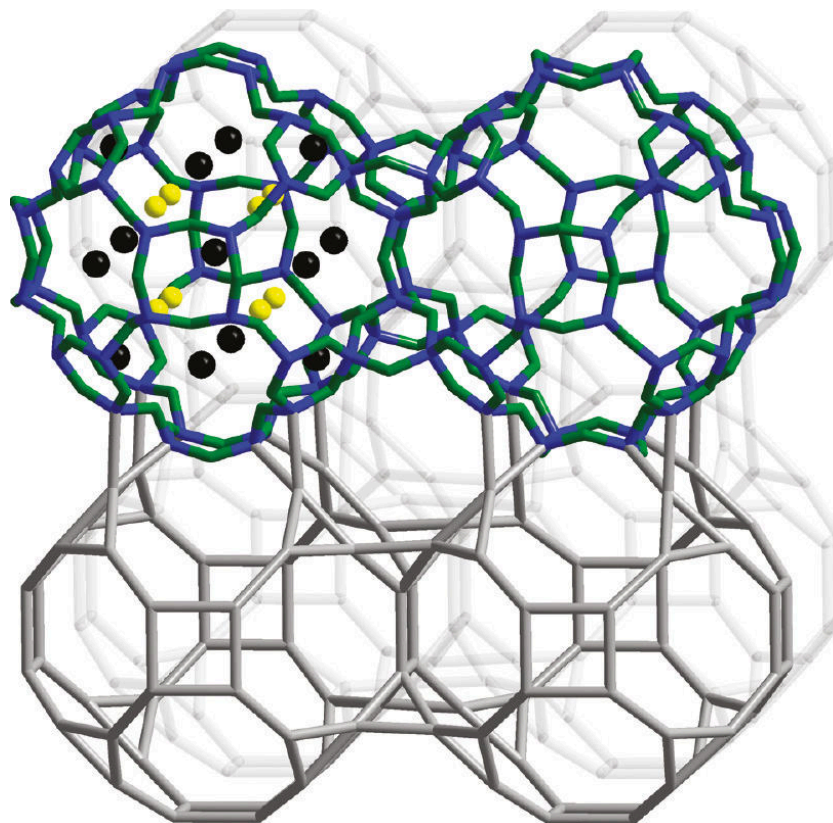
Figure 11. Interconnected $3^8 4^6 8^{12}$ cages in $Ba_{19}P_{36}O_{6+x}N_{66-x}Cl_{8+x}$ (x ≈ 4.54); top: drawing with P–N bonding and cage content (left); bottom: representation with only P–P linking.

Table 6. Coordination Sequences and Vertex symbols for the framework in $Ba_{19}P_{36}O_{6+x}N_{66-x}Cl_{8+x}$ (x ≈ 4.54) (analyzed with the program TOTOPOL).[a]

atom, Wyckoff symbol	Coordination Sequence	Vertex Symbol
P(1), 192*j*	1 4 8 17 32 46 71 95 129 166 199 241 309 346 407 476 539	3.3.8.8.8.8
P(2), 96*h*	1 4 9 18 32 50 70 95 128 166 212 259 296 344 412 467 530	3.4.8.8.8.8

[a] Treacy, M. M. J.; Srivilliputhur, S.; Foster, M. D.; Randall, K. TOTOPOL – A Topological Analysis Tool, Version 1.68, 2010: http://www.hypotheticalzeolites.net/NEWDATABASE/TOPO/upload_cif.html

The observed $[P_n(N/O)_n]$ ring sizes and their relative frequency, i.e., the cycle class sequence according to *Klee*,[43] are listed in Table 7 (calculated with the program TOPOLAN).[44] In contrast to the sodalite framework (*SOD*) or the framework of *LTA* that comprise cubic β-($4^6 6^8$) and α-($4^{12} 6^8 8^6$) cages, all ring sizes do exist in $Ba_{19}P_{36}O_{6+x}N_{66-x}Cl_{8+x}$ (x ≈ 4.54). Notably, many 3-rings are present, although they rarely occur in zeolite topologies (in only 15 of 194 framework types registered in the IZA database). However, when low framework densities should be achieved, small rings are relevant according to the theory of *Brunner* and *Meier*.[45] With a high 3-ring frequency of

19 and a framework density of 14.87 T/1000Å^3, which is rather low considering the typical range of zeolites (12.5–20.2 T/1000Å^3), this theory is supported by the findings in the case of $Ba_{19}P_{36}O_{6+x}N_{66-x}Cl_{8+x}$ ($x \approx 4.54$).

Table 7. Cycle class sequence from the framework in $Ba_{19}P_{36}O_{6+x}N_{66-x}Cl_{8+x}$ in comparison with frameworks *SOD* and *LTA*.

$P_n(O,N)_n$-rings	3	4	5	6	7	8	9	10
$Ba_{19}P_{36}O_{6+x}N_{66-x}Cl_{8+x}$	19	4	4	8	12	31	129	388
SOD	0	3	0	4	0	24	0	576
LTA	0	18	0	56	0	69	0	360

The $3^8 4^6 8^{12}$ cages in $Ba_{19}P_{36}O_{6+x}N_{66-x}Cl_{8+x}$ ($x \approx 4.54$) are slightly distorted from the symmetry of the regular polyhedron ($m\overline{3}m$). This distortion causes two different cages in the unit cell, which are crystallographically independent and thus the necessity of the 2-fold superstructure described in $Fm\overline{3}c$. Neglecting the superstructure reflections and accepting just slightly higher *R*-values, the structure can be described in $Pm\overline{3}m$ (crystallographic data of this basic structure are given in Tables 3 and 4) including only one less distorted cage. The number of independent atom sites is identical in both models; however, P and O/N atoms occupy more special positions in the approximate basic structure, while they occupy more general ones in the correct space group. To quantify the distortion of the cages in the $Fm\overline{3}c$ model and to clarify the difference to the model in $Pm\overline{3}m$, a conformation analysis of the 3- and 4-rings, i.e., the 6-membered $P_3(O,N)_3$ and 8-membered $P_4(O,N)_4$ rings,[46] has been performed calculating the torsion angle sequence (TAS see chapter 10.5, Table 9) as well as the displacement asymmetry (DAP, see chapter 10.5, Figure 14)[47] and the puckering parameters[48] with the program PARST97.[49] The 6-membered rings exhibit a chair conformation in both models, which, combined with a tiny interference of a sofa conformation, is more pronounced in $Fm\overline{3}c$. This can be clearly seen considering the respective values (chapter 10.5). A larger difference is found within the 8-membered $P_4(O,N)_4$ rings. While they are planar in $Pm\overline{3}m$ (all torsion angles are zero), a saddle conformation with an intermixture of a twist chair for the conformation in $Fm\overline{3}c$ is suggested by the values given in chapter 10.5.

In the Rietveld refinement, constraints were included to fit distances and angles within the tetrahedra into the usual range observed in phosphorus nitride network structures.[9,36,46] With a certain permitted deviation the distances P–(O,N) vary between 159.1 and 165.5 pm and the angles (O,N) –P–(O,N) between 99.0 and 119.2° (Table 8). The angles P–(O,N)–P

of the final model range between 121.5 and 141.2° (Table 8), comparable to angles in compounds like $P_4N_4(NH)_4 \cdot NH_3$[12] or SrP_2N_4.[50] Also within the corresponding hypothetical ideal SiO_2 framework generated by a distance-least-squares refinement with DLS76,[51] rather small angles Si–O–Si down to 159.684(2)° are existent. This might be the reason why this framework has not been realized in an oxidic system as of yet.

Table 8. Selected interatomic distances / pm and angles /° in $Ba_{19}P_{36}O_{6+x}N_{66-x}Cl_{8+x}$ (x ≈ 4.54) (esd's in parentheses).

Ba(1)–Cl (partially occupied)	311.0(12)	4 times
Ba(2)–Cl	317.6(4), 334.2(16)	3 times
Ba(3)–Cl	320.3(4)	8 times
Ba(1)–(O,N)	308.1(5), 309.4(4)	8 times
Ba(2)–(O,N)	288.6(4)–321.4(4)	7 times
P–(O,N)	159.1(6)–165.5(5)	8 times
P–(O,N)–P	121.5(3), 125.0(2), 125.2(3), 141.2(1)	
(O,N)–P–(O,N)	99.0(2)–119.2(2)	12 times

We assume a statistic O,N-distribution in the P/O/N network of $Ba_{19}P_{36}O_{6+x}N_{66-x}Cl_{8+x}$ (x ≈ 4.54). As there are no predestined positions for O or N and such statistic O,N-distributions were already observed in other P/O/N TX_2 networks,[9,6,7,52] this assumption is reasonable. Possible O,N ordering in $Ba_{19}P_{36}O_{6+x}N_{66-x}Cl_{8+x}$ (x ≈ 4.54) could only be analyzed by neutron diffraction. From the refined sum formula $Ba_{19}P_{36}O_{10.54}N_{61.46}Cl_{12.54}$ that is confirmed by semiquantitative EDX analysis within the accuracy of the method (calcd: Ba : Cl = 1.5, Ba : P = 0.5, P : (O,N) = 0.5, P : Cl = 2.9, N : O = 5.8; exptl: Ba : Cl = 1.3, Ba : P = 0.6, P : (O,N) = 0.4, P : Cl = 2.4, N : O = 4.4), on average 56 % PN_4 and 44 % PON_3 tetrahedra are present.

The framework in $Ba_{19}P_{36}O_{6+x}N_{66-x}Cl_{8+x}$ (x ≈ 4.54) provides a "free" volume of 4484.3 Å^3 (23.2 % of the cell volume). Within this volume, which comprises the 8-ring channels and the interior of the cages, the extra-framework ions Ba^{2+} and Cl^- are located. One Ba^{2+} site lies directly in the center of the cages coordinated by a cube of eight Cl^- ions at a distance of 320.3 pm (Figure 12, Ba(3)), corresponding to the content of one unit cell of the CsCl structure type. Around the $BaCl_8^{6-}$ units, 12 more Ba^{2+} ions are located within each cage. These ions are coordinated 10-fold by seven (O,N) atoms (288.6–321.4 pm) of the cage and three Cl^- ions (317.6 and 334.2 pm; Figure 12, Ba(2)). The Ba^{2+} ions along the 8-ring channels are arranged in pairs with an intrapair distance of 566.5 pm and Cl^- ions in between (Figure 12, Ba(1)). The four Cl^- positions are staggered from pair to pair

(cf. Figure 10) and have, due to their partial occupancy (about 40 %), with 311.0 pm the shortest Ba–Cl distance in $Ba_{19}P_{36}O_{6+x}N_{66-x}Cl_{8+x}$ (x ≈ 4.54). Furthermore, the Ba_{2+} ions involved in the pairs which have an interpair distance of 1342.7 pm are surrounded each by eight (O,N) atoms with distances between 308.1 and 309.4 pm. All Ba–Cl and Ba–(O,N) contacts, summarized in Table 8, range in the sum of the respective ionic radii.[53,54] Although the cages and channels are quite crowded with Ba^{2+} and Cl^-, there is still free space (about 38 Å^3) between the Ba^{2+} ions that are situated in the periphery of the cage interior in a distance of around 200 pm to the bridging atoms O,N. Replacing Cl^- and Br^- ions can also be partially introduced by adding NH_4Br to the starting material mixture. A replacement of Cl^- by Br^- could be proved obtaining cubic microcrystals (Figure 13) that contain the elements Ba, P, O, N, Cl, and Br (EDX analysis) and powder diffraction data where all reflections move to lower 2θ-values compared to the pure Cl^- containing compound (a = 2691.06(3) pm). No evidence was observed for incorporation of I^- or cations other than Ba^{2+}.
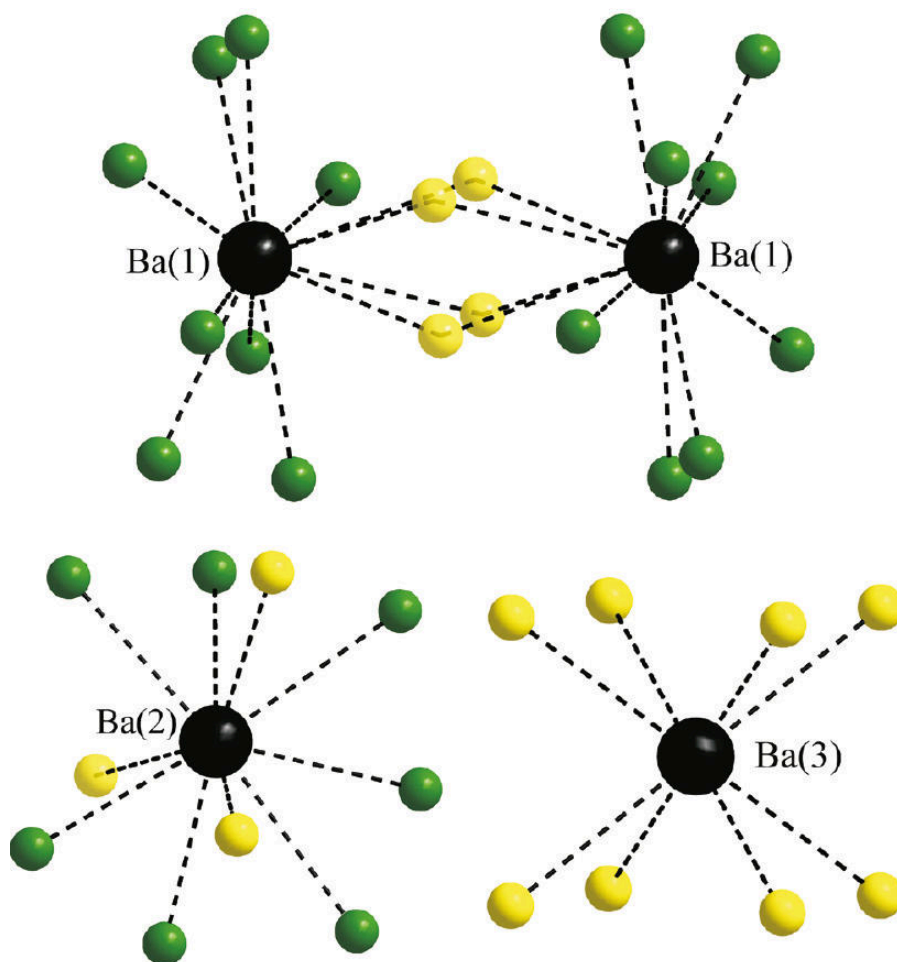
Figure 12. Coordination of the Ba sites in $Ba_{19}P_{36}O_{6+x}N_{66-x}Cl_{8+x}$ (x ≈ 4.54) (Ba^{2+} black, Cl^- yellow (partially occupied ones are hold transparent), (O,N) green).
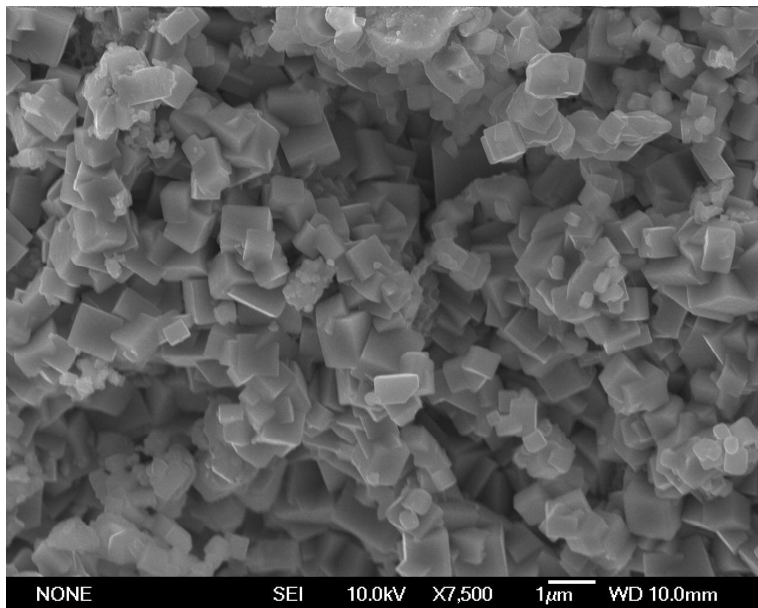
Figure 13. SEM image of "$Ba_{19}P_{36}O_{6+x}N_{66-x}Br_{8+x}$" as cubic microcrystals.

10.4   CONCLUSION

With the novel oxonitridophosphate $Ba_{19}P_{36}O_{6+x}N_{66-x}Cl_{8+x}$ (x ≈ 4.54), an unprecedented zeolite-like framework including a new CBU unit has been elucidated. Its discovery and its structure elucidation were highly challenging, as from a complex synthesis system only microcrystalline powder samples with side phases were available. However, applying a combination of high-resolution synchrotron powder diffraction and electron microscopic methods (SAED and STEM), ambiguous data could be clarified, and cubic ($Fm\overline{3}c$ (no. 226), a = 2685.41(3) pm) $Ba_{19}P_{36}O_{6+x}N_{66-x}Cl_{8+x}$ (x ≈ 4.54) could be established as a compound exhibiting a novel all-side vertex-sharing $P(O,N)_4$ tetrahedra topology that has been predicted but not observed as of yet. Confirmed and complemented with solid-state NMR spectroscopy, the structure model comprises Ba^{2+} and Cl^- ions which are incorporated in interlinked $3^8 4^6 8^{12}$ cages and in 8-ring channels with a free diameter of 292 pm. If this extra-framework material could be (partially) removed or exchanged by smaller ions, which will be the subject of future investigations, the title compound may be a representative for a small-pore zeolite that can usually be used in pressure swing adsorption (PSA) separation processes.[55–57] This or other applications seem to be desirable as $Ba_{19}P_{36}O_{6+x}N_{66-x}Cl_{8+x}$ (x ≈ 4.54) has a surprising thermal stability up to at least 1100 °C, a temperature where many common zeolites are already decomposed. With this stability, nitride materials would be interesting for catalytic processes that act at high temperatures.

Further improvement and development of the complex synthesis system must be another future goal. After the (oxo-)nitridosodalites and the *NPO* type materials, $Ba_{19}P_{36}O_{6+x}N_{66-x}Cl_{8+x}$ ($x \approx 4.54$) is another important example for the use of the multicomponent reactant system with phosphorus triamides, metal halides, and ammonium halides. A comprehensive investigation of the role of the NH_3 partial pressure as well as the templating effect of Ba^{2+} and Cl^- would allow one to purposefully optimize the synthesis. Other soft and large ions like Pb^{2+} or Sn^{2+} might as well be useful to establish a systematic route for the synthesis of nitridic zeolites and permit novel framework types with low framework densities and thus exploit the full potential of the nitride approach within zeolite chemistry.

10.5　SUPPORTING INFORMATION

In this chapter the symmetry of the 6-membered $P_3(O,N)_3$ and 8-membered $P_4(O,N)_4$ rings in the $3^8 4^6 8^{12}$ cages in $Ba_{19}P_{36}O_{6+x}N_{66-x}Cl_{8+x}$ is given.

Table 9. Torsion angle sequence (TAS) and puckering parameter for the 6-membered $P_3(O,N)_3$-rings in the structure models of $Ba_{19}P_{36}O_{6+x}N_{66-x}Cl_{8+x}$ in $Pm\overline{3}m$ and $Fm\overline{3}c$, respectively.

	$Pm\overline{3}m$	$Fm\overline{3}c$
TAS	3.4(4)/–3.4(4)/3.4(4) –3.4(4)/3.4(4)/–3.4(4)°	6.1(5)/–6.2(5)/6.1(5)/ –6.2(5)/6.1(5)/–6.2(5)°
puckering parameter	$q_2 = 0.000(4)$, $q_3 = Q_T = 0.333(3)$, $\theta = 180.0(68)°$	$q_2 = 0.000(4)$, $q_3 = Q_T = 0.061(4)$, $\theta = 180.0(38)°$
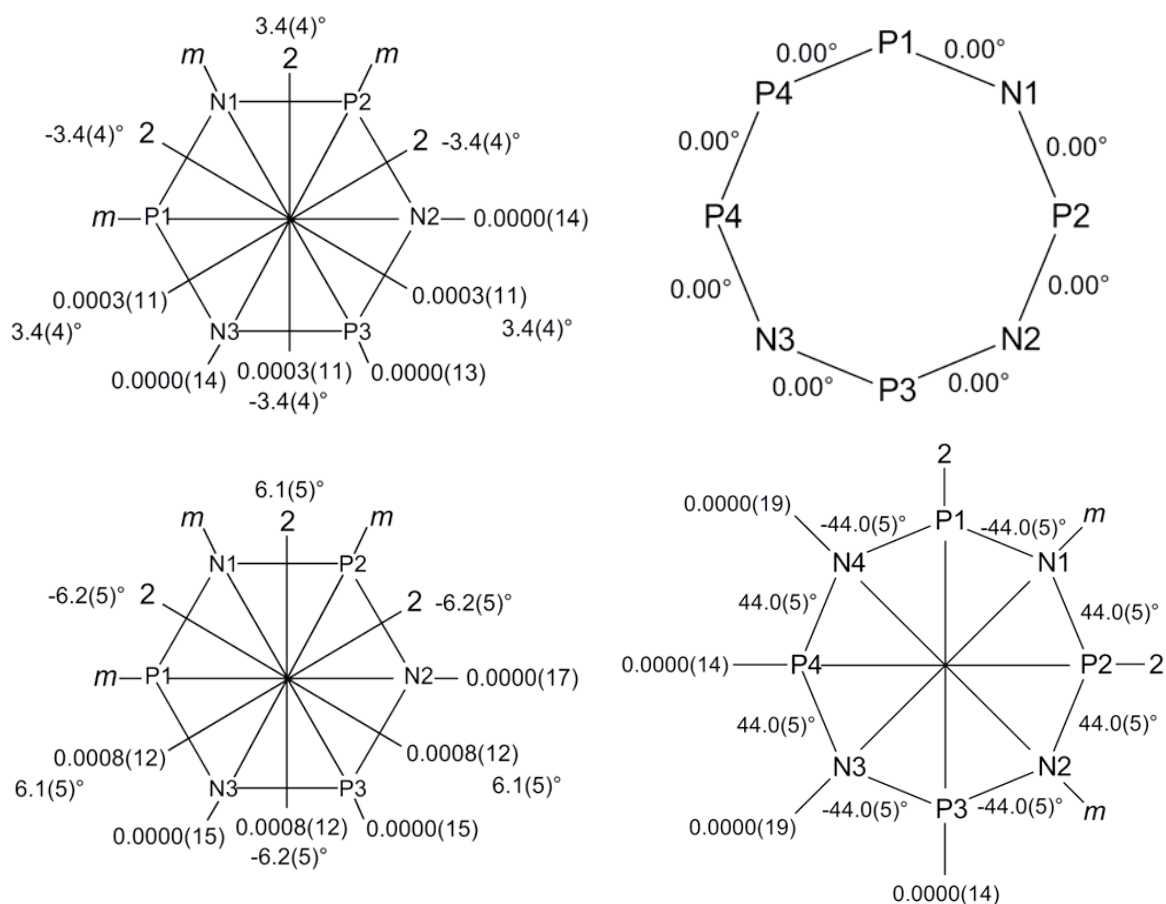
Figure 14. Symmetry of 6-membered $P_3(O,N)_3$ and 8-membered $P_4(O,N)_4$ rings in the $3^8 4^6 8^{12}$ cages in $Ba_{19}P_{36}O_{6+x}N_{66-x}Cl_{8+x}$; top: values calculated on basis of the refinement in space group $Pm\overline{3}m$, bottom: values calculated on basis of the refinement in space group $Fm\overline{3}c$; torsion angles in ° and displacement-asymmetry-parameter (DAP) for the mirror plane (*m*) and the twofold axes (2) are given.

For the 8-membered $P_4(O,N)_4$ rings in the $Fm\overline{3}c$ structure model a saddle conformation is suggested. The smallest DAP values are present for the mirror planes running through two N (0.0000(19) / 0.0000(18)) and the twofold rotation axes running through two P atoms each (0.0000(13) / 0.0000(14)) while visa versa for the respective symmetry elements running between the atoms the DAPs are high (0.2374(12)) (Figure 14). The saddle conformation is further confirmed by the TAS (44.0(5)/44.0(5)/–44.0(5)/–44.0(5)/44.0(5)/44.0(5)/–44.0(5)/–44.0(5)°), the puckering amplitudes ($q_2 = Q_T = 0.8776(58)$, $q_3 = 0.0000(58)$, $q_4 = 0.0000(42)$) and a phase angle $\varphi_2 = n(\pi/4)$ (for $n = 2m$ and $m = 1, 2, 3, …$). A phase angle φ_3 around $n(\pi/8)$ (for $n \notin N_0$) indicates an intermixture of a twist chair conformation. The values and the derivation of the conformations can be understood consulting a summary of the theory given in the literature.[46]

10.6   REFERENCES

[1]   A. K. Cheetham, G. Férey, T. Loiseau, *Angew. Chem.* **1999**, *111*, 3466; *Angew. Chem., Int. Ed.* **1999**, *38*, 3268.

[2]   S. Natarajan, S. Mandal, *Angew. Chem.* **2008**, *120*, 4876; *Angew. Chem., Int. Ed.* **2008**, *47*, 4798.

[3]   S. T. Wilson, B. M. Lok, C. A. Messina, T. R. Cannan, E. M. Flanigen, *J. Am. Chem. Soc.* **1982**, *104*, 1146.

[4]   a) J. L. Guth, H. Kessler, R. Wey, *Stud. Surf. Sci. Catal.* **1986**, *28*, 121; b) M. Estermann, L. B. McCusker, C. Baerlocher, M. Merrouche, H. Kessler, *Nature* **1991**, *352*, 320.

[5]   C. L. Bowes, G. A. Ozin, *Adv. Mater.* **1996,** *8*, 13.

[6]   a) W. Schnick, J. Lücke, *Angew. Chem.* **1992**, *104*, 208; *Angew. Chem., Int. Ed. Engl.* **1992**, *31*, 213; b) W. Schnick, J. Lücke, *Z. Anorg. Allg. Chem.* **1994**, *620*, 2014; c) W. Schnick, N. Stock, J. Lücke, M. Volkmann, M. Jansen, *Z. Anorg. Allg. Chem.* **1995**, *621*, 987; d) F. Wester, W. Schnick, *Z. Anorg. Allg. Chem.* **1996**, *622*, 1281.

[7]   N. Stock, E. Irran, W. Schnick, *Chem. Eur. J.* **1998**, *4*, 1822.

[8]   H. Huppertz, W. Schnick, *Angew. Chem.* **1997**, *109*, 2765; H. Huppertz, W. Schnick, *Angew. Chem., Int. Ed. Engl.* **1997**, *36*, 2651.

[9]   a) S. Correll, O. Oeckler, N. Stock, W. Schnick, *Angew. Chem.* **2003**, *115*, 3674; *Angew. Chem., Int. Ed.* **2003**, *42*, 3549; b) S. Correll, N. Stock, O. Oeckler, J. Senker, T. Nilges, W. Schnick, *Z. Anorg. Allg. Chem.* **2004**, *630*, 2205.

[10]   A. J. D. Barnes, T. J. Prior, M. G. Francesconi, *Chem. Commun.* **2007**, 4638.

[11]   S. Pagano, O. Oeckler, T. Schröder, W. Schnick, *Eur. J. Inorg. Chem.* **2009**, 2678.

[12]   F. Karau, W. Schnick, *Angew. Chem.* **2006**, *118*, 4617; *Angew. Chem., Int. Ed.* **2006**, *45*, 4505.

[13]   M. Pouchard, *Nature* **2006**, *442*, 878.

[14]   R. Klement, O. Koch, *Chem. Ber.* **1954**, *87*, 333.

[15]   W. Schnick, *Z. Naturforsch., B: J. Chem. Sci.* **1989**, *44*, 942.

[16]   S. Correll, Doctoral Thesis, Univ. Munich (LMU) **2006**.

[17]   S. Horstmann, W. Schnick, *Z. Naturforsch., B: J. Chem. Sci.* **1996**, *51*, 127.

[18]   a) D. B. Sowerby, L. F. Audrieth, *Chem. Ber.* **1961**, *94*, 2670; b) F. Golinski, H. Jacobs, *Z. Anorg. Allg. Chem.* **1994**, *620*, 965.

[19]   N. Stock, W. Schnick, *Z. Naturforsch., B: J. Chem. Sci.* **1996**, *51*, 1079.

[20]   J.-L. Hodeau, P. Bordet, M. Anne, A. Prat, A. N. Fitch, E. Dooryhee, G. Vaughan, A. K. Freund, *Proc. SPIE* **1998**, *3448*, 353.

[21]   A. A. Coelho, *TOPAS-Academic*, Version 4.1, Coelho Software, Brisbane, **2007**.

[22]   A. A. Coelho, *J. Appl. Crystallogr.* **2003**, *36*, 86.

[23]   G. Oszlányi, A. Sütő, *Acta Crystallogr., Sect. A: Found. Crystallogr.* **2004**, *60*, 134.

[24]   J. Bergmann, R. Kleeberg, A. Haase, B. Breidenstein, *Mater. Sci. Forum* **2000**, *347–349*, 303.

[25]   T. M. Sabine, B. A. Hunter, W. R. Sabine, C. J. J. Ball, *Appl. Crystallogr.* **1998**, *31*, 47.

[26]   R. J. Hill, I. C. J. Madsen, *Appl. Crystallogr.* **1984**, *17*, 297.

[27]   R. J. Hill, H. D. J. Flack, *Appl. Crystallogr.* **1987**, *20*, 356.

[28]   P.-H. Jouneau, P. Stadelmann, *Electron Microscopy Image Simulation (EMS On Line)*, Centre Interdépartemental de Microscopie Electronique, EPFL, Lausanne, **1998**, http://cecm.insa-lyon.fr/CIOLS/crystal1.pl.

[29]   R. K. Harris, E. D. Becker, S. M. Cabral de Menezes, R. Goodfellow, P. Granger, *Solid State NMR* **2002**, *22*, 458.

[30]   M. Hohwy, H. J. Jakobsen, M. Edén, M. H. Levitt, N. C. J. Nielsen, *Chem. Phys.* **1998**, *108*, 2686.

[31]   D. F. Shantz, J. Schmedt auf der Günne, H. Koller, R. F. J. Lobo, *Am. Chem. Soc.* **2000**, *122*, 6659.

[32]   J. C. C. Chan, H. Eckert, *J. Chem. Phys.* **2001**, *115*, 6095.

[33]   M. Roming, C. Feldmann, Y. S. Avadhut, J. Schmedt auf der Günne, *J. Chem. Mater.* **2008**, *20*, 5787.

[34]   F. Tessier, A. Navrotsky, A. Le Sauze, R. Marchand, *Chem. Mater.* **2000**, *12*, 148.

[35]   S. J. Sedlmaier, M. Eberspächer, W. Schnick, *Z. Anorg. Allg. Chem.* **2011**, *637*, 362.

[36]   a) K. Landskron, Doctoral Thesis, Univ. Munich (LMU) **2001**. (b) F. Karau, Doctoral Thesis, Univ. Munich (LMU), **2007**.

[37]   S. J. Sedlmaier, J. Schmedt auf der Günne, W. Schnick, *Dalton Trans.* **2009**, 4081.

[38]   E. J. Brunner, *Mol. Struct.* **1995**, *355*, 61.

[39]   M. D. Foster, M. M. J. Treacy, *A Database of Hypothetical Zeolite Structures*, http://www.hypotheticalzeolites.net, accessed June 2010.

[40]   L. B. McCusker, F. Liebau, G. Engelhardt, *Pure Appl. Chem.* **2001**, *73*, 381.

[41]   C. Baerlocher, L. B. McCusker, *Database of Zeolites Structures*, http://www.iza-structure.org/databases/, accessed November 2010.

[42]   M. O'Keeffe, M. A. Peskov, S. J. Ramsden, O. M. Yaghi, *Acc. Chem. Res.* **2008**, *41*, 1782.

[43]   W. E. Klee, *Z. Kristallogr.* **1987**, *179*, 67.

[44]   G. Thimm, S. Schumacher, W. Uhr, W. E. Klee, *TOPOLAN, Topological Analysis of Crystal Structures*, Univ. Karlsruhe, Germany, **1993**.

[45]   G. O. Brunner, W. M. Meier, *Nature* **1989,** *337*, 146.

[46]   N. Stock, Doctoral Thesis, Univ. Bayreuth, **1998**.

[47]   M. Nardelli, *Acta Crystallogr., Sect. C: Cryst. Struct. Commun.* **1983**, *39*, 1141.

[48]   D. Cremer, J. A. Pople, *J. Am. Chem. Soc.* **1975**, *97*, 1354.

[49]   M. Nardelli, *PARST97*, Univ. Parma, Italy, **1997**.

[50]   F. W. Karau, L. Seyfarth, O. Oeckler, J. Senker, K. Landskron, W. Schnick, *Chem. Eur. J.* **2007**, *13*, 6841.

[51]   C. Baerlocher, A. Hepp, W. M. Meier, *Distance Least Squares Refinement Program, DLS-76*, ETH, Zürich, **1977**.

[52]   J. M. Léger, J. Haines, C. Chateau, G. Bocquillon, M. W. Schmidt, S. Hull, F. Gorelli, A. Le Sauze, R. Marchand, *Phys. Chem. Miner.* **2001**, *28*, 388.

[53]   R. D. Shannon, *Acta Crystallogr., Sect. A: Found. Crystallogr.* **1976**, *32*, 751.

[54]   W. H. Baur, *Crystallogr. Rev.* **1987**, *1*, 59.

[55]   W. Zhu, F. Kapteijn, J. A. Moulijn, M. C. den Exter, J. C. Jansen, *Langmuir* **2000**, *16*, 3322.

[56]   D. H. Olson, U.S. Patent 6488741, **2002**.

[57]   D. H. Olson, M. A. Camblor, L. A. Villaescusa, G. H. Kuehl, *Microporous Mesoporous Mater.* **2004**, *67*, 27.

11. SrP₃N₅O: A Highly Condensed Layer Phosphate Structure Solved from a Nanocrystal by Automated Electron Diffraction Tomography

The difficulties that oppose identification of novel oxonitridophosphate compounds can sometimes be overcome by a combination of different analytical methods (see last chapter). Often, their discovery is fully prevented however. At this point, new methods are the only solution. From the year 2010 onward, the automated electron diffraction tomography (ADT), developed by *Kolb et al.* (Univ. Mainz) and promising structure determination on basis of nanocrystals, is applicable. With the two compounds presented in this and in the following chapter, this method could be established in this field.

ABSTRACT

The oxonitridophosphate SrP₃N₅O has been synthesized by heating a multicomponent reactant mixture that consisted of phosphoryl triamide $OP(NH_2)_3$, thiophosphoryl triamide $SP(NH_2)_3$, SrS, and NH_4Cl enclosed in evacuated and sealed silica-glass ampoules up to 750 °C. The compound was obtained as nanocrystalline powder with needle-shaped crystallites. The crystal structure was solved *ab initio* on the basis of electron diffraction data by means of automated electron diffraction tomography (ADT) and verified by Rietveld refinement with X-ray powder diffraction data. SrP₃N₅O crystallizes in the orthorhombic space group *Pnma* (no. 62) with unit-cell data of $a = 18.331(2)$, $b = 8.086(1)$, $c = 13.851(1)$ Å and Z = 16. The compound is a highly condensed layer phosphate with a degree of condensation $\kappa = ½$. The corrugated layers $_\infty^2\{(P_3N_5O)^{2-}\}$ consist of linked, triangular columns built up from $P(O,N)_4$ tetrahedra with 3-rings and triply binding nitrogen atoms. The Sr^{2+} ions are located between the layers and exhibit six-, eight-, and ninefold coordination. FT-IR and solid-state NMR spectra of SrP₃N₅O are discussed as well.

11.1   INTRODUCTION

Due to their abundance and diversity, silicates are not only one of the most important classes of minerals but also omnipresent in everyday life.[1] Besides building (e.g., cement) and ceramic materials, they are used as functional materials (zeolites as catalysts, substance separators, air and water conditioners, and so on)[2] and play an important role in future technologies (e.g., phosphors for phosphor-converted light-emitting diodes (pcLEDs)).[3] Such structural diversity associated with different properties and functionalities does not exist with respect to any other tetrahedra-based class of compounds. However, as SiO$_2$ and PON are isoelectronic, the silicate-analogous compound class of oxonitridophosphates can be expected to exhibit a similar structural richness to the silicates. The incorporation of nitrogen in a tetrahedral network has significant impact on properties, for example, higher stability due to more covalent bonding, and higher network charges or adjustable acidity / basicity. Moreover, in nitridic compounds, bridging N atoms are more common in threefold crosslinking situations or can even be fourfold-connecting.[4] Together with a larger flexibility in terms of bond lengths and bond angles, a wider range of structural features becomes possible. This can lead to novel networks that exhibit a variety of characteristics beyond those known for silicates. However, only relatively few oxonitridophosphates have been characterized to date as there are fundamental difficulties in terms of their synthesis. Furthermore, typical reaction products show poor crystallinity so that structure determination requires a combination of analytical methods such as powder X-ray diffraction, electron microscopic methods, and solid-state NMR spectroscopy. Structure elucidation is frequently impeded because samples notoriously contain nanosized crystals of the desired compounds accompanied by further unknown side phases. Nevertheless, the investigation of the oxonitridophosphates is rewarding as the few existing examples are exceedingly auspicious: besides the series $M^I_3 M^{III} P_3 O_9 N$ (M^I = Na, K; M^{III} = Al, Ga, In, Ti, V, Cr, Mn, Fe),[5] $M^I_2 M^{II}_2 P_3 O_9 N$ (M^I = Na; M^{II} = Mg, Mn, Fe, Co),[6] and $Cs_3 M^{II}_2 P_6 O_{17} N$ (M^{II} = Mg, Fe, Co),[7] open-framework structures are most intriguing. Whereas sodalite-type oxonitridophosphates[8] are microporous, $Ba_{19} P_{36} O_{6+x} N_{66-x} Cl_{8+x}$[9] and $Li_x H_{12-x-y+z}[P_{12} O_y N_{24-y}] X_z$ (X = Cl, Br)[10] exhibit unprecedented frameworks, with the latter representing the first nitridic zeolite-type *NPO*. In addition, the first nitridic clathrate $P_4 N_4 (NH)_4 \cdot (NH_3)$[11] with a unique cage structure that encapsulates ammonia molecules and the first closed layer phosphate $Sr_3 P_6 O_6 N_8$[12] suggest an immense potential for the structural chemistry of P/O/N compounds.

To meet the challenge of crystal structural analysis in which conventional methods such as single-crystal or powder X-ray diffraction fail, the new method of automated electron diffraction tomography (ADT)[13–15] has been developed over the last few years. It has been shown that ADT is an effective way for *ab initio* structure solution on the basis of electron diffraction data.[16–19] A tilt series is acquired from an arbitrarily oriented nanosized crystal to yield a complete 3D single-crystal diffraction dataset. Three-dimensional reconstruction of the reciprocal space delivers intensity data suitable for *ab initio* structure solution by using a kinematical approximation implemented in the program packages employed for single-crystal X-ray data. In this contribution, we report on the synthesis and structure elucidation of the novel oxonitridophosphate SrP_3N_5O, which exhibits a highly condensed layered structure made up of vertex-sharing $P(O,N)_4$ tetrahedra.

11.2   RESULTS AND DISCUSSION

11.2.1 Synthesis

Oxonitridophosphates can be synthesized from multicomponent reactant systems that consist of metal salts (e.g., halides, sulfides) and P/(O)/N-containing molecules, usually phosphoryl triamide $OP(NH_2)_3$ and thiophosphoryl triamide $SP(NH_2)_3$.[20,21] At approximately 750 °C, the latter act as P/N and P/O/N sources, respectively (Equations (1) and (2)), the joint thermal treatment enables the condensation of nitrogen-rich phosphates, and a controlled addition of oxygen is possible. Ammonium halides are often added as mineralizers to promote crystallization with a respectively adjusted ammonia partial pressure.

$$OP(NH_2)_3 \ \rightarrow \ PON + 2NH_3 \tag{1}$$

$$SP(NH_2)_3 \ \rightarrow \ HPN_2 + NH_3 + H_2S \ \rightarrow \ 1/3 \ P_3N_5 + 4/3 \ NH_3 + H_2S \tag{2}$$
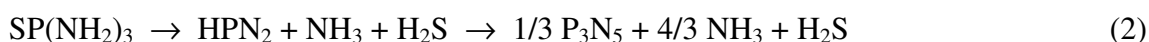
In such a multicomponent system, certain important parameters cannot be controlled independently (e.g., NH_3 partial pressure and amount of halide). Thus, a well-directed synthesis of specific phases without side phases is difficult and further complicated by the fact that the crystallization temperatures are in a range in which highly condensed phosphorus (oxo)nitrides PON and P_3N_5 already start to decompose.[22]

However, the synthesis conditions of SrP_3N_5O could be optimized to yield single-phase

products according to powder X-ray diffraction. Other starting materials such as Sr(N$_3$)$_2$[23] or [PN(NH$_2$)]$_3$[24] can also be employed, however, the best results so far were obtained with SrS, OP(NH$_2$)$_3$, SP(NH$_2$)$_3$, and NH$_4$Cl according to the procedure given in the Experimental Section. Higher temperatures and / or longer reaction times hardly increase crystallinity but favor the formation of decomposition products.[22] SrP$_3$N$_5$O is obtained as nanocrystalline powder with needle-shaped crystallites (Figure 1).
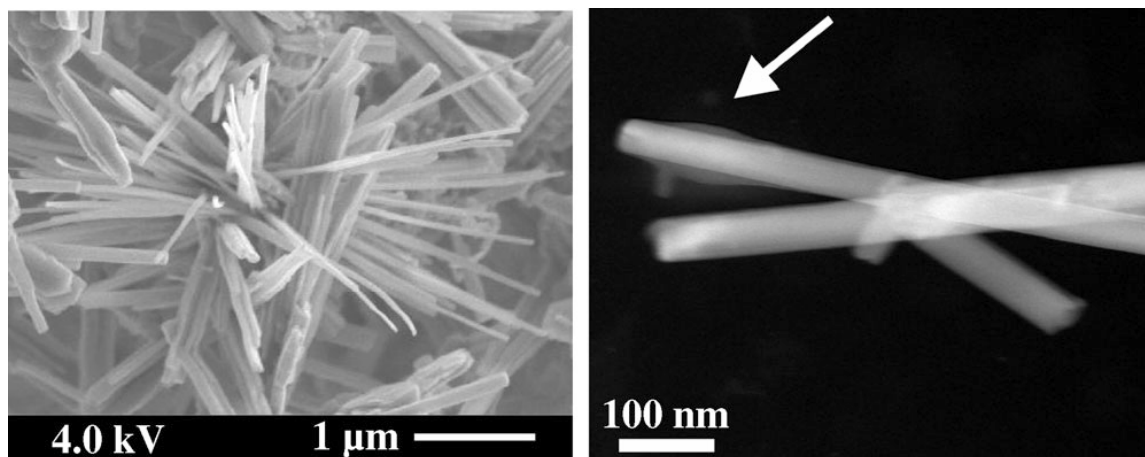
Figure 1. a) Secondary scattered electron image (left) and b) STEM image (right) of needle-shaped nanocrystals of SrP$_3$N$_5$O (the arrow points to the spot where the diffraction data were recorded).

11.2.2 Crystal Structure Analysis

Exploratory scanning transmission electron microscopy (STEM) and transmission electron microscopy (TEM) images (Figure 1) show that, besides the lath-shaped crystallites of SrP$_3$N$_5$O with a diameter of 80×20 nm^2 and a length up to 1000 nm, many shorter fragments are present. The small particles lead to reflection broadening in X-ray powder diffraction patterns, which is also very pronounced in high-resolution patterns measured with synchrotron radiation (ESRF (Grenoble), ID31, $\lambda = 0.4$ Å). Therefore, *ab initio* indexing and structure solution on the basis of powder diffraction data proved impossible.

As an alternative, single-crystal structure analysis was performed using ADT. Two tilt series with approximately orthogonal tilt axes were recorded from the tip of a nanosized crystal needle (Figure 1b) and covered tilt ranges of 100 and 95°, respectively. The effective tilt range was limited by surrounding crystals. Each measurement was carried out using precession electron diffraction (PED) for a further reduction of dynamical scattering effects and a more appropriate reflection integration.[13,14] Detailed information about the data collection is given in Table 1. According to reflection conditions and intensity

distribution, the space groups *Pnma* (no. 62) and *Pn2$_1$a* (no. 33) were derived. Figure 2 shows projections of the reconstructed reciprocal space volume along (010) and (01$\bar{1}$) in which the glide plane extinctions are visible. Merged integrated intensities from the two ADT data sets were used for *ab initio* structure solution by direct methods[25] with the kinematical assumption that intensities are proportional to F^2_{hkl}. The obtained structure clearly showed an inversion center, therefore the centrosymmetric space group *Pnma* (no. 62) was selected for the final model. Twenty-five independent atomic positions were obtained and correctly identified (four Sr, six P, and fifteen O/N). Thus the complete structure including all light atoms was obtained. Fourier maps do not show any significant residual electron density.
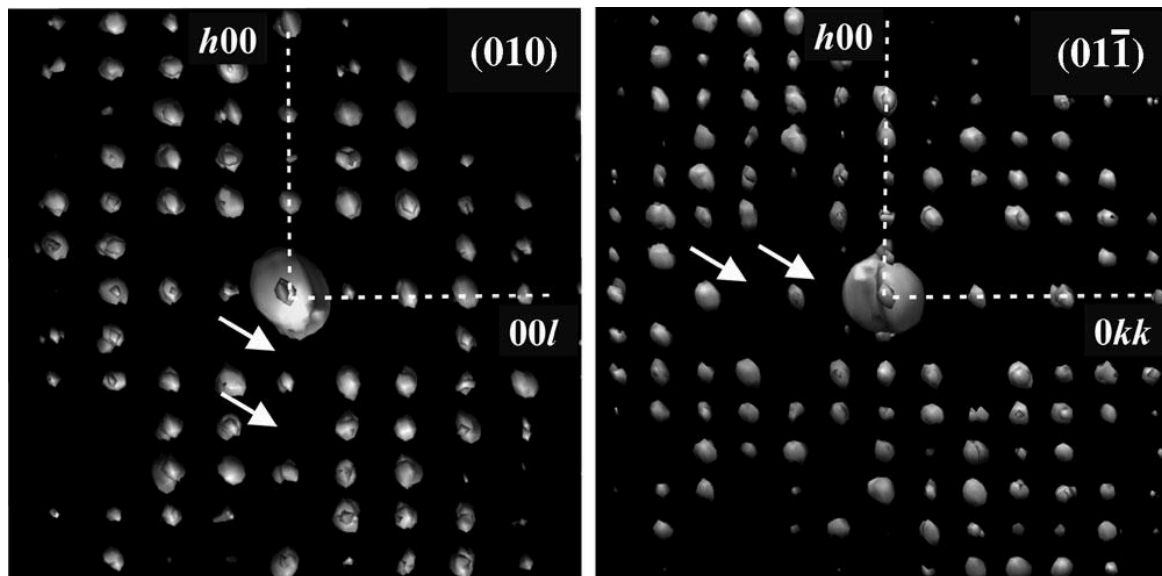
Figure 2. Three-dimensional reconstructed reciprocal space from ADT data: a) view along (010); b) view along (01$\bar{1}$); the reader should notice that these are projections of 3D diffraction volumes and not 2D diffraction patterns oriented along specific zone axes; the extinctions relative to the *a*-glide plane orthogonal to *c** and the *n*-glide plane orthogonal to *a** are indicated with white arrows.

Table 1. Crystallographic data for SrP$_3$N$_5$O (esd's in parentheses) as well as details of ADT data collection and realive structure solution refinement.

Crystal Structure Data	
formula	SrP$_3$N$_5$O
formula mass / g mol^{-1}	266.576
crystal system	orthorhombic
space group	*Pnma* (no. 62)
cell parameter / pm (from powder diffraction)	$a = 1833.1(2)$ $b = 808.6(1)$ $c = 1385.1(1)$
cell volume / 10^6 pm^3	$V = 2052.9(3)$
formula units / cell	Z = 16
X-ray density / g cm^{-3}	$\rho = 3.450$
crystal shape, crystal color	needle, colorless
crystal size	$1.0 \times 0.05 \times 0.02$

Data Collection	
diffractometer	Tecnai F30 S-TWIN TEM
radiation / Å	$\lambda = 0.01970$
temperature / K	T = 295(2)
tilt range /°	100/95
h, k, l indices	$-21 \leq h \leq 21$ $-9 \leq k \leq 9$ $-14 \leq l \leq 15$
measured reflections	8610
completeness / %	86
R_{int}	0.159

Structure Refinement	
solution method	direct methods[25]
refinement method	least-squares refinement on F^2[26]
independent reflections	1790
observed reflections (> 4σ)	1360
refined parameters	91
constraints / restraints	2 / 60
R indices [$F^2_o \geq 2\sigma(F_o)^2$]	$R1 = 0.299, wR2 = 0.662$
R indices (all data)	$R1 = 0.313, wR2 = 0.671$
GoF	2.528
weighting scheme	$w^{-1} = \sigma^2 F^2_o + (0.2000P)^2$ with P = $(F^2_o + 2F^2_c)/3$
max / min residual electron density / eÅ^{-3}	0.875 / -0.365

Table 2. Atom coordinates, Wyckoff symbols, and isotropic displacement parameters U_{iso} / Å^2 for the atoms in SrP$_3$N$_5$O in space group *Pnma* (esd's in parentheses); U_{eq} for Sr atoms is defined as one third of the trace of the orthogonalized U_{ij} tensor; c.n. = coordination number; occupancy of N(2)–O(14) is 0.9 and 0.1, respectively.

atom[c.n.]	Wyckoff symbol	x	y	z	U_{iso}/U_{eq}
Sr(1)[6]	4c	0.3729(5)	¼	0.7060(9)	0.065(3)
Sr(2)[8]	4c	0.4582(6)	¾	0.5686(10)	0.069(3)
Sr(3)[6]	4c	0.1801(6)	¼	0.4187(13)	0.082(4)
Sr(4)[9]	4c	0.4352(10)	¼	0.9874(11)	0.093(5)
P(1)[4]	8d	0.6162(6)	0.4314(11)	0.8601(9)	0.053(3)
P(2)[4]	8d	0.6524(6)	0.5672(12)	0.5262(10)	0.056(3)
P(3)[4]	8d	0.5549(6)	0.4329(11)	0.6729(9)	0.050(3)
P(4)[4]	8d	0.7062(6)	0.4296(12)	0.6938(10)	0.058(4)
P(5)[4]	8d	0.4709(6)	0.5617(11)	0.8288(10)	0.052(3)
P(6)[4]	8d	0.2575(9)	0.9298(16)	0.6378(13)	0.102(7)
N(1)[3]	8d	0.6253(6)	0.444(2)	0.7440(8)	0.065(6)
N/O(2)[2]	8d	0.5771(8)	0.501(3)	0.5687(10)	
N/O(3)[2]	4c	0.4529(16)	¾	0.854(2)	
N/O(4)[2]	4c	0.6425(16)	¾	0.4876(19)	
N/O(5)[2]	8d	0.7125(9)	0.5663(19)	0.6124(11)	
N/O(6)[2]	4c	0.7098(15)	¼	0.6434(17)	
N/O(7)[2]	8d	0.4908(9)	0.546(2)	0.7165(10)	
N/O(8)[2]	8d	0.7663(8)	0.440(2)	0.7752(12)	0.117(5)[a]
N/O(9)[2]	8d	0.5385(7)	0.501(3)	0.8913(12)	
N/O(10)[2]	8d	0.6802(10)	0.453(2)	0.4403(13)	
N/O(11)[2]	8d	0.5278(14)	¼	0.665(2)	
N/O(12)[2]	4c	0.6279(17)	¼	0.8963(18)	
N/O(13)[2]	4c	0.2637(15)	¾	0.685(2)	
N/O(14)[2]	4c	0.6781(8)	0.549(2)	0.9083(14)	
O(15)[1]	8d	0.4011(9)	0.452(2)	0.8534(18)	0.075(7)

[a] The value applies to all atoms N/O(2) to N/O(14).

Table 3. Anisotropic displacement parameters / Å^2 for the atoms in SrP$_3$N$_5$O in space group *Pnma* (esd's in parentheses); c.n. = coordination number.

atom[c.n.]	U11	U22	U33	U12	U13	U23
Sr(1)[6]	0.039(5)	0.124(8)	0.033(7)	0	0.000(5)	0
Sr(2)[8]	0.078(7)	0.063(5)	0.064(9)	0	0.002(6)	0
Sr(3)[6]	0.058(6)	0.086(7)	0.103(13)	0	–0.018(7)	0
Sr(4)[9]	0.159(14)	0.053(5)	0.066(10)	0	0.001(9)	0

Although the correct connectivity was obtained in one step, the structure model was rather rough. To obtain more precise atomic parameters for a detailed structure discussion, Rietveld refinement on the basis of powder X-ray diffraction data was attempted (results are given in the Experimental Section, Tables 6 and 7). Although a good fit with low *R* values was achieved and this can be taken as an independent confirmation of the

correctness of the structure model obtained by electron diffraction data, the precision of the structural parameters is just on the same order of magnitude. Indeed the severe reflection overlap due to particle-size broadening and the rather large unit cell means that groups of reflections contribute to each peak and only few isolated peaks are uniquely indexed (see Figure 3). The data to parameter ratio is therefore poor. The final structure model of SrP$_3$N$_5$O was taken from the refinement based on single-crystal ADT diffraction, as this benefits from more independent data than X-ray powder diffraction. The final residual is high when compared with standard refinement based on X-ray data, but is in the normal range for structure solution based on electron diffraction. Indeed, the performed refinement does not include corrections for residual dynamical scattering and geometrical distortions. The achieved model appears reliable since, for example, intentionally deleted atoms are reliably found again as the highest difference Fourier peaks. Lattice parameters were taken from the Rietveld refinement on account of its higher accuracy. Distances of P–(O,N) and (O,N)–(O,N) were restrained to be equal within a certain standard deviation, and overall displacement parameters were used for chemically equivalent light atoms. The Sr atoms could be refined anisotropically. Crystallographic data and further details about the structure refinement are summarized in Table 1; Table 2 shows the positional and displacement parameters for all atoms. The anisotropic displacement parameters are given in Table 3.
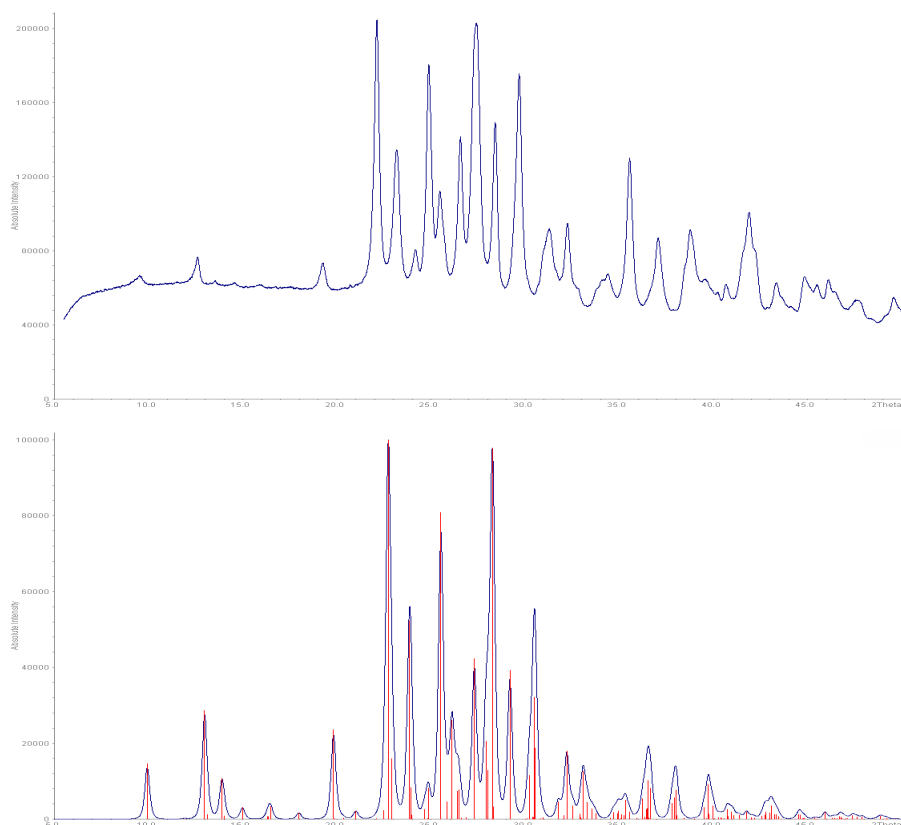
Figure 3. top: experimental powder diffraction pattern of SrP_3N_5O, bottom: calculated pattern based on the structure model solved from electron data (individual reflections indicated by red lines); Cu-$K_{\alpha 1}$, 154.0596 pm.

11.2.3 Structure Description and Discussion

The dimensionality of a tetrahedral substructure can be estimated from the sum formula and the respective degree of condensation κ, which is defined as the atomic ratio of tetrahedral centers and bridging atoms. In oxosilicate chemistry, orthosilicates are characterized by $\kappa = ¼$ (isolated $[SiO_4]^{4-}$, Q^0-type tetrahedra), silicate chains by $\kappa = \frac{1}{3}$ (e.g., pyroxene $CaMg[SiO_3]_2$, Q^2-type tetrahedra), layers by $\kappa = \frac{2}{5}$ (e.g., talc $Mg_3(OH)_2[Si_2O_5]_2$, Q^3-type), and finally frameworks with a maximum $\kappa = ½$ (e.g., zeolites, Q^4-type tetrahedra) in which every O bridges two tetrahedra.[1] Applying this concept to the title compound with $\kappa = ½$, one would expect a three-dimensional network of all-side vertex-sharing $P(O,N)_4$ tetrahedra. SrP_3N_5O, however, exhibits a layered structure isotypic with the rare-earth *meta*-oxoborates $RE(BO_2)_3$ (RE = Tb–Lu).[27] The structure consists of triangular columns that run along [010] that are interconnected to form corrugated layers that extend parallel to (100), with the Sr^{2+} ions being located between them (Figure 4). The triangular columns in the $^2_\infty\{(P_3N_5O)^{2-}\}$ anion are composed of Q^4- and Q^3-type $P(O,N)_4$ tetrahedra (with a ratio $Q^4/Q^3 = \frac{2}{1}$) with terminally bound oxygen and three-binding

nitrogen atoms. Their topology can be derived from that of the chlorophosphazene molecule P$_6$N$_7$Cl$_9$[28,29] (Figure 5), which is built of three condensed 3-rings. The columns are generated by substitution of all chlorine atoms by oxygen and nitrogen, respectively, and infinite interconnection of the resulting "P$_6$ON(O,N)$_{14}$" entities along [010]. These domed monomeric units are facing concave/concave and convex / convex and connect through six bridging O/N atoms; on one side there are three of the inner three tetrahedra, and on the other side three of the outer three tetrahedra, thus resulting in 4- and 6-rings, respectively (Figure 6). The O/N atoms that are not involved within a column are either bound terminally (O(15)) or interlink (O/N(11)) the triangular columns to form corrugated layers with a degree of condensation κ = ½.
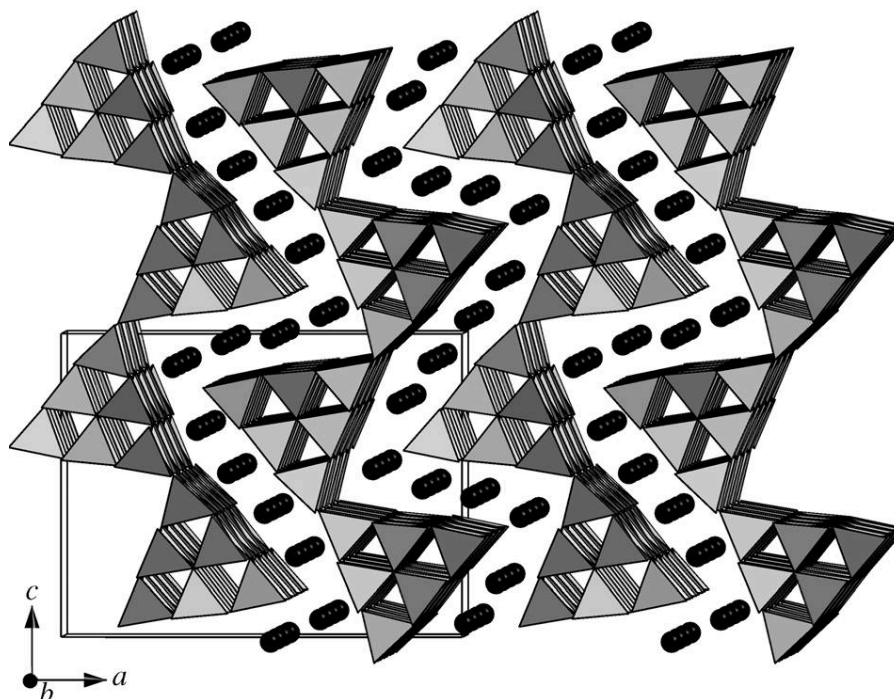
Figure 4. Crystal structure of SrP$_3$N$_5$O, view along [010]; corrugated layer ions $^{2}_{\infty}\{(P_3N_5O)^{2-}\}$ formed by interconnected triangular columns of vertex-sharing P(O,N)$_4$ tetrahedra separated by Sr^{2+} ions.
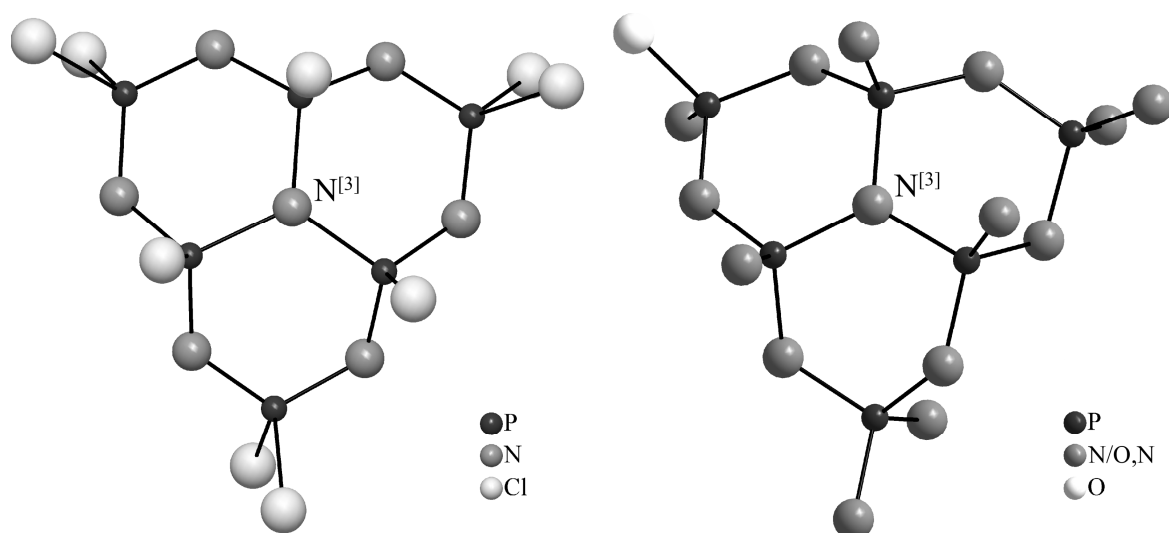
Figure 5. One single molecule of the chlorophosphazene P$_6$N$_7$Cl$_9$ (top)[28] and the respective formal building block in SrP$_3$N$_5$O (bottom).
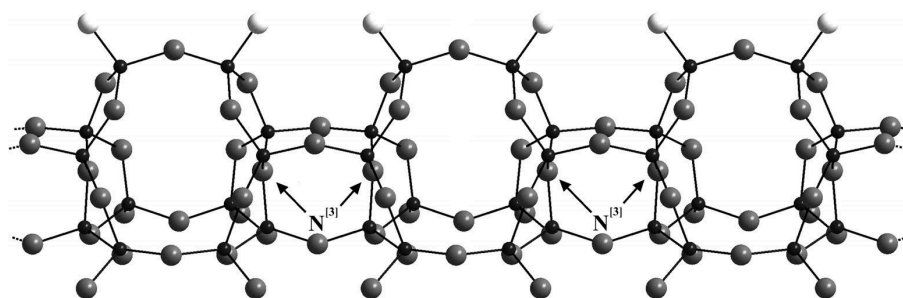
Figure 6. Connectivity of a single triangular column along [010] in SrP$_3$N$_5$O (P black, O/N gray, O white).

The bond lengths P–(O,N) and angles (O,N)–P–(O,N) within a tetrahedron, respectively, were restrained to be equal within a certain standard deviation. The resulting range of bond lengths (156.4–164.2 pm) corresponds to that usually observed in oxonitridophosphates. The resulting angles range between 106.4 and 114.9°, which is close to the values of the regular tetrahedron angle. The angles P–(O,N)–P between 118.5(12) and 145.0(5)° are also typical for P/O/N networks. Detailed information about bond lengths and angles are given in Table 4.

Table 4. Selected interatomic distances / pm and angles / ° in SrP$_3$N$_5$O (esd's in parentheses).

Sr(1)–(O,N)	249.9(17)–289.6(28)	6 times
Sr(2)–(O,N)	269.7(19)–302.4(20)	8 times
Sr(3)–(O,N)	250.4(19)–297.3(19)	6 times
Sr(4)–(O,N)	255.1(25), 300.7(22)	9 times
P–(O,N)	156.4(10)–164.2(12)	24 times
P–N(1)[3]–P	117.2(9), 120.6(10), 121.1(10)	
P–(O,N)–P	118.5(12)–145.0(5)	13 times
(O,N)–P–(O,N)	106.4(10)–114.9(12)	36 times

In phosphate chemistry, layer structures are quite unusual, although the layered *O'* form of $(P_2O_5)_x$ was discovered very early.[30] In pure oxophosphates, which are distinguished by discrete tetrahedra, chains and rings, no layer phosphates are known except few wide-meshed 2D structures in ultraphosphates.[31,32] This applies even more to nitridophosphates, in which a variety of structural motifs have been identified so far, for example, discrete PN_4 tetrahedra[33] and chains,[34] as well as three-dimensional networks in which the degree of condensation can reach values $\kappa > \frac{1}{2}$.[8,35–37] However, there are no layered structures except $Sr_3P_6O_6N_8$, a recently discovered single-layer phosphate with the highest degree of condensation of $\kappa = \frac{3}{7}$ observed for layer phosphates so far.[12] Triply binding nitrogen atoms $N^{[3]}$ are responsible for the high degree of condensation both in $Sr_3P_6O_6N_8$ and in the title compound. This feature is also resent in the structures of P_3N_5,[38] HP_4N_7,[39] P_4N_6O,[40] $Na_3P_6N_{11}$,[41] and $K_3P_6N_{11}$.[42]

According to the formula $^2_\infty[(P_6^{[4]}N_1^{[3]}N_9^{[2]}O_1^{[2]}O_1^{[1]})]^{4-}$ for the two-dimensional anion in SrP$_3$N$_5$O, three- and two-fold bridging as well as terminal atoms O/N are simultaneously involved. As the direct experimental differentiation between O and N is impossible by X-ray or electron diffraction on account of their similar scattering factors, a chemically reasonable assignment has been done by taking into account Pauling's rules and based on experiences with other oxonitridic compounds, for which solid-state NMR spectroscopic investigations and lattice-energy calculations have been helpful for proper assignment of O/N. $N^{[3]}$ were assumed to link three tetrahedra; the terminally bound position was assigned to oxygen $O^{[1]}$. For the two-fold bridging positions, an $N^{[2]}$ occupancy with a statistic admixture of 10 % $O^{[2]}$ was assumed. Other ordered or disordered models may be possible; the ratio N/O has to be 5 : 1, since the absence of hydrogen was proven by FT-IR spectroscopy (Figure 7) and elementary analysis. The suggested partially disordered model is in accordance with both the ^{31}P solid-state NMR spectroscopic investigation as well as the results of Madelung part of lattice energy (MAPLE) calculations.[43] In the ^{31}P solid-state NMR spectrum of SrP$_3$N$_5$O (Figure 8), a single signal with a chemical shift of δ_{iso} = -9.3 ppm is observed in a range typical for oxonitridophosphates, that is, δ_{iso} = -8.7 ppm (in oxonitridosodalites)[8] to δ_{iso} = +6.5 ppm (in *NPO*-type material).[10b] The large full width at half-maximum (FWHM) of δ_{iso} = 14.3 ppm of the peak indicates that six broadened ^{31}P resonances from slightly different surroundings (PN_4, PN_3O, or PN_2O_2) overlap. MAPLE calculations were carried out for 18 different O/N-ordered struc-ture models by using the formal ionic charges of the atoms (Table 5). No calculation yielded partial MAPLE values for O and N, respectively, that lie exclusively within the

typical ranges for O (2050–2800 kJ mol^{-1}) and N (5200–6300 kJ mol^{-1}).[44] However, the total MAPLE value averaged over all 18 models (327491 kJ mol^{-1}) is close to the sum of the MAPLE sum of the theoretical starting materials SrO and P_3N_5 (326232 kJ mol^{-1}; $\Delta = 0.4\ \%$).

Table 5. Total MAPLE for 18 O/N-ordered structure models; the rows indicate the ordered model by a fully occupancy of O at one respective two-fold bridging atomic position; with an occupancy of the remaining two-fold bridging positions and the three-fold bridging position by N and an occupancy of the terminal by O ordered models of SrP_3N_5O are given.

atomic position fully occupied with O	total MAPLE value / kJ mol^{-1}
O(14)	327936
O(10)	328204
O(9)	326726
O(8)	327753
O(7)	327248
O(5)	327873
O(2)	327250
O(3)/O(4)	327747
O(11)/O(12)	326770
O(3)/O(11)	327115
O(3)/O(12)	327047
O(4)/O(12)	327395
O(4)/O(11)	327230
O(3)/O(6)	327771
O(4)/O(6)	327906
O(6)/O(11)	327300
O(6)/O(12)	327371
O(6)/O(13)	328192
average Ø	327491, $\Delta = 0.4\ \%$
theoretical MAPLE value (SrO + P_3N_5)	326232
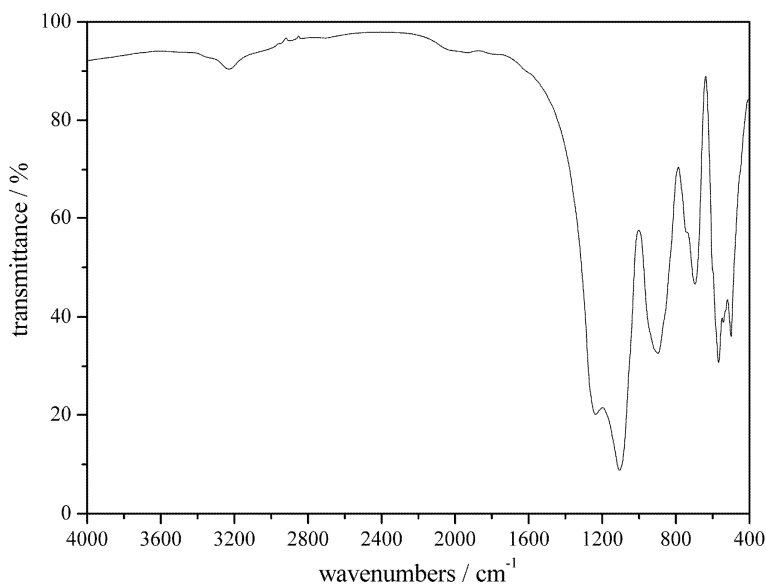
Figure 7. FT-IR spectrum of SrP$_3$N$_5$O (KBr pellet technique; 300 mg dried KBr and 2 mg sample); the FT-IR spectrum shows that SrP$_3$N$_5$O contains no stoichiometric amount of hydrogen. The weak signal around 3200 cm^{-1} comes from traces of water in the nanocrystalline powder sample or in the used KBr.
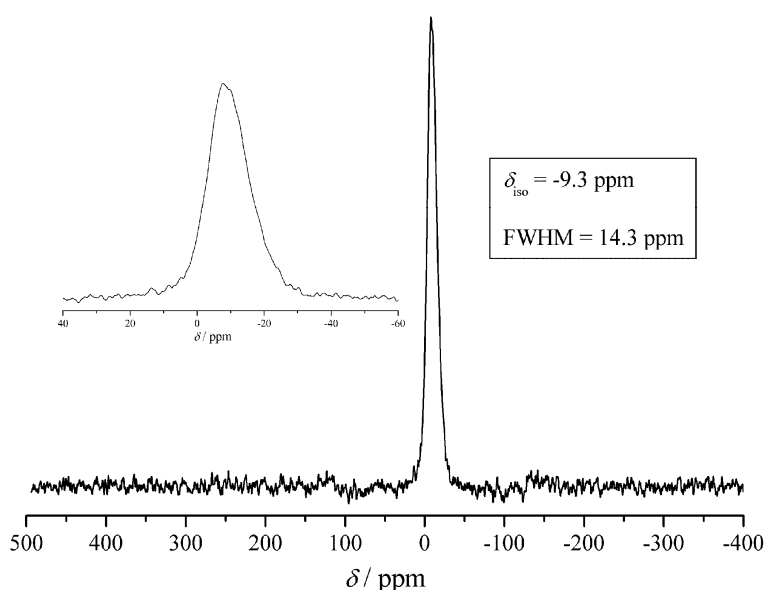
Figure 8. Solid-state ^{31}P MAS NMR spectrum of SrP$_3$N$_5$O.

The highly condensed, corrugated layers in SrP$_3$N$_5$O are held together by coordinating Sr^{2+} ions. The four crystallographically independent Sr^{2+} ions are surrounded six- to nine-fold by O and O/N atoms (Figure 9). More precisely, Sr(1) and Sr(3) are coordinated sixfold by four O/N atoms and two terminal oxygen atoms in a trigonal prismatic and pentagonal pyramidal way, respectively, in a distance range between 249.9(17) and 297.3(19) pm (Table 4). The latter is situated in the bends of the corrugated layers. Sr(2) and Sr(4), however, have a higher coordination number of eight and nine, respectively. Eight O/N atoms and seven O/N atoms plus two O atoms surround Sr(2) and Sr(4), respectively, in a cuboidal manner with distances between 266.6(24) and 307.8(24) pm,

whereas the coordination polyhedron of Sr(4) is capped with one further O/N. The Sr–O/N distances, summarized in Table 4, agree well with the sum of the ionic radii.[45,46]
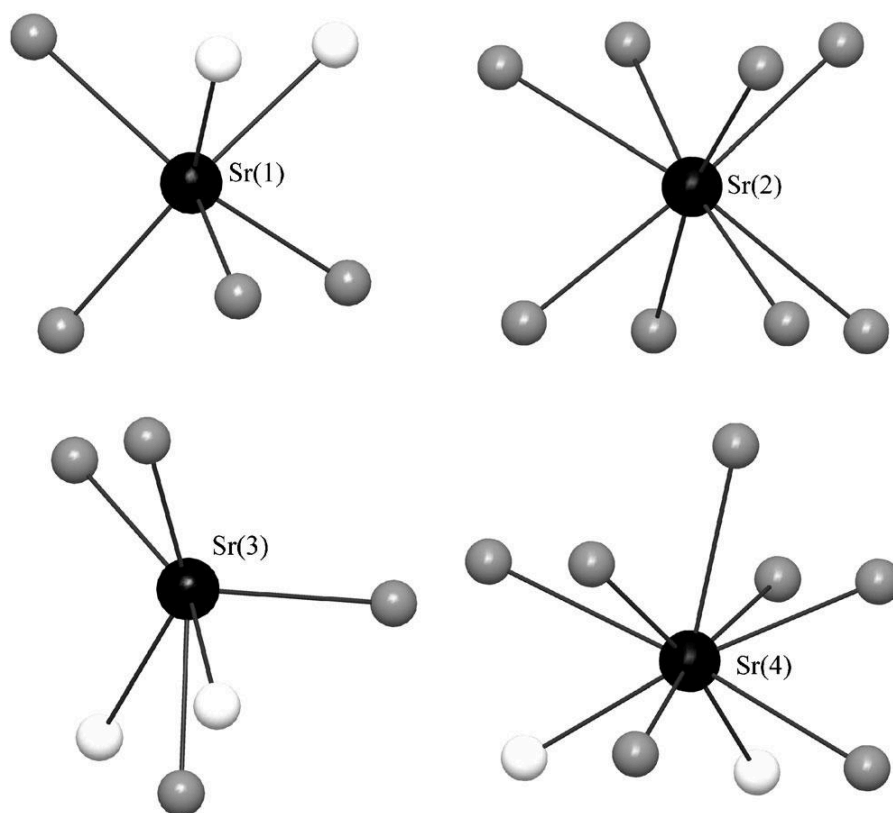
Figure 9. Coordination spheres of Sr^{2+} ions in SrP$_3$N$_5$O (Sr^{2+} black, O/N gray, O white).

11.3 CONCLUSION

In this contribution, we have presented the synthesis and the structure determination of the oxonitridophosphate SrP$_3$N$_5$O. The unexpected structure is exceptional for phosphates as well as for silicates and also for P/O/N compounds in general. Although the synthesis from a multicomponent reactant system could be optimized to yield single-phase samples, the small size of the crystallites did not allow for structural determination by traditional X-ray methods. Therefore, *ab initio* structure solution and refinement were performed using electron diffraction data and the newly developed ADT method. Due to the achieved results, at present ADT looks like the method of choice for starting a systematic investigation of oxonitridophosphates. In inhomogeneous samples with different foreign phases, novel compounds could be identified, structurally characterized and afterwards—with the knowledge of the sum formula—it may be possible to carry out a phase-pure synthesis.

SrP$_3$N$_5$O has a degree of condensation $\kappa = \frac{1}{2}$ and exhibits a highly condensed layer structure. It consists of vertex-sharing P(O,N)$_4$ tetrahedra that form interlinked triangular

columns. Given the motifs of condensed 3-rings and triply binding nitrogen atoms, the concept of (oxo)nitridophosphate chemistry introducing a nitridic component into tetradedra-based networks for generating a higher structural diversity is verified with SrP$_3$N$_5$O. Similar dense 2D structures also occur in single-layer oxonitridosilicates such as MIISi$_2$O$_2$N$_2$ (Ca, Sr, Ba).[47–49] It is possible that there is an isotypic CaP$_3$N$_5$O. This is indicated by similar needle-shaped nanocrystals observed in some SEM images. The latter and many further oxonitridophosphate phases in their typical nanocrystalline form can now be identified by the procedure shown in this paper. With the ADT method, the potential of a versatile structural P/O/N chemistry could be fully exploited.

11.4 EXPERIMENTAL SECTION

11.4.1 Synthesis

Phosphoryl triamide OP(NH$_2$)$_3$ and thiophosphoryl triamide SP(NH$_2$)$_3$ were synthesized according to the literature[20,21] similar to procedures described by *Correll*.[50] First, freshly distilled POCl$_3$ and PSCl$_3$ (Acros Organics, Geel, Belgium, 99 and 98 %, respectively; 10–20 mL), respectively, were added directly and slowly to liquid ammonia in a flame-dried three-necked 1 L flask. Subsequently, the elimination of NH$_4$Cl from the products was carried out performing a Soxhlet extraction with distilled Et$_2$NH in dry CH$_2$Cl$_2$ for 3 d. After drying in vacuo, OP(NH$_2$)$_3$ and SP(NH$_2$)$_3$ are available as starting materials in form of colorless, water-sensitive powders. Their purity was verified by powder X-ray diffraction.

SrP$_3$N$_5$O was synthesized employing a multicomponent reactant system. In a typical procedure, SrS (38.1 mg, 0.318 mmol; Sigma–Aldrich, 99.9 %; doped with 0.4 mg, 2.174 mmol EuS), OP(NH$_2$)$_3$ (20.5 mg, 0.216 mmol), SP(NH$_2$)$_3$ (47.9 mg, 0.431 mmol), and NH$_4$Cl (11.0 mg, 0.206 mmol; Fluka, puriss. p.a.) as mineralizer were thoroughly mixed and ground in an Ar-filled glovebox (MBraun, Garching, Germany; H$_2$O $\leq$ 0.2 ppm, O$_2$ $\leq$ 1.0 ppm) and transferred into a silica glass ampoule (wall thickness 2 mm, inner diameter 11 mm). The evacuated and sealed ampoule (length around 11 cm), was heated in a tube furnace to 200 and 750 °C with dwell times of 12 and 72 h (heating rate: 1 K min^{-1}, cooling rate: 0.1 K min^{-1}), respectively. The emerging condensation products NH$_3$ and H$_2$S are partially deposited as (NH$_4$)$_2$S together with NH$_4$Cl and small amounts of SrCl$_2$ at the places in the ampoule that cool first. After breaking the ampoules, the samples were washed with water and DMF to remove NH$_4$Cl, SrCl$_2$, and SrS. SrP$_3$N$_5$O was obtained as a

colorless, water- and air-resistant nanocrystalline powder. Elemental analysis calcd (%) for SrP$_3$N$_5$O (266.576 g mol^{-1}): Sr 32.9, P 34.9, N 26.3, O 6.0; found: Sr 33.7, P 30.5, N 22.4, O 8.9, Eu 1.6, S 0.24, H 0.16 (drying loss: 0.9 %).

11.4.2 SEM, TEM, ADT, and Structure Solution and Refinement

The SEM image (Figure 1a) was taken using a JSM-6500F electron microscope (JEOL Ltd., Tokyo, Japan) with a field-emission source at 4.0 kV. A powder sample was placed on a brass sample carrier fixed with self-adhesive carbon plates (Plano, Wetzlar, Germany) and sputtered with carbon (sputter device: BAL-TEC MED 020, BAL-TEC AG, Balzers, Netherlands).

For TEM and STEM investigations, the sample was suspended in ethanol and sprayed onto a carbon-coated copper grid using the sonifier described in ref. [13]. The TEM work was carried out using a Tecnai F30 STWIN transmission electron microscope equipped with a field-emission gun working at 300 kV. Electron diffraction patterns were acquired using a CCD camera (14-bit GATAN 794MSC).

ADT data acquisition was performed using a FISCHIONE tomography holder (tilt range ±70°), using the acquisition module described in ref. [52]. STEM images and diffraction patterns were collected using a mild illumination setting that resulted in an electron dose rate of 10–15 e Å^{-2} s^{-1}. STEM images were collected using a FISCHIONE high-angle annular dark-field detector (HAADF). Nano-electron diffraction was performed using a 10 mm C2 condenser aperture with a 50 nm beam on the sample. ADT data were collected in PED mode in steps of 1°. PED was performed using the NanoMEGAS SpinningStar unit.[52] The precession angle was kept at 0.6°, and the precession frequency was 100 Hz.

For data processing, including geometrical parameter optimization, 3D diffraction volume reconstruction, 3D visualization, automated cell-parameter determination and intensity integration, self-developed routines[53] and the software ADT-3D[54] were used. ESD for intensity was set to √(intensity). The *ab initio* structure solution was performed by direct methods implemented in SIR2008, included in the package Il Milione.[25] The structure refinement was performed with SHELXL97[26] using geometrical restraints on P(N,O)$_4$ tetrahedra.

11.4.3 Powder X-ray Diffraction

Powder X-ray diffraction patterns were recorded at 298 K using a Huber G670 Guinier imaging plate diffractometer with Ge(111) monochromated Cu-$K_{\alpha 1}$ radiation ($\lambda = 154.06$ pm). Rietveld refinement (Figure 10) was performed using the TOPAS package[55] with the structural parameters obtained by the ADT method as starting model. The reflection profiles were determined using the fundamental parameters approach (direct convolution of source emission profiles, axial instrument contributions and crystallite size and microstrain effects).[56] Preferred orientation of the crystallites was described with eighth-order spherical harmonics. An empirical 2θ-dependent absorption correction for the different absorption lengths of the Guinier geometry was applied. To describe peak broadening and shape anisotropy effects, the approach of *Le Bail* and *Jouanneaux*[57] was implemented. Overall displacement parameters have been used for P and N/O, respectively. Ten percent of all two-fold bridging N positions were occupied with O; the electroneutrality of the formula was retained. For an optimized tetrahedral geometry, distance restraints (1.65 Å for P–(N/O), 2.69 Å for (N/O)–(N/O)) have been included. Crystallographic data and further details of the data collection are summarized in Table 6. Table 7 shows the positional and displacement parameters for all atoms.[†]

Table 6. Crystallographic data of SrP$_3$N$_5$O (esd's in parentheses) and details of the X-ray powder diffraction data collection and respective Rietveld refinement.

Crystal Structure Data	
formula	SrP$_3$N$_5$O
formula mass / gmol^{-1}	266.576
crystal system	orthorhombic
space group	*Pnma* (no. 62)
cell parameters / pm	a = 1833.09(15)
	b = 808.59(5)
	c = 1385.05(10)
cell volume / Å^3	V = 2052.9(25)
formula units / cell	Z = 16
X-ray density / g·cm^{-3}	ρ = 3.4410(5)

Data collection	
diffractometer / radiation	Huber G670, λ = 1.540596 Å
temperature / K	T = 297(2)

---

† Further details of the crystal structure investigation may be obtained from Fachinformationszentrum Karlsruhe, 76344 Eggenstein-Leopoldshafen, Germany (fax: (+49)7247-808-666; e-mail: crysdata@fiz-karlsruhe.de, http://www.fiz-karlsruhe.de/request_for_deposited_data.html) on quoting the depository number CSD-423054.

2θ range /°	5.5–100.5
data points	18901
number of observed reflections	1154

Structure Refinement	
method of refinement	fundamental parameters model[56]
program used	TOPAS-Academic 4.1[55]
total number of parameters	175
background function / parameters	shifted Chebyshev / 44
number of atomic parameters	71
number of profile and other parameters	60
constaints	2
restraints	61
R indices	$R_p = 0.01388$ $wR_p = 0.01834$ $R_{bragg} = 0.0050$

Table 7. Atomic coordinates, Wyckoff symbols, occupancy and isotropic displacement parameters B_{eq} / Å^2 for the atoms in SrP_3N_5O (esd's in parentheses).

atom[c.n.]	Wyckoff symbol	x	y	z	B_{eq}
Sr(1)[6]	4c	0.3723(2)	¼	0.7074(2)	2.20(9)
Sr(2)[8]	4c	0.4636(2)	¾	0.5712(2)	1.02(9)
Sr(3)[6]	4c	0.1801(2)	¼	0.4158(3)	4.87(10)
Sr(4)[9]	4c	0.4337(2)	¼	0.9839(2)	7.34(13)
P(1)[4]	8d	0.6145(2)	0.4373(3)	0.8626(2)	
P(2)[4]	8d	0.6530(2)	0.5571(3)	0.5288(2)	
P(3)[4]	8d	0.5559(2)	0.4480(3)	0.6745(2)	2.67(7)[a]
P(4)[4]	8d	0.7084(2)	0.4252(3)	0.6889(3)	
P(5)[4]	8d	0.4671(2)	0.5627(3)	0.8262(2)	
P(6)[4]	8d	0.2567(2)	0.9234(4)	0.6236(2)	
N(1)[3]	8d	0.6287(1)	0.4454(4)	0.7502(2)	
N/O(2)[2]	8d	0.5758(1)	0.5332(4)	0.5740(1)	
N/O(3)[2]	4c	0.4317(3)	¾	0.8502(5)	
N/O(4)[2]	4c	0.6557(3)	¾	0.4824(3)	
N/O(5)[2]	8d	0.7143(2)	0.5605(3)	0.6111(1)	
N/O(6)[2]	4c	0.7234(4)	¼	0.6526(3)	
N/O(7)[2]	8d	0.4879(1)	0.5389(4)	0.7168(2)	
N/O(8)[2]	8d	0.7701(1)	0.4679(3)	0.7770(2)	0.20(10)[b]
N/O(9)[2]	8d	0.5437(1)	0.5512(3)	0.8898(2)	
N/O(10)[2]	8d	0.6845(1)	0.4787(3)	0.9281(2)	
N/O(11)[2]	8d	0.5328(3)	¼	0.6592(4)	
N/O(12)[2]	4c	0.5328(3)	¼	0.9006(4)	
N/O(13)[2]	4c	0.2316(3)	¾	0.6414(5)	
N/O(14)[2]	4c	0.6733(1)	0.4279(3)	0.4450(2)	
O(15)[1]	8d	0.4070(2)	0.4346(3)	0.8564(3)	

[a] The value applies to all atoms P(1) to P(6); [b] The value applies to all atoms N(1) to O(15).
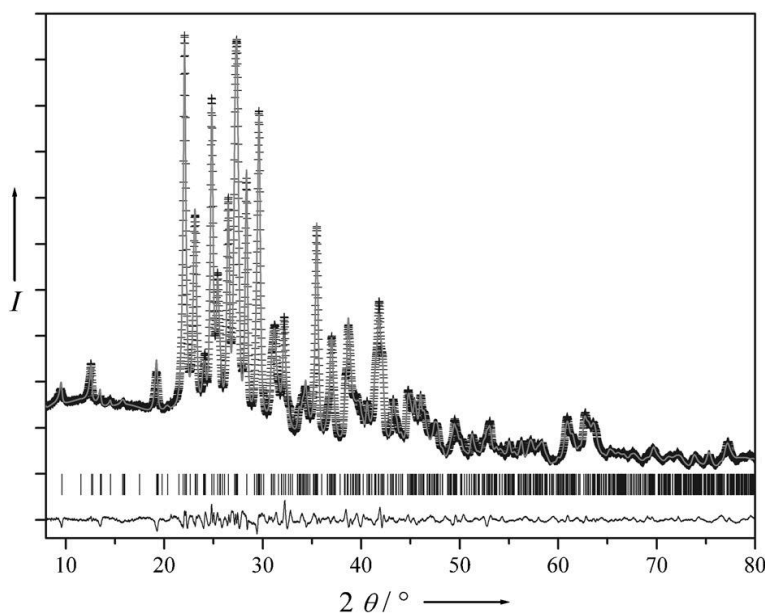
Figure 10. Observed (crosses) and calculated (gray line) powder diffraction pattern of SrP$_3$N$_5$O (Cu-$K_{\alpha 1}$, $\lambda = 154.0596$ pm) as well as difference profile of the Rietveld refinement; peak positions are marked by vertical lines.

11.4.4 ^{31}P Solid-state MAS NMR Spectroscopy

A ^{31}P NMR spectrum of SrP$_3$N$_5$O was recorded at ambient temperature using a Bruker Avance III spectrometer equipped with a commercial 2.5 mm MAS NMR spectroscopic double-resonance probe at a magnetic field of 11.7 T. The rotation frequency was 25 kHz. The chemical-shift values refer to a deshielding scale and 85 % H$_3$PO$_4$ was used as an external reference.

11.4.5 FT-IR Spectroscopy

An FT-IR spectrum of SrP$_3$N$_5$O was recorded in transmission geometry at room temperature in the range 4000–400 cm^{-1} using a Bruker IFS 66v/S spectrometer with the KBr pellet technique (2 mg of sample, 300 mg of dried KBr).

11.5 REFERENCES

[1]   F. Liebau, *Structural Chemistry of Silicates: Structure, Bonding, and Classification*, Springer, Berlin, **1985**.

[2]   A. K. Cheetham, G. Férey, T. Loiseau, *Angew. Chem.* **1999**, *111*, 3466; *Angew. Chem., Int. Ed.* **1999**, *38*, 3268.

[3]   a) H. A. Höppe, *Angew. Chem.* **2009**, *121*, 3626; *Angew. Chem., Int. Ed.* **2009**, *48*, 3572; b) W. Schnick, *Phys. Status Solidi RRL* **2009**, *3*, A113.

[4]   H. Huppertz, W. Schnick, *Angew. Chem.* **1996**, *108*, 2115; *Angew. Chem., Int. Ed. Engl.* **1996**, *35*, 1983.

[5]   W. Feldmann, *Z. Chem.* **1987**, *27*, 100.

[6]   R. Conanec, W. Feldmann, R. Marchand, Y. Laurent, *J. Solid State Chem.* **1996**, *121*, 418.

[7]   W. Feldmann, P. L'Haridon, R. Marchand, *J. Solid State Chem.* **2000**, *153*, 185.

[8]   N. Stock, E. Irran, W. Schnick, *Chem. Eur. J.* **1998**, *4*, 1822.

[9]   S. J. Sedlmaier, M. Döblinger, O. Oeckler, J. Weber, J. Schmedt auf der Günne, W. Schnick, *J. Am. Chem. Soc.* **2011**, *133*, 12069.

[10]   a) S. Correll, O. Oeckler, N. Stock, W. Schnick, *Angew. Chem.* **2003**, *115*, 3674; *Angew. Chem., Int. Ed.* **2003**, *42*, 3549; b) S. Correll, N. Stock, O. Oeckler, J. Senker, T. Nilges, W. Schnick, *Z. Anorg. Allg. Chem.* **2004**, *630*, 2205.

[11]   F. Karau, W. Schnick, *Angew. Chem.* **2006**, *118*, 4617; *Angew. Chem., Int. Ed.* **2006**, *45*, 4505.

[12]   S. J. Sedlmaier, J. Schmedt auf der Günne, W. Schnick, *Dalton Trans.* **2009**, 4081.

[13]   E. Mugnaioli, T. Gorelik, U. Kolb, *Ultramicroscopy* **2009**, *109*, 758.

[14]   U. Kolb, T. Gorelik, E. Mugnaioli, *Mater. Res. Soc. Symp. Proc.* **2009**, *1184*, GG01.

[15]   U. Kolb, E. Mugnaioli, T. E. Gorelik, *Cryst. Res. Technol.* **2011**, *46*, 542.

[16]   C. S. Birkel, E. Mugnaioli, T. Gorelik, U. Kolb, M. Panthöfer, W. Tremel, *J. Am. Chem. Soc.* **2010**, *132*, 9881.

[17]   I. Rozhdestvenskaya, E. Mugnaioli, M. Czank, W. Depmeier, U. Kolb, A. Reinholdt, T. Weirich, *Mineral. Mag.* **2010**, *74*, 159.

[18]   D. Denysenko, M. Grzywa, M. Tonigold, B. Streppel, I. Krkljus, M. Hirscher, E. Mugnaioli, U. Kolb, J. Hanss, D. Volkmer, *Chem. Eur. J.* **2011**, *17*, 1837.

[19]   I. Andrusenko, E. Mugnaioli, T. E. Gorelik, D. Koll, M. Panthöfer, W. Tremel, U. Kolb, *Acta Crystallogr., Sect. B: Struct. Sci.* **2011**, *67*, 218.

[20]   R. Klement, O. Koch, *Chem. Ber.* **1954**, *87*, 333.

[21]   W. Schnick, *Z. Naturforsch. B: J. Chem. Sci.* **1989**, *44*, 942.

[22]   F. Tessier, A. Navrotsky, A. Le Sauze, R. Marchand, *Chem. Mater.* **2000**, *12*, 148.

[23]   a) V. R. P. Verneker, M. Blais, *Mater. Res. Bull.* **1968**, *3*, 127; b) G. Brauer, *Handbuch der Präparativen Anorganischen Chemie*, Vol. 2, Ferdinand Enke, Stuttgart, **1978**, p. 930.

[24]   a) D. B. Sowerby, L. F. Audrieth, *Chem. Ber.* **1961**, *94*, 2670; b) F. Golinski, H. Jacobs, *Z. Anorg. Allg. Chem.* **1994**, *620*, 965.

[25]   M. C. Burla, R. Caliandro, M. Camalli, B. Carozzini, G. L. Cascarano, L. De Caro, D. Siliqi, G. Polidori, R. Spagna, C. Giacovazzo, *J. Appl. Crystallogr.* **2007**, *40*, 609.

[26]   a) G. M. Sheldrick, SHELXL97, Univ. Göttingen, **1997**; b) G. M. Sheldrick, *Acta Crystallogr., Sect. A: Found. Crystallogr.* **2008**, *64*, 112.

[27]   a) T. Nikelski, T. Schleid, *Z. Anorg. Allg. Chem.* **2003**, *629*, 1017; b) H. Emme, T. Nikelski, T. Schleid, R. Pöttgen, M. H. Möller, H. Huppertz, *Z. Naturforsch. B: J. Chem. Sci.* **2004**, *59*, 202; T. Nikelski, M. C. Schäfer, H. Huppertz, T. Schleid, *Z. Kristallogr. New Cryst. Struct.* **2008**, *223*, 177.

[28]   W. Harrison, J. Trotter, *J. Chem. Soc. Dalton Trans.* **1972**, 623.

[29]   H. N. Stokes, *Am. Chem. J.* **1897**, *19*, 782.

[30]   C. H. MacGillavry, H. C. J. De Decker, L. M. Nijland, *Nature* **1949**, *164*, 448.

[31]   A. Durif, *Crystal Chemistry of Condensed Phosphates*, Plenum Press, New York, **1995**.

[32]   R. Glaum, habilitation treatise, Univ. Gießen, **1999**.

[33]   W. Schnick, J. Lücke, *J. Solid State Chem.* **1990**, *87*, 101.

[34]   a) W. Schnick, V. Schultz-Coulon, *Angew. Chem.* **1993**, *105*, 308; *Angew. Chem., Int. Ed. Engl.* **1993**, *32*, 280; b) V. Schultz-Coulon, W. Schnick, *Z. Anorg. Allg. Chem.* **1997**, *623*, 69; c) S. J. Sedlmaier, M. Eberspächer, W. Schnick, *Z. Anorg. Allg. Chem.* **2011**, *637*, 362.

[35]   K. Landskron, E. Irran, W. Schnick, *Chem. Eur. J.* **1999**, *5*, 2548.

[36]   K. Landskron, S. Schmid, W. Schnick, *Z. Anorg. Allg. Chem.* **2001**, *627*, 2469.

[37]   W. Schnick, J. Lücke, *Z. Anorg. Allg. Chem.* **1990**, *588*, 19.

[38]   a) W. Schnick, J. Lücke, F. Krumeich, *Chem. Mater.* **1996**, *8*, 281; b) S. Horstmann, E. Irran, W. Schnick, *Angew. Chem.* **1997**, *109*, 1938; *Angew. Chem., Int. Ed. Engl.* **1997**, *36*, 1873; c) S. Horstmann, E. Irran, W. Schnick, *Z. Anorg. Allg. Chem.* **1998**, *624*, 620.

[39]   a) S. Horstmann, E. Irran, W. Schnick, *Angew. Chem.* **1997**, *109*, 2085; *Angew. Chem., Int. Ed. Engl.* **1997**, *36*, 1992; b) S. Horstmann, E. Irran, W. Schnick, *Z. Anorg. Allg. Chem.* **1998**, *624*, 221.

[40]   J. Ronis, B. Bondars, A. Vitola, T. Millers, J. Schneider, F. Frey, *J. Solid State Chem.* **1995**, *115*, 265.

[41]   A. Vitola, J. Ronis, T. Millers, *Latv. PSR Zinat. Akad. Vestis Kim. Ser.* **1990**, *1*, 35.

[42]   H. Jacobs, R. Nymwegen, *Z. Anorg. Allg. Chem.* **1997**, *623*, 429.

[43]   a) R. Hoppe, *Angew. Chem.* **1966**, *78*, 52; *Angew. Chem., Int. Ed. Engl.* **1966**, *5*, 95; b) R. Hoppe, *Angew. Chem.* **1970**, *82*, 7; *Angew. Chem., Int. Ed. Engl.* **1970**, *9*, 25.

[44]   H. A. Höppe, Doctoral Thesis, Univ. Munich (LMU), **2003**.

[45]   a) R. D. Shannon, C. T. Prewitt, *Acta Crystallogr., Sect. B: Struct. Sci.* **1969**, *25*, 925; b) R. D. Shannon, *Acta Crystallogr., Sect. A: Found. Crystallogr.* **1976**, *32*, 751.

[46]   W. H. Baur, *Crystallogr. Rev.* **1987**, *1*, 59.

[47]   H. A. Höppe, F. Stadler, O. Oeckler, W. Schnick, *Angew. Chem.* **2004**, *116*, 5656; *Angew. Chem., Int. Ed.* **2004**, *43*, 5540.

[48]   O. Oeckler, F. Stadler, T. Rosenthal, W. Schnick, *Solid State Sci.* **2007**, *9*, 205.

[49]   J. A. Kechele, O. Oeckler, F. Stadler, W. Schnick, *Solid State Sci.* **2009**, *11*, 537.

[50]   S. Correll, Doctoral Thesis, Univ. Munich (LMU), **2006**.

[51]   U. Kolb, T. Gorelik, C. Kübel, M. T. Otten, D. Hubert, *Ultramicroscopy* **2007**, *107*, 507.

[52]   NanoMEGAS, *Advanced Tools for Electron Diffraction*, NanoMEGAS, Brussels, **2004**.

[53]   U. Kolb, T. Gorelik, M. T. Otten, *Ultramicroscopy* **2008**, *108*, 763.

[54]   U. Heil, S. Schlitt, U. Kolb, T. Gorelik, E. Mugnaioli, E. Schömer, *ADT-3D: A Software Package for ADT Data Visualizing and Processing*, Cooperation with the Institute of Computer Science Johannes-Gutenberg University of Mainz (Germany), **2009**.

[55]   A. A. Coelho, *TOPAS-Academic*, Version 4.1, Coelho Software, Brisbane, **2007**.

[56]   J. Bergmann, R. Kleeberg, A. Haase, B. Breidenstein, *Mater. Sci. Forum* **2000**, *347–349*, 303.

[57]   A. Le Bail, A. Jouanneaux, *J. Appl. Crystallogr.* **1997**, *30*, 265.

12. Ba$_6$P$_{12}$N$_{17}$O$_9$Br$_3$ – A Column-Type Phosphate Structure Solved from Single Nanocrystal Data by Automated Electron Diffraction Tomography

Enrico Mugnaioli, Stefan J. Sedlmaier, Oliver Oeckler,

Ute Kolb, Wolfgang Schnick

ABSTRACT

Oxonitridophosphate Ba$_6$P$_{12}$N$_{17}$O$_9$Br$_3$ was synthesized by heating a multicomponent mixture of BaBr$_2$, BaS, phosphoryl triamide and thiophosphoryl triamide in an evacuated and sealed silica-glass ampoule to 750 °C. Ba$_6$P$_{12}$N$_{17}$O$_9$Br$_3$ was obtained as the main product as a nanocrystalline powder. The crystal structure was determined *ab initio* on the basis of electron diffraction data acquired from a single needleshaped nanocrystal by automated diffraction tomography. Ba$_6$P$_{12}$N$_{17}$O$_9$Br$_3$ crystallizes in the hexagonal space group $P6_3/m$ (no. 176) with unit cell parameters $a = 14.654(19)$, $c = 8.255(9)$ Å and $Z = 2$. Its structure includes triangular, column-shaped anions of $^1_\infty\{(P_{12}N_{17}O_9)^{9-}\}$, which are built from vertex-sharing P(O,N)$_4$ tetrahedra with 3-rings and three-coordinate nitrogen atoms. The 1D anions are separated by Ba^{2+} and Br$^-$ ions, which are arranged in channels parallel to the phosphate anions along [001]. The Ba^{2+} ions are eight- and nine-coordinated by Br$^-$ and O/N atoms, respectively.
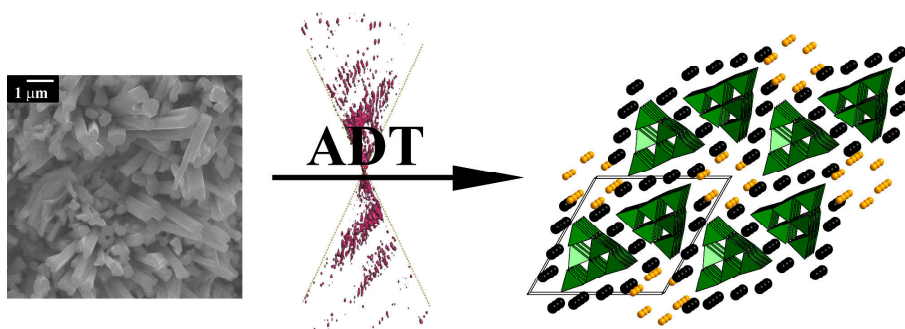
12.1   INTRODUCTION

Oxonitridophosphates represent a silicate-analogous class of compounds as the valence electron concentration of SiO_2 equals that of P/O/N, i.e. valence electron count = 16/3. Consequently, for P/O/N compounds a structural chemistry as complex as that of silicates is expected. The tetrahedron-based structures of (oxo)silicates are classified as ortho-silicates with isolated Q^0-type $[SiO_4]^{4-}$ tetrahedra, disilicates with Q^1-type tetrahedra, chain- and ring-type structures in different conformations with Q^2-type tetrahedra, ribbon- and layer-type structures with Q^3-type tetrahedra and 3D frameworks, in which Q^4-type tetrahedra are all-side vertex-connected to build diverse topologies.[1] Although there is a huge number of examples for each category of oxosilicates, such abundance has not been reported for oxonitridophosphates; however, due to the presence of nitrogen within the tetrahedron-based networks the structural variability should be even larger. N atoms may, more frequently than O atoms, interconnect three ($N^{[3]}$) or even four ($N^{[4]}$) tetrahedral centres and the corresponding bond lengths and angles are much more flexible.[2] The presence of nitrogen atoms can lead to 3D frameworks with a significantly higher degree of condensation than the maximum value possible in oxosilicates. The introduction of a more covalent bond character may improve properties such as chemical, thermal and mechanical stability, which is advantageous for the potential applications of oxonitrido-phosphate networks (e.g. new zeolites).[3] At present, only a comparably small number of P/O/N compounds is known; however, the individual representatives are different, which makes further research exciting.

The potential of the structural versatility of oxonitridophosphate chemistry has not been properly exploited to date because most P/O/N compounds elude identification and structural characterization. Typical reaction products are either amorphous or contain very small crystals, which often consist of various phases with different unknown compositions and cell parameters. As single crystals usually occur in the micro- or nanosize, structure characterization by single-crystal X-ray diffraction is not possible and has been substituted by combinations of different analytical methods such as powder (P)XRD and solid-state NMR spectroscopy.[4] Such an approach, however, cannot be used as a standard route for the structural investigation of oxonitridophosphate, because the assignment of different phases to contributions of PXRD or NMR signals is difficult and not always successful. High-resolution TEM can visualize single nanoparticles, but gathering 3D structural infor-mation by this technique is not straightforward when the cell parameters exceed 1 nm or when the high electron dose rate required results in fast deterioration and amorphization.[5]

Electron diffraction can deliver structural information from single nanocrystals with sub-Angstrom resolution and significantly milder illumination but is traditionally biased by data incompleteness and dynamic effects.[6] However, the recently-developed automated diffraction tomography (ADT) method for electron diffraction data acquisition and analysis[7–10] has proved to be a straightforward, fast and efficient method for structure solution of nanocrystalline materials, even if highly beam sensitive.[11–13] In conventional electron diffraction data acquisition, the crystal is manually oriented along low-index crystallographic zones, which is a time-consuming process and requires experience. In contrast, during ADT acquisition, the crystal is tilted along an arbitrary axis by steady steps, which exploits the full range of the TEM goniometer. ADT is able to deliver electron diffraction data with a higher completeness (up to 100% for orthorhombic or more symmetric crystal families) and a significant reduction of dynamic effects as the diffraction is collected off-zone.

A recent example of oxonitridophosphate structure determination by ADT is SrP_3N_5O.[14] There, the structural investigation was facilitated by the synthesis of a single-phase material. Nevertheless, the ADT approach is as efficient for multiphase systems, where bulk methods, such as PXRD, are limited by peak overlap.[15,16] The procedure is relatively straightforward when the compound of interest forms small crystals with well-defined morphologies and compositions so that recognition and isolation by low-resolution TEM imaging and energy-dispersive X-ray (EDX) spectroscopy can be performed. As this is the case for many P/O/N compounds, a systematic investigation of oxonitridophosphates has become possible.

Here, we report the synthesis and structure determination of a new oxonitridophosphate, $Ba_6P_{12}N_{17}O_9Br_3$, which has a rare column structure built of vertex-sharing $P(O,N)_4$ tetrahedra. Although $Ba_6P_{12}N_{17}O_9Br_3$ was the main synthetic product, its yield was limited by the presence of other phases.

12.2 RESULTS AND DISCUSSION

12.2.1 Synthesis

$Ba_6P_{12}N_{17}O_9Br_3$ was obtained by the reaction of a multicomponent system of $BaBr_2$, BaS, $PO(NH_2)_3$ and $PS(NH_2)_3$ in silica glass ampoules at 750 °C. Not all of the reaction parameters could be controlled independently in such a synthetic system (e.g. NH_3 partial pressure and amount of oxygen) so the optimal conditions for obtaining phase-pure pro-

ducts could not be determined. However, the procedure given in the Experimental Section yields $Ba_6P_{12}N_{17}O_9Br_3$ as the main product with at least two side phases. This can be concluded from the PXRD pattern as the strongest reflections can be assigned to the main reflections of $Ba_6P_{12}N_{17}O_9Br_3$ (Figure 1) and the remaining reflections cannot be jointly indexed. $Ba_6P_{12}N_{17}O_9Br_3$ was obtained as a nanocrystalline powder with rod-shaped crystallites.
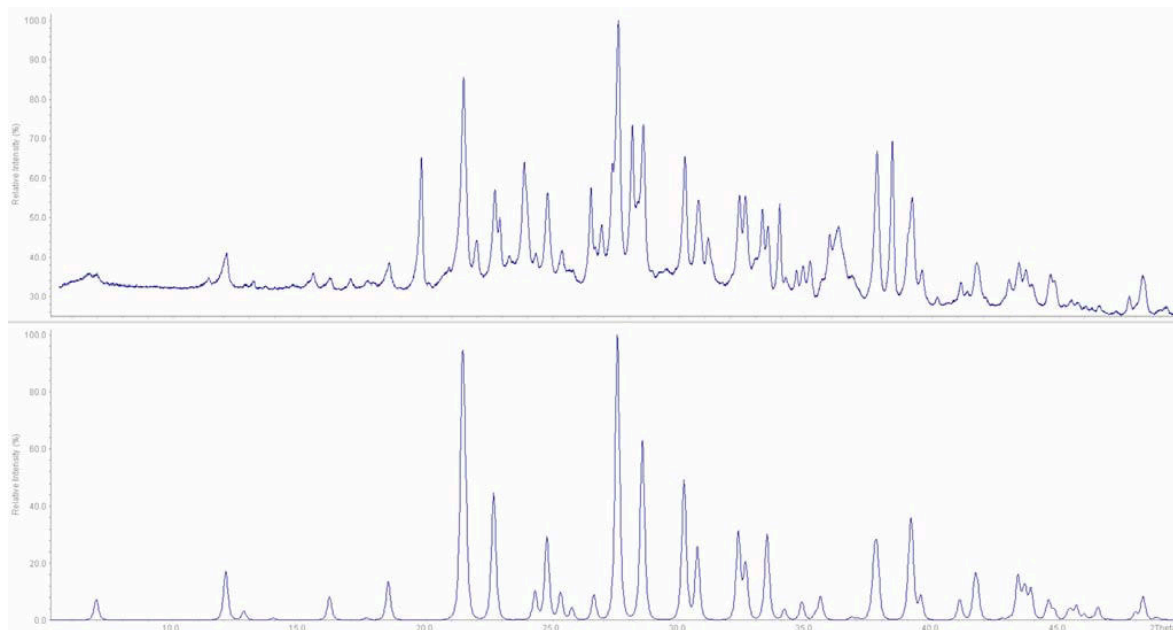

Figure 1. Top: experimental powder diffraction pattern; bottom: calculated pattern based on the structure model solved from electron data; Cu-$K_{\alpha 1}$, 154.0596 pm.

12.2.2 Crystal Structure Analysis

A rod-shaped crystal of around $500 \times 80 \times 80$ nm was selected for ADT. An ADT tilt series of $\pm 60°$ was acquired in steady steps of $1°$. The acquisition was coupled with precession of the electronic beam in order to improve reflection intensity integration.[9,17] After the 3D diffraction space was reconstructed,[8] a metrically hexagonal cell with parameters $a \approx 14.7$ Å and $c \approx 8.3$ Å was determined. The long direction of growth of the rod was parallel to c. On the basis of this cell, an intensity data set was integrated and treated according to the kinematical approximation.

The Laue symmetry was 6/m (internal residual $R_{sym} = 22\%$) but not 6/*mmm* ($R_{sym} = 32\%$). The extinction condition $00l$ with $l = 2n$ leads to space groups $P6_3$ (no. 173) and $P6_3/m$ (no. 176), and *ab initio* structure solution was achieved with the latter. The correct solution was the one with the best residual (R) and the best figure of merit. All

atom positions were determined at the first run and correctly identified using the default parameters. The structure model is in good agreement with the atomic ratio Ba/P/Br of 28 : 58 : 14 obtained by EDX spectroscopy (from the same crystal from which ADT data were acquired).

Table 1. Crystallographic data of $Ba_6P_{12}N_{17}O_9Br_3$ (esd's in parentheses) and details of ADT data collection, structure solution and refinement.

Crystal Structure Data	
formula	$Ba_6P_{12}N_{17}O_9Br_3$
formula mass / g mol^{-1}	1817.49
crystal system	hexagonal
space group	$P6_3/m$ (no. 176)
cell parameters / pm	$a = 1465.4(19)$
(from X-raypowder diffraction)	$c = 825.5(9)$
cell volume / Å^3	$V = 1535(3)$
formula units / cell	$Z = 2$
density / g cm^{-3}	$\rho_c = 3.932$
crystal shape, color	column, colorless
crystal size / µm	$0.50 \times 0.08 \times 0.08$
Data collection	
diffractometer / radiation	Tecnai F30 S-TWIN TEM, $\lambda = 0.01970$ Å
temperature / K	295(2)
tilt range / °	–60 / +60
h, k, l	$-19 \leq h \leq 19, -18 \leq k \leq 19, -10 \leq l \leq 10$
measured reflections	8520
completeness / %	99
resolution / Å	0.77
R_{int}	0.22
Structure Solution and Refinement	
structure solution method	direct methods[18]
structure refinement method	least-squares refinement on F^2 [19]
independent reflections	1343
independent reflections ($> 4\sigma$)	1121
refined parameters	35
constraints / restraints	2 / 21
R indices ($F_o^2 \geq 2\sigma (F_o)^2$)	$R1 = 0.276$ $wR2 = 0.649$
R indices (all data)	$R1 = 0.290$ $wR2 = 0.642$
GoF	2.192
weighting scheme	$w^{-1} = \sigma^2F_o^2 + (0.2000P)^2$ with $P = (F_o^2 + 2F_c^2)/3$
max./min. residual electron density / eÅ^{-3}	0.588 / –0.516

Accurate lattice parameters were determined from the eleven strongest peaks in the PXRD pattern, which were unambiguously assigned to the phase and uniquely indexed. The refinement of the structure of $Ba_6P_{12}N_{17}O_9Br_3$ was exclusively performed based on the ADT data, which provide a reliable and stable result as shown by the refinement of SrP_3N_5O.[14] The final residuals are high when compared with those of standard X-ray refinement but are in the normal range for structure refinement based on electron diffraction data. The P–(O,N) distances were restrained to be equal within a certain standard deviation, and overall displacement parameters were used for chemically equivalent, light atoms. Crystallographic data and further details concerning the structure refinement are summarized in Table 1. Table 2 shows the positional and displacement parameters for all atoms.

Table 2. Atomic coordinates, Wyckoff symbols, and isotropic displacement parameters U_{iso} / Å^2 for the atoms in $Ba_6P_{12}N_{17}O_9Br_3$ (space group $P6_3/m$, esd's in parentheses); c.n. = coordination number; occupancy of N(2)–N(5) and O(2)–O(5) is 5/6 and 1/6, respectively.

atom[c.n.]	Wyckoff symbol	x	y	z	U_{iso}/U_{eq}
Ba(1)[10]	6h	0.5791(4)	0.9657(4)	1/4	0.0549(16)
Ba(2)[10]	6h	0.9230(10)	0.1973(10)	1/4	0.121(4)
Br(1)	6h	0.1410(13)	0.1925(13)	1/4	0.104(4)
P(1)[4]	12i	0.7843(6)	0.3428(6)	0.4218(9)	0.045(2)
P(2)[4]	12i	0.8569(7)	0.5453(7)	0.5649(10)	0.050(2)
N(1)[3]	4f	2/3	1/3	0.420(3)	0.054(6)
N/O(2)[2]	12i	0.8715(8)	0.4604(8)	0.4610(15)	
N/O(3)[2]	12i	0.7828(9)	0.2627(7)	0.5595(14)	0.055(3)[a]
N/O(4)[2]	6h	0.8053(14)	0.3065(14)	¼	
N/O(5)[2]	6h	0.1091(15)	0.4586(16)	¼	
O(6)[1]	12i	0.9355(12)	0.6616(11)	0.493(2)	0.079(5)

[a] the value applies to all atoms N/O(2) to N/O(5)

12.2.3 Structure Description and Discussion

$Ba_6P_{12}N_{17}O_9Br_3$ exhibits a structure characterized by isolated columnar anions. The columns themselves, however, are highly condensed so that the overall degree of condensation (ratio of tetrahedral centres and bridging atoms), $\kappa = 0.46$, is rather high. Classification into the conventional categories of tetrahedral networks (see introduction) is not possible for $Ba_6P_{12}N_{17}O_9Br_3$. A comparably complex 1D anion has been observed in $Ce_{29}Si_{14}N_{43}O_7$.[20]
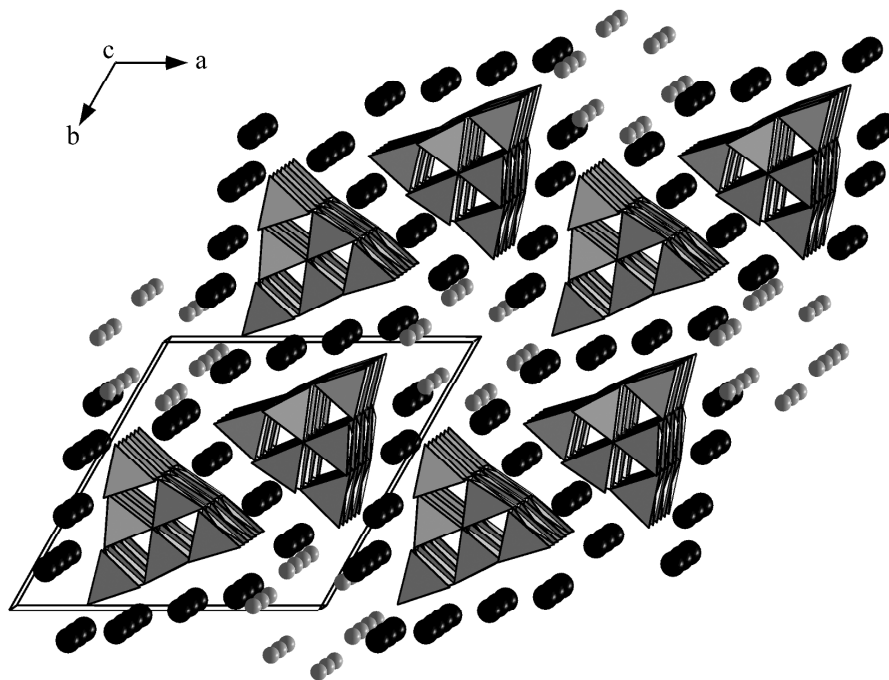
Figure 2. Crystal structure of $Ba_6P_{12}N_{17}O_9Br_3$, viewed along [001]; triangular column of ${}^1_\infty\{(P_{12}N_{17}O_9)^{9-}\}$ are built up from vertex-sharing $P(O,N)_4$ tetrahedra separated by Ba^{2+} ions (black) and Br^- (gray) ions to form channels along [001].

The structure of $Ba_6P_{12}N_{17}O_9Br_3$ can be derived from that of rare-earth metaborates $RE(BO_2)_3$ (RE = Tb–Lu)[21] and isotypic oxonitridophosphate SrP_3N_5O,[14] respectively. In these compounds, triangular columns, such as those in $Ba_6P_{12}N_{17}O_9Br_3$, form corrugated layers. Formally, the structure of $Ba_6P_{12}N_{17}O_9Br_3$ is obtained by cutting columns out of the layers, where the Br^- ions act as "chemical scissors". The triangular columns run along [001] with the Ba^{2+} and Br^- ions located between them (Figure 2). The ${}^1_\infty\{(P_{12}N_{17}O_9)^{9-}\}$ columns (Figure 3) are composed of Q^4- and Q^3-type $P(O,N)_4$ tetrahedra with a Q^4/Q^3 molar ratio of 1:1, which comprise terminally bound oxygen and three-coordinate nitrogen atoms. The formal building block for the complex anion corresponds to the chlorophosphazene $P_6N_7Cl_9$[22] (Figure 4), which is composed of three condensed 3-rings. The columns are generated by the formal substitution of all chlorine atoms by oxygen and nitrogen atoms and the infinite interconnection of the resulting $P_6O_3N(O,N)_{12}$ entities along [001]. These domed building units face concave/concave and convex/convex and are interconnected by six bridging O or N atoms. The linkage of these entities (on one side with three O/N atoms of their inner three tetrahedra and on the other side with three O/N atoms of their outer three tetrahedra) results in 4- and 6-rings, respectively (Figure 3). The O(6) atom does not interconnect the tetrahedra within a column and is terminally bound.
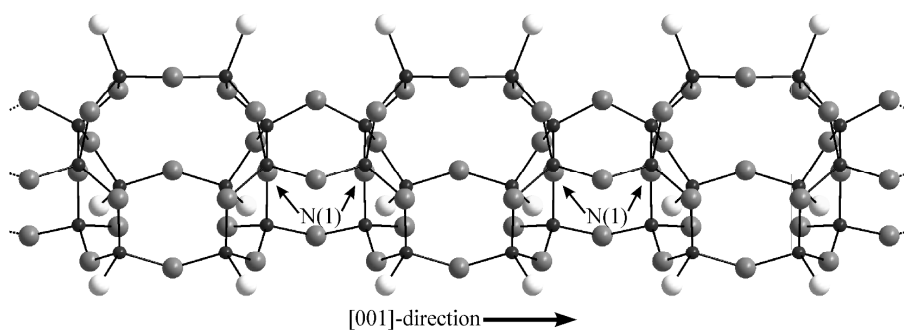
Figure 3. Structure of a single triangular column in $Ba_6P_{12}N_{17}O_9Br_3$ viewed along [100] (P black, O/N gray, O white); three-fold binding N(1) is indicated.
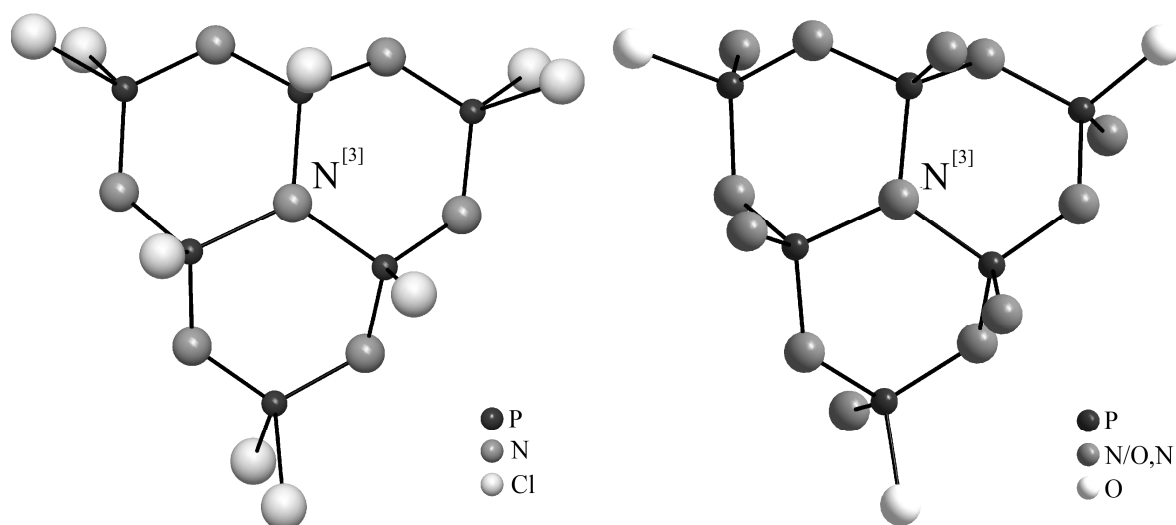

Figure 4. A single molecule of $P_6N_7Cl_9$ (left)[22] and corresponding formal building unit in $Ba_6P_{12}N_{17}O_9Br_3$ (right).

   The range of bond lengths (158.3–165.8 pm) corresponds to that usually observed in oxonitridophosphates. The resulting angles range between 107.9 and 111.1°, which is close to the values of the regular tetrahedron angle (109.5°). The angles P–(O,N)–P between 120.1 and 141.8° are also typical for P/O/N networks. More information about bond lengths and angles is given in Table 3.

Table 3. Selected interatomic distances / pm and angles / ° in $Ba_6P_{12}N_{17}O_9Br_3$ (esd's in parentheses).

Ba(1)-(O,N)	276.4(16)–320.3(12)	9 times
Ba(2)-(O,N)	288.0(31)–369.3(19)	8 times
Ba(1)-Br	348.0(24)	
Ba(2)-Br	316.0(22), 323.0(28)	
P-(O,N)	158.3(12)–165.8(10)	8 times
P-N(1)[3]-P	120.0(4), 120.0(5), 120.0(5)	
P-(O,N)-P	120.1(8)–141.8(5)	4 times
(O,N)-P-(O,N)	107.9(8)–111.1(9)	12 times

The formula $^1_\infty[(P^{[4]}_{12}N^{[3]}_2N^{[2]}_{15}O^{[2]}_3O^{[1]}_6)^{4-})]$ of the 1D anion in $Ba_6P_{12}N_{17}O_9Br_3$ involves two- and threefold bridging as well as terminal O/N atoms. As the direct experimental differentiation between O and N is impossible owing to their similar scattering factors, their reasonable assignment was based on Pauling's rules and experience with other oxonitridic compounds, for which solid-state NMR and lattice energy calculations have been helpful for proper O/N assignment. $N^{[3]}$ was assumed with full nitrogen occupancy as it links three tetrahedra. The terminally bound position was assigned to fully occupied $O^{[1]}$. For the twofold bridging positions, an $N^{[2]}$ occupancy with a statistical admixture of 1/6 $O^{[2]}$ was assumed. Other ordered or disordered models may also be possible, however, one has to stick to the atomic ratio N/O = 17 : 9 as long as the Br positions are fully occupied (as suggested by the refinement) and no hydrogen is present in the compound, which can be assumed by comparison with similar, hydrogen-free SrP_3N_5O (proved by elemental analysis).

The electrostatic plausibility for the structure model, also in respect of the atomic O/N ratio and their distribution, was verified with lattice energy calculations according to the Madelung part of lattice energy (MAPLE) concept.[23] The calculations were carried out for two differently O/Nordered structural models using the formal ionic charges of the atoms (Table 4). The total MAPLE value averaged over the two models (319181 kJmol^{-1}) is close to the sum of the total MAPLE values of the hypothetical starting materials $3BaBr_2$ + $9BaO$ + $9PON$ + $5P_3N_5$ (323053 kJmol^{-1}; Δ = 1.2%).

Table 4. Total MAPLE for two O/N-ordered structure models; the rows indicate the ordered model by a fully occupancy of O at one respective two-fold bridging atomic position; with an occupancy of the remaining two-fold bridging positions and the three-fold bridging position by N and an occupancy of the terminal by O, ordered models of $Ba_6P_{12}N_{17}O_9Br_3$ are given.

atomic position fully occupied with O	total MAPLE value / kJ·mol^{-1}
O(4)	318417
O(5)	319945
average Ø	319181, Δ = 1.2 %
theoretical MAPLE value ($3BaBr_2$ + $9BaO$ + $9PON$ + $5P_3N_5$)	323053

The columnar anions in $Ba_6P_{12}N_{17}O_9Br_3$ are separated by Ba^{2+} ions. Both crystallographically independent Ba^{2+} sites exhibit a coordination number of ten (Figure 5). Ba(1) is surrounded by nine O/N atoms and one Br$^-$ ion. The O/N atoms, including two terminal O atoms, are located at distances between 276.4 and 320.3 pm. The Ba(1)–Br distance is 348.0 pm. Ba(2) is surrounded by eight O/N atoms, four of which are terminal O atoms, and two Br–anions. The Ba(2)–(O,N) distances range from 288.0–369.3 pm

(Figure 5), whereas the Ba(2)–Br distances have values of 316.0 and 323.0 pm. All of the distances (Table 3) agree well with the sum of the respective ionic radii involved.[24,25]

The Br$^-$ ions in $Ba_6P_{12}N_{17}O_9Br_3$ are arranged to form channels along [001] (Figure 2). Staggered stacks of Br$^-$ triangles with a separation of 412.8 pm are arranged according to the 6_3 screw axis (Figure 6). The Br–Br distance within the triangles is 438.1 pm.
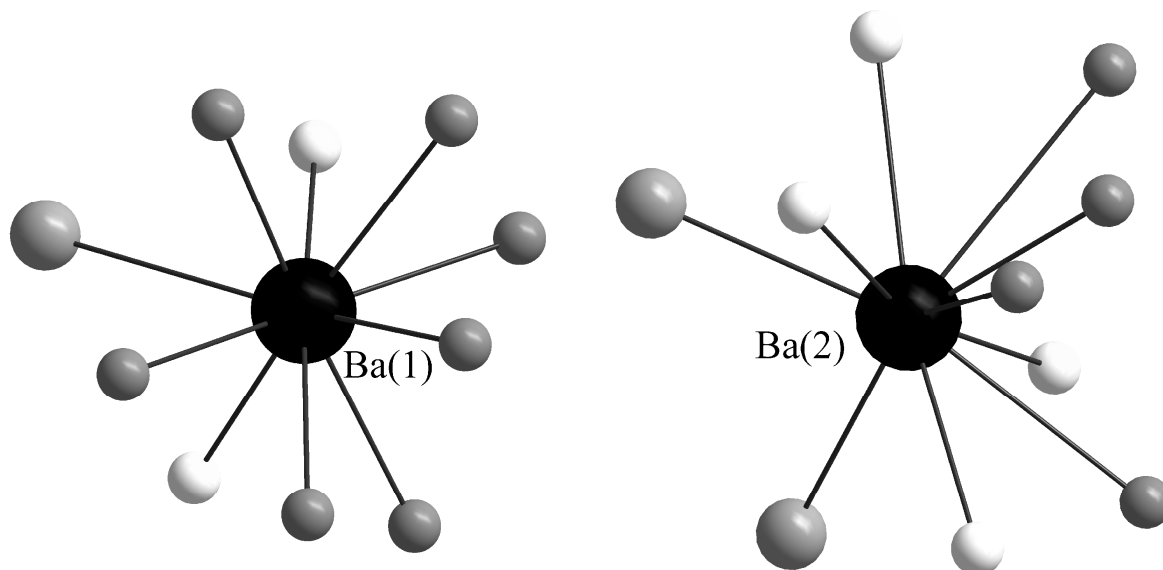
Figure 5. Coordination sphere of Ba^{2+} ion in $Ba_6P_{12}N_{17}O_9Br_3$ (Ba^{2+} black, Br$^-$ big gray, O/N small gray, O white).

438.1(21) pm

412.8(5) pm
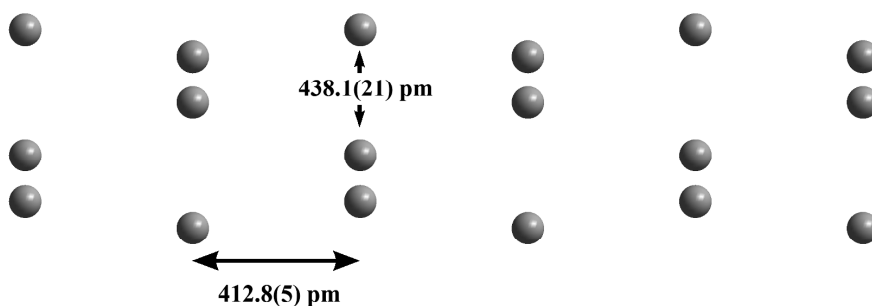
Figure 6. Arrangement of Br$^-$ ions in $Ba_6P_{12}N_{17}O_9Br_3$ along [001]; the Br$^-$ triple are ordered staggered.

12.3   CONCLUSION

The ADT method, now routinely operable, opens the chance to discover new compounds even from inhomogeneous and nanocrystalline samples. This chance should be grasped as the concept of oxonitridophosphates yields extraordinary compounds with open-framework structures, such as $P_4N_4(NH)_4(NH_3)$,[26] $Li_xH_{12-x-y+z}[P_{12}O_yN_{24-y}]X_z$

$(X = Cl, Br)^{[27]}$ and $Ba_{19}P_{36}O_{6+x}N_{66-x}Cl_{8+x}$,[4] and highly condensed layer structures, such as $Sr_3P_6O_6N_8$.[28] The ADT structure determination of SrP_3N_5O[14] has revealed a layer structure with a degree of condensation $\kappa = ½$, and $Ba_6P_{12}N_{17}O_9Br_3$ represents a further exceptional structure. To the best of our knowledge, such a highly condensed, 1D anion as that seen in $Ba_6P_{12}N_{17}O_9Br_3$ has not been observed in any tetrahedron-based class of compounds so far. $Ba_6P_{12}N_{17}O_9Br_3$ can be considered as a variant of SrP_3N_5O cut into snippets. The "chemical scissors" are Br^- ions, which form columns from corrugated layers and stabilize the channels in $Ba_6P_{12}N_{17}O_9Br_3$. Starting from this channel arrangement, it would be interesting to see if further cations, e.g. Li^+, can be incorporated. With an enlargement of the structure in the **<100>** directions and a simultaneous adaptation of the O/N ratio for charge equalization, this could lead to future lithium ion conductors.

One of our aims was the synthesis of phase-pure $Ba_6P_{12}N_{17}O_9Br_3$. Currently, at least two side phases are present in typical samples. These phases might be related to both SrP_3N_5O and $Ba_6P_{12}N_{17}O_9Br_3$. It can be imagined that structural cut-outs of (e.g. two or three) interlinked (double or triple) columns might be present as single-phase nanocrystals or nanodomains. Other intermediate compounds could exhibit crystal structures built up of finite pieces of a column (prism-like). As for SrP_3N_5O and $Ba_6P_{12}N_{17}O_9Br_3$, the systematic investigation of other oxonitridophosphate structures could benefit from singlecrystal electron diffraction data collected by ADT.

12.4 EXPERIMENTAL SECTION

12.4.1 Synthesis

Phosphoryl triamide and thiophosphoryl triamide were synthesized according to literature methods.[29–31] Freshly distilled $POCl_3$ (99%) or $PSCl_3$ (98%; both from Acros Organics, Geel, Belgium; 10–20 mL) were added directly and slowly to liquid ammonia in a flame-dried three-necked 1 L flask. Subsequently, the elimination of NH_4Cl from the products was carried out by a Soxhlet extraction with distilled Et_2NH in dry CH_2Cl_2 for 3 d. After drying in vacuo, $OP(NH_2)_3$ and $SP(NH_2)_3$ were available as starting materials in form of colourless, water sensitive powders. Their purity was verified by PXRD.

$Ba_6P_{12}N_{17}O_9Br_3$ was synthesized by a multicomponent system. In a typical procedure, $BaBr_2$ (35.7 mg, 0.120 mmol; Sigma–Aldrich, 99.999%), BaS (40.7 mg, 0.240 mmol; Sigma–Aldrich, 99.9%), $OP(NH_2)_3$ (27.4 mg, 0.288 mmol) and $SP(NH_2)_3$ (48.0 mg, 0.432 mmol) were thoroughly mixed and ground in an Ar-filled glovebox (MBraun,

Garching, Germany; H$_2$O $\leq$ 0.2 ppm, O$_2$ $\leq$ 1.0 ppm) and transferred into a silica glass ampoule (wall thickness 2 mm, inner diameter 11 mm). The evacuated and sealed ampoule (length around 11 cm), was heated in a tube furnace to 200 and 750 °C with dwell times of 12 and 48 h (heating and cooling rate: 1.0 Kmin^{-1}), respectively. The emerging condensation products NH$_3$ and H$_2$S were partially deposited as (NH$_4$)$_2$S at the places in the ampoule that cooled first. After breaking the ampoules, the samples were washed with water and *N,N*-dimethylformamide to remove NH$_4$Br, BaBr$_2$ and BaS. Ba$_6$P$_{12}$N$_{17}$O$_9$Br$_3$ was obtained as a heterogeneous, colourless, water and air resistant, nanocrystalline powder.

12.4.2 ADT Data Acquisition and Analysis

For data acquisition, the sample was suspended in ethanol and sprayed onto a carbon-coated copper grid using the sonifier described in ref.[9] ADT was performed with a Tecnai F30 S-TWIN TEM equipped with a field emission gun working at 300 kV. Electron diffraction patterns were acquired with a CCD camera (14-bit GATAN 794MSC). EDX spectra were recorded in STEM mode and quantified with Emispec ESVision software.

ADT data acquisition was performed with a FISCHIONE tomography holder, using the acquisition module described in ref.[7] STEM images and diffraction patterns were collected using a mild illumination setting. STEM images were collected by a FISCHIONE high angle annular dark field detector. Nano electron diffraction was performed with a 10 μm C2 condenser aperture with a 50 nm beam on the sample. ADT was coupled with precession of the electron beam (precession electron diffraction),[9,17] performed using the NanoMEGAS SpinningStar unit. The precession angle was kept at 1.2°. The ADT3D[8] software was used for data processing, which included geometrical parameter optimization, 3D diffraction volume reconstruction, 3D visualization, automated cell parameter determination and intensity integration. *Ab initio* structure solution was performed by direct methods implemented in SIR2008, included in the package IL MILIONE.[18] Structure refinement[†] was performed with the SHELX software.[19]

---

† Further details of the crystal structure investigation may be obtained from the Fachinformationszentrum Karlsruhe, 76344 Eggenstein-Leopoldshafen, Germany (fax: +49-7247-808-666; e-mail: crysdata@fiz-karlsruhe.de, http://www.fiz-karlsruhe.de/request_for_deposited_data.html) on quoting the depository number CSD-423468.

12.5 REFERENCES

[1]   F. Liebau, *Structural Chemistry of Silicates*, Springer, Berlin, **1985**.

[2]   M. Zeuner, S. Pagano, W. Schnick, *Angew. Chem.* **2011**, *123*, 7898; *Angew. Chem., Int. Ed.* **2011**, *50*, 7754.

[3]   R. Marchand, W. Schnick, N. Stock, *Adv. Inorg. Chem.* **2000**, *50*, 193.

[4]   S. J. Sedlmaier, M. Döblinger, O. Oeckler, J. Weber, J. Schmedt auf der Günne, W. Schnick, *J. Am. Chem. Soc.* **2011**, *133*, 12069.

[5]   U. Kolb, T. E. Gorelik, E. Mugnaioli, A. Stewart, *Polym. Rev.* **2010**, *50*, 385.

[6]   D. L. Dorset, *Structural Electron Crystallography*, Plenum Press, New York, **1995**.

[7]   U. Kolb, T. Gorelik, C. Kübel, M. T. Otten, D. Hubert, *Ultramicroscopy* **2007**, *107*, 507.

[8]   U. Kolb, T. Gorelik, M. T. Otten, *Ultramicroscopy* **2008**, *108*, 763.

[9]   E. Mugnaioli, T. Gorelik, U. Kolb, *Ultramicroscopy* **2009**, *109*, 758.

[10]   U. Kolb, E. Mugnaioli, T. Gorelik, *Cryst. Res. Technol.* **2011**, *46*, 542.

[11]   I. Rozhdestvenskaya, E. Mugnaioli, M. Czank, W. Depmeier, U. Kolb, A. Reinholdt, T. Weirich, *Mineral. Mag.* **2010**, *74*, 159.

[12]   D. Denysenko, M. Grzywa, M. Tonigold, B. Streppel, I. Krkljus, M. Hirscher, E. Mugnaioli, U. Kolb, J. Hanss, D. Volkmer, *Chem. Eur. J.* **2011**, *17*, 1837.

[13]   J. Jiang, J. L. Jorda, J. Yu, L. A. Baumes, E. Mugnaioli, M. J. Diaz-Cabanas, U. Kolb, A. Corma, *Science* **2011**, *333*, 1131.

[14]   S. J. Sedlmaier, E. Mugnaioli, O. Oeckler, U. Kolb, W. Schnick, *Chem. Eur. J.* **2011**, *17*, 11258.

[15]   C. S. Birkel, E. Mugnaioli, T. Gorelik, U. Kolb, M. Panthöfer, W. Tremel, *J. Am. Chem. Soc.* **2010**, *132*, 9881.

[16]   M. Gemmi, J. Fischer, M. Merlini, S. Poli, P. Fumagalli, E. Mugnaioli, U. Kolb, *Earth Planet. Sci. Lett.* **2011**, *310*, 422.

[17]   R. Vincent, P. A. Midgley, *Ultramicroscopy* **1994**, *53*, 271.

[18]   M. C. Burla, R. Caliandro, M. Camalli, B. Carozzini, G. L. Cascarano, L. De Caro, D. Siliqi, G. Polidori, R. Spagna, C. Giacovazzo, *J. Appl. Crystallogr.* **2007**, *40*, 609.

[19]   G. M. Sheldrick, *Acta Crystallogr., Sect. A: Found. Crystallogr.* **2008**, *64*, 112.

[20]   C. Schmolke, Doctoral Thesis, Univ. Munich (LMU) **2010**, pp. 143.

[21]   a) T. Nikelski, T. Schleid, *Z. Anorg. Allg. Chem.* **2003**, *629*, 1017; b) H. Emme, T. Nikelski, T. Schleid, R. Pöttgen, M. H. Möller, H. Huppertz, *Z. Naturforsch. B*

2004, *59*, 202; T. Nikelski, M. C. Schäfer, H. Huppertz, T. Schleid, *Z. Kristallogr. New Cryst. Struct.* **2008**, *223*, 177.

[22]   W. Harrison, J. Trotter, *J. Chem. Soc., Dalton Trans.* **1972**, 623.

[23]   a) R. Hoppe, *Angew. Chem.* **1966**, *78*, 52; *Angew. Chem., Int. Ed. Engl.* **1966**, *5*, 95; b) R. Hoppe, *Angew. Chem.* **1970**, *82*, 7; *Angew. Chem., Int. Ed. Engl.* **1970**, *9*, 25.

[24]   a) R. D. Shannon, C. T. Prewitt, *Acta Crystallogr., Sect. B: Struct. Sci.* **1969**, *25*, 925; b) R. D. Shannon, *Acta Crystallogr., Sect. A: Found. Crystallogr.* **1976**, *32*, 751.

[25]   W. H. Baur, *Crystallogr. Rev.* **1987**, *1*, 59.

[26]   F. Karau, W. Schnick, *Angew. Chem.* **2006**, *118*, 4617; *Angew. Chem., Int. Ed.* **2006**, *45*, 4505.

[27]   a) S. Correll, O. Oeckler, N. Stock, W. Schnick, *Angew. Chem.* **2003**, *115*, 3674; *Angew. Chem., Int. Ed.* **2003**, *42*, 3549; b) S. Correll, N. Stock, O. Oeckler, J. Senker, T. Nilges, W. Schnick, *Z. Anorg. Allg. Chem.* **2004**, *630*, 2205.

[28]   S. J. Sedlmaier, J. Schmedt auf der Günne, W. Schnick, *Dalton Trans.* **2009**, 4081.

[29]   R. Klement, O. Koch, *Chem. Ber.* **1954**, *87*, 333.

[30]   W. Schnick, *Z. Naturforsch. B* **1989**, *44*, 942.

[31]   S. Correll, Doctoral Thesis, Univ. Munich (LMU) **2006**.

13. Template-free Inorganic Synthesis of Silica-Based Nanotubes and their Self-Assembley to Mesocrystals

The same approach that resulted in novel, crystalline oxonitridophosphates (see last three chapters) has been applied in this case. The molecules $PO(NH_2)_3$ and $PS(NH_2)_3$ were transformed with liquid $SiCl_4$ in order to synthesize a silicon oxonitridophosphate, but the system behaved differently:

ABSTRACT

A novel synthesis approach for silica-based nanotubes (NTs) was discovered in the purely inorganic system containing the molecular compounds $OP(NH_2)_3$, $SP(NH_2)_3$ and $SiCl_4$ in evacuated and sealed silica glass ampoules. Without any solvent or structure directing template the amorphous NTs self-organise to form orthogonally ordered, 3D hyperbranched mesocrystals, exhibiting an interesting material for nanofluidic device applications.
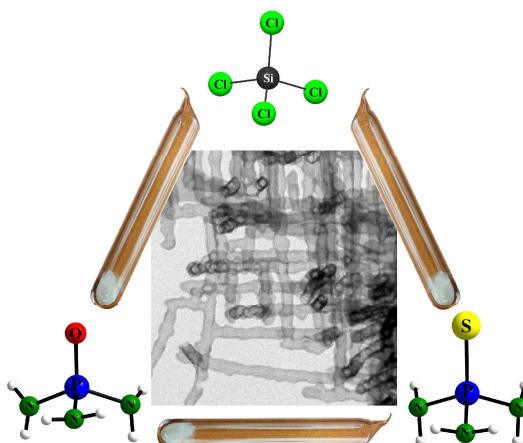
13.1   INTRODUCTION WITH RESULTS AND DISCUSSION

Silica, the most abundant solid compound on earth, occurs in a multitude of crystalline and amorphous forms and has been used for a diverse range of applications (e.g. as ceramics, quartz oscillators) for a long time.[1,2] The discovery of one-dimensional silica nanotubes (NTs)[3] has generated considerable attention towards the search for further functionalities, e.g. in gas storage, drug/gene-delivery, sensing, catalysis or nanofluidic systems.[4] Triggered by this high potential, research concerning new synthesis methods for silica-based hollow NTs is a topic of great interest. While two-dimensional, layered compounds exhibit an intrinsic rolling up tendency,[5,6] the preparation of purposeful NTs of three-dimensional, isotropicmaterials like silica, however, usually requires structure-directing templates.[7,8] Therefore, physical templates such as porous alumina membranes or previously fabricated nanowires in combination with atomic layer deposition (ALD), organic surfactants in self-assembled gels or biological templates were drawn into consideration.[3,9–14] In principle, these methods allow a precisely controlled growth of silica NTs. In some cases, however, the template-assisted synthesis exhibits laborious multiple-step reactions with partially toxic organic substances involved. Apart from that the process of removal of the template could be a severe problem causing collapse of a newly prepared tubular silica nanostructure.[4]

Silica (SiO_2) is isoelectronic to phosphorus oxonitride (PON) and phosphorus oxonitride imide (PN(NH)) while a structural analogy is consequent. The related compound classes of nitridophosphates and oxonitridophosphates exhibit structural chemistry with many variants including e.g. highly condensed layered as well as openframework structures.[15–20] In the course of our systematic investigation of these silicate-analogous compound classes, we discovered a novel approach for a template- and solvent-free synthesis of silicabased NTs. In a purely inorganic reaction, actually trying to synthesise a silicon oxonitridophosphate, we simply performed a reaction of a mixture of phosphoryl triamide $OP(NH_2)_3$[21] and thiophosphoryl triamide $SP(NH_2)_3$[7,22] with silicon tetrachloride $SiCl_4$ in a closed system of a sealed silica glass ampoule (see chapter 13.2.1). For systematically exploring the system, we performed the synthesis at different temperatures from 300 to 700 °C (in steps of 100 °C) while maintaining all other conditions constant. Additionally, some of the syntheses were carried out with an increased amount of $SiCl_4$ in the ampoule. A structure-directing agent was not added at any step of the synthesis. The synthesis products were mainly recovered as homogeneous, dry, grey solids.
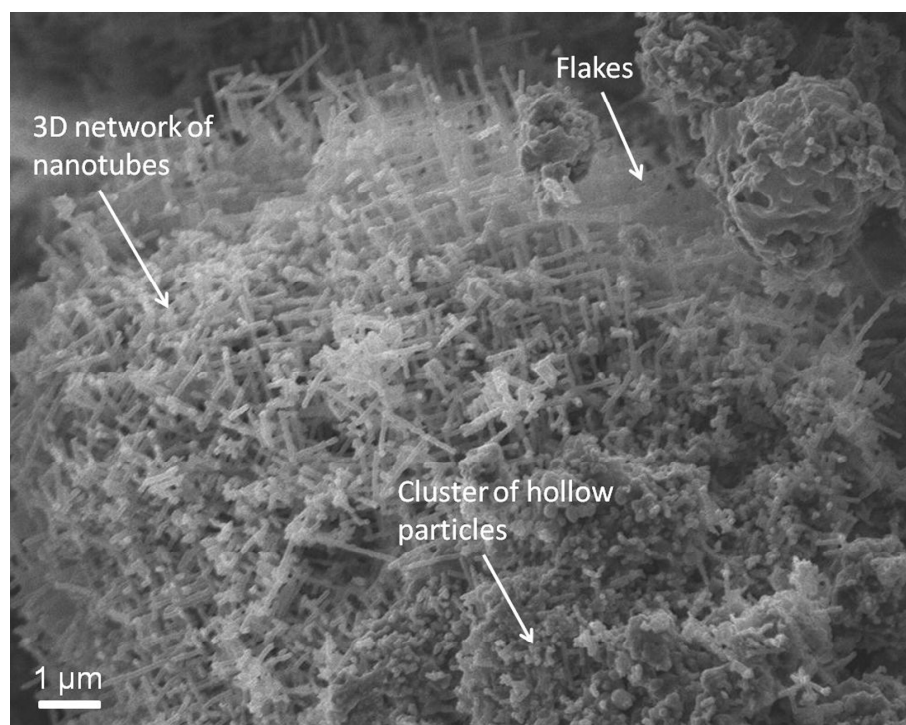
Figure 1. SEM images of the as-synthesized sample showing nanotubes tending to form 3D networks, shapeless flakes and cluster of particles.

A scanning electron microscopy (SEM) image of a representative as-synthesised sample is shown in Figure 1. Overall, the reaction products consist of three different morphologies. There are vitreous, shapeless flakes as the main product, amorphous clusters of hollow particles, and finally, although no structure-directing agent was added, amorphous silica-based NTs that usually form nettings. The length of the NTs goes up to several micrometers, while the hollow particles as the shortest version of the NTs are the lower endpoint with a size less than 150 nm. Our systematic series of experiments performed at different synthesis temperatures from 300 to 700 °C shows, besides the reproducibility, a temperature dependency concerning the relative amount of NTs and hollow particles and the cross-sectional dimensions of the NTs. Although all morphologies emerge at each synthesis temperature, the NT structures are rather more frequent at higher temperatures than at lower ones and vice versa for the hollow particles.

Transmission electron microscopy (TEM) studies reveal a bamboo-like growth of the NTs (see Figure 2b) which is also observed for CN_x NTs.[23] From TEM images the mean cross-sectional diameters and wall thicknesses of the NTs have been determined for each synthesis temperature. The wall thicknesses decrease from 24(3) nm for a synthesis temperature of 300 °C to 15(2) nm for 700 °C. The diameters are narrower when the synthesis is performed at higher temperatures. They range from 126(24) nm for a synthesis

temperature of 300 °C down to 72(17) nm for 700 °C. The large deviation is due to the bamboo-like structure. Accordingly, with our new template-free approach a control concerning the diameter of silicabased NTs is feasible. The observed cross-sectional dimensions are within the typical range reported for silica nanotubes.[4] For a deeper insight into the system and more detailed analysis of the different morphologies, we performed a series of further TEM investigations. Bright-field images of a typical vitreous flake and an array of NTs synthesised at 700 °C are shown in Figure 2a and b. The flake appears porous with differently sized holes indicating intensive gas formation. The NTs have a partially lopsided growth and are orthogonally branched in all three directions in space as already illustrated in Figure 1. Furthermore, the hollow nature of the NTs is clearly observable in Figure 2b, where identification of walls by a different mass–thickness contrast is possible. This is even more evident in Figure 2c, where an exemplary, high-magnification TEM image of a single tube, synthesised at 700 °C, is presented. As is obvious in Figure 2d, where different shaped hollow particles as the shortest version of NTs are shown, all NTs are originally closed. Open ends are only generated by breakage during sample preparation (Figure 2c). Electron diffraction (ED) experiments (insertion in Figure 2a and b) for all morphologies showed no Bragg intensities. Consequently, as already suggested by powder diffraction measurements of samples, the flakes as well as the tube structure are characterised as amorphous. This amorphous character is definitely present from the beginning (as-synthesised material) and was confirmed by independent measurements using acceleration voltages of 80 and 300 kV. No difference in shape was observed, when working under these different conditions. In addition the NTs were found to be surprisingly stable under electron bombardment.
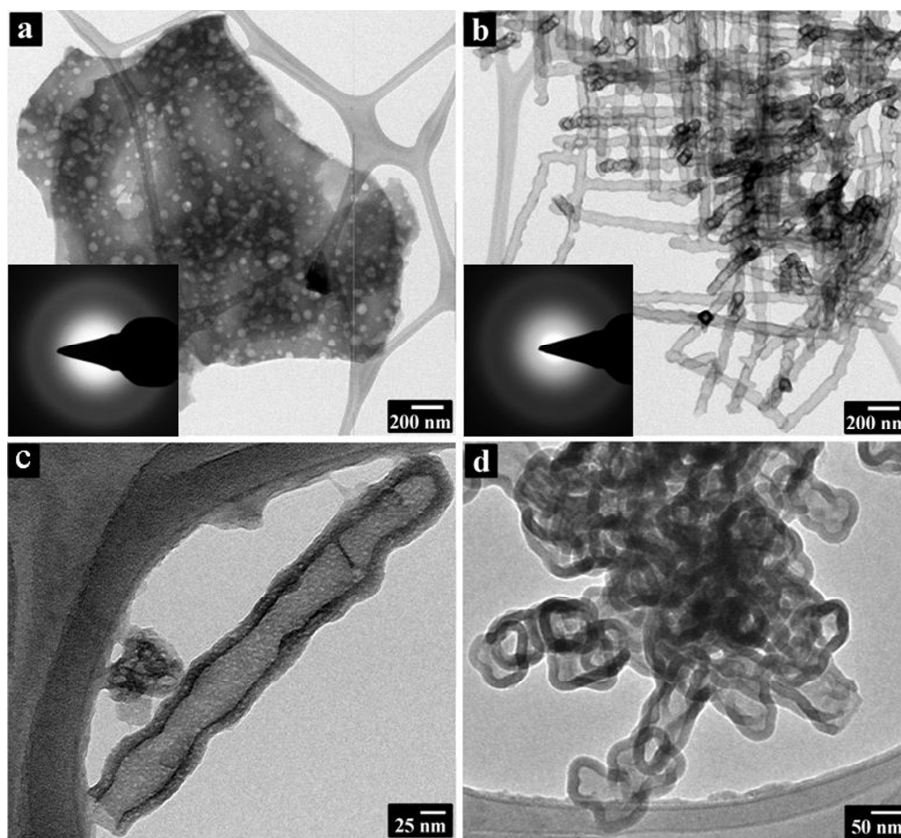
Figure 2. TEM images of as-synthesized samples of a) an amorphous flake with different sized pores, b) an array of orthogonally branched silica-based NTs (both with ED pattern as insertion), c) single silica-based NT synthesized at 700 °C and d) a cluster of hollow particles synthesized at 400 °C.

Investigations concerning the composition were performed employing energy dispersive X-ray spectroscopy (EDX). Using the TEM, we extensively analysed the different morphologies in a sample synthesised at 700 °C (Figure 1) by recording a number of spectra at different spots. For both, the flakes and the NTs, the elements Si, P, O and N were detected (see Figure 3). Semi-quantitative analyses resulted in an approximate atomic ratio of Si : P of 4 : 1 for the NTs which was inverted (1 : 4) for the flake material. While O is predominantly incorporated in the NTs (together with Si), N is mainly contained in the flakes (together with P). Another result from the EDX investigation is that the composition of the hollow particles is similar to that of the NTs. Hence one can conclude that the NTs and the hollow particles exhibit the same material. Consequently, from our template- and solvent-free inorganic synthesis approach two products, namely (Si)/P/(O)/N amorphous flakes and phosphorus- and nitrogen-doped silica or even phosphorus-doped silicon oxonitride NTs are yielded. In addition to these determined compositions, regarding the starting materials ($OP(NH_2)_3$, $SP(NH_2)_3$), one can assume that hydrogen is more or less present in all structures. This is not separately verified for each structure but experiences with other oxonitridophosphates[17,18] and infrared spectra from the material do suggest

this. Assuming that the materials are most probably built up from 3D interconnected SiX_4 and PX_4 tetrahedra, respectively, hydrogen is either included in connecting positions X as –NH– or as terminal –OH or –NH_2 groups. As we know from the chemistry of nitridosilicates or nitridophosphates, these functionalities can also exist after high temperature treatment. The mixing of Si/P/O/N/NH in the materials is also fully comprehensible regarding the structural chemistry of crystalline SiO_2, PON and PN(NH). All three compounds exhibit the cristobalite structure type[1,24,25] so that continuous solid solutions $Si_{1-x}P_xO_{2-x-y}N_x(NH)_y$ ($x \leq 1$, $y \leq 2$ and $x + y \leq 2$) seem possible.
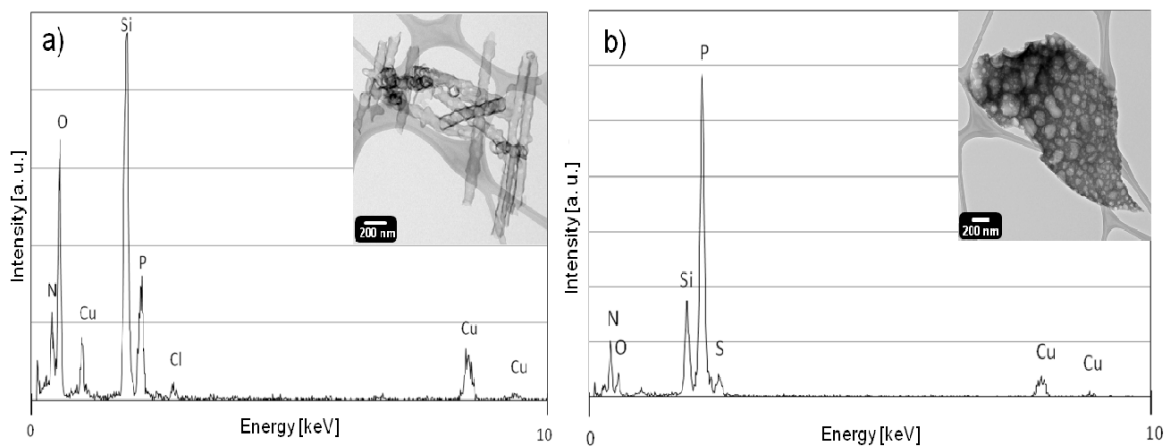

Figure 3. EDX measurements of a) SiO_2-based NTs and b) a flake; Cu results from the copper grid, Cl and S, respectively, from the starting materials.

An important critical condition for the silica-based NTs is definitely the content of oxygen in the mixture of starting materials. As rather little O is introduced by our synthesis approach, the yield of flakes is much higher than that of the NTs. However, the reaction with the highest possible O content, the transformation of only $OP(NH_2)_3$ with $SiCl_4$, resulted not in the formation of NTs but in a vitreous Si/P/O/N compound. In contrast, the reaction of only $SP(NH_2)_3$ with $SiCl_4$ yielded no NTs as well but a nanocrystalline Si/P/N compound different from the only known phase $SiPN_3$ in this system.[26] This indicates that interplay between the different reactants is responsible for the NT growth.
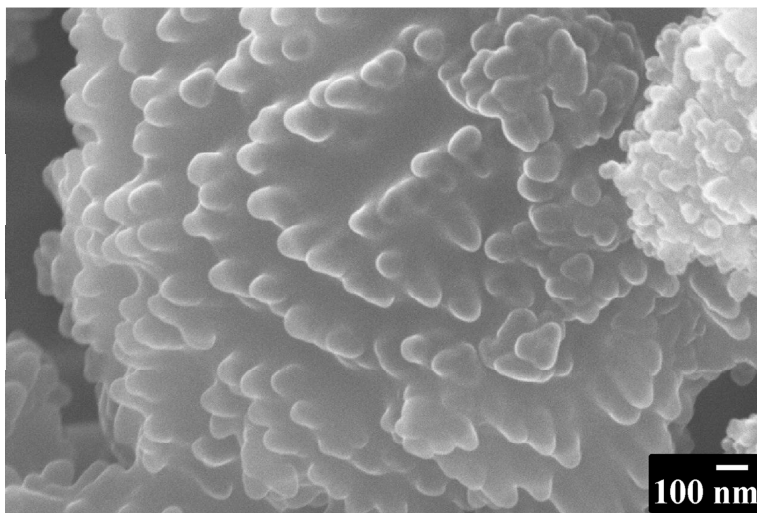
Figure 4. SEM image of a polymeric agglomeration indicating the starting point for NT growth.

As a first hypothesis we visualize the growth of the silica-based NTs as follows: starting from weakly condensed inorganic polymer agglomerations Si/(P)/O/(N) nuclei are built and form small cells (hollow particles) filled with gas. The polymer agglomeration in Figure 4 is a sign of such a starting point. While elevating the temperature in the following, more gas (NH_3, HCl, H_2S) is generated within the condensation process and the cells become more and more elongated and combine to more or less long and hyperbranched NTs. Thereby it seems that the growth is accompanied by a respective self-separating process towards Si/O and P/N resulting in a dropout of the flake material. This is comprehensible regarding the higher oxophilia of Si and NTs found growing nearby or on top of the flake material. The elongation and combination of the shapeable hollow particles are probably driven by the reduced pressure in the system (here, an ampoule), which also assists length growth in other assemblies.[27] Branching has mostly been observed orthogonally. This is probably effected by a maximal repulsion of the branches. Although of course further investigations are necessary, this model seems probable as NT structures are more frequently found at higher temperatures, while hollow particles are more frequently found at lower temperatures (see above).

As indicated, the described synthesis depends on the amount of $SiCl_4$. If the amount of $SiCl_4$ is increased to excess (67.6 ml, 0.589 mmol) keeping all other parameters like pressure, heating rate and dwell time constant, at a synthesis temperature of 700 °C impressive 3D assemblies of hyperbranched silica-based NTs are obtained. As presented in the SEM images in Figure 5, mesocrystals with octahedral habitus are formed. These well-regulated nanopipe systems that can be isolated from the surface of the flake materials,

afford interesting opportunities for constructing novel 3D nanofluidic devices. While other fabrication methods for inorganic nanofluidic devices usually require multiple production steps associated with templates,[9,28–30] our method exhibits a simple one-pot synthesis comprising only one single step. Another benefit in this context is that the silica-based NTs involve N, so harder and more thermally and chemically stable pipes could be provided for e.g. bioseparation[31] or fast mass transport[32] in nanofluidic devices. Strong N-doped silica is also interesting as glasses with variable refractive indices in optical applications (e.g. fiber Bragg gratings).[33]

In conclusion, a novel inorganic solvent-free synthesis approach for silica-based NTs is presented. This exceedingly interesting and promising system has to be further investigated with respect to the yield increase and growth mechanism. A detailed analysis is also desirable as this pure inorganic system creates fascinating mesostructures that are similarly found in nature.[34]
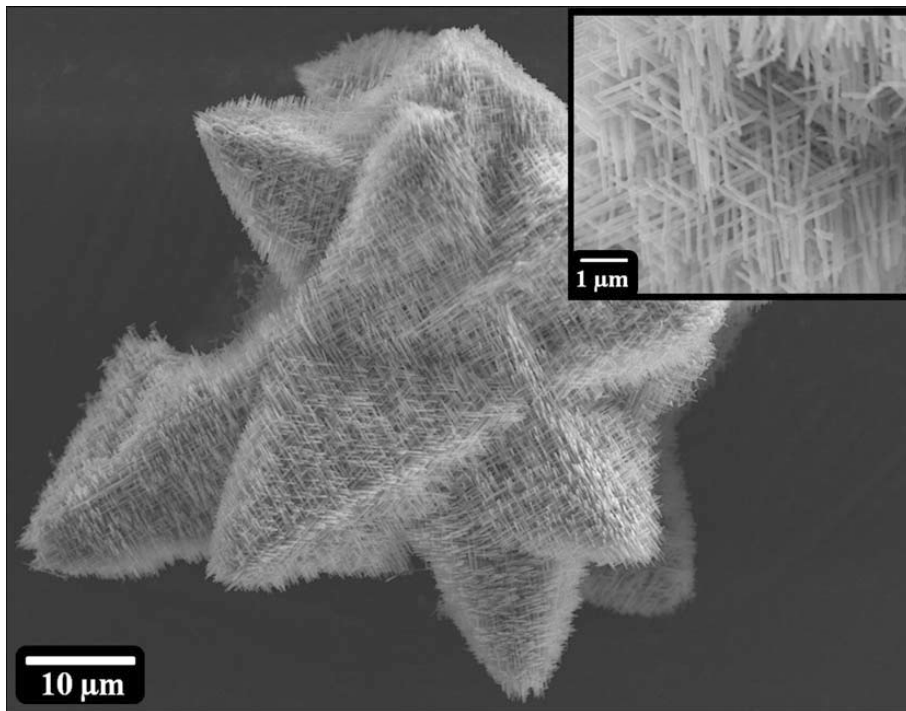

Figure 5. SEM images of an as-synthesized sample showing an isolated intergrown mesocrystals and a zoomed-in view into the mesocrystal.

13.2   EXPERIMENTAL DETAILS

13.2.1 Synthesis

In a typical procedure, OP(NH$_2$)$_3$ (18.6 mg, 0.196 mmol) and SP(NH$_2$)$_3$[21,22] (70.0 mg, 0.630 mmol) were thoroughly mixed and ground in an argon-filled glovebox and transferred into a flame-dried silica glass ampoule (wall thickness 2 mm, inner diameter 11 mm). While using dry nitrogen[35] as inert gas, SiCl$_4$ (33.8 µl, 0.294 mmol; Sigma-Aldrich, 99.998 %) was added and dropped onto the mixture of the triamides. After freezing with liquid N$_2$, the ampoule was sealed (to a length of approx. 11 cm) under reduced pressure and subsequently heated in a conventional tube furnace in horizontal position to 200 °C and different target temperatures from 300 – 700 °C (in steps of 100 °C) with dwell times of 12 and 48 h (heating and cooling rate: 1 Kmin^{-1}), respectively. Emerging condensation products such as NH$_3$, H$_2$S and HCl are (partially) deposited as (NH$_4$)$_2$S and NH$_4$Cl at the places in the ampoule that cool first. After breaking the ampoules, the samples were recovered as dry, gray solids.

13.2.2 Electron Microscopy and EDX measurements

First morphological investigations of the reaction products were made on a JSM-6500F scanning electron microscope (SEM) (JEOL Ltd., Tokyo, Japan) with a field emission source operated at 4.0 to 12.0 kV. All images shown are secondary electron images. The chemical composition was studied with an energy-dispersive X-ray spectrometry (EDS) detector model 7418 (Oxford Instruments, Oxfordshire, UK). Powders were placed on a brass sample carrier fixed with self-adhesive carbon plates (Plano, Wetzlar, Germany). The samples were sputtered with carbon (sputter device: BAL-TEC MED 020, BAL-TEC AG, Balzers, Netherlands) before loading them into the SEM chamber, since the reaction products were not electrically conducting.

To obtain more detailed information about the NTs and flakes, a FEI Titan 80–300 S/TEM transmission electron microscope (TEM) with a field emission gun, a Gatan Tridiem image filter and an EDAX EDS detector for analytical measurements was employed. Diffraction patterns were recorded with a Gatan UltraScan 1000 (2k × 2k) CCD camera. For sample preparation, the grayish solids were suspended in ethanol (99.9 %), ultrasonicated for 10 min and few drops of the suspension were placed on a copper grid coated with an amorphous, holey carbon layer (Lacey S166-2, PLANO). After plasmacleaning for 10-30 s, the TEM measurements were performed at 300 and 80 kV,

respectively. For this, the grids were mounted on a double tilt holder with a maximum tilt angle of 30°.

The chemical composition of the reaction products were investigated with EDX also on the FEI Titan 80–300 S/TEM.

13.3   REFERENCES

[1]   P. J. Heaney, *Rev. Mineral.* **1994**, *29*, 1.

[2]   G. H. Beall, *Rev. Mineral.* **1994**, *29*, 469.

[3]   H. Nakamura, Y. Matsui, *J. Am. Chem. Soc.* **1995**, *117*, 2651.

[4]   X. Yang, H. Tang, K. Cao, H. Song, W. Sheng, Q. Wu, *J. Mater. Chem.* **2011**, *21*, 6122.

[5]   R. Tenne, L. Margulis, M. Genut, G. Hodes, *Nature* **1992**, *360*, 444.

[6]   a) L. Margulis, G. Salitra, R. Tenne, M. Talianker, *Nature* **1993**, *365*, 113; b) M. Hershfinkel, L. A. Gheber, V. Volterra, J. L. Hutchison, L. Margulis, R. Tenne, *J. Am. Chem. Soc.* **1994**, *116*, 1914.

[7]   R. Tenne, *Angew. Chem.* **2003**, *115*, 5280; *Angew. Chem., Int. Ed.* **2003**, *42*, 5124.

[8]   C. N. Rao, A. Govindaraj, *Adv. Mater.* **2009**, *21*, 4208.

[9]   M. Zhang, Y. Bando, K. Wada, K. Kurashima, *J. Mater. Sci. Lett.* **1999**, *18*, 1911.

[10]   S. O. Obare, N. R. Jana, C. J. Murphy, *Nano Lett.* **2001**, *1*, 601.

[11]   J.-X. Wang, L.-X. Wen, Z.-H. Wang, M. Wang, L. Shao, J.-F. Chen, *Scr. Mater.* **2004**, *51*, 1035.

[12]   R. Fan, Y. Y. Wu, D. Y. Li, M. Yue, A. Majumdar, P. D. Yang, *J. Am. Chem. Soc.* **2003**, *125*, 5254.

[13]   W. L. Liu, K. Alim, A. A. Balandina, D. M. Mathews, J. A. Dodds, *Appl. Phys. Lett.* **2005**, *86*, 253108.

[14]   M. Numata, K. Sugiyasu, T. Hasegawa, S. Shinkai, *Angew. Chem., Int. Ed.* **2004**, *43*, 3279.

[15]   W. Schnick, *Angew. Chem.* **1993**, *105*, 846; *Angew. Chem., Int. Ed. Engl.* **1993**, *32*, 806.

[16]   a) S. Correll, O. Oeckler, N. Stock, W. Schnick, *Angew. Chem.* **2003**, *115*, 3674; *Angew. Chem., Int. Ed.* **2003**, *42*, 3549; b) S. Correll, N. Stock, O. Oeckler, J. Senker, T. Nilges, W. Schnick, *Z. Anorg. Allg. Chem.* **2004**, *630*, 2205.

[17]   N. Stock, E. Irran, W. Schnick, *Chem. Eur. J.* **1998**, *4*, 1822.

[18] S. J. Sedlmaier, E. Mugnaioli, O. Oeckler, U. Kolb, W. Schnick, *Chem. Eur. J.* **2011**, *17*, 11258.

[19] S. J. Sedlmaier, M. Döblinger, O. Oeckler, J. Weber, J. Schmedt auf der Günne, W. Schnick *J. Am. Chem. Soc.* **2011**, *133*, 12069.

[20] F. Karau, W. Schnick *Angew. Chem.* **2006**, *118*, 4617; *Angew. Chem., Int. Ed.* **2006**, *45*, 4505.

[21] R. Klement, O. Koch, *Chem. Ber.* **1954**, *87*, 333.

[22] W. Schnick, *Z. Naturforsch., B: J. Chem. Sci.* **1989**, *44*, 942.

[23] A. A. Koós, M. Dowling, K. Jurkschat, A. Crossley, N. Grobert, *Carbon* **2009**, *47*, 30.

[24] J.-M. Léger, J. Haines, L. S. de Oliveira, C. Chateau, A. Le Sauze, R. Marchand, *J. Phys.: Condens. Matter* **1996**, *8*, L773.

[25] W. Schnick, J. Lücke, *Z. Anorg. Allg. Chem.* **1992**, *610*, 121.

[26] H. P. Baldus, W. Schnick, J. Lücke, U. Wannagat, G. Bogedain *Chem. Mater.* **1993**, *5*, 845.

[27] S. Krylyuk, A. V. Davydov, I. Levin, *ACS Nano* **2011**, *5*, 656.

[28] C. R. Martin, *Science* **1994**, *226*, 1961.

[29] J. Goldberger, R. Fan, P. D. Yang, *Acc. Chem. Res.* **2006**, *39*, 239.

[30] J. Zhu, H. Peng, S. T. Connor, Y. Cui, *Small* **2009**, *5*, 437.

[31] D. T. Mitchell, S. B. Lee, L. Trofon, N. Li, T. K. Nevanen, H. Sőderlund, C. R. Martin, *J. Am. Chem. Soc.* **2002**, *124*, 11864.

[32] J. K. Holt, H. G. Park, Y. Wang, M. Stadermann, A. B. Artyukhin, C. P. Grigoropoulos, A. Noy, O. Bakajin, *Science* **2006**, *312*, 1034.

[33] R. R. Khrapko, K. M. Golant, E. M. Dianov, A. L. Tomashuk, *Adv. Sci. Technol.* **1999**, *17*, 541.

[34] J. Aizenberg, J. C. Weaver, M. S. Thanawala, V. C. Sundar, D. E. Morse, P. Fratzl, *Science*, **2005**, *309*, 275.

[35] Inert gas N_2 was previously purified by piping it through columns filled with blue gel (Merck KGaA, Darmstadt, Germany), KOH pellets (Merck KGaA, purum), molecular sieve (Merck KGaA, 3 Å), Granulopent® (granulated P_4O_{10}, Roth GmbH, Karlsruhe, Germany, ≥ 99%), BTS catalyzer (Sigma-Aldrich, St. Louis, USA).

14. Summary

14.1   Objective of the thesis

The P/O/N chemistry, including the compound classes of oxonitridophosphates and phosphorus oxonitrides, theoretically exhibits a structural chemistry going beyond the already very versatile one known for silicates. Until now, except for few examples, it was not possible to realize this potential, mainly due to preparative difficulties. In order to discover unprecedented tetrahedral networks and so to exploit the potential of P/O/N chemistry, the objective of this thesis was the synthesis, identification and characterization of oxonitridophosphates and phosphorus oxonitrides.

The challenge has been mastered by developing and applying different synthesis strategies and analyzing the reaction products with different suitable investigation methods. An essential element in this thesis was the high-pressure route. This frequently used synthesis tool improved not only the crystallinity of products but made many compounds accessible for the first time. The development of a novel activated PON starting material played also a very important role: several compounds resulted from it. For structural investigation, in most cases, powder X-ray diffraction has been used. *Ab initio* solved structures (direct methods and charge flipping) were refined with the Rietveld method. Solid-state NMR spectroscopic methods corroborated and supplemented the refined structures in many cases. Furthermore, the new method of automated electron diffraction tomography (ADT) could be introduced in this field. With two ADT structure determinations the potential of this new structure determination tool has been pointed out. This all together expanded P/O/N chemistry significantly. Considering the described synthetic and analytical strategies, identification of novel oxonitridophosphates and phosphorus oxonitrides should become much easier in the future.

The results summarized in the following, reflect the variety of P/O/N chemistry, the success of covered synthesis strategies and the powerful analytical methods used.

14.2   Tetrametaphosphimates $Tl_4(PO_2NH)_4 \cdot H_2O$ and $Ca_2(PO_2NH)_4 \cdot 8H_2O$ (chapter 2, page 10 and chapter 3, page 26)

Tetrathallium(I) tetra-μ-imidocyclotetraphosphate monohydrate, $Tl_4(PO_2NH)_4 \cdot H_2O$, and Dicalcium tetra-μ-imidocyclotetraphosphate octahydrate, $Ca_2(PO_2NH)_4 \cdot 8H_2O$, were obtained by evaporation of respective combined aqueous solutions ($K_4(PO_2NH)_4 \cdot 4H_2O$ and $TlOOCCH_3$ and $Ca(NO_3)_2 \cdot 4H_2O$, respectively). The structure determinations were

performed by single-crystal X-ray diffraction methods. For $Tl_4(PO_2NH)_4 \cdot H_2O$, in addition to the basic structure ($P\bar{1}$ (no. 2), $a = 928.3(2)$, $b = 974.6(2)$, $c = 1018.0(2)$ pm, $\alpha = 74.47(3)$, $\beta = 64.68(3)$, $\gamma = 78.81(3)°$, Z = 2), satellite reflections indicate a fourfold super-structure ($A\bar{1}$, $a = 928.0(2)$, $b = 3897.1(8)$, $c = 2035.4(4)$, $\alpha = 74.47(3)$, $\beta = 64.68(3)$, $\gamma = 78.81(3)°$, Z = 16) that is described by an $a \times 4b \times 2c$, A-centered supercell that mainly concerns one thallium site of the basic structure. In order to reduce the number of parameters, this superstructure was handled as a commensurate occupancy modulation using the structural description in (3 + 1)-dimensional superspace ($P\bar{1}(\alpha\beta\gamma)$, q = 0.25b* + 0.5c*) with a single harmonic wave function. For $Ca_2(PO_2NH)_4 \cdot 8H_2O$ (*Pbcn* (no. 60), $a = 1700.6(3)$, $b = 1069.3(2)$, $c = 963.2(2)$ pm, Z = 4) structure determination ran straight forward. The crystal structures of $Tl_4(PO_2NH)_4 \cdot H_2O$ and $Ca_2(PO_2NH)_4 \cdot 8H_2O$ consist of infinite columns of the cyclic $(PO_2NH)_4^{4-}$ ions (saddle conformation) which are interconnected by N–H⋯O hydrogen bonds. These columns are hold together by coordination to the metal ions and a complex hydrogen bonding network with crystal water molecules involved. FT-IR spectra of the compounds have been measured and relevant bands were assigned. The structures were verified by ^{31}P solid-state NMR spectroscopy. The thermal behavior of $Tl_4(PO_2NH)_4 \cdot H_2O$ and $Ca_2(PO_2NH)_4 \cdot 8H_2O$ were discussed as well.

14.3   Ammonium *catena*-polyphosphate IV [NH₄PO₃]ₓ (chapter 4, page 40)

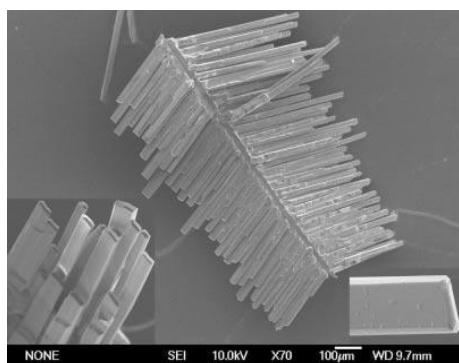In the course of the synthesis of phosphorus oxonitride PON polymorph IV of *catena*-polyphosphate $[NH_4PO_3]_x$ was synthesized phase-purely by heating $NH_4H_2PO_4$ in a tube furnace in an ammonia gas flow with an elevated NH_3 partial pressure. From obtained pseudo-merohedrally twinned single crystals of $[NH_4PO_3]_x$ IV X-ray structure determination ($P2_1/c$ (no. 14), $a = 2270.3(5)$, $b = 458.14(9)$, $c = 1445.1(3)$ pm, $\beta = 108.56(3)°$, Z = 4) of only the second of five modifications of $[NH_4PO_3]_x$ was achieved. The parallel [010] running *catena*-polyphosphate chain anions

Figure 14.1. REM images of [NH₄PO₃].

with a chain-periodicity $P = 2$ and a stretching factor $f_s = 0.94$ are interconnected through extensive hydrogen bonding towards the ammonium ions. Due to 'chemical twinning' a novel *catena*-polyphosphate structure type is realized in $[NH_4PO_3]_x$ IV. The vibrational spectra of $[NH_4PO_3]_x$ IV corroborated the chain structure with its periodicity $P = 2$.

14.4   Amorphous 'PO$_{0.88}$N$_{1.24}$H$_{0.56}$' as precursor and starting material

As crystalline β-cristobalite PON is non-reactive and thus not suitable as starting material for the synthesis of oxonitridophosphates, another PON starting material has been developed. At multi-gram scale, an amorphous phosphorus oxonitride imide with the composition PO$_{0.88}$N$_{1.24}$H$_{0.56}$ has been prepared by heating the mixture PO(NH$_2$)$_3$ / 3NH$_4$Cl that results from the reaction of POCl$_3$ with ammonia, in an ammonia gas flow. It turned out to be as precondensed that it is shortly before the crystallization to β-cristobalite PON and thus excellently suitable as precursor and starting material. Besides exhibiting a single-source precursor for β-cristobalite and quartz PON, four new compounds resulted from this amorphous PON. The preparation method, which is described in detail in chapter 5 (H$_3$P$_8$O$_8$N$_9$), shows great prospect as with it different P/O/N/H compositions for differently intended products can be continuously designed.

14.5   Interrupted network of H$_3$P$_8$O$_8$N$_9$ (chapter 5, page 52)

The first crystalline phosphorus oxonitride imide, H$_3$P$_8$O$_8$N$_9$, was synthesized by means of high-pressure high-temperature conditions, treating the highly reactive phosphorus oxo-
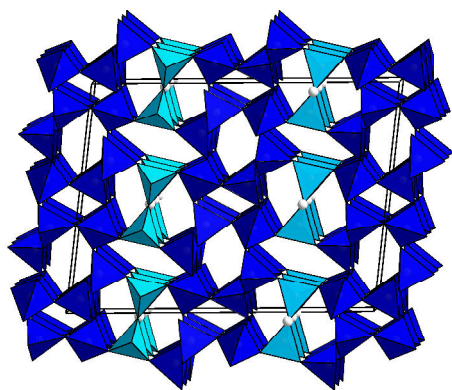

nitride imide precursor at 12 GPa and 750 °C with using a multianvil assembly. The crystal structure of H$_3$P$_8$O$_8$N$_9$ was determined *ab initio* from X-ray powder diffraction data (*C*2/*c* (no. 15), $a = 1352.11(7)$, $b = 479.83(3)$, $c = 1820.42(9)$ pm, $\beta = 96.955(4)°$, Z = 4) and exhibits a highly condensed (κ = 0.47), three-dimensional but interrupted network, which is composed of all-side vertex sharing (Q^4) and only three-fold connecting

Figure 14.2.   Crystal structure of H$_3$P$_8$O$_8$N$_9$.

(Q^3) P(O,N)$_4$ tetrahedra in a ratio Q^4 : Q^3 of 3 : 1. The structure, including 4-rings as the smallest ring size, can be subdivided in alternating open-branched zweier double-layers {oB,2$^2_\infty$}[^{2}P$_3$(O,N)$_7$] and layers containing pair-wise linked Q^3-tetrahedra parallel (001). Information on hydrogen in H$_3$P$_8$O$_8$N$_9$ were gained by ^{1}H 1D MAS, 2D homo- and heteronuclear (together with ^{31}P) correlation NMR spectroscopy and a ^{1}H spin-diffusion experiment with a hard-pulse sequence, designed for selective excitation of a single resonance. Two hydrogen sites with a ratio in multiplicity of 2 : 1 were identified and assigned to Wyckoff positions 8*f* and 4*e*.

14.6   New phosphorus(V) oxonitride polymorph δ-PON (chapter 6, page 76)

δ-PON was synthesized by treating the amorphous PON precursor at high-pressure high-temperature conditions of 12 GPa and 13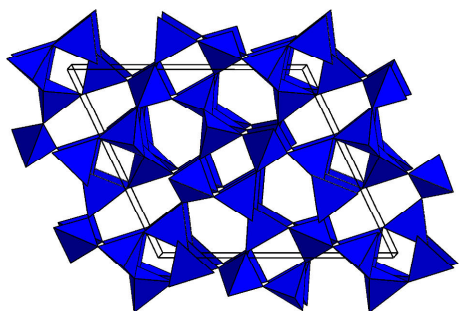50 °C using a multianvil assembly. The crystal structure of δ-PON was elucidated *ab initio* from laboratory X-ray powder diffraction data using the charge-flipping algorithm for structure solution and the Rietveld method for structure refinement ($P2_1/c$ (no. 14), $a =$ 1224.72(2), $b = 483.618(6)$, $c = 1086.04(2)$ pm, $\beta = 115.8026(8)°$, Z = 16). The structure is made up from all-side vertex-sharing

Figure 14.3. Crystal structure of δ-PON.

$P(O,N)_4$ tetrahedra and forms a 3D-network, which was not known before, even not for SiO_2. The topology, characterized through 4- and 6-rings, was predicted as SiO_2-modification in the space group *Aea*2 (Predicted Crystallography Open Database, entry 3102887). The structure of δ-PON and the predicted structure are related through a common aristotype in the space group *Cmce*. δ-PON exhibits, after cristobalite-, moganite- and quartz-PON only the fourth polymorph for PON.

14.7   Highly condensed layered oxonitridophosphates $M_3P_6O_6N_8$ (M = Sr, Ba) (chapter 7, page 88 and chapter 8, page 100)

$Sr_3P_6O_6N_8$ and $Ba_3P_6O_6N_8$ were prepared by means of a high-pressure high-temperature synthesis of 6 GPa and 920 °C using a multianvil assem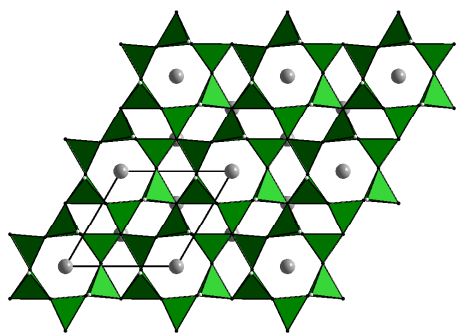bly starting from the amorphous phosphorus oxonitride imide and the metal azides $Sr(N_3)_2$ and $Ba(N_3)_2$, respectively. Their crystal structure was solved *ab initio* on the basis of powder X-ray diffraction data by direct methods and refined by the Rietveld method ($P\overline{3}$ (no. 147), $Sr_3P_6O_6N_8$: $a = 729.667(5)$, $c = 602.603(5)$ pm, $Ba_3P_6O_6N_8$: $a = 740.227(9)$, $c = 631.436(11)$ pm,   Z = 1).   The structure of $M_3P_6O_6N_8$ (M = Sr, Ba) is built up from

Figure 14.4. Crystal structure of $Sr_3P_6O_6N_8$.

two-dimensional, single layer anions $[P_6O_6N_8]^{6-}$ parallel (001) and Sr^{2+} and Ba^{2+} ions, respectively, in-between. The anions are composed of vertex-sharing Q^3-type PON_3 tetrahedra, which form condensed 4- and 6-rings with twofold and threefold N atoms involved within the layer. The O atoms are bound terminally. The layer structure exhibits a very high degree of condensation κ = 0.43.

14.8 *Catena*-polynitridophosphate Zn₂PN₃ (chapter 9, page 104)

Phase-pure Zn_2PN_3 was synthesized by means of high-pressure high-temperature conditions (1200 °C, 8 GPa) starting from Zn_3N_2 and P_3N_5 utilizing a multianvil assembly.
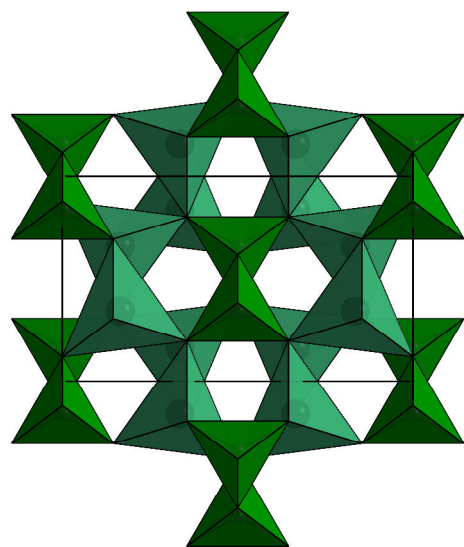

The crystal structure of Zn_2PN_3, refined from powder X-ray diffraction data by the Rietveld method using the atomic parameters of isotypic Mg_2PN_3 as starting values ($Cmc2_1$ (no. 36), $a = 937.847(6)$, $b = 547.696(4)$, $c = 492.396(3)$ pm, $Z = 4$), comprises *catena*-polynitridophosphate chain anions running parallel [001] with a chain periodicity $P = 2$ and a stretching factor $f_s = 0.88$ and interconnecting Zn^{2+} ions. The structure exhibits a pseudo-hexagonal symmetry and can be reduced to the wurtzite structure type. FT-IR and Raman spectra as well as a ^{31}P MAS NMR spectrum corroborate the structure of

Figure 14.5. Crystal structure of Zn_2PN_3.

Zn_2PN_3. The thermal behavior of Zn_2PN_3 was analyzed as well.

14.9 Novel zeolite-like framework topology in Ba₁₉P₃₆O₆₊ₓN₆₆₋ₓCl₈₊ₓ (x ≈ 4.54) (chapter 10, page 119)

The oxonitridophosphate $Ba_{19}P_{36}O_{6+x}N_{66-x}Cl_{8+x}$ ($x \approx 4.54$) has been synthesized by heating a multicomponent reactant mixture consisting of phosphoryl triamide $OP(NH_2)_3$,
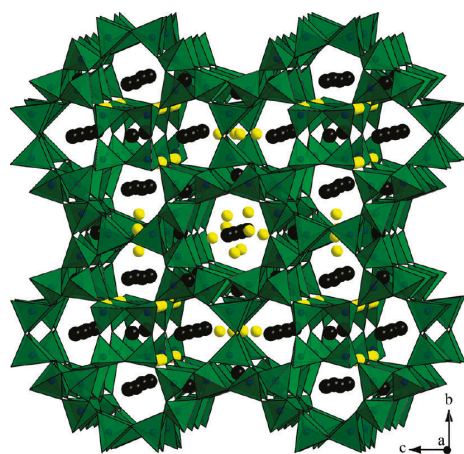

thiophosphoryl triamide $SP(NH_2)_3$, BaS, and NH_4Cl enclosed in an evacuated and sealed silica glass ampoule up to 750 °C. The crystal structure was elucidated *ab initio* from high-resolution synchrotron powder diffraction data ($\lambda = 39.998$ pm) applying the charge-flipping algorithm supported by independent symmetry information derived from electron diffraction (ED) and scanning transmission electron microscopy (STEM). The structure of

Figure 14.6. Crystal structure of $Ba_{19}P_{36}O_{6+x}N_{66-x}Cl_{8+x}$.

$Ba_{19}P_{36}O_{6+x}N_{66-x}Cl_{8+x}$ ($x \approx 4.54$) ($Fm\overline{3}c$ (no. 226),

$a = 2685.41(3)$ pm, $Z = 8$) comprises all-side vertex sharing $P(O,N)_4$ tetrahedra forming slightly distorted $3^8 4^6 8^{12}$ cages representing a novel composite building unit (CBU). Interlinked through their 4-rings and additional 3-rings, the cages build up a 3D network

with a framework density FD = 14.87 T / 1000 Å^3 and a 3D 8-ring channel system. Ba^{2+} and Cl^- as extra-framework ions are located within the cages and channels of the framework. The structural model is corroborated by ^{31}P double-quantum (DQ) / single-quantum (SQ) and triple-quantum (TQ) / single-quantum (SQ) 2D correlation MAS NMR spectroscopy. According to $^{31}P\{^1H\}$ C-REDOR NMR measurements, the H content is less than one H atom per unit cell.

14.10 Highly condensed layer oxonitridophosphate SrP_3N_5O (chapter 11, page 148)

The oxonitridophosphate SrP_3N_5O has been synthesized by heating a multicomponent reactant mixture that consisted of phosphoryl triamide $OP(NH_2)_3$, thiophosphoryl triamide
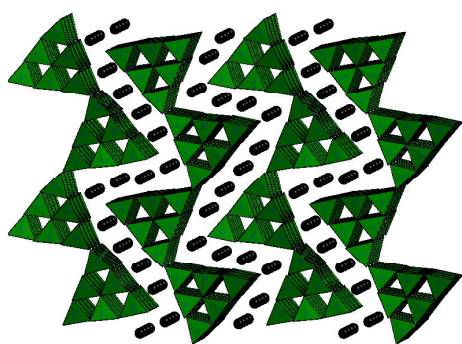

$SP(NH_2)_3$, SrS, and NH_4Cl enclosed in evacuated and sealed silica-glass ampoules up to 750 °C. The compound was obtained as nanocrystalline powder with needle-shaped crystallites. The crystal structure was solved *ab initio* on the basis of electron diffraction data by means of automated electron diffraction tomography (ADT) and verified by Rietveld refinement with X-ray powder diffraction

Figure 14.7. Crystal structure of $Sr_3P_6O_6N_8$.

data. SrP_3N_5O crystallizes in the orthorhombic space group *Pnma* (no. 62) with unit-cell data of $a = 18.331(2)$, $b = 8.086(1)$, $c = 13.851(1)$ Å and Z = 16. The compound is a highly condensed layer phosphate with a degree of condensation $\kappa = ½$. The corrugated layers $^2_\infty\{(P_3N_5O)^{2-}\}$ consist of linked, triangular columns built up from $P(O,N)_4$ tetrahedra with 3-rings and triply binding nitrogen atoms. The Sr^{2+} ions are located between the layers and exhibit six-, eight-, and ninefold coordination. FT-IR and solid-state NMR spectra of SrP_3N_5O are discussed as well.

14.11   Column-type oxonitridophosphate Ba$_6$P$_{12}$N$_{17}$O$_9$Br$_3$ (chapter 12, page 171)

The oxonitridophosphate Ba$_6$P$_{12}$N$_{17}$O$_9$Br$_3$ was synthesized by heating a multicomponent reactant mixture including BaBr$_2$, BaS, phosphoryl triamide OP(NH$_2$)$_3$ and thiophosphoryl
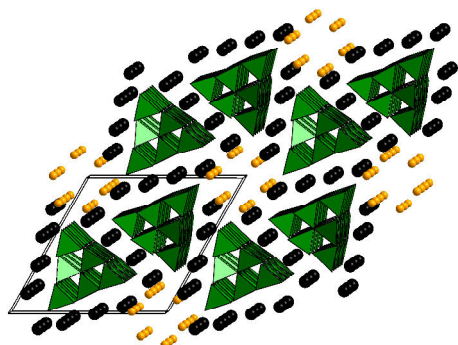
triamide SP(NH$_2$)$_3$, enclosed in evacuated and sealed silica-glass ampoules, up to 750°C. The compound was obtained as main product in a nanocrystalline powder. The crystal structure was determined *ab initio* on basis of electron diffraction data acquired from a needle-shaped nanocrystal by means of automated electron diffraction tomography (ADT). Ba$_6$P$_{12}$N$_{17}$O$_9$Br$_3$ crystallizes in the hexagonal space group *P*6$_3$/*m* (no. 176) with unit-cell parameters of

Figure 14.8.   Crystal   structure   of Ba$_6$P$_{12}$N$_{17}$O$_9$Br$_3$.

a = 14.654(19), c = 8.255(9) Å and Z = 2. Its structure includes triangular, column-shaped anions $^1_\infty${(P$_{12}$N$_{17}$O$_9$)$^{9-}$} built up from vertex-sharing P(O,N)$_4$ tetrahedra with 3-rings and triply binding nitrogen atoms. The one-dimensionally extended anions are separated by Ba^{2+} and Br$^-$ ions, the latter arranged in channels parallel to the phosphate anions along [001]. The Ba^{2+} ions are coordinated eight-, and ninefold, respectively, by Br$^-$ and O/N atoms.

14.12   Nanotubes in the Si/P/O/N system (chapter 13, page 185)

A novel synthesis approach for silica-based nanotubes (NTs) was discovered in a pure inorganic system consisting of the phosphoryl triamides OP(NH$_2$)$_3$ and SP(NH$_2$)$_3$ and

SiCl$_4$. Directly, without using any solvent, the molecules are transformed in the closed system of an evacuated and sealed silica glass ampoule at temperatures from 300 to 700 °C. Besides the formation of vitreous, mainly P/N containing, flakes-like morphologies, amorphous silica-based NTs occur without adding any structure-directing template to the synthesis. By analyzing a series of synthesis products by transmission electron microscopy the NTs were found to be composed of
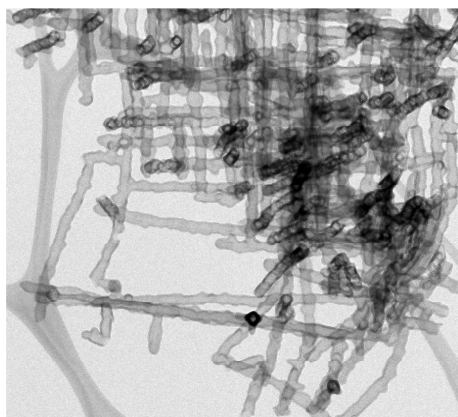
Figure 14.9.   Orthogonally   branched silica-based NTs.

mainly Si/O and less P/N and grow bamboo-like to several micrometers in length and,

dependent on the temperature, to 126 to 72 nm in diameter. Furthermore the NTs were frequently observed to grow orthogonally branched in all three directions in space. It is suggested that the growth starts from low condensed P/O/N/H polymer agglomerations and proceeds by a self-separating process of Si / O accumulation first to hollow particles and further to NTs with forming closed ends. The chemical system and its dependency on different parameters are thoroughly discussed. The building of 3D hyperbranched mesocrystals of these new, amorphous silica-based NTs make them interesting for application in nanofluidic devices.

15.   Appendix

This appendix contains a collection of ^{31}P solid-state NMR chemical shift values of P/(O)/N compounds (15.1.). Furthermore, the list of publications building up this doctoral thesis (15.2.) and publications beyond this thesis (15.3.) are additionally given below in reverse chronological order. Contributions to conferences and a summary of the CSD numbers with which crystallographic data of the newly (via X-ray and electron diffraction) characterized compunds can be retrieved at Fachinformationszentrum Karlsruhe, 76344 Eggenstein-Leopoldshafen, Germany (fax: (+49)7247-808-666; e-mail: crysdata@fiz-karlsruhe.de) are given in chapters 15.4 and 15.5, respectively.

15.1   List of ^{31}P solid-state NMR chemical shift values of P/(O)/N compounds

P/O/N compound and reference	chemical shift value δ_{iso} / ppm
α-P_3N_5 W. Schnick, J. Lücke, F. Krumeich, *Chem. Mater.* **1996**, *8*, 281.	–46, –65
γ-P_3N_5 K. Landskron, H. Huppertz, J. Senker, W. Schnick, *Z. Anorg. Allg. Chem.* **2002**, *628*, 1465.	–11.9, –101.7
HP_4N_7 S. Hostmann, E. Irran, W. Schnick, *Z. Anorg. Allg. Chem.* **1998**, *624*, 221.	–26
$H_3P_8O_8N_9$ S. J. Sedlmaier, V. R. Celinski, J. Schmedt auf der Günne, W. Schnick, *Chem. Eur. J.* **2012**, *18*, 4358.	–31.9
PON (cristobalite) S. J. Sedlmaier, W. Schnick, unpublished work.	–26.3
$PO_{0.88}N_{1.24}H_{0.56}$ (amorphous) J. Holz, Bachelor Thesis, Univ. Munich (LMU), **2008**.	–38
δ-PON D. Baumann, S. J. Sedlmaier, W. Schnick, *Angew. Chem.* **2012**, *124*, 4785; *Angew. Chem. Int. Ed.* **2012**, *51*, 4707.	–32.1

Li/Na PON-glasses A. Le Sauze, L. Montagne, G. Palavit, R. Marchand, *J. Non-Cryst. Solids* **2001**, *293-295*, 81.	PO_4: ~ –20 PO_3N: ~ –10 PO_2N_2: ~ 0
$LiPN_2$ H.-P. Baldus, W. Schnick, J. Lücke, U. Wannagat, G. Bogedain, *Chem. Mater.* **1993**, *5*, 845.	0.0
$NaPN_2$ K. Landskron, S. Schmid, W. Schnick, *Z. Anorg. Allg. Chem.* **2001**, *627*, 2469.	–15.0
NaP_4N_7 K. Landskron, Doctoral Thesis, Univ. Munich (LMU), **2001**.	–23.5, –25.0
KP_4N_7 K. Landskron, Doctoral Thesis, Univ. Munich (LMU), **2001**.	–0.4, –1.7
RbP_4N_7 K. Landskron, Doctoral Thesis, Univ. Munich (LMU), **2001**.	–19.6, –28.2
CsP_4N_7 K. Landskron, Doctoral Thesis, Univ. Munich (LMU), **2001**.	–21.6, –31.9
$Rb_3P_6N_{11}$ K. Landskron, Doctoral Thesis, Univ. Munich (LMU), **2001**.	–7.4
$Cs_3P_6N_{11}$ K. Landskron, Doctoral Thesis, Univ. Munich (LMU), **2001**.	–8.9
$SiPN_3$ H.-P. Baldus, W. Schnick, J. Lücke, U. Wannagat, G. Bogedain, *Chem. Mater.* **1993**, *5*, 845.	–12
Mg_2PN_3 a) S. J. Sedlmaier, W. Schnick, unpublished result; b) V. Schultz-Coulon, W. Schnick, *Z. Anorg. Allg. Chem.* **1997**, *623*, 69.	22.8
Zn_2PN_3 S. J. Sedlmaier, M. Eberspächer, W. Schnick, *Z. Anorg. Allg. Chem.* **2011**, *637*, 362.	42.8
SrP_2N_4 F. W. Karau, L. Seyfarth, O. Oeckler, J. Senker, K. Landskron, W. Schnick, *Chem. Eur. J.* **2007**, *13*, 6841.	–27.8, –23.4, –17.1, -15.5, –14.1, intensity ratio: 1:1:3:2:1
CaP_2N_4 K. Landskron, Doctoral Thesis, Univ. Munich (LMU), **2001**.	–20.0, –15.9, –5.2, –3.6, –2.6

Li$_7$PN$_4$ R. Lauterbach, Diploma Thesis, Univ. Bayreuth, **1996**.	49.2, 54.6
Oxonitridosodalite Li$_{5.8}$H$_{2.2}$[P$_{12}$N$_{18}$O$_6$]I$_2$ N. Stock, E. Irran, W. Schnick, *Chem. Eur. J.* **1998**, *4*, 1822.	–8.7, half width: 8 ppm
Zn$_8$[P$_{12}$N$_{24}$]O$_2$ F. Karau, O. Oeckler, F. Schäfers, R. Niewa, W. Schnick, *Z. Anorg. Allg. Chem.* **2007**, *633*, 1333.	1.8
Li$_{12-x}$H$_{x-y+z}$[P$_{12}$O$_y$N$_{24-y}$]X$_z$ (X = Cl, Br) S. Correll, N. Stock, O. Oeckler, J. Senker, T. Nilges, W. Schnick, *Z. Anorg. Allg. Chem.* **2004**, *630*, 2205.	6.53(1), –0.06(2), half width: 6.81(2) ppm, 10.58(3), intensity ratio: 2:3
Sr$_3$P$_6$O$_6$N$_8$ S. J. Sedlmaier, J. Schmedt auf der Günne, W. Schnick, *Dalton Trans.* **2009**, 4081.	2.6
SrP$_3$N$_5$O S. J. Sedlmaier, E. Mugnaioli, O. Oeckler, U. Kolb, W. Schnick, *Chem. Eur. J.* **2011**, *17*, 11258.	–9.3, half width: 14.3 ppm

15.2   Publications within this thesis

17. Template-free Inorganic Synthesis of Silica-Based Nanotubes and their Self-Assembley to Mesocrystals

    S. J. Sedlmaier, T. Dennenwaldt, C. Scheu, and W. Schnick

    J. Mater. Chem. **2012**, *22*, 15511-15513.

16. An Unprecedented AB$_2$ Tetrahedra Network Structure Type in a High-Pressure Phase of Phosphorus Oxonitride (PON)

    D. Baumann, S. J. Sedlmaier, and W. Schnick

    Angew. Chem. **2012**, *124*, 4785-4787; *Angew. Chem., Int. Ed.* **2012**, *51*, 4707-4709.

15. High-Pressure Synthesis and Crystal Structure of Ba$_3$P$_6$O$_6$N$_8$

    S. J. Sedlmaier, D. Weber, and W. Schnick

    Z. Kristallogr. – New Cryst. Struct. **2012**, *227*, 1-2.

14. High-pressure Synthesis and Structural Investigation of $H_3P_8O_8N_9$: A New Phosphorus(V) Oxonitride Imide with an Interrupted Framework Structure

S. J. Sedlmaier, V. R. Celinski, J. Schmedt auf der Günne, und W. Schnick

Chem. Eur. J. **2012**, *18*, 4358-4366.

13. $Ba_6P_{12}N_{17}O_9Br_3$ – A Column-Type Phosphate Structure Solved from Single Nanocrystal Data Obtained by Automated Electron Diffraction Tomography

E. Mugnaioli, S. J. Sedlmaier, O. Oeckler, U. Kolb, and W. Schnick

Eur. J. Inorg. Chem. **2012**, 121-125.

12. Synthesis and Characterization of $Ca_2(PO_2NH)_4 \cdot 8H_2O$

S. J. Sedlmaier, S. R. Römer, and W. Schnick

Z. Anorg. Allg. Chem. **2011**, *637*, 2228-2232.

11. Unprecedented Zeolite-Like Framework Topology Constructed from Cages with 3-Rings in a Barium Oxonitridophosphate

S. J. Sedlmaier, M. Döblinger, O. Oeckler, J. Weber, J. Schmedt auf der Günne, and W. Schnick

J. Am. Chem. Soc. **2011**, *133*, 12069-12078.

10. SrP_3N_5O – A Highly Condensed Layer Phosphate Structure Solved from a Nanocrystal by Automated Electron Diffraction Tomography

S. J. Sedlmaier, E. Mugnaioli, O. Oeckler, U. Kolb, and W. Schnick

Chem. Eur. J. **2011**, *17*, 11258-11265.

9. High-Pressure Synthesis, Crystal Structure and Characterization of Zn_2PN_3 – A New Catena-polynitridophosphate

S. J. Sedlmaier, M. Eberspächer, and W. Schnick

Z. Anorg. Allg. Chem. **2011**, *637*, 362-367.

8. $Sr_3P_6O_6N_8$ – A Highly Condensed Layered Phosphate

S. J. Sedlmaier, J. Schmedt auf der Günne, and W. Schnick

Dalton Trans. **2009**, 4081-4084.

7. Crystal Structure of Ammonium Catena-polyphosphate IV [NH$_4$PO$_3$]$_x$

    S. J. Sedlmaier and W. Schnick

    Z. Anorg. Allg. Chem. **2008**, *634*, 1501-1505.

6. Tl$_4$(PO$_2$NH)$_4$ · H$_2$O – a Modulated Tetrametaphosphimate

    S. J. Sedlmaier, O. Oeckler, and W. Schnick

    Solid State Sci. **2008**, *10*, 1150-1158.

15.3   Publications beyond this thesis

5. Luminescence Tuning of MOFs via Ligand to Metal and Metal to Metal Energy
    Transfer by Co-Doping of [Gd$_2$Cl$_6$(bipy)$_3$] · 2bipy with Europium and Terbium

    P. R. Matthes, C. J. Höller, M. Mai, J. Heck, S. J. Sedlmaier, S. Schmiechen, C.
    Feldmann, W. Schnick, and K. Müller-Buschbaum

    J. Mater. Chem. **2012**, *22*, 10179-10187.

4. Synthesis, Crystal Structures and Properties of the Trimetaphosphimates
    Na$_2$M(PO$_2$NH)$_3$ · 2H$_2$O with M = K, Tl

    S. J. Sedlmaier, D. Johrendt, O. Oeckler, and W. Schnick

    Z. Anorg. Allg. Chem. **2007**, *633*, 2217-2222.

3. Crystal Structures of Incommensurately Modulated Ln(PO$_3$)$_3$ (Ln = Tb–Yb) and
    Commensurate Gd(PO$_3$)$_3$ and Lu(PO$_3$)$_3$

    H. A. Höppe and S. J. Sedlmaier

    Inorg. Chem. **2007**, *46*, 3467-3474.

2. Synthesis, crystal structures and properties of the trimetaphosphimates
    NaBa(PO$_2$NH)$_3$, KSr(PO$_2$NH)$_3$ · 4H$_2$O and NH$_4$Sr(PO$_2$NH)$_3$ · 4H$_2$O

    S. Correll, S. Sedlmaier, and W. Schnick

    Solid State Sci. **2005**, *7*, 1261-1271.

1. Synthese, Kristallstruktur und Eigenschaften von Chrom(III)-trimetaphosphimat-Heptahydrat, Cr(PO$_2$NH)$_3$ · 7H$_2$O

   S. Correll, S. Sedlmaier, and W. Schnick

   Z. Anorg. Allg. Chem. **2005**, *631*, 1359-1364.

15.4 Contributions to conferences

8. "Synthesis, Identification and Characterization of Novel, Condensed Oxonitridophosphates and Phosphorus Oxonitrides" (oral presentation)

   <u>S. J. Sedlmaier</u>, W. Schnick

   Red Kite Crystallographers meeting, Oxford, United Kingdom, 2012.

7. „Neue Phosphoroxonitride" (oral presentation)

   <u>S. J. Sedlmaier</u>, V. R. Celinski, J. Schmedt auf der Günne, W. Schnick

   Hirschegg-Seminar on Solid-state Chemistry, Hirschegg, Austria, 2011.

6. "PON durch ADT" (oral presentation)

   <u>S. J. Sedlmaier</u>, E. Mugnaioli, O. Oeckler, U. Kolb, W. Schnick

   Hemdsärmelkolloquium – Symposium on Solid-state Chemistry, Dresden, 2011.

5. "HP/HT-Synthesis of Nitride Materials" (poster presentation)

   <u>S. Schneider</u>, F. Pucher, D. Baumann, S. Sedlmaier, R. Römer, F. Karau, W. Schnick

   4th Berichtskolloquium for the SPP 1236, Hünfeld, 2011.

4. "Ba$_{19}$[P$_{36}$O$_6$N$_{66}$]Cl$_8$: An Oxonitridophosphate with an Unprecedented Zeolite-like Framework Topology" (poster presentation)

   <u>S. J. Sedlmaier</u>, M. Döblinger, O. Oeckler, W. Schnick

   16th International Zeolite Conference 2010 (IZC joint with 7th IMMS), Sorrento, Italien, 2010.

3. „Das Oxonitridophosphat $Sr_3P_6O_6N_8$ – Synthese und Struktur" (oral presentation)

    <u>S. J. Sedlmaier</u>, J. Schmedt auf der Günne, W. Schnick

    Hirschegg-Seminar on Solid-state Chemistry, Hirschegg, Austria, 2009.

2. „$Tl_4(PO_2NH)_4 \cdot H_2O$ – Ein moduliertes Tetrametaphosphimat und seine Strukturlösung in 3+1 D" (oral presentation)

    <u>S. J. Sedlmaier</u>, O. Oeckler, W. Schnick

    Hirschegg-Seminar on Solid-state Chemistry, Hirschegg, Austria, 2007.

1. "Ln(PO$_3$)$_3$ – commensurate or incommensurate?" (poster presentation)

    <u>H. A. Höppe</u>, S. J. Sedlmaier

    14th Annual Conference of the German Crystallographic Society, Freiburg i. Breisgau, 2006.

15.5   Deposited crystallographic data

Compound	CSD-Number
$Tl_4(PO_2NH)_4 \cdot H_2O$	418498
$Ca_2(PO_2NH)_4 \cdot 8H_2O$	423118
$[NH_4PO_3]_x$	419184
$H_3P_8O_8N_9$	423298
δ-PON	423589
$Sr_3P_6O_6N_8$	419864
$Ba_3P_6O_6N_8$	710077
Zn_2PN_3	422150
$Ba_{19}P_{36}O_{6+x}N_{66-x}Cl_{8+x}$ $(x \approx 4.54)$	422769
SrP_3N_5O	423054
$Ba_6P_{12}N_{17}O_9Br_3$	423468

<u>Stefan</u> Josef Sedlmaier

Personal Information	
born	10/04/1981
in	Freising, Germany

Education	
01/2007 – 11/2011	Doctoral studies in the group of Prof. Dr. W. Schnick at the Department of Chemistry, Ludwig-Maximilians-Universität München with the aim of awarding the doctorate; Doctoral thesis entitled: "Synthesis, Identification, and Characterization of novel, condensed Oxonitridophosphates and Phosphorus Oxonitrides"
11/2006	**Master of Science** (Chemistry) at Ludwig-Maximilians-Universität München with Prof. Dr. W. Schnick Master thesis entitled: "Neue strukturelle Aspekte bei Imidocyclophosphaten"
10/2004 – 11/2006	Studies of Chemistry (Master) at Ludwig-Maximilians-Universität München
10/2004	**Bachelor of Science** (Chemistry and Biochemistry) at Ludwig-Maximilians-Universität München with Prof. Dr. W. Schnick Bachelor thesis entitled: "Synthese, Charakterisierung und Eigenschaften neuer Trimetaphosphimate"
10/2001 – 10/2004	Studies of Chemistry and Biochemistry (Bachelor) at Ludwig-Maximilians-Universität München
2001	**Allgemeine Hochschulreife** at Gabelsberger-Gymnasium Mainburg
09/1992 – 06/2001	Secondary school at Gabelsberger-Gymnasium Mainburg
09/1991 – 07/1992	Extended elementary school at Volksschule Nandlstadt
09/1987 – 07/1991	Elementary school at Volksschule Nandlstadt

Awards and Scholarships	
30/06/2011	**Holleman-Wiberg Book award**, in recognition for achievements during Doctoral reserach, Ludwig-Maximilians-Universität München (in the course of the 23. Egon-Wiberg-lecture)
18/06–03/07/2009	**Member (*Young researcher*) of Nobel Laureate Meeting**, Lindau
2007	**Dr. Klaus Römer-Stiftung award** for outstanding achievements in master studies
10/2007 – 09/2009	**Doctoral scholarship,** Stiftung Stipendien-Fonds of 'Verband der Chemischen Industrie e.V.'
2006	**Book Prize** for outstanding achievements in studies, Ludwig-Maximilians-Universität München

Munich, 16/11/2011